UNIVERSITY OF SOUTHAMPTON

FACULTY OF SCIENCE

AN INVESTIGATION OF STIMULATED RAMAN SCATTERING IN GASES USING A TUNABLE LASER

by

Marcos Tadeu Tavares Pacheco

A thesis submitted for the degree of

Doctor of Philosophy

May 1986

UNIVERSITY OF SOUTHAMPTON

ABSTRACT

FACULTY OF SCIENCE

Doctor of Philosophy

AN INVESTIGATION OF STIMULATED RAMAN SCATTERING IN GASES USING A TUNABLE LASER

by

Marcos Tadeu Tavares Pacheco

This thesis describes investigations made of the two nonlinear optical processes of Stimulated Raman Scattering (SRS) and Four-Wave Mixing (FWM), carried out both in simple gases, when they were perfomed in various guided and unguided configurations, and in liquids, when they were perfomed in an unguided arrangement.

To make a detailed comparison between experiment and theory a well defined pump beam is required. The development and operation of a laser capable of producing such a beam, an excimer pumped dye laser, is described in the initial part of this thesis. This laser was then used for an unguided SRS experiment to provide results such as tuning range and SRS threshold pump power, against which the perfomance of the guided configuration can be compared.

The properties of hollow, cylindrical capillaries are then described along with theoretical expressions for SRS and FWM. Both numerical and analytical solutions are presented and the conversion efficiencies for the Stokes components are worked out for several configurations.

A detailed analysis of parametric processes in guided and unguided cells is made and the experimental results compared with the predictions based in the numerical model and calculations for the phase match angle.

In the final part of the thesis several arrangements to reach high Raman conversion efficiency in liquids and gases are discussed and the main conclusion is that the use of a waveguide in a Raman oscillator-amplifier configuration can provide good conversion efficiency for high order Stokes components and an improvement in the spatial characteristics of the generated beam.

To Eld

CONTENTS

CHAPTER ONE

Introduction

Some kinds of selective interactions of radiation with matter, like spectroscopy and photochemistry as well as applications where the radiation wavelength must be in a low absorption region of the material (due to the long interaction length of the pump radiation with the medium), created a need for high-power tunable lasers in the near and middle infrared region. Several advances have been made in tunable coherent light sources in recent years in terms of high power, spectral brightness and directionality. To date, however, most of the tunable sources that have been developed operate over only a limited range of the spectrum, and in general, the best sources tend to be limited to the visible region.

Several methods of generating tunable radiation in the 1.5–20 μm region have therefore been investigated. Semiconductor diode lasers have been discontinuously tuned over the range 4–30μm, but they usually required low temperature operating conditions and each diode has only a limited tuning range.

Nonlinear crystals have been used in optical parametric oscillators to down-convert fixed frequency laser radiation and produce a tunable source over the region of interest. The problems here, however, include the small margin between the power threshold for the process and damage of the crystal.

Recently, interest has been shown in techniques where the tunability of a well-established source in the visible, like a dye laser, can be shifted directly into the infrared by Stimulated Raman Scattering (SRS). In particular, in Stimulated Electronic Raman Scattering in atomic vapours, since the large shifts available (20,000 → 30,000 cm^{-1}) allowed the typical dye laser tunability to be shifted well into the infrared. However, serious limitations are imposed by various competing processes and the heat pipes necessary to maintain the atomic (metal) vapours prove to be somewhat inconvenient.

Another approach involves SRS in simple molecular gases such as H_2 or CH_4, using the tunable output of lasers already

operating in the near-infrared region of the spectrum. Such lasers include the so called "vibronic" lasers (e.g. nickel or cobalt doped magnesium fluoride; alexandrite) and colour or F-centre lasers. These lasers have so far been tuned over the range 0.8 → 3.5 μm and so a single shift in, say, H_2 (4155 cm^{-1}), would cover the entire middle infrared region of the spectrum. The problem so far with this approach is the difficulty in obtaining high enough output powers to reach SRS threshold in the molecular gases, due to the small Raman gain coefficient in this region of the spectrum.

The approach to be considered in the work of this thesis is to again use SRS of the output from visible dye lasers, using simple molecular gases such as H_2 and CH_4. These gases have relatively large Raman shifts, i.e. 4155 cm^{-1} for H_2. The middle infrared region is covered not just by the tunable 1st Stokes shifted radiation, but by the multiple Stokes shifted components. It is necessary , therefore, that good efficiencies be obtained for conversion to the higher order Stokes components. One method of ensuring this is to perform the SRS process using a waveguide in a Raman oscillator-amplifier configuration.

In this thesis the work was aimed towards establishing the perfomance and limitations and giving a general assessment of the nonlinear optical interactions Stimulated Raman Scattering and Four Wave Mixing when carried out in guided and unguided configurations. A well-behaved and well-characterised pump beam is necessary to enable one to make careful comparison between theory and experiment. The output of a carefully designed dye laser and a Nd:YAG laser and its harmonics were used as the pump beam.

In chapter 2, the design of this laser is described, including the measurement of the laser parameters.

In chapter 3 the general theory of SRS and FWM is presented and an analytical expression is derived for the first Stokes pulse intensity including pump depletion. The general solution of the system of coupled equations is carried out numerically and finally, an extension of this theory to include the beam profile and temporal behaviour is presented and the overall solution presented and discussed.

Chapter 4 shows the experimental results for H_2 in an unguided and guided cell when pumped by the dye laser described in Chapter 2. A comparison between the experimental and predicted value for the SRS threshold pump pulse power is made and the tuning range

for the Stokes components in each case is discussed.

In chapter 5 an analysis of parametric processes in a waveguide and an unguided cell is carried out and the results of the experimental investigations are presented.

In chapter 6 experimental arrangements to reach a high conversion efficiency into first Stokes and high order Stokes components are investigated and the influence of the main factors which usually limit the conversion efficiency is discussed.

Finally in Chapter 7 several experimental arrangements for producing 1.5μm radiation are described, including SRS in liquids and the use of a mode locked Nd:YAG laser in a synchronously pumped oscillator configuration.

CHAPTER TWO

Dye Laser Design for SRS experiments

2.1 Introduction

The development of the dye laser has provided powerful continuously tunable sources with a narrow linewidth in the visible region of the EM spectrum. The threshold for SRS in the superfluorescent mode is readily reached by these sources.

The dye laser output beam should be of reasonably good quality in order to achieve a high value for the product intensity x length inside the Raman medium and also when we use capillary waveguide [Berry et al (1982/83)], to get a good transmission and very low coupling losses [Abrams (1972)]. Beside that a diffraction limited beam will allow a better understanding of the interacting processes inside the Raman medium.

This chapter is divided basically into two main parts. The first part deals with the dye laser oscillator, where we try to get two out of the three requirements given above, i.e., narrow linewidth and a good beam quality. The low damage threshold for the diffraction grating and for the dye cell surface limits the pump pulse energy and, consequently, the output energy of the oscillator stage. In the second part we describe techniques to increase the power of the whole system with a minimum deterioration of the characteristics of the beam generated in the dye oscillator.

2.2 Dye laser oscillator components

There are two main kinds of design for this sort of dye laser cavity. One of them uses a beam expander between the dye cell and diffraction grating, so that a narrow linewidth can be obtained in the tuning range(figure 2.1a). The other design uses the diffraction grating at a grazing incidence angle and a mirror, figure 2.2b.

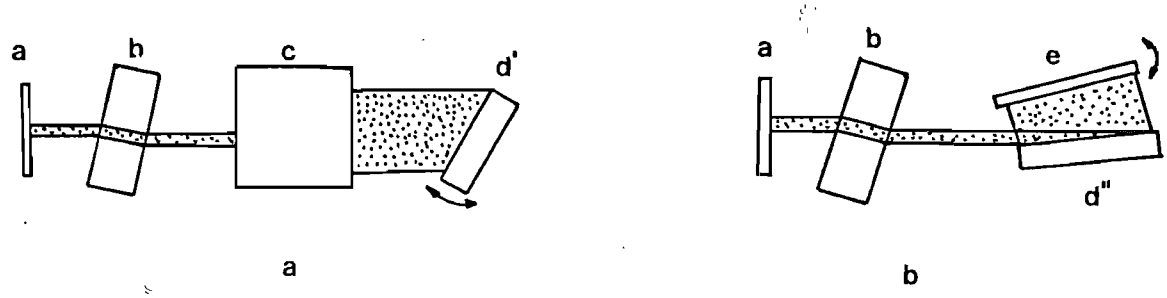

Figure 2.1.Scheme for dye laser cavities.(a) with beam expander.(b) without beam expander.
(a) output coupler, (b) dye cell, (c) beam expander, (d) diffraction grating at Littrow mode,(e)diffraction grating at grazing incidence,
(f) high reflectivity tuning mirror.

The second configuration is more suitable for producing single longitudinal mode operation, because besides the fact that the cavity length can be made very short, the laser beam is incident twice on the diffraction grating surface during each round trip. The linewidth produced in this case is within a factor of two of the cavity free spectral range, resulting in a nearly single longitudinal mode operation. The disadvantage of such a system is the very low output energy due to the low efficiency of the grating at high angles of incidence.

We have chosen configuration 2.1a, where the grating is in a Littrow mode arrangement [Bernhardt et al (1981)], because its efficiency is greater than the grazing incidence arrangement. A beam expander is used to expand the laser beam and to fill the diffraction grating surface with a low divergence beam, since this leads to the greatest frequency narrowing.A telescopic beam expander was reported by Hansch (1972), which was widely adopted and used commercially. However the telescope is not easy to align, nor is it cheap. Another option to expand the beam is to use a prism near grazing incidence angle, so that we get an expanded beam at the grating incidence plane. Hanna et al (1975) compared the prism beam expander perfomance with that of a telescope. For a nitrogen laser pumped dye laser it was found that in practice it is easier to use the prism than a telescope and that it gives linewidths which are just as narrow.

In this work the first system was chosen in order to get more efficiency from the diffraction grating and a four prism beam expander was used.

2.2.1 Diffraction grating

The use of a diffraction grating in the dye oscillator provides a narrow linewidth and tuning in the dye emission range.In a diffraction grating a periodical structure provides phase matching for a given wavelength at a specific direction. If the cavity optical axis is made coincident with this direction and the dye medium provides gain enough to overcome the losses at this wavelength, we will have oscillations at that wavelength, figure 2.2..

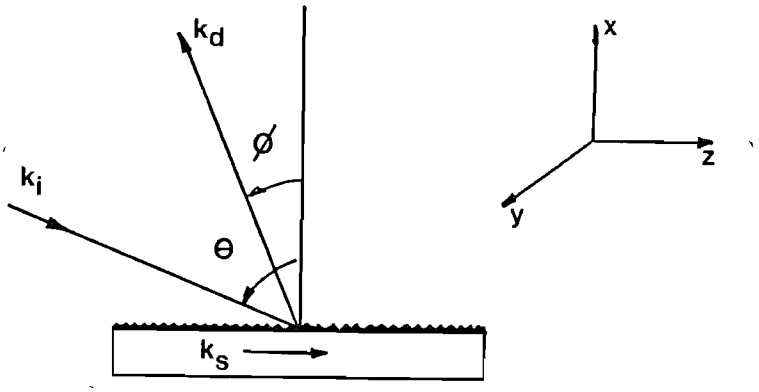

Figure 2.2. Incident and diffracted beams for a diffraction grating.

From the phase match condition at the xz plane we have,

$$k_{iz}=k_{dz}+mk_s \qquad 2.1$$

where k_{iz} and k_{dz} are the wavevector component in the z direction of the incident and diffracted beam respectively. k_s is the "wave vector" of the periodical structure and is defined as,

$$k_s=2\pi/\Lambda \qquad 2.2$$

where Λ is the spatial grating period. From the geometry of figure 2.2 we write,

$$\sin\theta/\lambda_i + \sin\phi/\lambda_d = m/\Lambda \qquad 2.3$$

where m is the grating diffraction order. For $\lambda_i=\lambda_d$ we have the value of the radiation wavelength as a function of the incident angle on the diffraction grating.

$$\lambda = (\Lambda/m).(\sin\theta+\sin\phi) \qquad 2.4$$

The value of m should be kept as low as possible. A grating working with many diffraction orders causes undesirable feedback of other wavelengths when we have an active medium with wide gain bandwidth.

For the grazing incidence configuration we have $\theta\simeq 90^\circ$ and for m=1 we can write,

$$\lambda=\Lambda(1+\sin\phi) \qquad 2.5$$

in the Littrow mode situation we have $\theta=\phi$ and expression 2.4 becomes,

$$\lambda=2\Lambda\sin\phi \qquad 2.6$$

In order to cover the whole dye tuning range and to avoid high diffraction orders, the spatial grating period Λ should satisfy the inequality,

$$\lambda_{max}/2 < \Lambda < \lambda_{min} \qquad 2.7$$

where λ_{max} and λ_{min} are the maximum and the minimum value of wavelength for which we can have laser action inside the oscillator.

2.2.1.1. **Cavity bandwidth**

The single pass bandwidth of the cavity (full width) is given by Hanna et al (1975),

$$\delta\lambda=2(\partial\lambda/\partial\phi)\delta\theta \qquad 2.8$$

where $\delta\theta$ is the half angle divergence of the superfluorescent beam incident on the grating. The angular dispersion can be found by the first derivative of expression 2.4 with respect to ϕ.

$$\partial\lambda/\partial\phi=\Lambda\cos\phi/2 \quad \text{for grazing incidence} \qquad 2.9$$

$$\partial\lambda/\partial\phi=\Lambda\cos\phi \quad \text{for Littrow mode} \qquad 2.10$$

The factor two in the grazing incidence dispersion is due to the fact that the beam is diffracted twice before returning to the dye cell. The value of $\delta\theta$ depends on the relation between the cavity length and the confocal parameter which is defined by the radius **a** of the active dye region cross-section. In order to get a diffraction limited beam and maximum pulse output energy the dye laser cavity should be design in a way that the distance from the dye cell to the diffraction grating is given by (Appendix 1)

$$c= \pi a^2/\lambda \qquad 2.11$$

the beam divergence at the grating surface is

$$\delta\theta= 2\sqrt{2}\ \lambda/\pi L'\cos\phi \qquad 2.12$$

where L' is the illuminated length of the grating.

If L' is equal to L the main diffraction lobe of the slit function, defined by the active dye region cross-section, just fills the grating length.

When the cavity length is smaller than the length given by expression 2.11 we will not have a diffraction limited beam coming out the cavity, since in this case high diffraction order will be reflected into the pumping region. That is usually the case when one uses a prism beam expander set-up, the first prism is placed very close to the dye cell in order to keep the cavity length as small as possible. In this case the spot size at the grating surface is given by the radius of the active region cross-section multiplied by the expansion factorM, due to the beam expander and the half angle divergence at the grating surface can be written as

$$\delta\theta=\lambda/\pi Ma \qquad 2.13$$

Using expression 2.8 one can calculate the full width single pass cavity bandwidth for each case.

	Littrow mode	grazing incidence
With no beam expander and d≥c	$4\sqrt{2}\ \lambda\Lambda/\pi L$	$2\sqrt{2}\ \lambda\Lambda/\pi L$.
With beam expander and d<c	$4\lambda\Lambda/\pi L$	$2\lambda\Lambda/\pi L$

where $c= \pi a^2/\lambda$

In this work we use the Littrow mode configuration with a beam expander. It will make the radius of the active dye region be multiplied by a large factor (typically > 50) and the distance from the dye cell to the first prism beam expander very small producing a non difraction limited beam. However in the vertical plane the beam does not have any magnification and in terms of high diffraction order modes reflected back into the pumping region one can still consider the distance between the dye cell and the grating regardless the prisms beam expander set-up since it has no effect on the beam divergence in the vertical plane. Usually this distance is equal or bigger than the value given in expression 2.11 and the beam is diffraction limited in this plane. So in our case the cavity bandwidth is given by,

$$\delta\lambda= 2(\Lambda\cos\phi).\lambda/(\pi Ma) \qquad 2.14$$

or

$$\delta\lambda=4\lambda\Lambda/\pi L \qquad 2.15$$

in terms of usual unities we can write

$$\delta\tilde{\nu}=4\times10^6/(\pi LN\lambda) \qquad 2.16$$

where $\delta\tilde{\nu}$ is the full bandwitdth in cm^{-1}.

L is the grating length in cm.

Figure 2.3. Cavity bandwidth against the dye laser wavelength. Curves A,B and C correspond to N=1900,2400 and 3200 respectively. The symbols show the variation of the needed magnification to fill the grating length, (Δ) for N=1900 g/mm, (∇) for N=2400 g/mm and (+) for N= 3200 g/mm. The variation of the grating incidence angle to cover the whole dye tuning range is given in the upper part of this diagram.

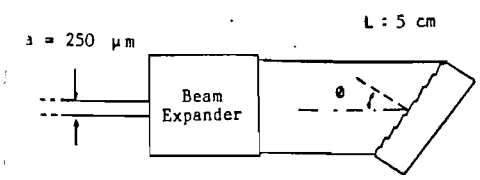

Angle Variation: (Φ)

31°30' to 35°05' for N = 1900 g/mm

41°18' to 46°33' for N = 2400 g/mm

61°38' to 75°28' for N = 3200 g/mm

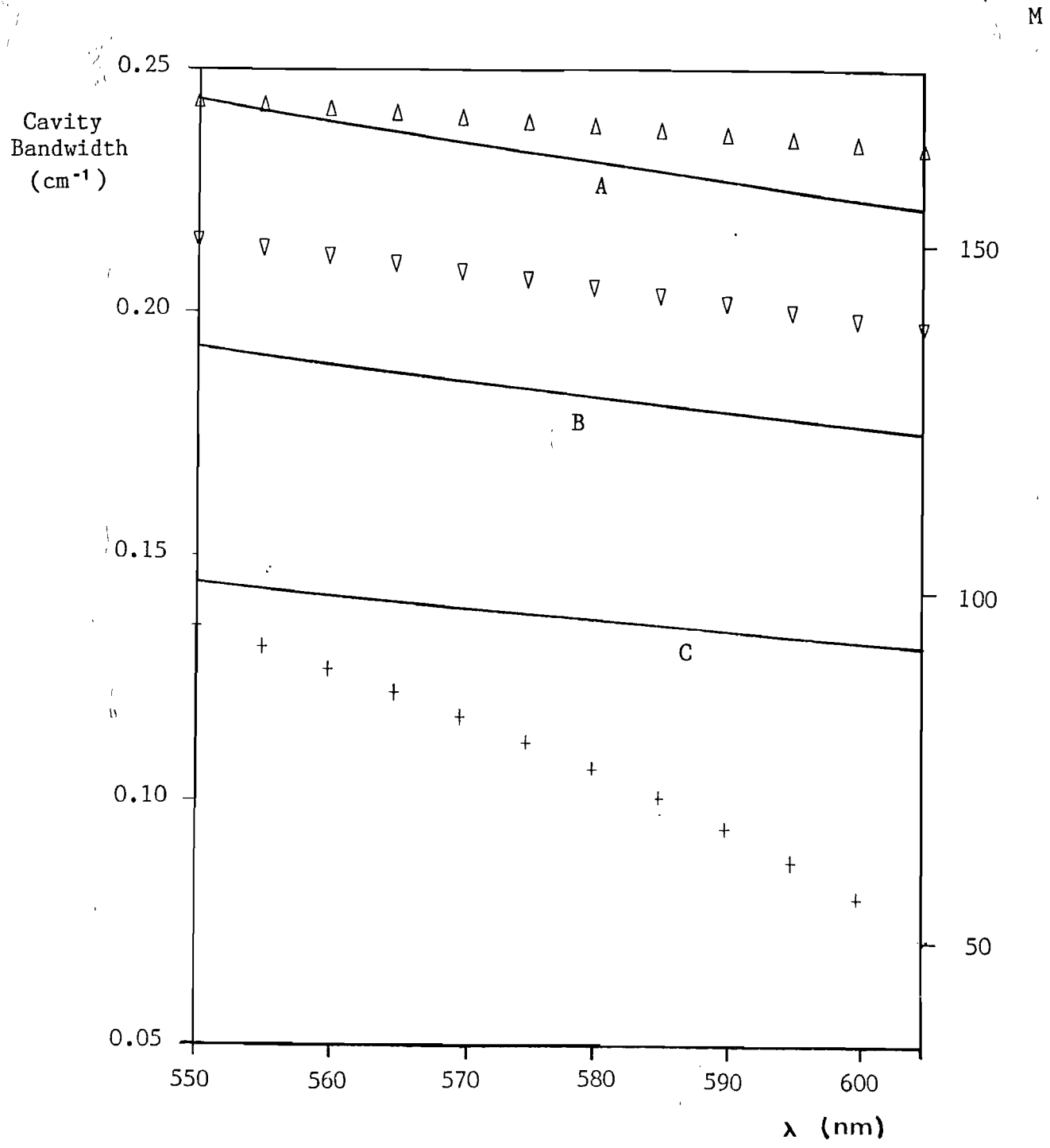

N is the number of grooves per mm.

λ is the wavelength in nm.

In figure 2.3 we have the variation of the cavity bandwidth against the wavelength.

2.2.2. **Beam expander – prisms**

A telescope is generally used in order to achieve a dye laser output beam with a narrow spectral width. It expands and collimates the beam onto a grating. The configuration however has some problems; for a dye laser being pumped by pulses of the order of nanoseconds we need to have a cavity length short enough to allow a sufficient number of cavity round trips during the excitation time,and this is particularly difficult when one uses a telescope as a beam expander. In addition to that it is not easy to ensure an accurate matching between the cavity optics and the dye cell over a wide range of wavelengths.[T.Kasuka et al (1978)]This is because the amount of diffraction present is wavelength dependent and therefore requires telescope re-adjustment for optimum operation at any new chosen wavelength. An alternative arrangement is the use of a prism at a large angle of incidence. The very simplicity and compactness of the cavity, the easy alignment and the comparative economy of the optical components lead us to choose this system to expand the beam in the dye cavity.

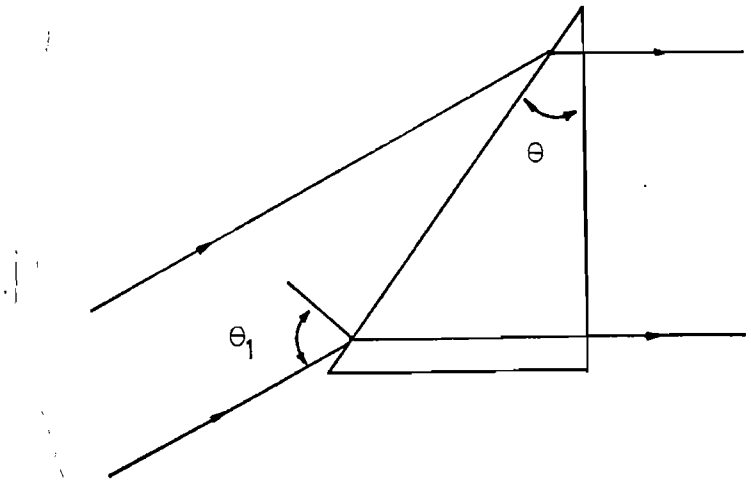

Figure 2.4. Single prism beam expander with output beam normal to the exit prism surface.

Figure 2.4 shows the single prism beam expander with the input angle such that the output beam is normal to the prism exit surface. The beam of light undergoes an expansion M_0 in the plane of incidence given by, [Hanna et al (1975)]

$$M_0=\sqrt{1 - \sin^2\theta_1/n^2}/\cos\theta_1 \qquad 2.17$$

where **n** is the prism refractive index. In everyday use however, we might not have the output beam normal to the exit surface. The two main consequences of that are:

(i) a reduction in the magnification due to the contraction of the beam size at the exit surface.

(ii) possibility of internal total reflection that appears for some values of the input and apex angles.

The overall magnification for a general case can be separated into two factors. The first one gives the magnification produced by the entrance prism surface,

$$C_1=\cos\theta_2/\cos\theta_1 \qquad 2.18$$

where θ_1 and θ_2 are shown in figure 2.5.

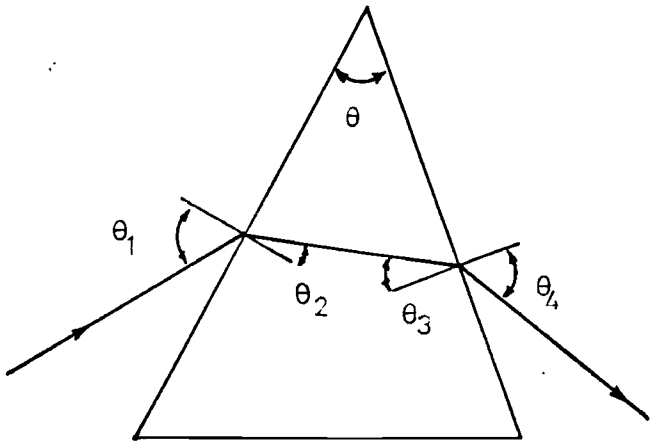

Figure 2.5. The relevant angles for a beam prism beam expander calculation.

The second factor gives a contraction of the beam diameter at the exit surface and it is given by,

$$C_2=\cos\theta_4/\cos\theta_3 \qquad 2.19$$

so the total magnification can be written as,

$$M = C_1 . C_2 \qquad 2.20$$

The maximum value assumed by C_2 is unity, when the output beam is normal to the exit surface. In this case expression 2.20 is reduced into expression 2.17,

$$M = C_1 = M_0 \qquad 2.21$$

thus the value of C_1 is given by the prism magnification when we have the output beam normal to the exit surface. The factor C_2 depends on the apex and input angles and is given by

$$C_2 = C(\theta, \theta_1) = \frac{\sqrt{1 - n^2(\sin\theta_1 . \cos\theta/n - \sin\theta \sqrt{1 - (\sin^2\theta_1/n^2)})^2}}{\sqrt{1 - (\sin\theta_1 . \cos\theta/n - \sin\theta \sqrt{1 - (\sin^2\theta_1/n^2)})^2}} \qquad 2.22$$

figure 2.6 shows a curve for the variation of C_2 against the input angle for a apex angle of 30° and several prism refractive indices. The maximum value for C_2 is given for an input angle of

$$\theta_1 = \text{arc } \sin(n \sin\theta) \qquad 2.23$$

that corresponds to a exit surface normal to the output beam. From expression 2.23 and figure 2.6 one can observe that a large value for the refractive index will correspond to a large value for θ_1.

2.2.2.1 Internal total reflection

The condition for total internal reflection can be derived directly from expression 2.22,

$$\left| \sin\theta_1 . \cos\theta - \sin\theta \sqrt{n^2 - \sin^2\theta_1} \right| > 1 \qquad 2.24$$

In figure 2.7 we have a set of curves for the apex angle θ versus the input angle θ_1 from 2.24 with an equallity sign introduced. In those graphs the region above each curve represents the range of the set of angles (θ, θ_1) which will produce total reflection inside the prism.

We can define three regions for the apex angle variation and

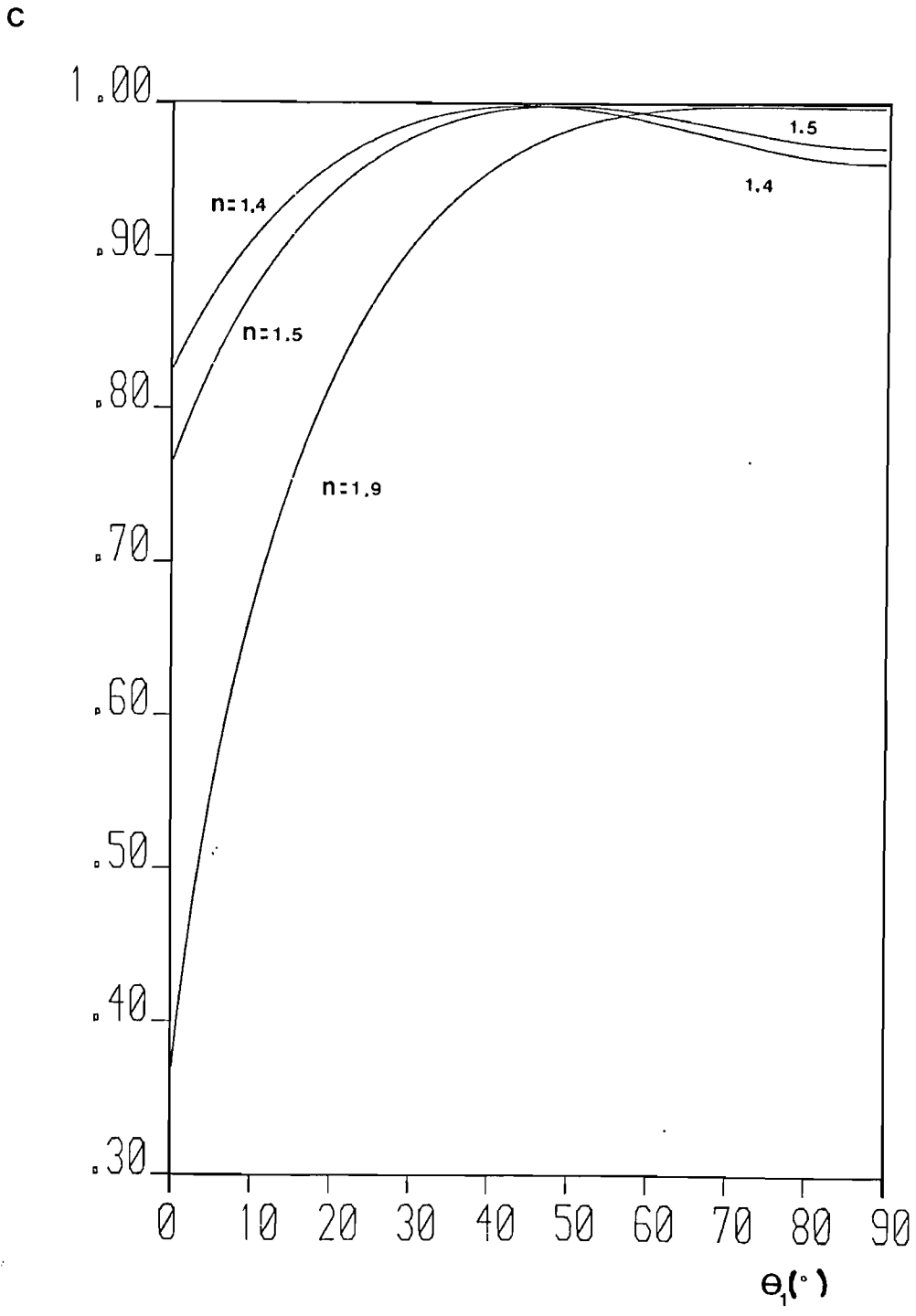

Figure 2.6. Curve for the C factor against the angle of incidence for three refractive indices 1.4, 1.5 and 1.9 and a apex angle of 30°.

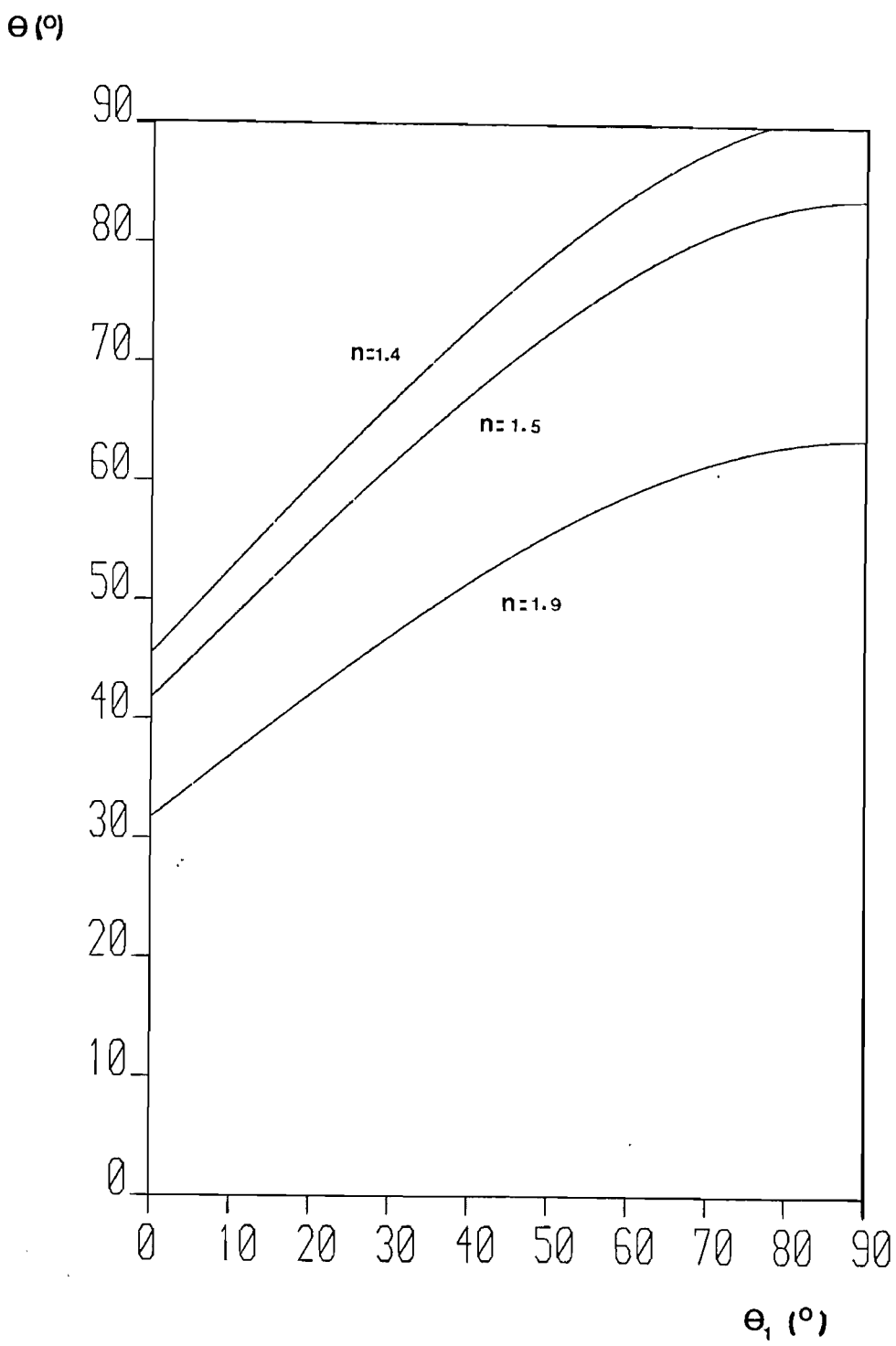

Figure 2.7. Curve of maximum apex angle against the angle of incidence for three refractive indices 1.4, 1.5 and 1.9.

these regions are given in terms of the prism refractive index.The first region is defined as,

$$0^\circ < \theta < \text{arc sin } 1/n \qquad 2.25$$

for this range of apex angles any input angle can be used without causing internal reflection. The second region is defined as,

$$\text{arc sin } 1/n < \theta < 2 \text{ arc sin } 1/n \qquad 2.26$$

for this range of θ there are certain values for θ_1 that will give total internal reflection. From figure 2.7 for a given apex angle we can read off a minimum value for the input angle. One can see that when the refractive index and the apex are increased simultaneously the condition for useful operation becomes rather restrictive.

The third region is defined for an apex angle in the range

$$\theta > 2 \text{ arc sin } 1/n \qquad 2.27$$

In this region any input angle will produce total internal reflection and therefore it represents a region where the prism cannot be used as a beam expander element. A detailed deduction of expressions 2.25,2.26 and 2.27 is given in Appendix 2.

2.2.2.2 **Prism dispersion**

The prism dispersion is small when compared with the grating dispersion, even when one uses a single prism to provide the whole magnification,the prism dispersion can still be neglected in relation to the grating dispersion [Nair (1977)]. Usually however, the number of prism used is hardly one, due to the high transmission losses that one single prim will produce.For a typical beam expander configuration four prisms are used. The input angle can be made smaller than the one for the single prism configuration and this drastically reduces the transmission losses and the prism dispersion that is proportional to the tangent of the internal input angle. Besides that, a multiple prism configuration allows an arrangement in compensating pairs to reduce the overall dispersion, figure 2.8

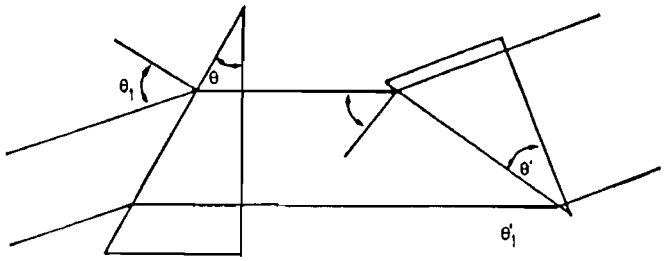

Figure 2.8. Arrangement of compensating pair prism

2.2.3 **Laser dyes**

The energy levels for a typical organic dye are shown in figure 2.9. Each electronic level is actually a band composed of a continuum of vibrational and rotational levels. The lowest energy absorption is caused by absorption from the electronic S_0 ground state to the first excited state S_1. This strong absorption is usually in the visible region of the spectrum.

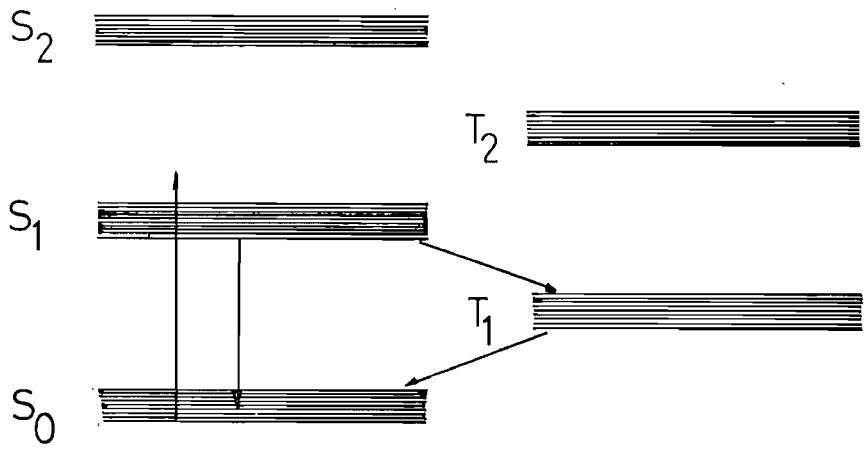

Figure 2.9. Energy level diagram of a typical organic molecule.

Several classes of organic compounds have been demonstrated to give laser action when conveniently pumped. In practice, however, coumarin and rhodamine dyes are the most widely used owing to their high laser yield, photostability, available tuning spectral range and high solubility in convenient solvents. In figure 2.10 we have the absorption and fluorescent emission spectra of rhodamine 6G and B.[Sahar et al (1977)]

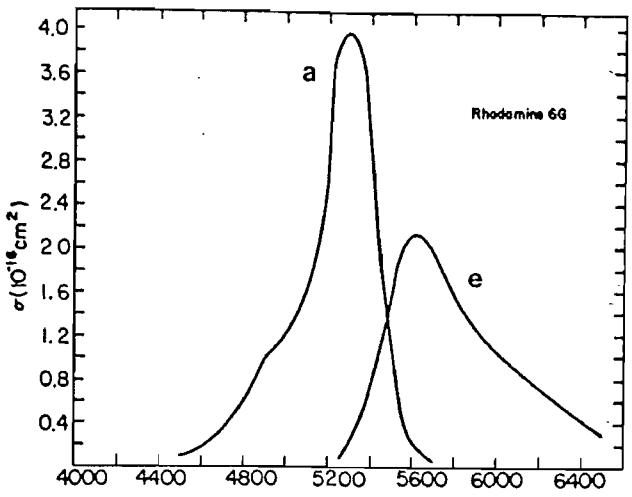

Figure 2.10. Absorption and emission spectra for rhodamine 6G.

The tuning range curve for the dye laser will be different from the emission curve due to the absorption by the excited state and ground state. The overlapping between the curves will shift the tuning range peak to long wavelengths.

2.2.3.1 **The rhodamine 6G**

Rhodamine 6G is the most efficient dye and also it has the best stability of all known dyes. Consequently much interest has been shown in dye lasers employing it as the lasing medium. We briefly review some relevant performance results obtained with Rhodamine 6G. Shank et al (1970) measured the small signal gain under N_2 laser pumping and Govindanunny (1980) repeated the Shank experiment for different solvents coming to the conclusion that in solvent of low refractive index and high polarity, Rh6G has its highest gain per unit pump power. The performance of Rh6G under high intensity 248nm wavelength pumping was reported by V.I.Tomin (1978). The dye was dissolved in ethyl alcohol (EtOH) and experiments carried out at concentrations of 0.5×10^{-3} to 5.0×10^{-3} Mol/L. The dye showed a constant efficiency for a range of pump energies, typically around 5% in a simple cavity formed by a high reflecting mirror, cell and the output coupler. McKee et al (1979) using a similar configuration observed an efficiency of 10% for a concentration of 1.3×10^{-3} Mol/L. Investigations were made using a Q-switched frequency doubled Nd:YAG laser as pump source. [Moore et al (1978)] The cavity used consists of a flowing dye cell between two mirrors and a longitudinal pumping

geometry. The dye was dissolved in methanol at a concentration of 0.75 x 10^{-4} Mol/L. The untuned laser emission efficiency was 40% at 559nm, with a bandwidth of aproximatelly 10% of the full fluorescent emission width. Damage to the dye cell windows was noted for a pump intensity of 400 MW/cm^2 (coated windows). The absorption cross-section for 532nm pump wavelength was measured to be σ=4.24 x 10^{-16} cm^2 by P.R.Hammond (1979).

2.2.4 Dye oscillator design

The parameters analysed in this section are concerned with the spatial quality and output energy of the laser beam generated in the dye oscillator. We will discuss in particular the influence of the cylindrical lens, the dye concentration and the pump energy.

2.2.4.1 Cavity length

The light emitted from the excited region of the dye cell gets out through the cell windows and is diffracted by the output aperture. In order to keep the beam divergence small we need to avoid the reflection of the high diffraction orders by the rear mirror.

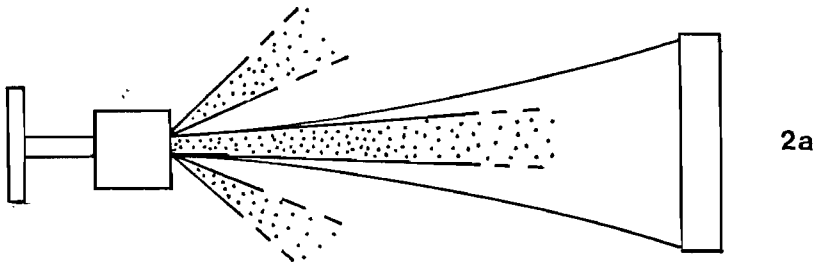

Figure 2.11. Diffracted light from the excited region.

The rear mirror should be placed at such a distance from the dye cell that only the main lobe, which subtends an angle of δ with the cavity axis (the Airy disk), is reflected back to the excited region of the dye cell.

$$\delta=0.61\lambda/a \qquad 2.28$$

The distance **d** between the dye cell and the rear mirror will be referred to as the cavity length providing the dye cell is very close

to the output coupler. Thus we may write the angle subtended by the excited region at the rear mirror as,

$$\theta = a/d \qquad 2.29$$

if this angle is kept smaller than the main lobe angle no secundary lobe will be reflected back into excited region,

$$a/d \leq 0.61\lambda/a \qquad 2.30$$

or

$$d \geq 1.64a^2/\lambda \qquad 2.31$$

in relation 2.31 the equality sets the smallest cavity length that can be used to produce a diffraction limited beam, for a given beam waist and wavelength. For a wavelength of 580 nm and a=400 μm we need a cavity length longer than 45 cm. A long cavity will reduce the pulse output energy as a result of the small nunber of round trips during the excitation time and due to the fact that not the whole energy of the central lobe is reflected back into the pumping region. One solution is to decrease the parameter

$$a^2/\lambda \qquad 2.32$$

so that we could satisfy condition 2.31 with shorter cavity lengths.

In a cavity with a prism beam expander the condition 2.31 will hardly be satisfied in the horizontal plane unless a long cavity could be used. Thus for this kind of oscillator the output beam will have different divergences on each plane. The divergence on the horizontal plane will be larger than the one on the vertical plane due to the reflection of high diffraction orders into the excited region.

2.2.4.2 **Active region**

The size of the active region of the dye cell plays a very inportant role in determining the beam quality, figure 2.12.

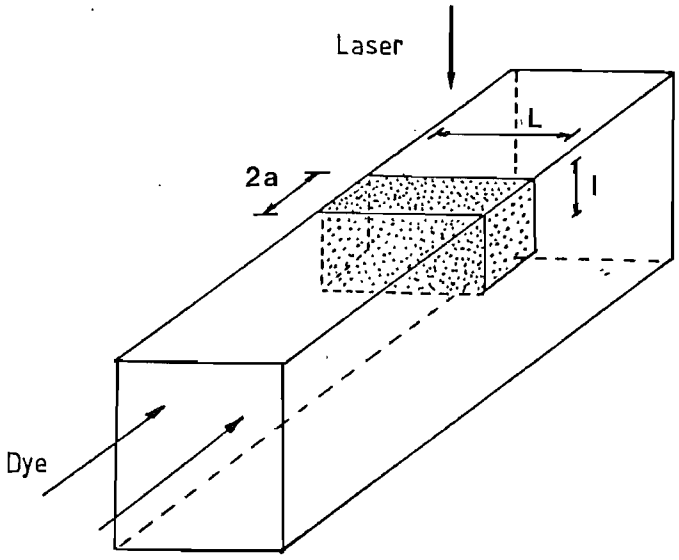

Figure 2.12. Dye cell active region for a transversely pumping configuration

The dimensions of the excited region define the minimum cavity length that can be used and consequently the spatial quality and energy of the output beam. By changing the dye concentration and the focal length of the cylindrical lens we should get a square-like shape for the excited region. It will maximize the energy transference from the excited molecules into the oscillating mode.

The surface dimension (2a) is related to the focal length of the lens used to collimate the beam on the cell surface and to the divergence of the pump radiation,

$$a=\delta f \qquad 2.33$$

where δ is the half divergence of the pump laser beam and **f** is the equivalent focal length of the system used to reduce the pump beam dimensions.

The penetration depth inside the dye cell is given in terms of the absorption cross section(σ), the ground state concentration (C_0) and the path length (l),

$$I_{tr}= I_{in}.\exp(-\sigma C_0 l) \qquad 2.34$$

This expression can be used only when we assume absence of saturation in the medium, otherwise the absorption coefficient would be smaller.When the exponent of expression 2.34 is equal to unity we have $l=l_0$, where l_0 is the penetration depth, i.e. the length for which

most of the pump energy has been absorbed by the dye medium, as long as $l_0<L$, where L is the cell thickness we will have,

$$l_0=1/C_0.\sigma \qquad 2.35$$

or

$$l_0=(1.66\times10^{-21})/C_0.\sigma \qquad 2.36$$

for C_0 in Mol/L
σ in cm^2
l_0 in cm

Thus we can control the surface dimension (2a) by choosing a convenient focal length and the depth (l_0) by adjusting the dye concentration. By choosing suitable values of these two parameters we can satisfy the expression,

$$2a=l_0 \qquad 2.37$$

making use of expressions 2.33 and 2.36 we can rewrite the expression 2.37 as,

$$f.C_0=(8.3\times10^{-22})/\delta\sigma \qquad 2.38$$

where f is in cm
C_0 is in Mol/L
δ is in radian (half pump divergence)
σ is in cm^2

For a pump laser with a half divergence of 2 mrad and a dye absorption cross-section of 2.4×10^{-17} cm^2, we need a focal length of 8.7 cm for a dye concentration of 2×10^{-3} Mol/L in order to get a square-like shape for the excited region with dimensions 346 μm x 346 μm.

2.2.5 **Design abstract**

A design scheme can be seen in figure 2.13. The focal length of the cylindrical lengs, f, defines the value of a and C_0 through expressions 2.33 and 2.38 respectively. The cavity length is obtained by the condition 2.31.

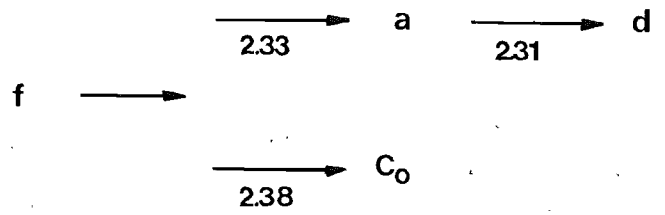

Figure 2.13. Scheme for dye oscillator design using the expression given in this section.

For a small value of **a** we can be above the lower limit of condition 2.31 and still use a short cavity length. In this way we obtain a very low beam divergence and a high energy efficiency due to the elevated number of round trips in the cavity. Besides that the cavity mode spacing is increased and one can attempt single longitudinal mode operation. A small value of **a** usually solves most of the design difficulties but it brings out two problems:the cell threshold energy damage is easily reached due to the high pump intensity on its surface and the required beam magnification in order to illuminates the whole diffraction gration length becomes very large increasing the transmission losses in the prims beam expander.

2.3 **Experimental results and parameters**

2.3.1 **Laser pump sources**

Three different radiation sources were used to pump the dye laser oscillator throughout the experiments. Two of them came from a excimer laser and the other was the second harmonic of a Nd:YAG laser.

2.3.1.1 **Excimer laser - 351 nm**

Active medium - XeF
Wavelength - 351 nm
Gas mixture - Helium (99.995%) ⇒ 2.260 mbar
Xenon (99.99 %) ⇒ 20 mbar
Helium+ 5% Fluorine (99.9%) ⇒ 220 mbar
Half beam divergence - 2.5 mrad (vertical plane)
Output energy - 32 mJ
Pulse width(FWHM) - 14 nsec

The addition of Argon to the mixture leads to a considerable

improvement in performance while at the same time leading to a reduction in pulse energy fluctuation. The decrease of power output with the number of pulse can be partly compensated by adding small amounts (~ 10 mbar) of the halogen-buffer gas mixture. This postpone the need for new fillings which is very useful due to the high cost of Xenon and other gases, but this method only works until approximately 50% of the original inserted amount remains.

2.3.1.2 **Excimer laser - 308 nm**

Active medium - XeCl
Wavelength - 308 nm
Gas mixture - Xenon (99.99%) ⇒ 75 mbar
Neon 70 (70% Ne + 30% He) ⇒ 2425 mbar
Helium + 5% HCl (99.995%) ⇒ 100 mbar
Half beam divergence - 2.5 mrad (vertical plane)
Output energy - 140 mJ
Pulse width - 20 nsec

The decrease of output energy with number of pulses is less than for the XeF mixture, and one can go up to 3.5 x 10^6 pulses before the output pulse energy drops down to a half of its initial value, that is a factor of ~7 better than the previous gas mixture. However the short wavelength emitted requires lens and dye cells made of silica.

2.3.1.3 **Second harmonic of a Nd:YAG**

Active medium - Nd:YAG rod
Wavelength - 1064 nm → 532 nm
Half beam divergence - 0.55 mrad
Output energy - 40 mJ
Pulse width - 15 nsec

A telescopic resonator was designed for the Nd:YAG laser cavity [Hanna et al (1981)]. A two times magnification was provided by the AR coated lenses and a fast Q-switch was used. The output mirror is flat and the rear concave mirror with a high reflectivity at 1.064 μm has a curvature of five meters. The cavity length is 1.15 meters and produces a TEM_{00} beam waist size at the output coupler of 1.25 mm. This cavity was usually allowed to operate with many transverse modes in order to get more output energy. This was done by using a 5.5 mm

diameter aperture placed between the Nd:YAG rod and the output coupler, i.e. just 0.5 mm less than the rod diameter. For single transverse mode operation a 3.5 mm diameter aperture was used. In order to avoid internal oscillation modes between the Nd:YAG rod ends and the cylinder walls we use a rod with grooves on the lateral surface and a 0.5 wedge end surface. The free running output energy (no Q-switch) was 300 mJ per pulse and 180 mJ in a Q-switched pulse.

The generation of 532nm radiation was done by using a KD*P type II crystal. The doubling crystal was placed just outside the output mirror. The unfocused output beam has a intensity of 325 MW/cm^2 on the crystal surface, which has a pump power damage threshold of 400 MW/cm^2. As a large part of the pump energy goes through the doubling crystal without being used we decided to place another doubling crystal after the first one to use this remaining pump pulse energy. The second doubling crystal was a KDP type I wich is not so efficient as the first one. The pump radiation was focused down in this second crystal by mean of a cylindrical lens.

Figure 2.14 shows the temporal profile of the pump pulse for the three different pump systems. The short spikes in the 532nm pulses are due to the oscillation of several longitudinal modes inside the Nd:YAG laser cavity.

Table I summarizes the pump sources characteristics.

Table I

	E (mJ)	τ (nsec)	λ (nm)	Half div. (mrad)	σ (cm^2)
XeF	32	14	351	2.5	3.1×10^{-17}(a)
XeCl	140	20	308	2.5	3.1×10^{-17}(a)
Nd:YAG 2nd harm.	40	15	532	0.55	4.24×10^{-16}(b)

(a) H. Telle et al (1981)

(b) P. Hammond (1979)

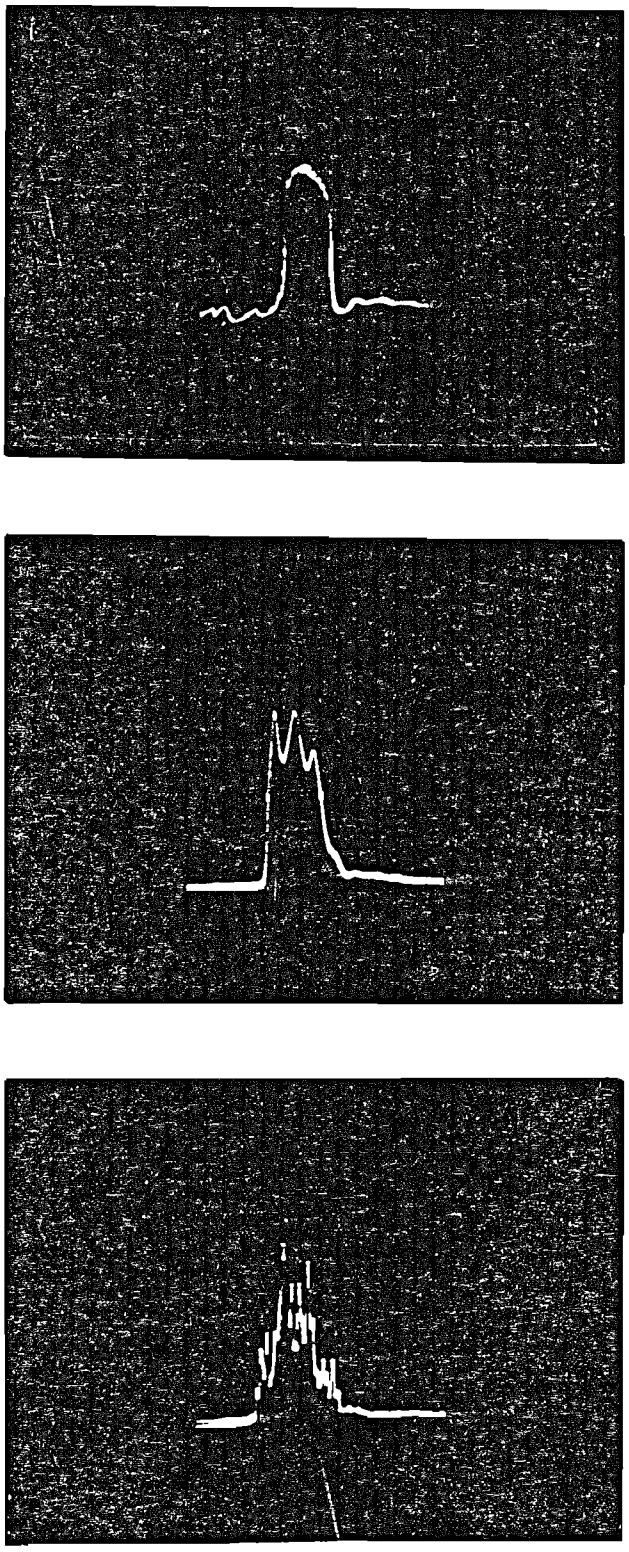

Figure2.14. Pump pulses used in the experiments.(a) XeCl excimer laser,(b) XeF excimer laser and (c) second harmonic of Nd:YAG laser.

2.3.2 Dye oscillator components

2.3.2.1 Dye solvents

The effect of solvents on the dye laser gain was investigated by T. Govindanunny (1980) under ultraviolet (337.1nm) radiation pumping. Amongst the solvents studied the alcohols displayed the highest gain. We ran the dye oscillator with ethanol (XeF) and methanol (XeF, XeCl and 2nd harmonic of Nd:YAG) as the solvents for the rhodamine 6G.

	Ethanol	Methanol
Refractive index	1.3576	1.3288
Absorption peak	531 nm	530 nm
Fluorescence peak	558 nm	556 nm
Absorption Cross-section	2.27×10^{-17} cm^2	2.51×10^{-17} cm^2

2.3.2.2 Dimensions for the active region

By following the design scheme given in section 2.2.5 we chose a focal length of 5 cm for the cylindrical lens. From expression 2.33 we have for the radius of the active region,

$$a=\delta f$$

$$\delta=2.5 \text{ mrad} \quad f= 5 \text{ cm}$$

$$\Rightarrow a= 125\ \mu m$$

the dye cell thickness is 1 cm. In order to avoid oscillations between the cell surfaces and to minimize the reflection losses, the cell was positioned as shown in figure 2.15.

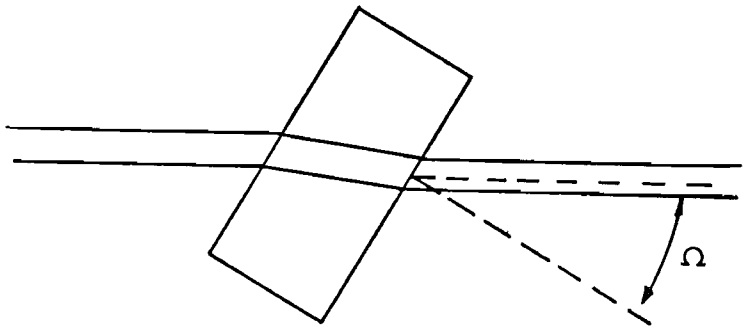

Figure 2.15. Positioning of the dye cell in relation to the cavity axis in order to avoid reflections from the cell surfaces.

2.3.2.3 **Dye concentration**

From condition 2.37 we can work out the correct concentration for the dye oscillator. Using the expression 2.38 we have,

$$f.C_0=8.3\times10^{-22}/\delta\sigma$$

f= 5.0 cm

δ= 2.5 mrad

σ= 3.2×10^{-17} cm^2 (at 351 nm)

$$\Rightarrow \quad C_0=2.1 \times 10^{-3} \text{ Mol/L}$$

2.3.2.4 **Minimum cavity length**

Knowing the dimensions of the excited region we may use the expression 2.31 to get the value for the shortest allowed cavity length.

$$d_{min}=1.64a^2/\lambda \qquad 2.39$$

a= 125 μm

λ= 580 nm

$$\Rightarrow d_{min}= 4.4 \text{ cm}$$

2.3.2.5 **Diffraction grating**

The number of grooves per mm for the diffraction grating is given by expression 2.7. It is related to the dye tunning range, which for ultraviolet pump radiation is typically 570 → 605 nm.

$$302.5 < \Lambda < 570 \text{ nm}$$

or

$$1754 \text{ grooves/mm} < N < 3306 \text{ grooves/mm}$$

We used a diffraction grating with Λ=416.7 nm, or N=2400 grooves/mm. As we have mentioned in section 2.2.1.1 the angle the grating normal makes with the cavity axis changes with the tuned wavelength (figure 2.3). The shortest wavelength in the tuning range will correspond to the smallest grating angle, and it will define the maximum required beam dimension to fill the whole grating length.

$$D_{max} = L.\cos\theta_{\lambda min} \qquad 2.40$$

for λ_{min}= 573 nm ⇒ $\theta_{\lambda min}$= 43° 26'

L= 5 cm

we have ⇒ D_{max}=3.63 cm

The dye laser beam diffraction from the grating at this angle will be about 55% as given by B.Racz et al (1981).

2.3.2.6 **Beam expander**

With the values of the active region and beam dimensions we can determine the required magnification.

$$M=3.63 \text{ cm}/250 \ \mu\text{m} = 145$$

For a four prism beam expander we need a magnification of 3.47 per prism in order to reach the overall magnification of 145. The input angle for each prism is worked out by using expression 2.20 with the value of C_2 given by 2.22,

$$M=C_1.C_2$$

$$C_1=M_o=\frac{\sqrt{1 - \sin^2\theta_1/n^2}}{\cos\theta_1}$$

where θ_1 is the input angle and n the prism refractive index. The energy transmission losses per prisms per round trip can be calculated by using the expressions,

$$R= 1 - (T_1T_2)^2 \qquad 2.41$$

$$T_1= 1 - \frac{Tg^2(\theta_1-\theta_2)}{Tg^2(\theta_1+\theta_2)} \qquad 2.42$$

$$T_2= 1 - \frac{Tg^2(\theta_3-\theta_4)}{Tg^2(\theta_3+\theta_4)} \qquad 2.43$$

The angles $\theta_1,\theta_2,\theta_3$ and θ_4 are defined in the figure 2.5. The expressions for the transmission losses calculation were taken from Appendix 3 where a detailed analysis is presented.

In our four prism beam expander set- up the first prism surface is 13 mm long and the last one is 45 mm long. The prism apex angle were chosen by following condition 2.25,

$$\theta_{apex} < \text{arc sin}(1/n)$$

for $n=1.57$

we have $\Rightarrow \theta_{apex} < 40°$

in table II we give the geometrical characteristics and transmission losses for each prism and in table III the input angle and the reflection losses for the case when a single prism is being used to produce the whole required magnification; the transmission losses for the four prisms combination is shown in the same table.

Table II

	Apex angle	Input angle	Reflection losses (round trip)
Prism 1	36°42'	76°57'	33.5%
Prism 2	24°00'	77°38'	34.7%
Prism 3	34°12'	77°00'	33.6%
Prism 4	32°00'	77°03'	33.6%

Table III

	Apex angle	Input angle	Reflection losses (round trip)
Single prism	32°	87°00'	96.8%
Four prism	table II	table II	80.8%

2.3.2.7 **Dye circulation**

To avoid over heating of the laser dye we should keep the substance circulating so that every time a pump pulse reaches the cell surface it will excite a new portion of the dye. To get this we need a dye flowing system with a minimum flow rate given the expression,

$$F_{min}=2.R.a.L.l$$

for a pump pulse repetition rate (R) of 10 pps and a volume (2aLl) where l is the cell depth we have a minimum flowing rate of 1.1 liter per hour. The dye circulating system that we built gives a minimum flowing rate of 1.5 litre/hour and a maximum of 3.0 liter/hour. In this circulating system we have available a built in cooling unit in

case we need to run the laser at very high repetition rates.

The final scheme for the dye laser oscillator is shown in figure 2.16. The total cavity length is 16 cm which gives a separation of 0.03 cm^{-1} between the cavity longitudinal modes. The beam expander is formed by four prism which produce the required magnification with a low transmission loss.

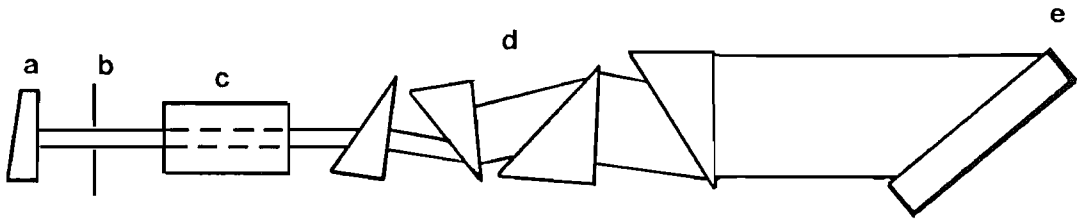

Figure 2.16. Final arrangement used for the dye oscillator. (a) output coupler, (b) intracavity aperture, (c) dye cell, (d) prism beam expander, (e) diffraction grating.

In table IV we summarize the cavity parameter calculation with all three pump wavelengths. We assume a tuning range of 570 to 605 nm with a maximum at 573 nm for the ultraviolet pumping source and 555 to 595 nm and a peak conversion at 560 nm for the pumping with 532 nm wavelength radiation.

Table V

Pump wavelength (nm)	a (μm)	C_o (Mol/L)	d_{min} (cm)	$\Delta\tilde{\nu}$ (cm^{-1})	M	BE trans. losses
351	125	2.1×10^{-3}	4.5	0.2	145	80.8%
308	125	2.1×10^{-3}	4.5	0.2	145	80.8%
532	110	1.8×10^{-4}	3.5	0.2	170	83.1%

Grating length: 5 cm

Number of groves per mm: 2400

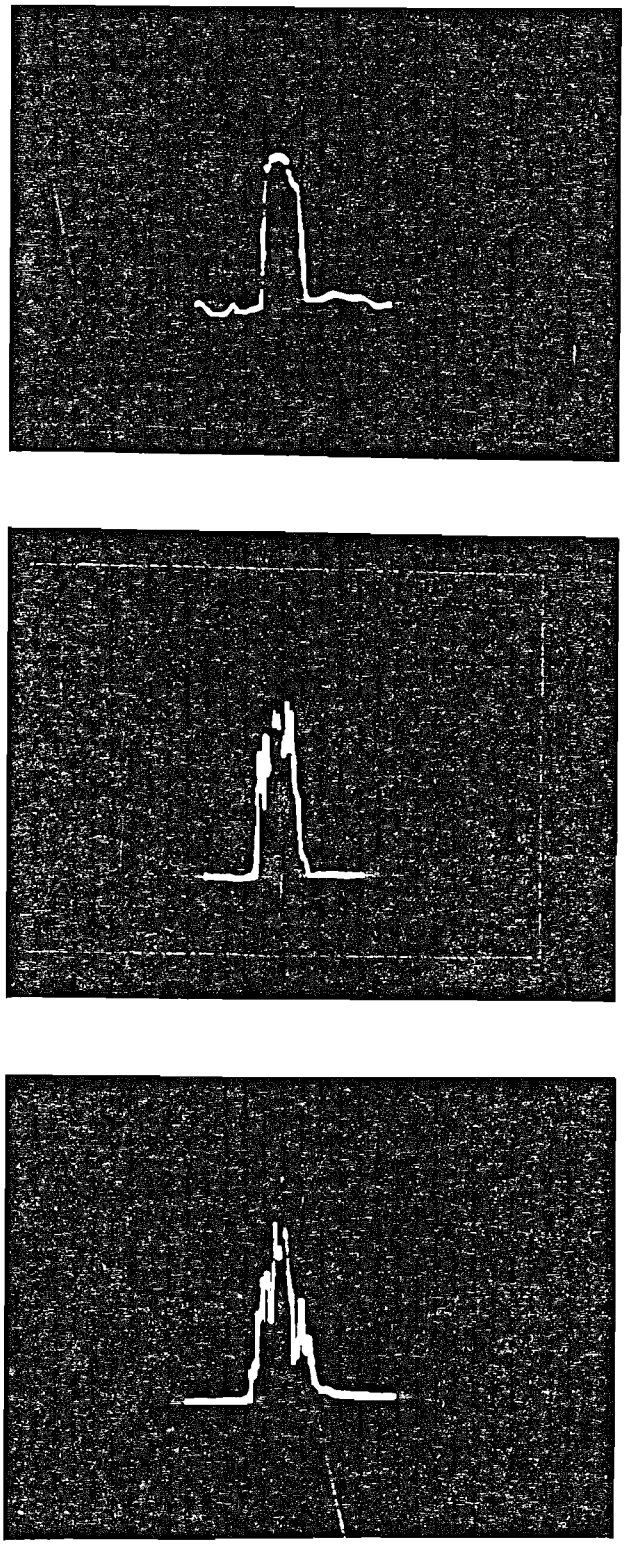

Figure2.17. Dye laser pulses under different pumping sources.(a) Xecl excimer laser, (b) XeF excimer laser and (c) second harmonic of Nd:YAG laser.

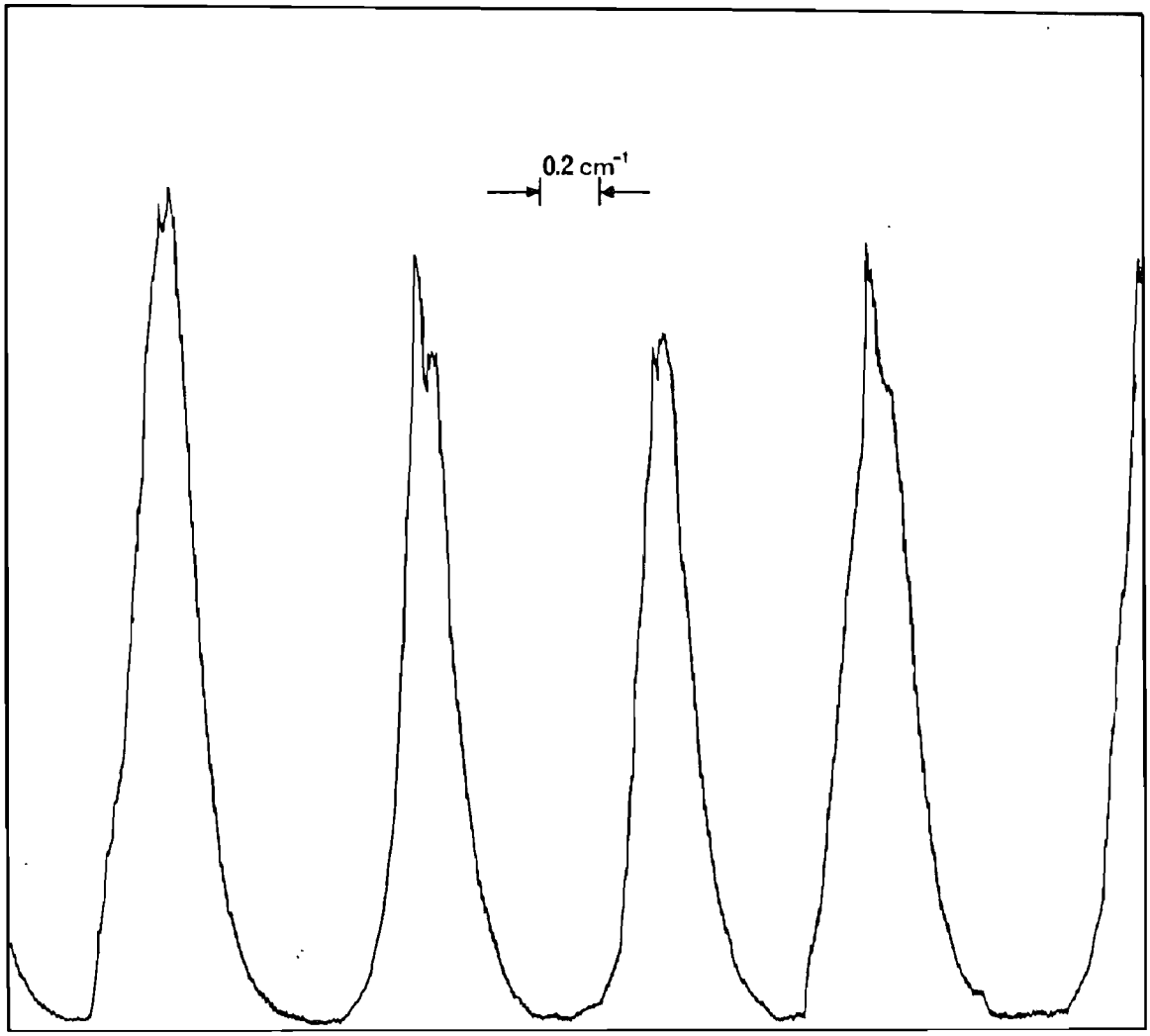

Figure 2.18. Fabry-Perot transmission curve for the dye laser pulse.

2.3.3 Dye oscillator experimental results

2.3.3.1 Pulse shape

The time dependence of the dye oscillator output pulse was measured with a vacuum photodiode and a digital analyser 632 Tektronix. All the measurements were made at the wavelength corresponding to the maximum output pulse energy in the dye tuning range. Figure 2.17 displays the dye laser pulse shapes under the three different pumping sources.

2.3.3.2 Pulse linewidth

An piezoelectrically scanned Fabry–Perot was used to measure the linewidth of the pulse. The Fabry–Perot has a FSR of 1.0 cm^{-1} and a resolution of 0.08 cm^{-1} (its finesse is 12.5) in the visible region of the spectrum. The measured linewidth was 0.21 cm^{-1} for the dye laser radiation under any pumping source condition, figure 2.18.

2.3.3.3 Beam profile

The beam profile was measured by using a lens to expand the beam and fill most of the surface of a diode array with 128 diodes per cm, placed at 1 metre away from the dye oscillator output. During these measurements we have a pinhole inside the dye laser cavity to discriminate against high transverse order mode oscillation. The photograph from the transient digitiser display is shown in figure 2.19. The shape was essentially the same for all the pumping sources.

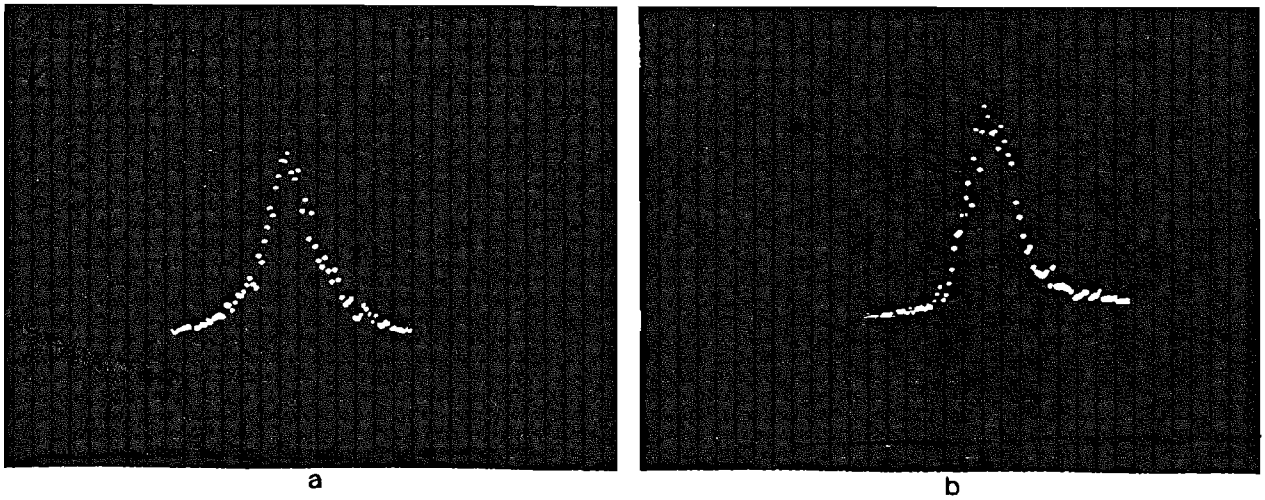

Figure 2.19. Dye oscillator beam profile.
(a) horizontal plane,
(b) vertical plane.

2.3.3.4 Dye oscillator tuning range

The dye laser tuning range was measured by using a monochromator and a PIN diode as detector. The electrical signal was processed in a box-car wich has a time constant of 10 nsec and the pump repetition rate was 7 pulses per second. The dye concentration for ultraviolet pumping radiation was 2.0×10^{-3} Mol/L and ten times less for pumping with 532nm wavelength radiation. The tuning range is defined by the two extreme wavelengths at which the dye laser pulse energy is comparable to the amplified spontaneous emission (ASE). The ASE energy level was measured by blocking the diffraction grating. We observed a tuning range of 568 nm → 602 nm for uv pump and 551 nm → 579 for 532nm pump wavelength.

The dye oscillator output pulse energy shows a strong dependence on the flow rate. For the laser running at 7 pps the output energy drops down to 15% of its initial value after 1 minute the circulating cooling system is turn off.

The beam is horizontally polarized as we expected due to the polarization selection in the prism beam expander. The beam is very close to diffraction limited and table V summarizes the results under all pumping conditions.

Table V

Pump wavelength	Dye pulse width(nsec)	Tuning range	Available pump energy	Dye output energy (μJ)	Efficiency (%)
351 nm	12	568→602nm	3.7mJ	200 (20)	5.4 (0.5)
308 nm	14	568→602nm	24mJ	1400 (400)	5.8 (1.7)
532 nm	12	551→579nm	4mJ	650 (100)	16.3 (2.5)

The values for the dye output energy and efficiency indicated between brackets are for the cavity with a pinhole inside. The diameter of this aperture was chosen such that a diffraction limited beam was produced by the dye laser.

2.4 Dye amplifier

The energy produced in the dye oscillator is not enough to excite SRS in gases. This low energy is basically due to the losses introduced by the intracavity elements and the limition on the pump pulse energy in order to avoid damage on the dye cell surface and on the diffraction grating.

To overcome these problems a two stage dye amplifier was used. The details of this design are described in this section.The two main problems we had to deal with were the strong amplification of the spontaneous emission inside the active region and the distortion of the input beam profile due to the nonuniform pump intensity distribution inside the active region along the direction transverse to the input beam axis.

The use of two amplifiers instead of a single long amplifier cell is to minimise the amplified spontaneous emission. In a single amplifier cell the ASE is going to be amplified along the whole cell length. By dividing the cell in two short cells we can manage to get less ASE signal in the second amplifier stage by placing it as far as possible from the first stage and by using pinholes between the cells.

2.4.1 Dye amplifier theory

The dye amplifier has been analysed by several authors. Usually the analysis neglects the variation of the pump intensity into the medium, because it reduces the complication of the numerical treatment considerably. Since the transverse dimensions of the excited region are small compared with its length, this assumption does not affect the results for the gain G appreciably. However, when one considers the intensity beam profile rather than the overall output energy we must take in account the shape of the excited region. This shape is mainly determined by the pump radiation absorption , the pump beam diffraction and the dye saturation.

2.4.1.1 Pump intensity distribution

The pump intensity distribution inside the amplifier cell determines the quality of the amplified beam. The best intensity

distribution is the one which produces a uniform gain across the input beam cross section. The intensity inside the cell is defined basically by the focal length of the cylindrical lens, the dye concentration and the absorption cross section at the pump wavelength. Assuming the divergence of the pump beam is very small, the beam waist will be formed at the focal plane of the cylindrical lens and by shifting it we can have the maximum pump intensity outside, on the surface or inside the dye amplifier cell (DAC).

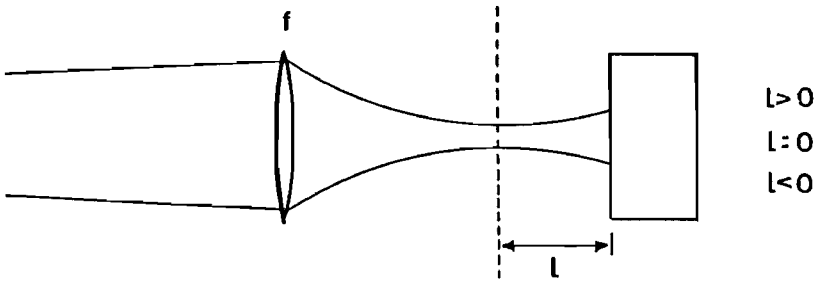

Figure 2.20. Position of the pump beam waist relatively to the cell surface.

In the first and the second case the beam diverges inside the cell and consequently the maximum intensity inside the dye solution will be the one on the DAC entrance surface. This divergence will reduce the pump intensity inside the dye medium and if we consider the pump radiation absorption by the dye molecules as well, this intensity will drop down quite abruptly inside the DAC, figure 2.21,

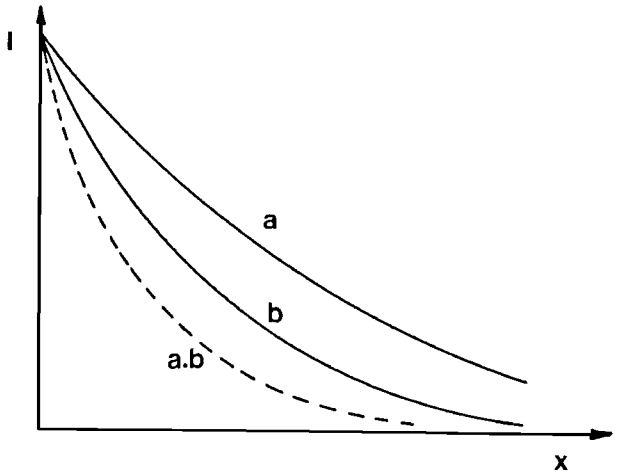

Figure 2.21. Pump intensity variation inside the dye amplify cell.

where P_0 in figure 2.21 is the pump power and **A** the cross section area in the pump beam direction as a function of the length inside the DAC.

The linear absorption coefficient α can be worked out from expression 2.34,

$$\alpha(cm^{-1}) = 6.02 \times 10^{20} . C_0 \sigma \qquad 2.44$$

This non uniform pump intensity brings out two problems. The first one is the strong distortion suffered by the amplified beam, since the amplification is not uniform or even symmetrical along the cross section of the input beam; the portion of the beam close to the DAC entrance surface will have a very much higher amplification than the other parts of the beam. The second problem is the amplifier efficiency because only part of the dye input beam cross section is going through the region with a high number of dye excited molecules, this will correspond to an input signal with less energy than actually we have available in the signal, producing a low gain and low output energy for the DAC.

If we place the beam waist inside the cell, figure 2.22, the increasing of the pump intensity between the cell entrance surface and the beam waist position can compensate for the attenuation caused by the pump radiation absorption if a convenient choice of parameters is made.

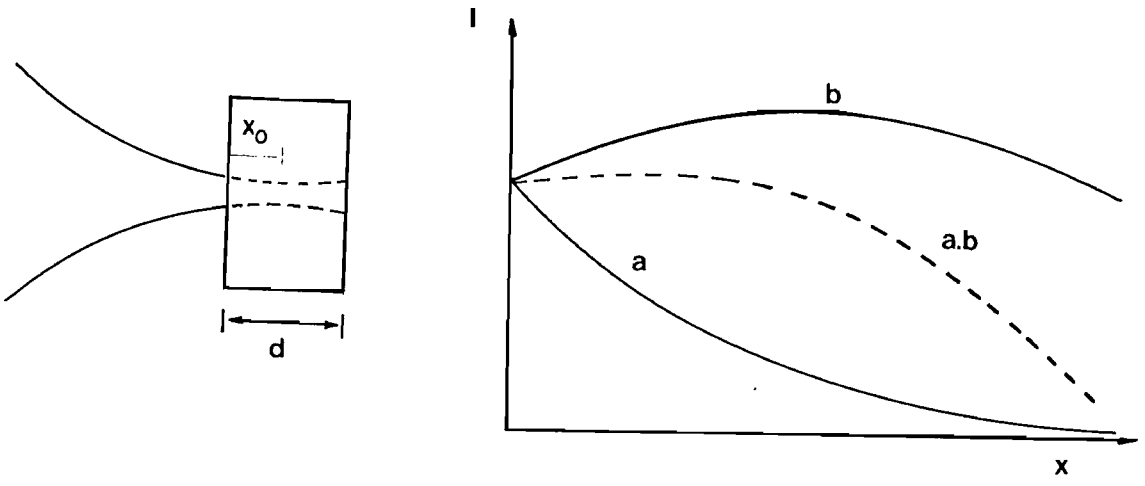

Figure 2.22 Pump beam waist formed inside the dye amplify cell.

The pump intensity inside the cell will be,

$$I(x) = (P_0/A) . \exp(-\alpha x) \qquad 2.45$$

where

$$A=2[x'(D/2f - \delta) + f\delta].L \qquad 2.46$$

$$x'=|x - x_0| \qquad x_0<d$$

x' is the distance to the beam waist.
x_0 is the beam waist position.
D is the pump beam dimension at the cylindrical lens.
f is the focal length of the cylindrical lens.
δ is the pump beam half divergence.
L is the cell pumped length.
d is the cell depth.
n is the dye solvent refractive index.

Usually the pump pulse intensities are high enough to saturate the dye solution and its effect must be considered in the calculation. The attenuation coefficient given by expression 2.44 is redefined as, [C.G.Morgan (1979)]

$$\alpha=\alpha_0/(1+I/I_s) \qquad 2.47$$

$$I_s=h\nu/2\sigma\tau \qquad 2.48$$

where

Is is the saturation intensity.
ν is the pump optical frequency.
σ is the absorption cross section for dye molecules at the pump wavelength.
τ is the lifetime of the excited state.

and equation 2.53 becomes,

$$I(x)=\{P_0/2L[|x-x_0|(D/2f-\delta) + f\delta]\}.\exp[-\alpha_0 x/(1+I(x)/I_s)] \qquad 2.49$$

In figures 2.23 to 2.26 we show the numerical solution for this equation under several different conditions. In these curves two regions can be identified, the region near the cell entrance surface where the pump intensity remains quite unchangeing and the region away

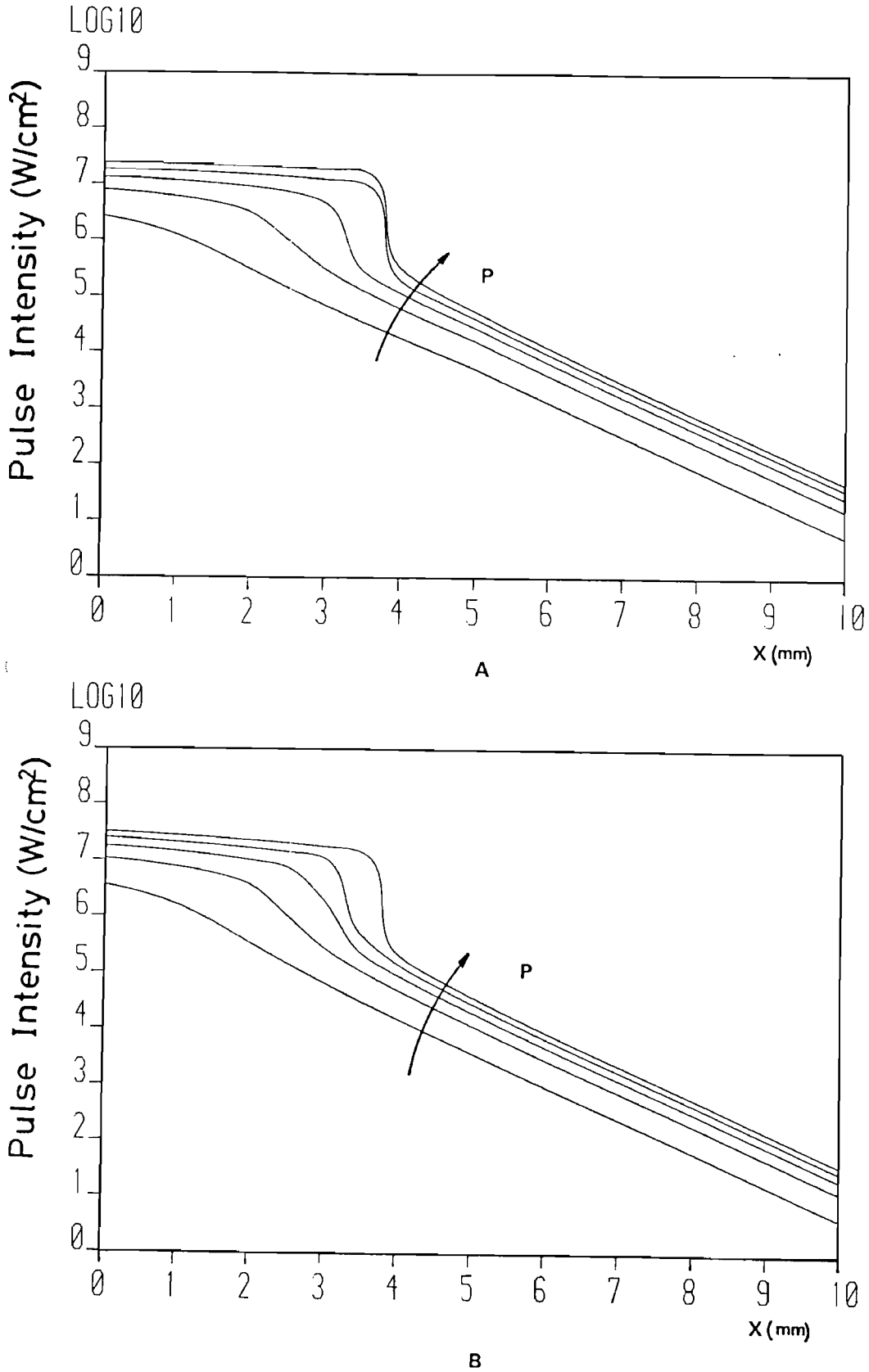

Figure 2.23. Pump intensity variation inside the dye amplifier cell for five differentes pump power: 0.67MW, 2.0MW, 3.4MW, 4.7MW and 6.04MW. (a) pump beam waist at the center of the cell,(b) pump beam waist at the cell entrance surface.

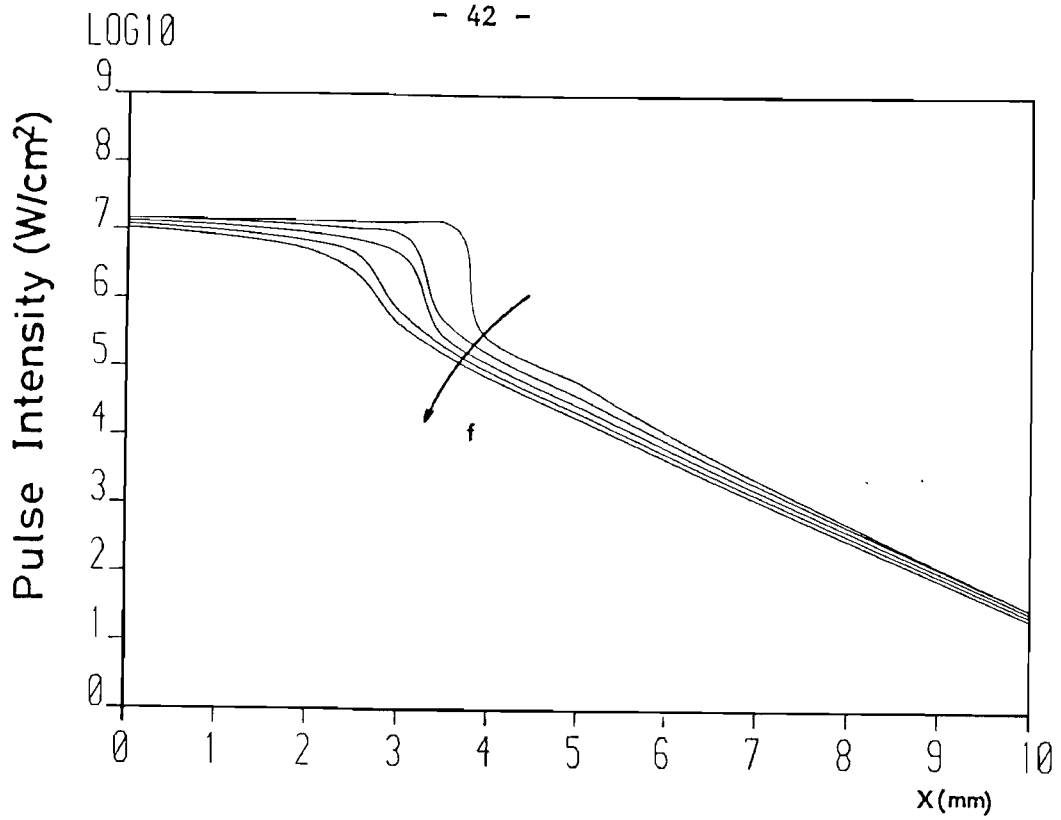

Figure2.24. Pump intensity variation inside the amplifier cell for five differents focal length of the cylindrical lens: 10 cm, 15 cm, 20 cm, 25 cm and 30 cm.

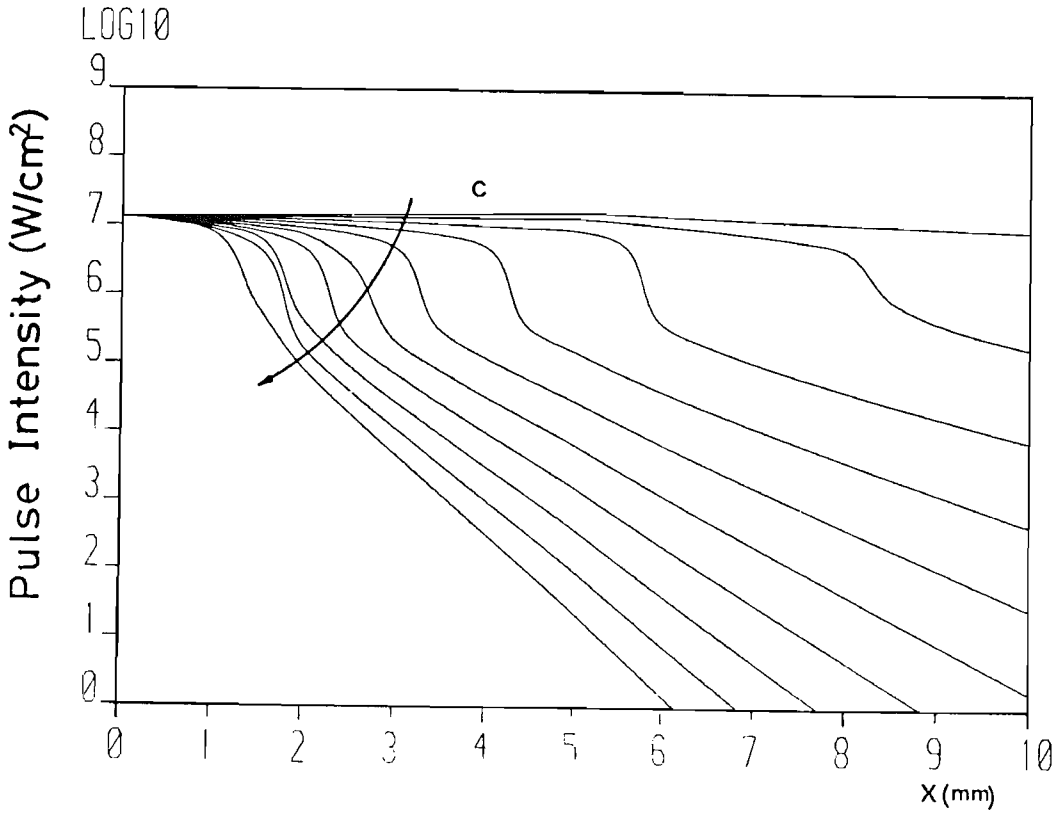

Figure 2.25. Pump intensity variation inside the amplifier cell for ten differents dye concentrations: 1.0, 2.5, 4.0, 5.5, 7.0, 8.5, 10.0, 11.5, 13.0 and 14.5 (10^{-4} Mol/liter).

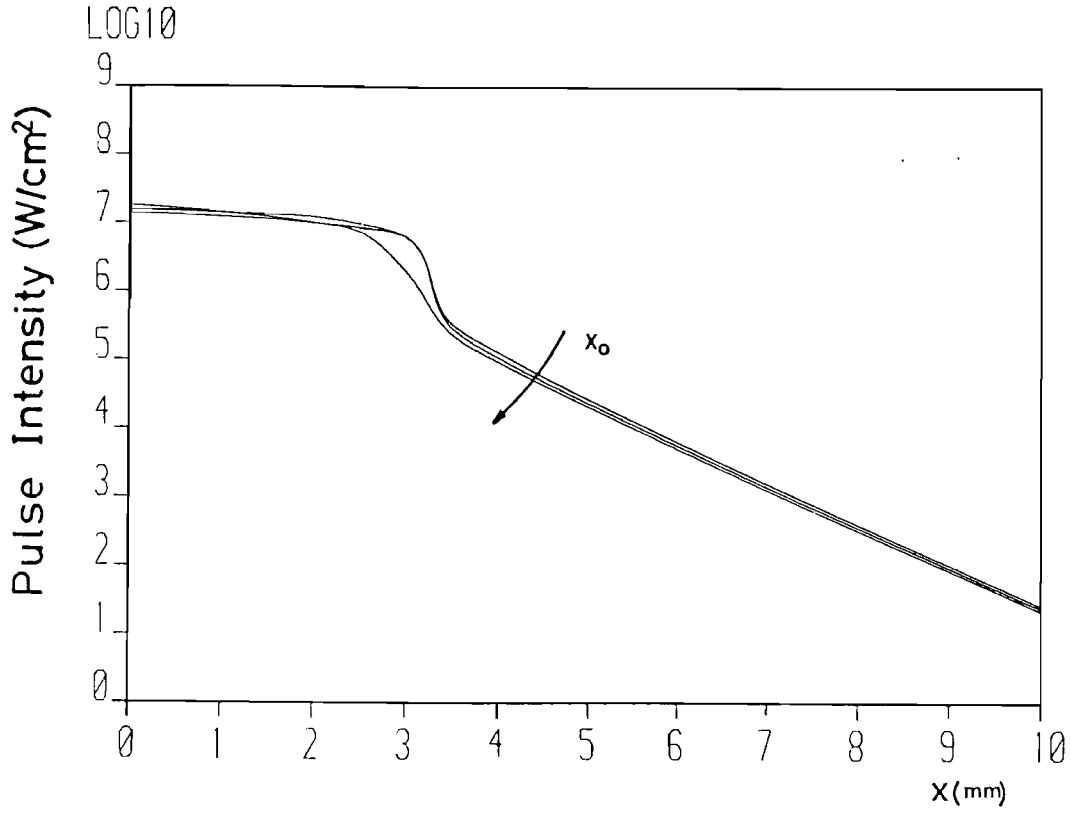

Figure 2.26. Pump intensity variation inside the amplifier cell for three position of the beam waist inside the cell: 0.0, 2.0mm and 4.0mm.

from the cell entrance where there is no saturation absorption any more and the intensity falls rapidly with distance due to the combined effects of absorption and beam expansion. The parameters used for these calculation were:

$L = 2.0$ cm

$D = 1.5$ cm

$\delta = 2.5$ mrad

$\sigma = 3.1 \times 10^{-17}$ cm^2

$d = 1.0$ cm

$\lambda_p = 308$ nm

$\tau = 5$ nsec

In figures 2.23a and 2.23b we have the intensity variation for several pump power values. In both cases a low pumping power produces a strong variation of the pump intensity near the cell entrance inside the cell. We will define this variation in terms of the percentage of the pump intensity variation by unit of length divided by the pump intensity at the cell surface,

$$\Delta I(\%) = \Delta I / I_0 \qquad 2.50$$

we are interested in characterising the pump intensity variation from x=0 to x=2 mm, since the maximum beam waist diameter will be 1.75 mm, this range of distance will cover the whole input beam profile cross section. With the waist located at the middle of the cell, figure 2.23a, the intensity variation is 54%/mm for the minimum pump intensity 700 kW/cm^2, and it drops down to only 6%/mm when we have the maximum pump intensity. The beam waist shift in the direction perpendicular to the surface does not change the strong variation of the pump intensity inside the dye when we pump the cell with a low pump power,figure 2.23b, however the situation is quite diferent for high pump power levels, the variation jumps from 6%/mm to 15%/mm.

The influence of the focal length is analysed in figure 2.24. A short focal length produces a very small pump intensity variation, due to the high pump intensity produced inside the medium which saturates the dye molecules and reduces the attenuation coefficient. The value of $\Delta I(\%)$ for the shortest focal length, 10 cm, is only 4%/mm. As the focal length increases the pump intensity is reduced

inside the medium and the attenuation becomes very strong leading to a high variation,i.e, for a 35 cm focal length the variation is 21%/mm.

The effect of increasing the dye concentration is shown in figure 2.25. A very weak dye concentration, 0.1×10^{-3} Mol/L will have a low attenuation and the intensity profile will be determined almost only by the focal length itself. When the dye concentration is increased the linear absorption coefficient increaes and the usual pattern returns. The intensity variation is 3%/mm for the weakest dye concentration and it goes up to 34% /mm for the strongest one, at which we will have the maximum gain for the medium but strong beam distortion will occur too.

Finally figure 2.26 shows the intensity variation along the cell depth for three positions of the beam waist. For the parameters we are using, specially the focal length of 20 cm, the position of the beam waist does not seen to be very important, the positioning the of it at the cell surface will still produce an intensity variation of 22%/mm as we can see in the enlarged section of figure 2.26, while the other beam waist position produce a $\Delta I(\%)$ of less than 13%/mm. The parameters used for this last calculation were used in the experimental set up. The focal length of the cylindrical lens is determined by the pump beam dimension at the cell surface and the laser pump divergence. The pump pulse energy, the dye concentration and beam waist position were chosen via numerical calculation in order to produce a small intensity variation close to the cell surface. We have a $\Delta I(\%) = 12\%$ /mm along the cross section of the input beam.

2.4.2 **ASE reduction**

The amplified spontaneous emission was reduced firstly by using two short amplifiers instead of a long one. They were placed as far as possible from each other, the high ASE divergence will reduce the input ASE in the second stage. In this way we have some reduction of the ASE level by limiting the length of the active region and avoiding the interstage coupling. But we still have a reasonable amount of ASE at the dye laser output, enough to produce SRS in systems with a very low pump power Raman threshold. One way to reduce the ASE level still more is by using an extra dye cell (unpumped) placed between each amplifier stage. Depending on the power levels involved we can classify this inter stage dye cell as saturated or

linear absorbers. In the first case the energy in the dye laser pulse is enough to saturate the dye solution while the high divergence of the ASE beam produces a very low intensity at the satured absorber. When the dye laser pulse energy is not very high, which is usually the case before the amplifier cell, there is no saturation effect taking place, but still the ASE radiation is going to be strongly attenuated because its radiation wavelength is shorter than the dye laser wavelength and consequently the absorption coefficient will be higher for the ASE component. In figure 2.27 we can see the effect of the linear absorber placed between the two amplifier cells. One can notice from this figure that only the begining of the tuning range undergoes any distortion due to the inclusion of the cell, and this disappears almost completely for longer wavelengths due to the small dye absorption cross section in this region.

The ASE reduces the dye laser efficiency if the ASE signal gets strong and depletes the dye excited molecules, however the ASE after the last stage is not very important unless we are using a Raman cell with a very low pump power threshold. For this kind of Raman cell a small amount of ASE will produce SRS simultaneously to the dye laser beam and this will reduce the efficiency of the SRS process because then the Raman components generated by the ASE beam can divert energy from the main scattering signal via parametric processes. In order to overcome this problem we used a dye cell after the last amplifier as well, so that the ASE was greatly reduced. This dye cell acts as a saturable absorber in this case because the power levels involved at the dye output will be very high

2.5 **Experimental results for the complete system**

In figure 2.28 we show the general set up for the dye laser pumped by the excimer and the second harmonic of the Nd:YAG laser.

Two delay lines were used to match in time the input signal and pump pulse inside each amplifier stage for the 532nm pumping wavelength; each line provides a delay adjust of five nanoseconds. The first dye amplifier is 10mm long and the second is 20 mm long and 3mm wide due to the laminar flowing. The concentrations were 1.4×10^{-3} Mol/L and 0.7×10^{-3} Mol/L for the first and the secondamplifier respectively when they are being pumped by the excimer laser and 1.2×10^{-4} Mol/L and 0.6×10^{-4} when they are pumped by the 532nm

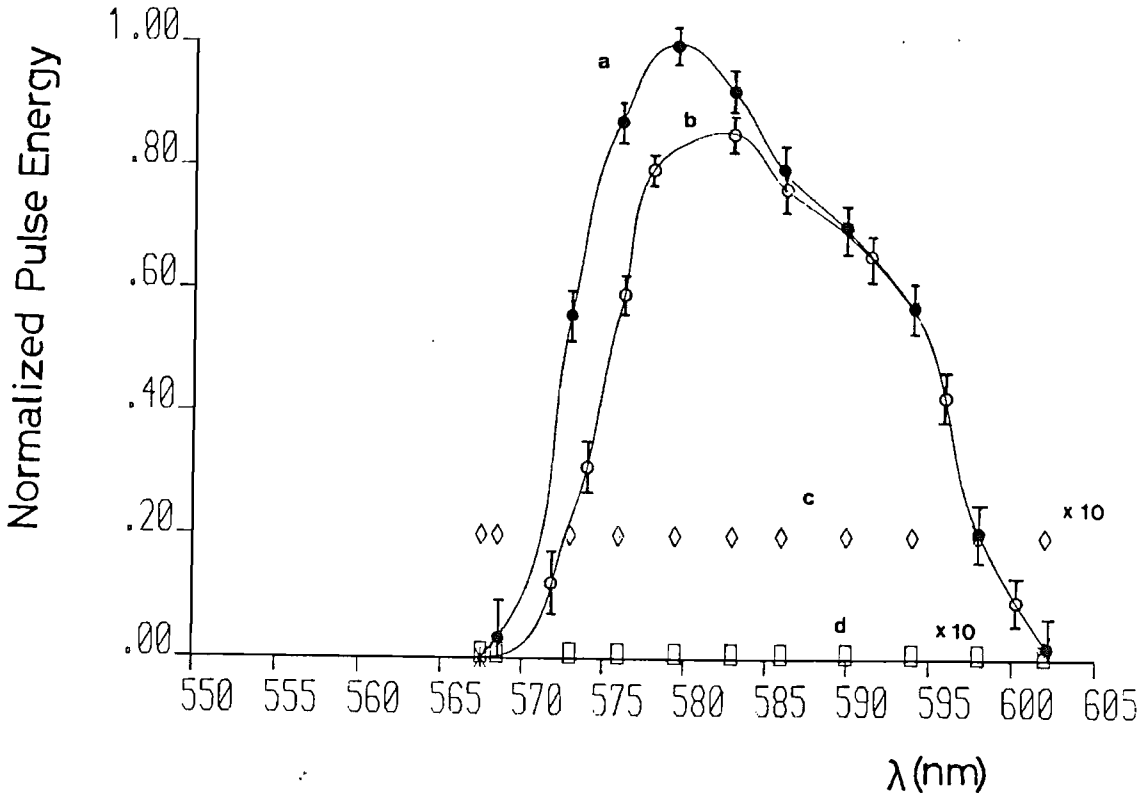

Figure2.27. The effect of the linear absorber on the dye tuning range:a) tuning range for the laser without linear absorber,b) tuning range for the laser with linear absorber,c) ASE energy level for the laser without linear absorber, d) ASE energy level at the dye laser output with linear absorber.

Figure 2.28. Dye laser pumping arrangement, (a) by an excimer laser and (b) by the second harmonic of a Nd:YAG laser.

ex – excimer laser
b – total reflector
c – cylindrical lens
d – diffraction grating
e – prisms beam expander
f – dye oscillator cell
g – cavity output coupler
h – aperture
f – dye amplifier cell
bs – beam spliter
dc – doubling frequency crystal
ny – Nd:YAG laser
dl – delay line
sl – spherical lens
as – absorber

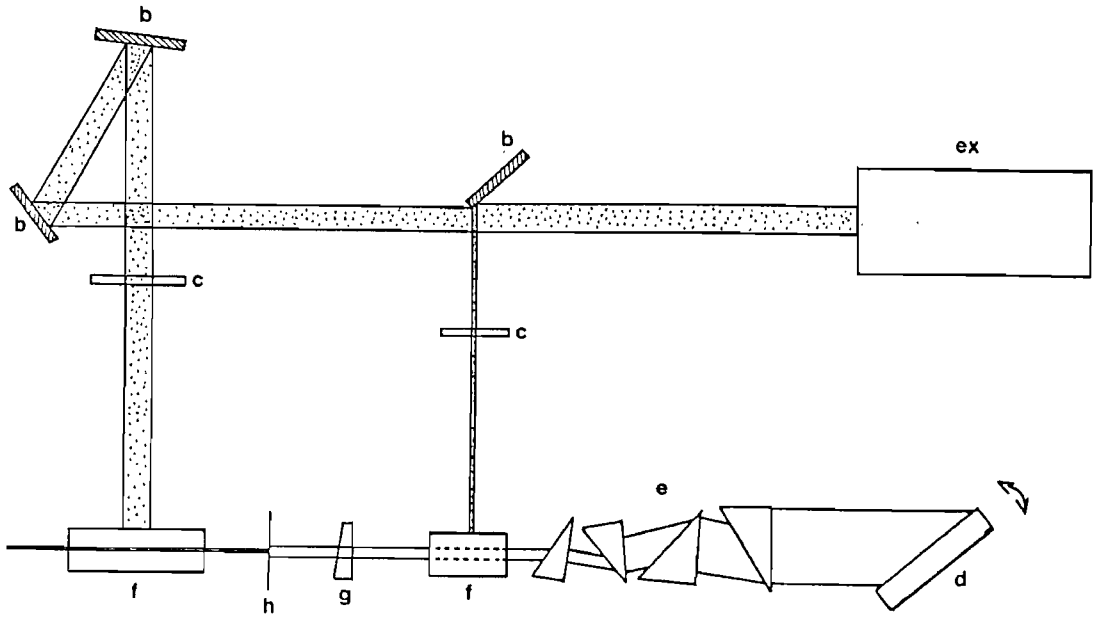
b
b
b
ex
c
c
e
f
h
g
f
d

2.28a

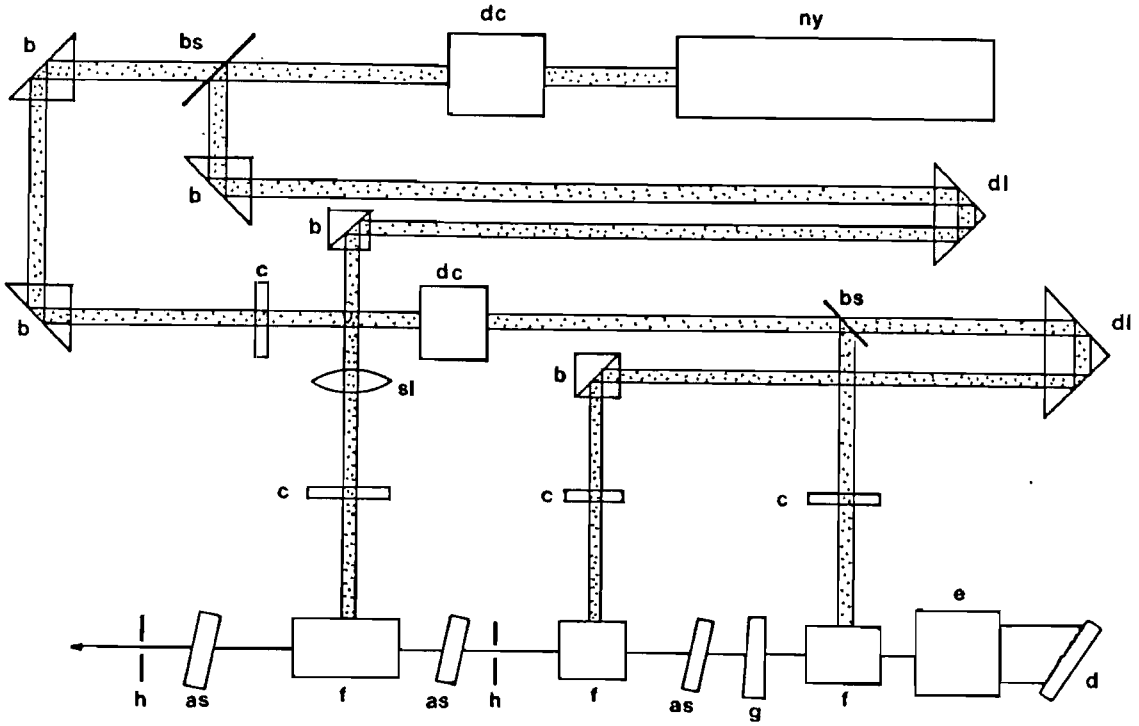
dc
ny
b
bs
b
dl
b
c
dc
bs
dl
b
sl
b
c
c
c
e
h
as
f
as
h
f
as
g
f
d

2.28b

radiation wavelength. Linear absorbers were placed between each stage and a saturable absorber was placed after the last amplifier cell. The dye concentration in the these cell was 1.0×10^{-3} in all the measurements. The laser dye was usually replaced every four weeks, when the output energy started to drop down and the beam distortion increased. The inter stage pinhole avoided the amplification of the non diffraction limited portion of the beam as well as blocking part of the ASE beam coming from the previous stage. The dye laser pulse energy after the last amplifier is about 12 mJ for any pumping system we used.

When no ASE prevention was used, the ASE level in this case is 2 mJ, measured by blocking the dye oscillator cavity. With the pinholes and the absorbers the dye output pulse energy is 5 mJ and the ASE level less than 200 μJ. With this dye output pulse energy we measured the output beam quality. The beam waist was imaged on the diode array surface and its value worked out from the geometric optics and the curve produced by the photodiodes, then the spot size was measured directly without any imaging and the beam divergence was calculated. By comparing the measured beam divergence with the divergence which the measured beam waist should produce for a diffraction limited beam one can obtain information on the quality of the dye laser beam. In the vertical direction two divergence values agree quite well, however in the horizontal plane the divergence worked out from the spot size measument was 1.4 bigger than the value expected for the measured beam waist.

2.6 Phase conjugation and the dye laser

In order to get more power and a better beam quality for the dye laser we tried the phase conjugation scheme shown in figure 2.29.

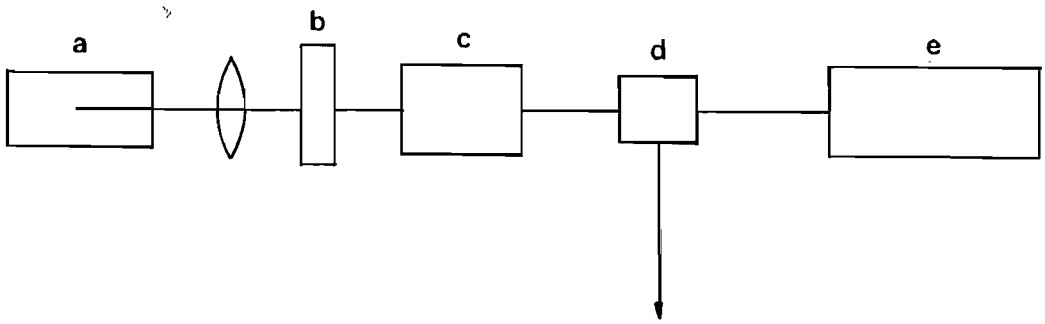

Figure 2.29. Scheme of the dye laser using phase conjugation.
(a) Brillouin cell, (b) $\lambda/4$ polarization change,
(c) dye amplifier cell, (d) beam splitter,
(e) dye oscillator.

The beam coming out of the dye oscillator goes through a polarizer and the dye amplifier cell. After the dye amplifier a quarter wave-plate was placed to change the beam polarization from linear to a circular. Then the dye laser beam is focused inside the phase conjugation medium by the lens f_1. The conjugated beam goes through the quarter wave-plate which changes its polarization back to linear but now in the vertical direction. The beam is amplified again and is separated from the forward beam by the polarizer. The energy of the phase conjugated dye laser beam (PCD) depends on the transmission losses of the polarizer, the quarter wave-plate and the efficiency of the phase conjugate mirror. As the quarter wave-plate device we used a Pockels cell and latter a Fresnel romb. The latter showed a smaller transmission loss. The polarizer was substituted by a calcite crystal where the forward and the backward beams are laterally shifted by 2 mm by double refraction and the phase conjugated beam is extracted via a prism as shown in figure 2.30. The Fresnel romb and calcite crystal were used in the final measurements. The phase conjugation medium was acetone which gives the lowest dye pulse power threshold among the liquids we tried.

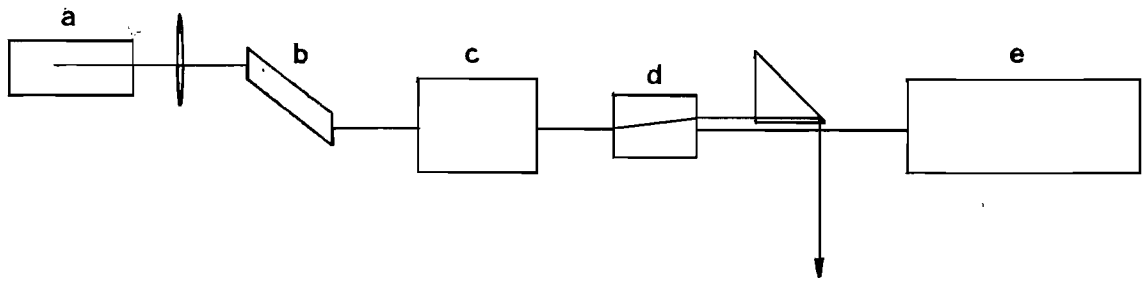

Figure 2.30. Scheme for the dye laser with phase conjugation used during the experiments.
(a) Brillouin cell - acetone, (b) Fresnel romb, (c) dye amplifier cell, (d) calcite beam splliter, (e) dye oscillator.

In table VI we give the results for several arrangements. One can notice that a low dye output energy produces the highest efficiency. This is due to the non saturation of the dye amplifier. The forward and the backward (conjugated) beam cross the DAC excited region at the same time and this reduces the expected gain for the

conjugated signal. This shows how important it is to have a high efficiency from the phase conjugation cell, because if we can get enough conjugated energy in the phase conjugated beam without needing to inject a large amount of dye laser energy into the Brillouin cell, the dye amplifier will not be depleted when the backward beam goes through it and consequently the conjugated beam can be amplified properly.

Table VI

configuration	Dye laser output energy (mJ)	PCD output energy(mJ)	Efficiency
PC + pol.	1.5	1.1	73%
PC + pol.	8.0	3.0	37%
FR + pol.	5.0	3.0	60%
FR + pol.	8.0	4.0	50%
FR + calc.	9.0	4.5	50%

PC= Pockels cell

pol.= polarizer

FR= Fresnel romb

Efficiency= Energy(PCD)/Energy(dye laser)

The phase conjugation efficiency was measured as a function of the input energy for a 15 cm focal length lens. For a input dye pulse energy of 5 mJ the efficiency was 16% and this value does not change very much for higher values of the input energy.

We can summarize our conclusions about the phase conjugation scheme for dye lasers in this way:

1. We had a energy reduction of a factor of 2, but the pulse time duration was reduced by a factor of 4. Thus we end up with less pulse energy and more pulse power.

2. The phase conjugation eliminates the ASE completely. Thus the PCD beam is totally free of spurious untuning radiation.

3. The intensity distribution along the beam cross section is very much better for the PCD. It resembles the intensity distribution coming from the dye oscillator.

4. The phase conjugation arrangement implies an inclusion of four new elements in the dye laser, although their alingnment is not critical at all due to the phase reproduction in the backward beam.

In figure 2.31 we display the pulse shape at different points of the arrangement. It starts with the pulse of the Nd:YAG laser, τ=20 nsec, and it ends with the PCD pulse, τ= 3 nsec.

CHAPTER THREE

Stimulated Raman Scattering—theory

3.1 Introduction

Spontaneous Raman scattering has been well known for approximately fifty years. In this process one photon is absorbed by a molecule or atom which is raised to a virtual level from which a photon of different frequency is radiated to leave the molecule in some level other than the original state. Only a small fraction of the input photon are scattered in this inelastic way and the emitted photon's direction is not correlated with the direction of the input beam, figure 3.1.

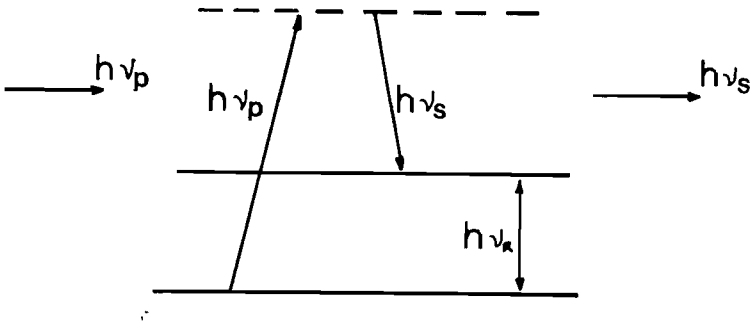

Figure 3.1. Scheme showing the emission of a Stokes photon in terms of energy level.

When the intensity, and hence number density of pump photons is increased, the number of scattered Stokes photons per interval of time, which was proportional to the number of incident photons, begins to be proportional to the number of scattered photons as well. This happens because a large number of incident photons generates a sufficient number of scattered photons for these to start induceing transitions themselves. The scattered photons generated by these induced transitions are identical to the incoming Stokes photons. This process is called stimulated Raman scattering. The two main differences between this process and spontaneous Raman scattering are the high conversion efficiency of these generated scattered photons for the former process, and the directionality of

the generated Stokes photons, figure 3.2.

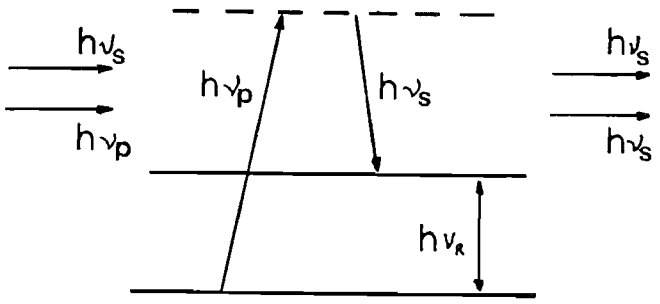

Figure 3.2. Scheme showing the stimulated emission of a Stokes photon in terms of energy levels.

The advent of the laser made it possible to observe stimulated Raman scattering (SRS). One of the first observations was made by Eckhardt et al (1962). They found that when a ruby laser beam was incident on a cell containing nitrobenzene, a stimulated Raman beam was generated.

The generated radiation at the frequency which is lower than pump optical frequency by a single energy difference in the scattering species($h\nu_r$ in figure 3.1) is called the "first Stokes" beam, which will henceforth be referred to as the "S_1 component" of the incident beam in a particular medium. The energy transfered from the pump beam to the S_1 component can be so large that the first Stokes radiation can reach intensities of the same order of magnitude as the pump intensity, which is depleted accordingly. The efficiency of the SRS process can be very high. In principle the photon conversion efficiency can reach 100%. However, for a pump beam with nonuniforme (e.g. Gaussian) spatial and temporal profile the conversion efficiency will be lower due to the low intensity in the wings of the profile. Thus the S_1 component can be Raman scattered itself since it can reach high intensity levels, to generate the "second Stokes" beam, S_2, with twice the frequency shiftν_r towards lower frequencies. Further repetition of this Raman process generates the S_3, S_4 ... components. In a general notation we have

$$\nu_n = \nu_0 - n.\nu_r \qquad 3.1$$

where ν_n is the optical frequency of the S_n component, ν_0 is the pump frequency and ν_r is the frequency Raman shift provided by the medium.

Scattered generated radiation with frequency higher than the pump frequency is called anti-Stokes radiation. In figure 3.3 we show schematically the anti-Stokes generation.

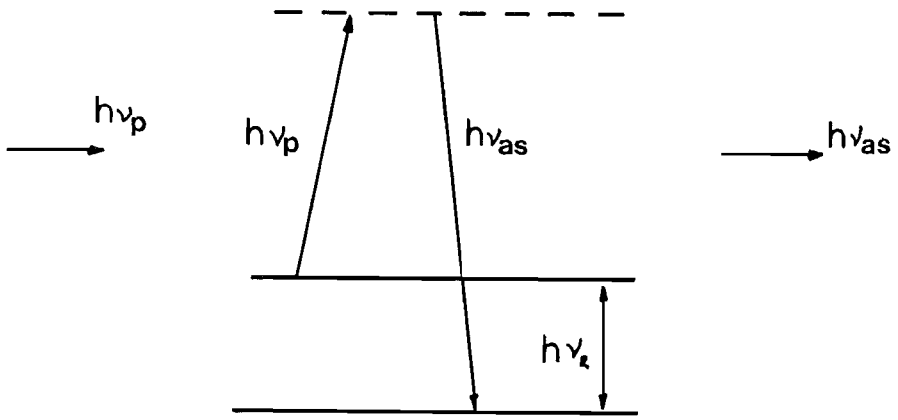

Figure 3.3. Scheme showing the emission of an anti-Stokes photon in terms of energy level.

Stimulated anti-Stokes Raman scattering, analagous to Stokes Raman scattering can also occur, but for a net gain to be achieved for the anti-Stokes photons, and hence high efficiency of anti-Stokes generation via this process, it is necessary to have population inversion, i.e. more molecules in the initial excited state. In thermal equilibrium this does not occur and yet powerfull anti-Stokes emission is observed once threshold for Stokes generation is exceeded. The explanation for this is that anti-Stokes radiation can be generated via another process involving a parametric interaction of the waves inside the Raman medium. While there is more than one beam present in the medium with frequencies separated by a multiple of the medium Raman shift, four-wave mixing can occur to generate either additional Stokes or anti-Stokes components. These four-wave mixing or parametric processes are characterized by the need for phase matching if they are to be efficient. Compared with the SRS process the parametric processes are rather inefficient because their generated intensities are proportional to the intensities of the involved beams, while in the

SRS or Raman process there is an exponential dependence on the input intensity. However, the radiation generated parametrically is quite important as we will see later in this work, not only in the anti-Stokes generation but even in the Stokes generation itself when, despite the low efficiency, it can provide seed radiation a few orders of magnitude above the noise level background and be amplified by the SRS process. A detailed analysis of these parametric process is made in chapter five of this work.

In this chapter we analyse the intensity of a general Stokes wave as a function of the the pump intensity, the length of the interacting medium and the pressure. An analytical solution is found for a simplified case and a complete numerical analysis of the whole system of equations is carried out.

3.2 SRS - Plane wave analysis

In this section the basic equations governing the Raman and parametric process will be derived. Much of the work presented in this section has been derived from Hanna et al (1979), Lorrain and Corson (1970) and Butcher (1964).

Maxwell's equations for a medium where the total density of charges is zero and the only current is given by the displacement current are given by

$$\nabla.\vec{d} = 0 \qquad 3.2$$

$$\nabla.\vec{b} = 0 \qquad 3.3$$

$$\nabla \times \vec{e} = -\partial\vec{b}/\partial t \qquad 3.4$$

$$\nabla \times \vec{h} = \partial\vec{d}/\partial t \qquad 3.5$$

and the constitutive relations

$$\vec{d} = \varepsilon_r.\varepsilon_0.\vec{e} \qquad 3.6$$

$$\vec{h} = \vec{b}/\mu_0 \qquad 3.7$$

where

$\vec{d}$ is the electric displacement, [d]=Coulombs/m^2

$\vec{b}$ is the magnetic induction, [b]= tesla

$\vec{e}$ is the electric field strength, [e]=volt/m

$\vec{h}$ is the magnetic field intensity, [h]=ampere/m

ε_r is the relative permeabillity

ε_0= 8.854 x 10^{-12} Farad/m

μ_0= 1.255 x 10^{-6} Henry/m

By applying the operator ∇x in the equation 3.4 and substituting 3.5 in the result we have:

$$\nabla \times \nabla \times \vec{e} = -\partial(\nabla x \vec{b})/\partial t = -\mu_0(\partial^2\vec{d}/\partial t^2) \qquad 3.8$$

Equation 3.8 may be Fourier transformed into the frequency domain. Considering a component with a harmonic time variation we have

$$\vec{d} = \vec{D}.\cos(\omega t) = Re[\vec{D}.\exp(-j\omega t)] \qquad 3.9$$

$$\vec{e} = \vec{E}.\cos(wt) = Re[\vec{E}.\exp(-jwt)]$$

$$\nabla \times \nabla \times \vec{E} = \mu_0\omega^2\vec{D} \qquad 3.10$$

Using the vector relation

$$\nabla \times \nabla \times \vec{a} = -\nabla^2\vec{a} + \nabla(\nabla.\vec{a}) \qquad 3.11$$

and the fact that we have the total density of charges equal to zero, we can write equation 3.10 in the form

$$\nabla^2\vec{E} = -\mu_0\omega^2\vec{D} \qquad 3.12$$

and assuming a plane polarized wave with the E vector parallel to the x-axis and forward propagation along the z-axis, we have

$$d^2E/dz^2 = -\mu_0\omega^2D \qquad 3.13$$

Expression 3.6 can be written for an isotropic medium in a more general form to include the medium polarization,

$$D = \varepsilon_0 E + P \qquad 3.14$$

where P is the polarization which is set up when the medium is subjected to a electrical field E. For a small electrical field intensity E the polarization may be expressed as

$$P = \varepsilon_0 \chi E \qquad 3.15$$

where χ is a dimensionless parameter known as the linear electric susceptibility of the medium.

At high field strengths the polarization is given by

$$P = \varepsilon_0 \chi E + \varepsilon_0 k^{(2)} \chi^{(2)} E^2 + \varepsilon_0 k^{(3)} \chi^{(3)} E^3 + \ldots \qquad 3.16$$

$$[\chi^{(n)}] = (m/V)^{n-1}$$

where the quantities $\chi^{(2)}$, $\chi^{(3)}$, etc., are called the nonlinear susceptibilities of the medium and the numerical factor $k^{(n)}$ is determined by the particular circumstances of the scattering process being considered, for example degeneracy in the interacting fields affects the value of $k^{(n)}$.

Thus we may write the electric displacement as

$$D = \varepsilon E + P_{NL} \qquad 3.17$$

where

$$\varepsilon = \varepsilon_0 (1+\chi) \qquad 3.18$$

$$P_{NL} = \varepsilon_0 k^{(2)} \chi^{(2)} E^2 + \varepsilon_0 k^{(3)} \chi^{(3)} E^3 + \ldots \qquad 3.19$$

Substituting 3.17 in 3.13 we have

$$\partial^2 E / \partial z^2 = -\mu_0 \varepsilon \omega^2 E^2 - \mu_0 \omega^2 P_{NL} \qquad 3.20$$

The electrical field is now taken in the form of a superposition of running waves,

$$E = \tilde{E} \exp(+jkz) \qquad 3.21$$

where k is the wavevector in the medium,

$$k = (\mu_0 \epsilon)^{\frac{1}{2}} \omega \qquad 3.22$$

and the signal + and - mean forward and backward propagation along z. For forward-propagating waves 3.20 becomes

$$d^2E/dz^2 + 2jkdE/dz = -\mu_0 \omega^2 P_{NL} \exp(-jkz) \qquad 3.23$$

where, to simplify the notation, we have dropped the tilde on E.

Assuming E is a slowly varying envelope function, i.e., the fractional growth of the envelope in a distance of the order of a wavelength should be small, the second E derivative may be dropped, and the equation 23.23 becomes,

$$dE/dz = (j\omega/2\epsilon_0 cn) P_{NL} \exp(-jkz) \qquad 3.24$$

Each term in the expression of the nonlinear polarization corresponds to a set of nonlinear phenomena. In this work we are interested in the term with a cubic electric field dependence which gives rise to SRS and four wave mixing. The term "stimulated" arises from the fact that the induced polarisation is proportional to the electric field at the same frequency. For the case of SRS the nonlinear polarisation is given by Hanna et al (1979) as

$$P_{SRS}(\omega_{S1}) = (3/2)\epsilon_0 \chi(-\omega_{S1}; \omega_P, -\omega_P, \omega_S) E_P \overset{*}{E_P} E_S \qquad 3.25$$

and for the four wave mixing parametric process as

$$P_{FWM} = (3/2)\epsilon_0 \chi(-\omega_1; \omega_2, \omega_3, \omega_4) E_2 E_3 E_4 \exp(j\Delta kz) \qquad 3.26$$

where Δk is the phase mismatch factor and k_i is the wavevector in the medium for the interacting fields,

$$\Delta k = -k_1 + k_2 + k_3 + k_4 \qquad 3.27$$

When the involved field energies are very large and/or the interaction length is long enough, we will have several Stokes

components being generated by sucessives Raman shifts. Besides that we need to account for the parametric processes as well. The generalized non linear polarization including SRS and four wave mixing terms is

$$P_{NL}(\omega_i)\exp(-jk_iz)= (3/2)\varepsilon_0\Sigma(\chi(-\omega_i;\omega_{i-1},-\omega_j,\omega_{j+1})E_{i-1}E_j^*E_{j+1}.$$

$$\exp(-j\Delta k_{i-1,j}.z)-\chi(-\omega_i;\omega_{i+1},-\omega_j,\omega_{j+1})E_{i+1}.$$

$$E_jE_{j+1}^*\exp(j\Delta_{i,j}.z)) \qquad 3.28$$

The summation is over all possible contributing processes. The negative values of j denote anti-Stokes components and the positive values denote Stoke components. The phase mismatch Δk is given by

$$\Delta k_{i,j}= k_j - k_{j+1} - k_i + k_{i+1} \qquad 3.29$$

Only the imaginary part of the susceptibility will be considerer, since at resonance only this part remains

$$\chi = \chi' - j\chi''$$

Then we have

$$\chi(-\omega_i;\omega_{i+1},-\omega_j,\omega_{j+1}) \Rightarrow -j\chi''(-\omega i;\omega_{i+1},-\omega_j,\omega_{j+1})$$

and to simplify the notation we will use

$$\chi''(-\omega_i;\omega_{i+1},-\omega_j,\omega_{j+1})=\chi(i,j) \qquad 3.30$$

Introducing the value of P_{NL} given in equation 3.28 into the equation for the slowly-varying field envelope, 3.24, we have

$$dE_i/dz= (3\omega_i/4cn_i)\Sigma(\chi(i-1,j)E_{i-1}E_j^*E_{j+1}.\exp(-j\Delta k_{i-1,j}.z)$$

$$-\chi(i,j)E_{i+1}E_jE_{j+1}^*.\exp(j\Delta k_{i,j}.z)) \qquad 3.31$$

The attenuation will be added phenomenologically by inserting the parameter α_i which characterizes the linear absoption

of the component S_i by the medium.

$$dE_i/dz = (3\omega_i/4cn_i)[\Sigma(\chi(i-1,j)E_{i-1}E^{*}_{j}E_{j+1}.\exp(-j\Delta k_{i-1,j}.z)$$

$$- \chi(i,j)E_{i+1}E_{j}E^{*}_{j+1}.\exp(j\Delta k_{i,j}.z))] - \alpha_i E_i \qquad 3.32$$

3.3 First Stokes – analytical treatment

3.3.1 First Stokes gain coefficient

If we allow only the first Stokes generation in a lossless medium, we can write the equation for its electrical field from equation 3.32,

$$dE_i/dz = (3\omega_1/4cn_1)\chi(0,0)E_0E_0E_1 \qquad 3.33$$

A similar equation may be written for the pump electrical field. But if we assume for the moment a low pump conversion to the first Stokes component we can assume a negligible pump field variation along z. Thus the solution for the equation 3.33 is given by

$$E_1(z) = E_1(0).\exp[(3\omega_1/4cn_1)\chi(0,0)E_0E_0z] \qquad 3.34$$

or in terms of the time averaged intensities,

$$I = (cn\varepsilon_0/2)E^2$$

$$I_1(z) = I_1(0)\exp[(3\omega_1/c^2\varepsilon_0n_0n_1)\chi(0,0)I_0z] \qquad 3.35$$

thus the exponential gain is

$$G = (3\omega_1/c^2\varepsilon_0n_0n_1)\chi(0,0)I_0z \qquad 3.36$$

and the gain coefficient can be defined using the relation 3.30 as

$$g = -(3\omega_1/c^2\varepsilon_0n_0n_1)\chi \qquad 3.37$$

The Raman susceptibility is given by Hanna et al (1979),

$$\chi = \frac{N/6\hbar\varepsilon_0}{\Omega_{fg}+\omega_1-\omega_0+i\Gamma}.|\alpha|^2 \qquad 3.38$$

where α is the polarisability, Ω_{fg} is the frequency difference of the transition levels and Γ is the half width of the transition resonance curve. The polarisability is related to the Raman scattering cross-section, $d\sigma/d\Omega$, through the expression

$$d\sigma/d\Omega = \frac{\omega_1^3.\omega_0}{(4\pi\varepsilon_0 c^2)^2}.|\alpha|^2 \qquad 3.39$$

Thus, combining equations 3.38, 3.39 and assuming $\Omega_{fg}=\omega_0-\omega_1$ we have the gain coefficient at resonance in terms of the Raman scatering cross-section:

$$g = \frac{8\pi^2c^2}{\hbar\omega_1^2.\omega_0 n_1 n_0}.(N/\Gamma).(d\sigma/d\Omega)_{photon} \qquad 3.40$$

The differential cross-section $(d\sigma/d\Omega)_{photon}$ is defined in terms of the number of photons scattered per unit solid angle and it is related to the quoted intensity scattering differential cross-section via the ratio of the pump and Stokes frequency, [Hanna et al (1985)]

$$(d\sigma/d\Omega)_{photon} = (\omega_0/\omega_1).(d\sigma/d\Omega)_{intensity} \qquad 3.41$$

Thus the gain coefficient becomes

$$g = \frac{8\pi^2c^2}{\hbar.\omega_1^3.n_0 n_1}.(N/\Gamma).(d\sigma/d\Omega)_{intensity} \qquad 3.42$$

3.3.2 **Gain coefficient parameters**

3.3.2.1 **Number density - N**

The population density N can be considered as depending linearly on pressure, which is a good enough first approximation, although conversion tables must be consulted for high pressures.

$$N = P/KT \qquad 3.43$$

or

$$N = (7.25 \times 10^{27}).\ \frac{P(atm)}{T(^{\circ}K)}.\ C \quad [m^{-3}] \qquad 3.44$$

The factor C represents the fraction of the total number of molecules in the initial level for the Raman transition. At room temperature the appropriate values for C, are [Laycock (1978)]

$C = 0.67$ (for J=1) in H_2

$C = 0.387$ (for J=2) in D_2

$C = 1.0$ for CH_4

3.3.2.2 Spontaneous Raman linewidth

The FWHM linewidth 2Γ (rad/sec) depends in a rather more complex way on the pressure. At low pressures the linewidth is doppler broadened and therefore depends on the mean thermal velocities of the molecules and on the relative directions of Stokes and pump beams. It results in a linewidth for backward SRS bigger than the linewidth for forward SRS by a factor of $(\omega_0+\omega_1)/(\omega_0-\omega_1)$. However, as the pressure is increased the mean free path of the molecules decreases and collisions are happening so fast that the doppler effect corresponds to the velocity of the molecules averaged over several collisions and consequently we get a narrower and narrower linewidth. This is the Dicke narrowing effect or collisional narrowing, Dicke (1953). As the pressure is increased further, the normal pressure broadening effects take over, the proximity of other molecules is enough to appreciably affect the internal energy levels of the molecules. The full width half maximum Raman linewidth is given by Owyoung (1978) for hydrogen in the range from 0.5 to 100 amagats.

$$\Delta\omega = 2\Gamma = 2\pi[D_0 k^2/(\pi\rho) + a\rho] \qquad 3.45$$

where

$$D_0 = 1.39 \text{ cm}^2.\text{amagats/sec.}$$

$$a = 51.3 \text{ MHz/amagat}$$

D_0 is the self-diffusion constant, k is the difference between the wavevectors of the pump and first Stokes photons, ρ is the gas density in amagats and **a** is the pressure-broadening coeffcient.

For methane we have [Taira et al (1982)]

$$\Delta\omega = 2\Gamma = 2\pi(b + a\rho) \qquad 3.46$$

where

$$b = 9.6 \text{ GHz}$$

$$a = 360 \text{ MHz/amagat}$$

In the pressure broadening region the Raman linewidth is proportional to the pressure (and hence the number density), so from expression 3.42 we can see that the Raman gain coefficient is independent of pressure in this region. However if the coherence time of the pump laser, given by the inverse of the laser linewidth

$$T_C = 1/(2\pi\Delta\nu) \text{ Hz}$$

is shorter than the coherence time for the Raman transition, which is given by the inverse of the Raman transition linewidth

$$T_d = 1/\Delta\omega$$

then the incoming laser beam can see an excitation built up earlier in the pulse that is incoherent with it. The SRS process can then be influenced by the finite laser linewidth and the latter can no longer be treated as monochromatic. However, it has been shown that the pump laser in such a case can be regard as quasi-monochromatic provided that the coherence time remains longer than the group-lag time T_g, defined as [Akhmanov et al (1974)],

$$T_g = L[(1/v_g(\lambda_0))-(1/v_g(\lambda_1))] \qquad 3.47$$

where

$$v_g(\lambda) = c[n(\lambda)-\lambda.dn/d\lambda] \qquad 3.48$$

For a gas with low dispersion we may make the approximation

$$v_g(\lambda) \simeq cn(\lambda) \qquad 3.49$$

and thus we have

$$T_g = \frac{L.}{c}[n(\lambda_0)-n(\lambda_1)] \qquad 3.50$$

The refractive index as a function of the wavelength and the pressure can be expressed as

$$n(\lambda) = 1 + p.f(\lambda) \qquad 3.51$$

by substituting 3.51 into 3.50 we have

$$T_g = \frac{L.}{c}[f(\lambda_0)-f(\lambda_1)].p \qquad 3.52$$

From expression 3.52 we may notice that the lag time is directly proportional to the pressure due to the increase in the gas dispersion. So for a pump system in which the coherence time is not greater than the lag time, the actual Raman gain coefficient can be affected by an increase in the gas pressure even if we are in the pressure broadening region, because for a larger value of T_g the pump can no longer be regarded as monochromatic and the laser linewidth should be taken in account in the calculations.

The dye laser used in the experiments produces pulses with duration of 12→14 nsec and a linewidth of 0.21 cm^{-1}, it produces a coherence time of 25 psec. The Raman transition coherence time in hydrogen is of order of 300→100 psec at pressures of 10→30 atmospheres. To settle the question of whether the pump beam can be considered as monochromatic we need to compare the laser coherence

time with the group lag time. In order to work out the lag time for hydrogen we will make use of the four- parameter equation for the hydrogen dispersion given by Peck and Huang (1977),

$$10^6(n-1)= \frac{14895.6}{180.7-\sigma^2} + \frac{4903.7}{92-\sigma^2} \qquad 3.53$$

where σ is $1/\lambda$ in μm^{-1}

then the lag time can be calculated through equation 3.52 and we observe that it is very much smaller than the laser coherence time for L<1 metre, even at pressures as high as 60 atmospheres.

	P= 10 atm	P= 60 atm
T_c coherence time	25 psec	25 psec
T_d transition time	312 psec	52 psec
T_g lag time	0.05 psec	0.27 psec

Then a pump with a broad linewidth compared with the Raman linewidth can be regarded as monochromatic in terms of Raman gain coefficient if the duration of the shortest pulse inside the pulse envelope is bigger than the group lag time in the Raman medium.

3.3.2.3 Differential cross section

We need to find a value of $d\sigma/d\Omega$ for a specific medium under a certain pump wavelength. Most of the differential Raman scattering cross sections are given in the literature relative to the cross section of the Q-branch of N_2 at some particular exciting frequency $\tilde{\nu}_n$. To find $d\sigma/d\Omega$ for a particular medium x we may use the expression given by [Schrötter and Klöckner(1979)],

$$(d\sigma/d\Omega)_{x,\tilde{\nu}_n} = (d\sigma/d\Omega)_{N_2}\tilde{\nu}.\Sigma_j.(\tilde{\nu}_n-\tilde{\nu}_x)^4/(\tilde{\nu}_n-2331)^4 \qquad 3.54$$

The first factor on the right side of equation 3.54 is the differential Raman scattering cross section for N_2 at the exciting frequency $\tilde{\nu}_n$. For $\tilde{\nu}_n$= 19436.4 (λ=514.5 nm) we have from Schrötter and Klöckner

$$(d\sigma/d\Omega)_{N_2,\tilde{\nu}_N} = 43.2 \times 10^{-32} \text{ cm}^2/\text{sr} \qquad 3.55$$

the second factor is the "relative normalized differential Raman scattering cross section" defined by Schrötter and Klöckner. The third factor includes the Raman frequency shift $\tilde{\nu}_x$ which characterises the new medium.

To transform the Raman cross section given in expression 3.54 to the one at the pump wavelength $\tilde{\nu}_p$ we use the following expression,

$$(d\sigma/d\Omega)_{x,\tilde{\nu}_p} = (d\sigma/d\Omega)_{x,\tilde{\nu}_N} \cdot \frac{\left[\dfrac{1}{\tilde{\Omega}_{ig}-\tilde{\nu}_p} + \dfrac{1}{\tilde{\Omega}_{ig}+\tilde{\nu}_p}\right]^2 \cdot (\tilde{\nu}_p-\tilde{\nu}_x)^4}{\left[\dfrac{1}{\tilde{\Omega}_{ig}-\tilde{\nu}_n} + \dfrac{1}{\tilde{\Omega}_{ig}+\tilde{\nu}_n}\right]^2 (\tilde{\nu}_n-\tilde{\nu}_x)^4} \qquad 3.56$$

Ω_{ig} is the frequency of the transition from the initial Raman level **g** to the dominant intermediate level **i** in the Raman process. Using the value for $(d\sigma/d\Omega)_{N_2,\tilde{\nu}_N}$ and $\tilde{\nu}_n$ we can write 3.56 as

$$(d\sigma/d\Omega)_{x,\tilde{\nu}_p} = 5.05\text{x}10^{-48} \cdot \Sigma_j \cdot (\tilde{\nu}_p-\tilde{\nu}_x)^4 \cdot F \ [\text{cm}^2/\text{sr}] \qquad 3.57$$

where

$$F = \frac{\left[\dfrac{1}{\tilde{\Omega}_{ig}-\tilde{\nu}_p} + \dfrac{1}{\tilde{\Omega}_{ig}+\tilde{\nu}_p}\right]^2}{\left[\dfrac{1}{\tilde{\Omega}_{ig}-\tilde{\nu}_n} + \dfrac{1}{\tilde{\Omega}_{ig}+\tilde{\nu}_n}\right]^2} \qquad 3.58$$

The value of **F** does not change very much in the near infrared region as we can see from figure 3.4. Thus, using equations 3.42, 3.45, 3.54 and 3.57 we can calculate the steady state Raman gain coefficient. Table I gives results of the calculation for H_2, D_2 and CH_4. The value of Σ_j for methane was taken as a average of the given values in the references **d,e,f**. The value of **F** was considered as equal to 1.0 and the linewidth for D_2 and H_2 were

Figure 3.4. Correction factor for the differential Raman cross section due to influence of electronic levels as a function of pump wavelength in hydrogen.

Figure 3.5. Analytical solution for the first Stokes component given in terms of normalized 1st Stokes pulse energy in relatively to input pump pulse energy as a function of interaction length, for three different initial energy for Stokes component.

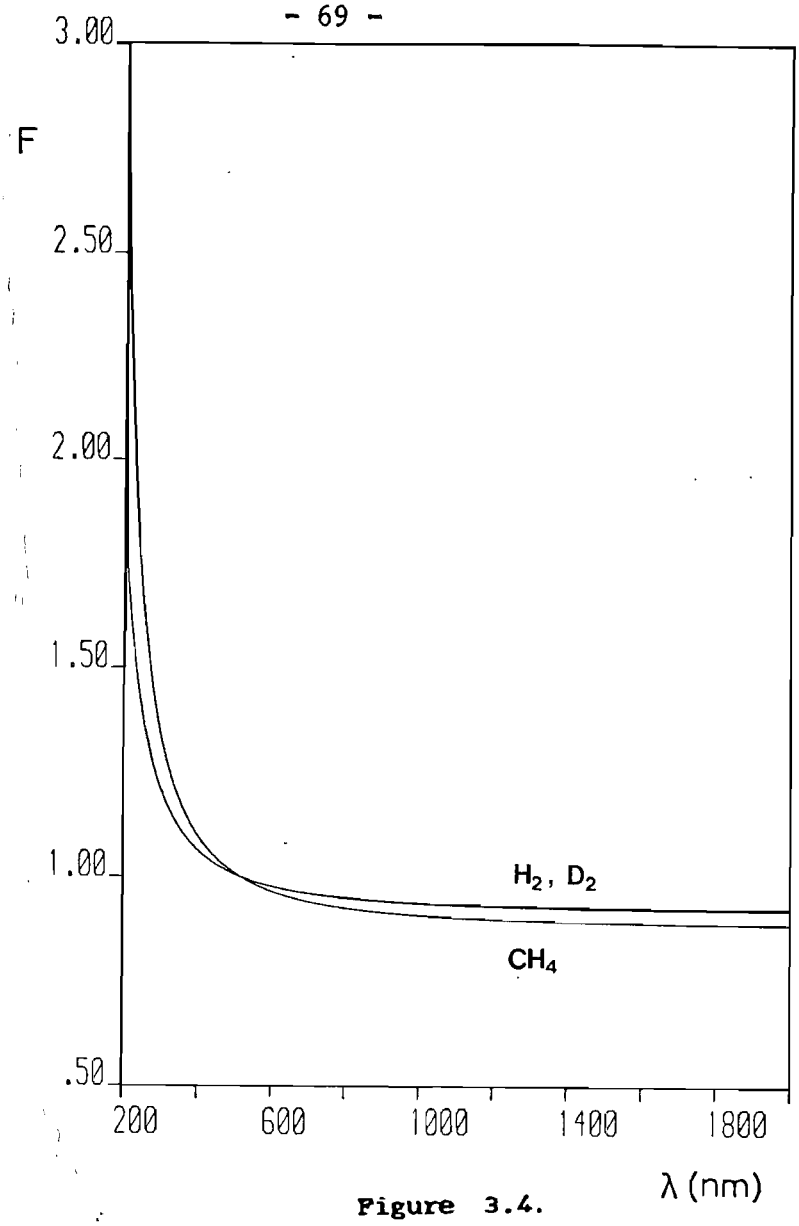

Figure 3.4.

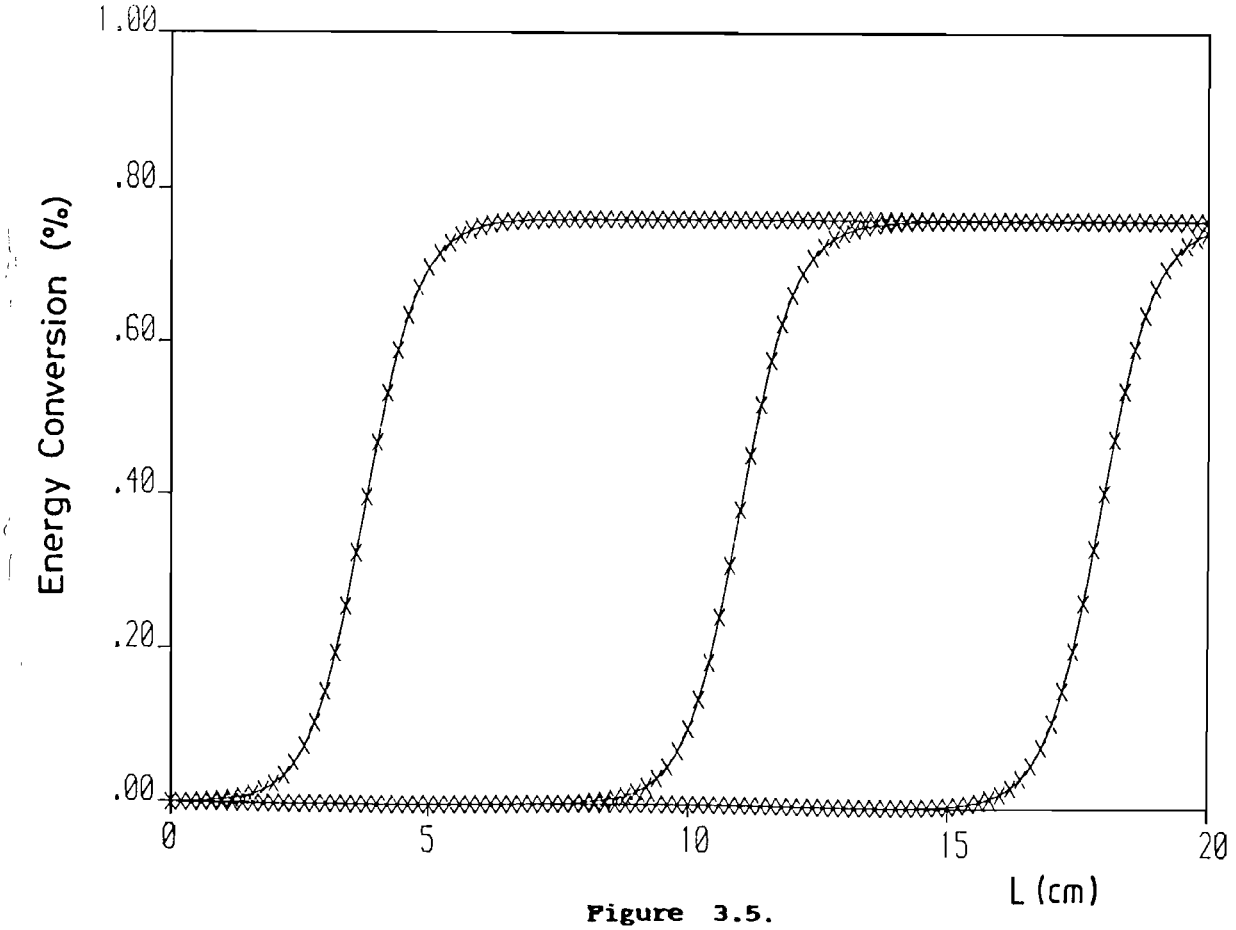

Figure 3.5.

assumed to be the same and in the pressure broadening region that makes the the Raman gain coefficient pratically pressure independent.

Raman medium	Raman shift ν_x (cm^{-1})	Σ_j	g(cm/GW) [P in atm]
H_2	4156[a]	3.6[b]	$1.85/\lambda_s(\mu m)$
D_2	2986[a]	2.6[c]	$0.78/\lambda_s(\mu m)$
CH_4	2917[a]	9.03[d,e,f]	$(P/P+27)/\lambda_s(\mu m)$

(a) Schrötter and Klöckner, (1979)
(b) Fenner et al, (1979)
(c) Murphy et al, (1979)
(d) Fouche et al, (1972)
(e) Penney et al, (1972)
(f) Kamiyama et al, (1974)

3.3.3 First Stokes – analytical solution

The equation 3.32 for the electric field can be put in terms of the intensity and the gain coefficient for the first Stokes component (expression 3.42),

$$dI_i/dz = g_i I_i I_{i-1} - g_i' I_i I_{i+1} + \Sigma \text{ parametric terms} - \beta I_i \qquad 3.59$$

where

$$g_i = (\chi_i/\chi_1).(\omega_i^2 k_1/\omega_1^2 k_i).g_1 \qquad 3.60$$

and

$$g_i' = (\chi_{i+1}/\chi_i).g_i \qquad 3.61$$

The component intensity attenuation is characterised by the coefficient β. Equation 3.59 may be simplified if we neglect the parametric terms and consider a lossless medium. These assumptions

are quite reasonable for the first Stokes component for gases in an unguided system, due to the small influence of the four wave mixing processes in the growing of the first Stokes intensity and to the very low gas absorption at the used pump wavelengths. Under these assumptions we may write the equation 3.59 as

$$dI_0/dz = g_0 I_0 I_{-1} - g_0' I_0 I_1 \qquad 3.62$$

$$dI_1/dz = g_1 I_1 I_0 - g_1' I_1 I_2 \qquad 3.63$$

When we consider a Raman amplifier for the first Stokes radiation, the input intensity for the S_1 component is very much stronger than the initial intensity for any other Stokes or anti-Stokes component

$$I_1^0 \gg I_i^0 \quad (i \neq 0) \qquad 3.64$$

and consequently we may assume that the pump radiation exchanges energy mainly with the S_1 component. In this case the terms containing the second Stokes and first anti-Stokes intensities can be dropped out of equations 3.62 and 3.63,

$$dI_0/dz = -g_0' I_0 I_1 \qquad 3.65$$

$$dI_1/dz = g_1 I_1 I_0 \qquad 3.66$$

the solution is,

$$I_1(z) = \frac{\alpha . \exp(\gamma z)}{A + \exp(\gamma z)} \qquad 3.67$$

where

$$\alpha = I_1^0 + (g_1/g_0')I_0^0 \qquad 3.68$$

$$A = (g_1/g_0').(I_0^0/I_1^0) \qquad 3.69$$

$$\gamma = g_0' I_1^0 + g_1 I_0^0 \qquad 3.70$$

$$g_o' = (\omega_o/\omega_1)^2.(k_1/k_o).g_1 \simeq (\lambda_1/\lambda_o).g_1 \qquad 3.71$$

and I_1° and I_o° are the input intensities for the first Stokes and the pump beam.

In diagram 3.5 we show the first Stokes normalized intensity against the interaction length for several values of the input intensity I_1°. Equation 3.67 was used to get these curves and the Raman medium is hydrogen at 30 atmospheres pumped by the dye laser. In this diagram we include the case where the first Stokes input intensity is given by the noise background,i.e, spontaneous emission, in this case we no longer satisfy the condition 3.64. Later in this chapter we will give the numerical solution for these equation and we will be able to evaluate the discrepancy produced by the analytical solution when one considers the Raman oscillator case.

3.3.3.1 Noise intensity

In the absence of radiation at frequencies other than that of the pump laser in the equations no polarization is produced and so no SRS occurs. Initially there must be a build up of S_1 intensity through spontaneous scattering. The noise background from which the process starts is equivalent to one photon per mode of the generated field [Mostowski and Raymer (1981), Hanna et al (1979)]. From radiation theory the density of modes in the frequency range between ω and $\omega+d\omega$ per steradian and for a given polarization is given by

$$\rho(\omega) = \omega^2 d\omega/8\pi^3 c^3 \qquad 3.72$$

We consider the nonlinear medium to be irradiated by the pump beam over a cylindrical region of radius w_o and length L. We need to consider only the noise emitted in such a direction that it travels along the length of the cylinder, because only that noise component will undergo the full amplification provided by the medium. The cylindrical region has a solid angle

$$d\Omega \sim \pi\theta_m^2$$

where θ_m is the angle subtended by the beam and cylindrical axes. The cylindrical volume is

$$V= \pi w_0^2 L$$

thus the total number of modes is

$$V\rho(\omega)d\Omega= \omega^2 d\omega L w_0^2 \theta_m^2/8\pi c^3 \qquad 3.73$$

The photon energy is $\hbar\omega$ and the radiation travels the length L in a time L/c, thus the noise power can be written as

$$P_n= \hbar\omega^3 d\omega w_0^2 \theta m^2/8\pi c^2 \qquad 3.74$$

For a gaussian beam we have, $\theta_m= \lambda/\pi w_0$ and it produces a noise power of

$$P_n= h\nu d\nu \qquad 3.75$$

where ν is the optical frequency expressed in Hertz.

The noise intensity for the assumed cylindrical geometry is given by

$$I_n= h\nu d\nu/\pi w_0^2 \qquad 3.76$$

For a capillary waveguide we have the angle $\theta_m= \mu_{11}\lambda/2\pi a$ for the fundamental mode EH_{11} [Marcatili and Schmeltzer (1964)], it produces a noise intensity of

$$I_{nc}= (\mu_{11}/2)^2 . h\nu d\nu/\pi a^2 \qquad 3.77$$

where **a** is the capillary radius. For a Raman linewidth of 0.21cm^{-1} and a pump wavelength of 575 nm with a beam waist size of 66.7 microns, which matches the EH_{11} mode for a capillary with a 200 micron bore diameter we have for the noise intensity in a unguided structure,

$$I_n= 1.6 \times 10^{-5} \ W/cm^2 \qquad 3.78$$

and for the guided structure,

$$I_{nc} = 1.0 \times 10^{-5} \text{ W/cm}^2 \qquad 3.79$$

For the tight focusing condition,i.e. L≫b the cylindrical geometry does not hold any more and by using Kogelnik and Li' expression for the beam diffraction the expression 3.76 becomes

$$I_{TF} = I_n.[1 + \frac{(L/b)^2}{3}] \qquad 3.80$$

$$b = 2\pi w_0^2/\lambda$$

The expressions 3.76, 3.77 and 3.80 give the noise intensity value under several situations, so that we can work out the Raman exponential gain necessary to reach SRS threshold in each case. However if one is interested in the final intensity of a given Stokes component a precise knowledge of the noise intensity is not required because it undergoes a large exponential amplification and the final value is usually determined by saturation. In diagram 3.5 we have used equation 3.80 to determine the value of I_1° for the case where the Stokes input intensity is defined by the noise background.

3.4 **Numerical model**

Equation 3.32 may be recast into a pair of equations by using the notation,

$$E_i = |E_i|.\exp(+j\phi_i) \qquad 3.81$$

where E_i and ϕ_i are functions of z. The derivative of 3.81 gives,

$$dE_i/dz = (d|E_i|/dz)\exp(j\phi_i) + j(d\phi_i/dz)|E_i|\exp(j\phi_i) \qquad 3.82$$

By separating equation 3.32 into real and imaginary parts and comparing with the terms in equation 3.82 we find,

$$d|E_i|/dz=(3\omega_i/4n_ic).$$
$$[\Sigma_j\chi(i-1,j)|E_{i-1}||E_j^*||E_{j+1}|\cos(-\Delta k_{i-1,j}.z+\phi_{i-1}-\phi_i+\phi_{j+1}-\phi_j)$$
$$-\chi(i,j)|E_{i+1}||E_j||E_{j+1}^*|\cos(\Delta k_{i,j}.z+\phi_{i+1}-\phi_i-\phi_{j+1}+\phi_j)]$$
$$-\alpha_i|E_i| \qquad 3.83$$

$$d\phi_i/dz=(3\omega_i/4n_ic|E_i|).$$
$$\Sigma_j\ \chi(i-1,j)|E_{i-1}||E_j^*||E_{j+1}|\sin(-\Delta k_{i-1,j}.z+\phi_{i-1}-\phi_i+\phi_{j+1}-\phi_j)$$
$$-\chi(i,j)|E_{i+1}||E_j||E_{j+1}^*|\sin(\Delta k_{i,j}.z+\phi_{i+1}-\phi_i-\phi_{j+1}+\phi_j) \qquad 3.85$$

These equations may also be normalized by dividing each field amplitude by the undepleted pump field amplitude and using equation 3.37 as to get equations 3.83 and 3.84 as a function of the first Stokes electrical field gain coefficient.

$$dA_i/d\zeta=(n_1\omega_i/n_i\omega_1).$$
$$[\Sigma_j\ Q(i-1,j)A_{i-1}A_jA_{j+1}\cos(-\Delta k_{i-1,j}.(\zeta_f/gI_o)+\phi_{i-1}-\phi_i+\phi_{j+1}-\phi_j)$$
$$-Q(i,j)A_{i+1}A_jA_{j+1}\cos(\Delta k_{i,j}.(\zeta_f/gI_o)+\phi_{i+1}-\phi_i-\phi_{j+1}+\phi_j)]$$
$$-(\alpha_i/gI_o)A_i \qquad 3.86$$

$$d\phi_i/dz=(n_1\omega_i/n_i\omega_1).(1/A_i).$$
$$\Sigma_j\ Q(i-1,j)A_{i-1}A_jA_{j+1}\sin(-\Delta k_{i-1,j}.(\zeta_f/gI_o)+\phi_{i-1}-\phi_i+\phi_{j+1}-\phi_j)$$
$$-Q(i,j)A_{i+1}A_jA_{j+1}\sin(\Delta k_{i,j}.(\zeta_f/gI_o)+\phi_{i+1}-\phi_i-\phi_{j+1}+\phi_j) \qquad 3.87$$

where

$$A_k=|E_k|/|E_o| \qquad 3.87$$

$$Q(i,j)=\chi(i,j)/\chi(0,0) \qquad 3.88$$

$$\zeta_f=g_fI_oz \qquad 3.89$$

$$g_f=3\omega_1\chi(0,0)/2c^2\varepsilon_on_on_1 \qquad 3.90$$

The initial values for the phases ϕ_i are taken as zero [J.H.Newton and G.M.Schindler (1981)] and for the normalized amplitudes are calculated either from expressions 3.77 and 3.80 when we have an oscillator (or superfluorescent amplifier), or from the electrical field correponding to the input component energy in the case of a Raman amplifier.

The set of equations 3.85→3.86 are the main equations that govern the Raman conversion for the plane wave case, they have been used by Komine and Stappaerts (1979) to find the conversion efficiency for a pump beam very loosely focused into the Raman cell.These equations have been solved numerically by Newton and Schindler for the case of the Raman amplifier. In this present work we will solve these equations numerically for the case of the Raman amplifier and Raman oscillator. From these solutions we will treat a more complicated case– that is, when a given intensity distribution over the beam cross section is considered, as well as a general pulse shape in the time domain. In chapter 5 these equations will make part of the procedure to select the most important parametric terms to determine the Stokes components efficiency.

3.4.1 **Plane wave solution**

The first step to solve numerically the set of equations 3.85→3.86 is to determine the number of Stokes componentsin which we are interested. In our case we are going to use the range of pump wavelengths 550nm→605nm produced in the dye laser and if we have hydrogen as the Raman medium we will have at most four Stokes shifts. The number of anti-Stokes components is not limited by the photon energy but by the gas absorption and the influence of these components in the four-wave mixing processes. We will keep the first and the second anti-Stokes components since they can provide a relatively small value for the mismatch factor and can reach reasonably high energy levels by interactions with the pump radiation and/or the first Stokes components.

When we take in account **n** components we have a set of **2n** equations, where each one has **2n-4** terms, 2 of them corresponding to the usual Raman cascade process and **2(n-3)** to the parametric processes. Thus for a choice of seven components (4 Stokes, 2 anti-Stokes and the pump radiation) we will have 14 first order differential equations to be solved simultaneously, each of them with 2 cascade terms and 8 parametric terms.

In chapter five a procedure to reduce the number of parametric terms will be given, it considers not only the energy in the components which take part in the process but the coherence length as well.

To integrate the system of first-order differential equations we used a variable-order variable-step Adams method. A description of this numerical method and its practical implementation can be found in G.Hall and J.M.Watt (1976). Figure 3.6 shows the plot of the solution for the set of equations for a pump wavelength of 575 nm and a temperature of 298°K. A beam waist of 200 μm was used, it makes the cell length (40cm) slightly shorter than the confocal parameter. This figure shows the behaviour of the Stokes and pump components when only the pump signal is injected in the Raman medium. In the first diagram, figure 3.6a, only the cascade processes were assumed to occur in the Raman medium and in figure 3.6b we included all the parametric processes which can occur for the components choice we have. The gas pressure in figure 3.6a and 3.6b is 30 atmospheres and the effect of the parametric interaction can be seen more clearly when one reduces the gas dispersion through the gas pressure reduction, figure 3.6c.

As we can notice in this diagram (diagram 3.6c) components which have not even reached the threshold for a certainvalue of Raman exponential gain when only the cascade interaction was considered (diagram 3.6a), now show a reasonable conversion efficiency for the same value of Raman exponential gain. While the low order Stokes components have their maximum conversion efficiency considerably reduced.

Figure 3.7 shows the case when the first Stokes component does not grow from the noise level but from an input seed radiation with a pulse energy equal to 1.0% of the input pump pulse energy, all the other components are still growing from the noise background. The general behaviour of the components does not change very much compared with the Raman oscillator situation, since new high order Stokes components appear and the low order Stokes components have their peak conversion efficiency reduced. However, this second effect is less strong in the amplifier case as we may see from diagram 3.7c where the gas pressure is only 10 atmospheres. The peak conversion efficiency for the first Stokes does not differ very much from the one obtained with the cascade processes only, although after this peak has been reached a strong parametric interaction takes place and the whole conversion efficiency for this component is greatly reduced. The vertical axis in diagrams 3.6 and 3.7 shows the quantum efficiency for each

Figure 3.6. Numerical solution for the set of equations given in terms of quantum conversion as a function of the Raman exponential gain for the Raman oscillator.

(□) pump,

(×) S1,

(+) S2,

(▽) S3,

(△) S4.

(a) only cascade terms, (b) cascade and parametric terms at 30 atmospherics pressure, (c) cascade and parametric terms at 10 atmospheres pressure.

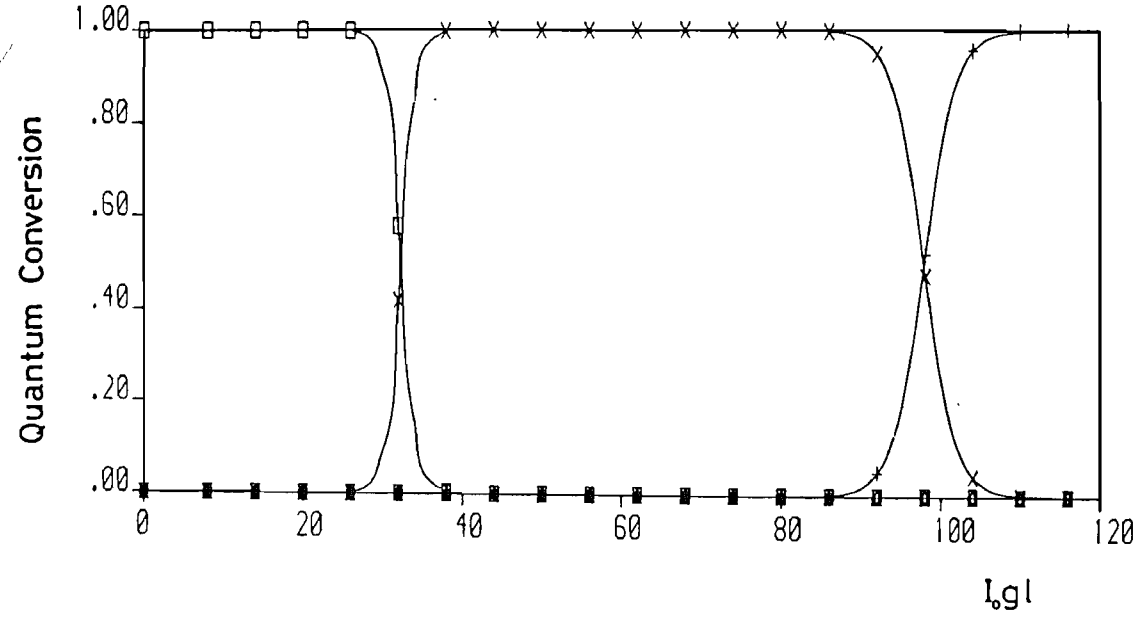
Quantum Conversion
1.00
.80
.60
.40
.20
.00
0
20
40
60
80
100
120
I₀gl

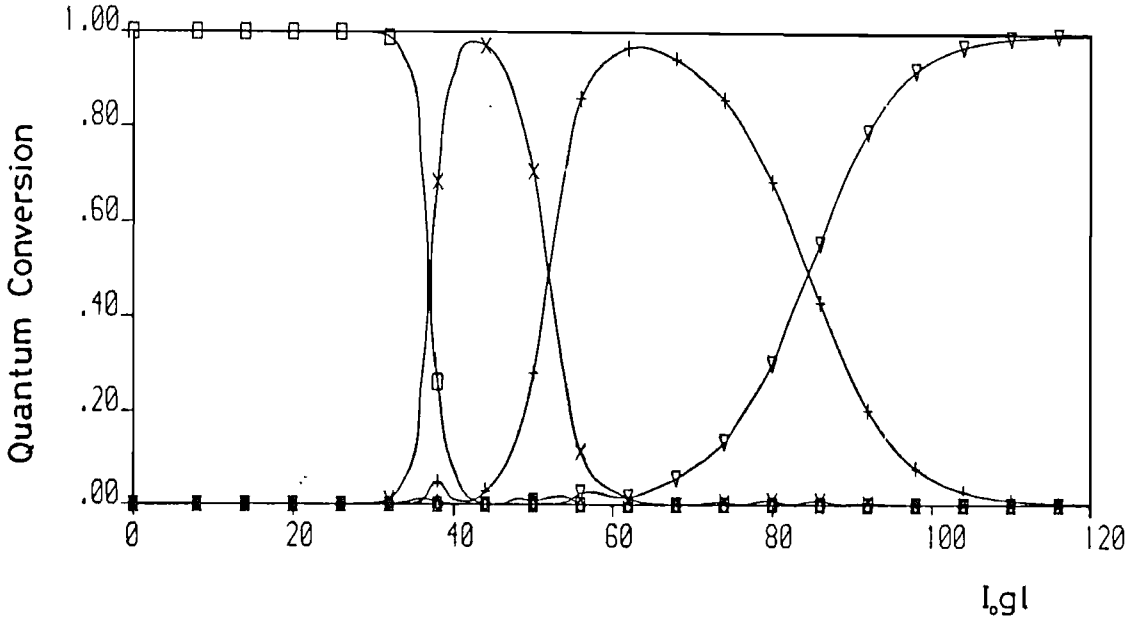
Quantum Conversion
1.00
.80
.60
.40
.20
.00
0
20
40
60
80
100
120
I₀gl

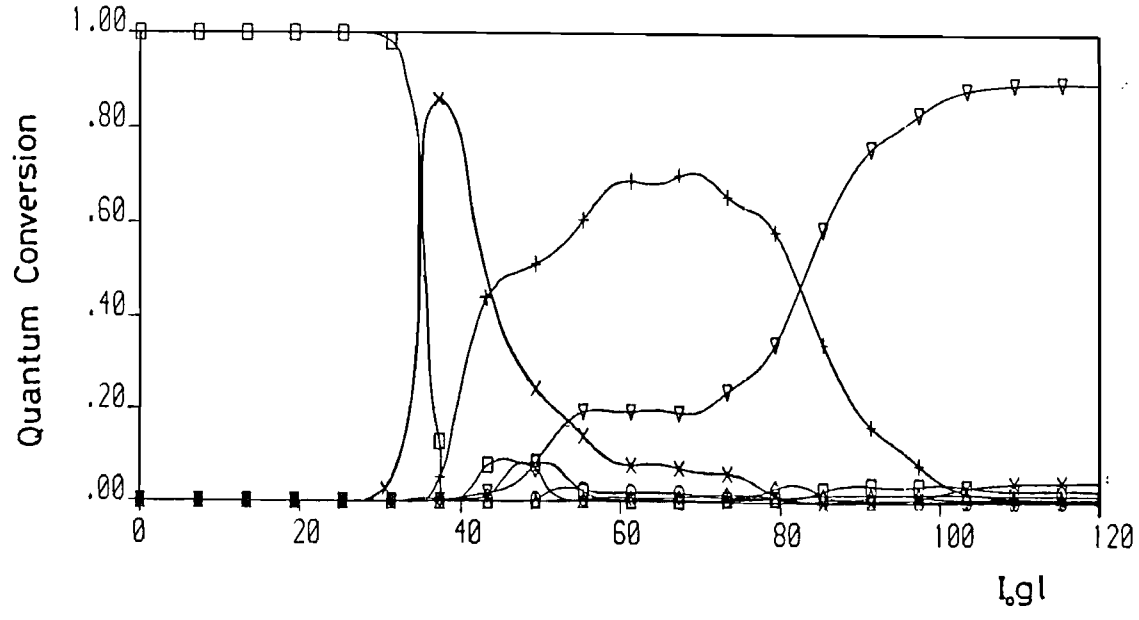
Quantum Conversion
1.00
.80
.60
.40
.20
.00
0
20
40
60
80
100
120
I₀gl

Figure 3.6.

Figure 3.7. Numerical solution for the set of equation given in terms of quantum conversion as a function of the Raman exponential gain for Raman amplifier.

(□) pump,

(×) S1,

(+) S2,

(▽) S3,

(△) S4.

(a) only cascade terms, (b) cascade and parametric terms at 30 atmospherics pressure, (c) cascade and parametric terms at 10 amospheres pressure.

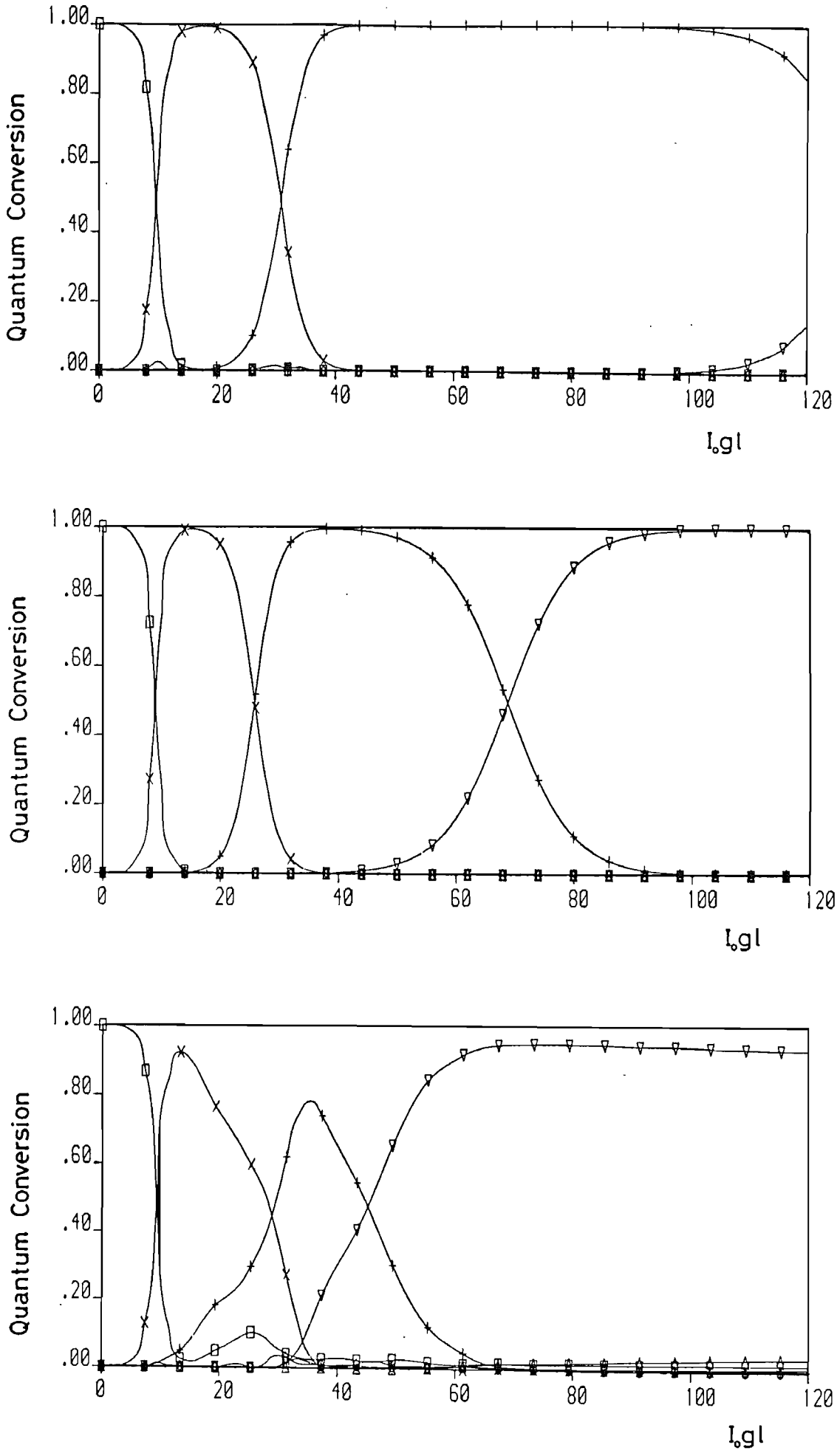

Figure 3.7.

component in relation to the pump, defined as,

$$\eta_i=(n_i\lambda_i/n_o\lambda_o).A_i^2$$

and in the horizontal axis we have the variable ζ defined as,

$$\zeta=2\zeta_f=2gzI_o \qquad 3.91$$

in order to allow the results be presented in terms of the energy gain coefficient rather than the field gain coefficient.

The main characteristic of these solutions is the 100% quantum conversion efficiency reached by each component when we have the cascade processes only or when the gas pressure is high enough to avoid any efficient energy transfer among the components via parametric processes, which means that for a given range of ζ it is possible to have essentially only a single Stokes component generated within a specific region of the Raman cell. The reason for this is the assumption of a uniform intensity distribution and a flat top pulse shape in the time domain, thus there is no part of the intensity profile at the edge of the beam cross section or at the begining of the pulse shape that is not used in the non linear interaction.

The analytical expression for the first Stokes intensity derived in section 3.3.3 is compared with the numerical solution in figure 3.8. On the vertical axis we have the quantum conversion efficiency η_i and on the horizontal axis the Raman exponetial gain. As we expected we notice a better agreement between the analytical and numerical solution in the case of the Raman amplifier, when the first Stokes does not start from the noise level but from an input pulse energy very much higher than the initial pulse energy for any other Stokes component. Figure 3.8a shows the analytical and the numerical calculation when only the cascade processes are considered, the agreement is quite good, even for the oscillator case where the assumption that the pump beam changes energy only with the first Stokes beam is not quite fullfilled. In figure 3.8b and 3.8c the parametric processes were included in the numerical calculation, and a gas pressure of 20 atmospheres was used. In this case the assumption does not hold any more and there is strong coupling between the pump beam and the other Stokes components, but for the

Figure 3.8. Comparison between the analytical and numerical solution for the first Stokes component under several circumstances. The solutions are given in terms of quantum conversion as a function of the Raman exponential gain. (a) only cascade terms in a Raman oscillator and Raman amplifier cells, (b) cascade and parametric terms in a Raman oscillator cell, (c) cascade and parametric terms in a Raman amplifier cell. The * indicates the analytical solution and the continuous line the numerical solution.

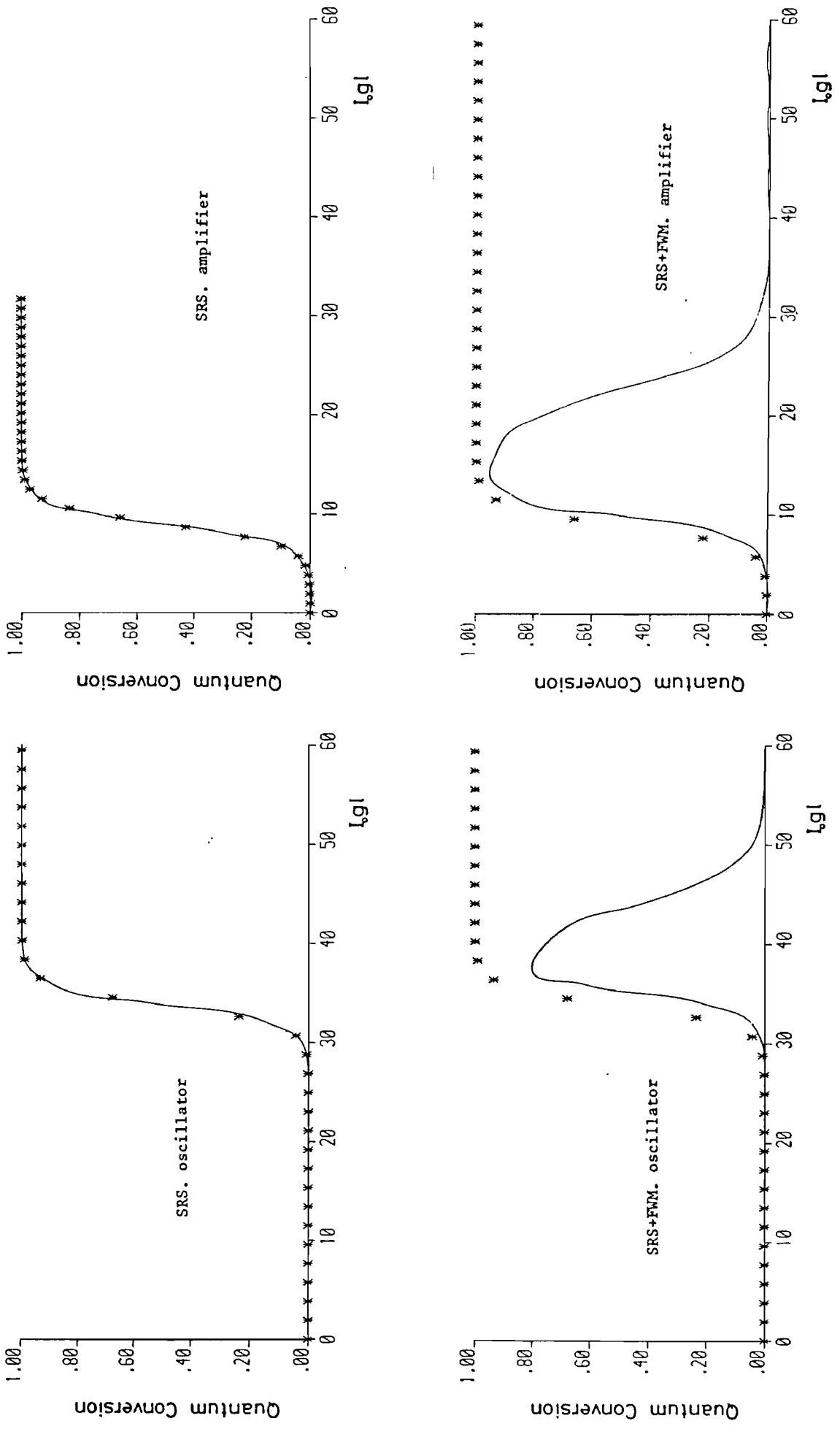
SRS. amplifier
SRS+FWM. amplifier
SRS. oscillator
SRS+FWM. oscillator
Quantum Conversion
1gI
1.00
.80
.60
.40
.20
.00
0
10
20
30
40
50
60

Figure 3.8.

case of the Ramam amplifier we still have a reasonable agreement between the numerical and analytical calculation up to the point where the first Stokes reaches its maximum conversion efficiency. As a conclusion we may say that the expression 3.67 describes very well the Stokes intensity behaviour for the case of the Raman oscillator and Raman amplifier when only the cascade processes are assumed to occur and it shows a fairly good agreement for the case of the Raman amplifier with the parametric processes included.

3.4.1.1 The ζ variable

The ζ variable expressed as a function of the energy gain coefficient may be interpreted as the first Stokes gain coefficient for an undepleted pump beam, i.e. the first Stokes energy level is not enough to drive appreciable energy out from the pump beam. This generalized coordinate ζ as defined in equation 3.89 or 3.91 is a product of the pump intensity, the interaction length and the Raman gain coefficient. However, due to the normalization used, ζ can not be interpreted as a variation of any of these parameters directly, except the interaction length. Thus the horizontal axis in figures 3.6,3.7 and 3.8 correspond to the position inside the Raman cell. If we need the solution to be presented in terms of the input pump energy, the set of equations must be solved a number of times, each one corresponding to a given input pump pulse energy. The reasons for this are the initial conditions, the parametric terms and the attenuation factor. The initial electric field value and other electric field strengths in the program are normalized in relation to the input pump electric field strength, not in relation to ζ. Thus at each run with a new input pump energy a new normalized input electric field needs to be used. For the parametric processes we have the factor $\Delta k\zeta/I_0 g$, then if ζ variation is interpreted as an input pump pulse energy variation the value of I_0 can not be kept constant any more. The same happens with the attenuation coefficient, $\alpha/I_0 g$. The value of α should be changed on each run so that we keep the attenuation independent of the input pump energy.

For a pure Raman process in a lossless medium, ζ can be interpreted as the variation of z, g or I_0 independently, however for the general case, when the parametric processes and attenuation are included it is not possible to assume that any more. As for the

normalized initial value for the electric field we can say that its variation for the superfluorescent amplifier has a very small influence on the component intensity since their values are given by saturation. But the same cannot be said for the four wave mixing mismatch factor and the attenuation coefficient, because they play a very important role in determining the maximum value of intensity which a given component can reach.

3.4.2 **Beam radial profile**

The total photon conversion obtained from the solution of the set of equations 3.85 → 3.86 does not agree with most of the stimulated Raman scattering experimental results. Usually several Stokes shifts are observed simultaneously at the output of the Raman cell and the conversion efficiency is not 100%. One explanation for this behaviour is the non uniform intensity distribution along the pump beam cross section. For a given pump pulse energy we may have a large range of intensities over the beam cross section. The central part of the beam, due to its higher intensity, will generate SRS initially, while the rest of the beam energy will go through the medium without being converted to Stokes radiation. When the interaction length is long enough to produce a reasonable Raman exponential gain these intensities located off axis will start to show SRS as well, but the long interaction length will affect the central part of the beam differently, since for this part of the beam profile the SRS process has started already and any increase in the Raman exponential gain may start a secondary cascade process where the first Stokes beam starts to generate a higher order Stokes shift. Thus as the observation plane is moved along the Raman gain region or the pump pulse energy is increased, we may have a high order Stokes shift being generated at the central part of the pump pulse beam surrounded by a ring of a lower order Stokes component. So the possibility of multiple simultaneous Stokes shift coming out of the Raman cell is quite likely for a beam where there is a transverse profile. Then, as we usually have a Gaussian-like beam profile for the pump radiation we should take into account this intensity variation in our numerical calculation.

The pulse power for a given Stokes component can written as,

$$P_i = \int_S I_i dA \qquad 3.92$$

where S is the beam cross section area. from equation 3.87 we may relate the i_{th} component intensity to the intensity of the undepleted pump pulse,.

$$I_i/I_0^0 = (n_i/n_0)A_i^2 \qquad 3.93$$

and then the expression 3.92 can be written in terms of the undepleted pump intensity,

$$P_i = (n_i/n_0) \int_S A_i^2 . I_0^0 . dA \qquad 3.94$$

For an axially symmetrical beam we have

$$P_i = (2\pi n_i/n_0) \int_0^\infty A_i^2 . I_0^0(r) r dr \qquad 3.95$$

The values for A_i are obtained from the solution of the set of equations 3.86→3.87 as a function of ζ, thus we must do the change of variables

$$r \rightarrow \zeta \qquad 3.96$$

Let's assume a Gaussian variation for the undepleted pump beam intensity along the radius of the cross section.

$$I_0^0(r) = I_M . \exp(-2r^2/w_0^2) \qquad 3.97$$

Where w_0 is the beam spot size defined as the distance from the beam axis where the electric field strength is reduced to 1/e of its maximum value. The first derivative of the expression 3.97 in relation to r can be written as,

$$dI_0^0(r)/dr = -(4r/w_0^2) . I_0^0(r) \qquad 3.98$$

By substituting this derivative into expression 3.95 we have the pulse power for a general component given by,

$$P_i = (\pi w_0^2 n_i / 2n_0) \int_0^{I_M} A_i^2 . d[I_0^0(r)] \qquad 3.99$$

The pulse power for the undepleted pump can be worked out from,

$$P_0^0 = \int_0^{2\pi} \int_0^{\infty} I_M . \exp(-2r^2/w_0^2) . r dr d\theta \qquad 3.100$$

and by solving the integral we have,

$$P_0^0 = (\pi w_0^2/2) . I_M \qquad 3.101$$

Thus we may define th ratio of the power of the i_{th} component to the power of the undepleted pump pulse,

$$R_i = P_i / P_0^0 \qquad 3.102$$

and by using expression 3. 99 and 3.101 we can express R_i as

$$R_i = [n_i/(n_0 I_M)] . \int_0^{I_M} A_i^2 . d[I_0^0(r)] \qquad 3.103$$

The whole expression 3.103 can be put in terms of the variable ζ by making use of the relation 3.89,

$$R_i(\zeta) = [n_i/(n_0 \zeta)] \int_0^{\zeta} A_i^2(\zeta') d\zeta' \qquad 3.104$$

Then using the solution A_i for the set of equations for the plane wave aproximation we may take into account the radial intensity variation of the beam via expression 3.104. To make the numerical model closer to the experimental conditions the pulse shape in time should be considered as well. In the next section we show the mathematical formulation for this aproach.

3.4.4 **Pulse shape**

The pulse energy for a given component may be obtained through the integral,

$$\epsilon_i = \int_{-\infty}^{\infty} P_i dt \qquad 3.105$$

and using the normalized power defined in equation 3.102 we may express the pulse energy for a general component as a function of the pulse power of the undepleted pump beam.

$$\epsilon_i = \int_{-\infty}^{\infty} R_i(\zeta).P_0^0(t).dt \qquad 3.106$$

At this point we must carry out another change of variables. The whole integral should be expressed in terms of ζ since the solution for the plane wave case is given as a function of this variable. This change can be performed via the transformation,

$$t \rightarrow P_0^0(t) \qquad 3.107$$

and the first derivative of $P_0^0(t)$ in relation to t being indicated by $[P_0^0(t)]'$,

$$[P_0^0(t)\quad]' = dP_0^0(t)/dt \qquad 3.108$$

By substituting expression 3.108 into equation 3.106 we have

$$\epsilon_i = \int_{-\infty}^{\infty} R_i(\zeta).\frac{P_0^0(t)}{[P_0^0(t)]'}.d[P_0^0(t)] \qquad 3.109$$

but as $P_0^0(t)$ can be related to ζ we may work out the energy for a given conponent as a function of ζ. Letus assume a gaussian time dependence for the undepleted pump power,

$$P_0^0(t) = P_M.\exp(-t^2/\tau_0^2) \qquad 3.110$$

where P_M is the peak power for the undepleted pulse beam and τ_0 is given by,

$$\tau_0 = 0.6T_{FWHM} \qquad 3.111$$

and T_{FWHM} is the full width half maximum time. The first derivative of $P_0^0(t)$ in relation to t can be expressed as,

$$[P_0^0(t)]' = (-2/\tau_0).\sqrt{\ln[P_M/P_0^0(t)]}\ .\ P_0^0(t) \qquad 3.112$$

and by substituting expression 3.112 into the integral 3.109 we find,

$$\epsilon_i = \tau_0 \int_0^{P_M} R_i / \sqrt{\ln[P_M/P_0^0(t)]}.d[P_0^0(t)] \qquad 3.113$$

If we use the relationship

$$\zeta' = g.I_0^0(t).z = S.P_0^0(t) \qquad 3.114$$

$$\zeta = S.P_M \qquad 3.115$$

we can write the integral 3.113 as a function of ζ only,

$$\epsilon_i(\zeta) = (\tau_0/S_0).\int_0^{\zeta} R_i(\zeta')/\sqrt{[\ln(\zeta/\zeta')]}.d\zeta' \qquad 3.116$$

or

$$\epsilon_i(\zeta) = (0.6T_{FWHM}/S) \int_0^{\zeta} R_i(\zeta')/\sqrt{\ln(\zeta/\zeta')}.d\zeta' \qquad 3.117$$

The energy into the undepleted pump pulse can be worked out through expressions 3.105 and 3.110,

$$\epsilon_0^0 = (0.5\sqrt{\pi}/\sqrt{\ln 2}).T_{FWHM}.P_M \simeq 1.06.T_{FWHM}.P_M \qquad 3.118$$

thus the expression 3.117 can be normalized to the input pump pulse energy ϵ_0^0,

$$\epsilon_{in}(\zeta) = (0.56/\zeta) \int_0^{\zeta} [R_i(\zeta')/\sqrt{\ln(\zeta/\zeta')}].d\zeta' \qquad 3.119$$

and the quantum conversion efficiency can be obtained for the i_{th} component,

$$\eta_i(\zeta) = (0.56/\zeta).(\lambda_i/\lambda_0) \int_0^{\zeta} [R_i(\zeta')/\sqrt{\ln(\zeta/\zeta')}].d\zeta' \qquad 3.120$$

We considered another pulse shape in time for the beam as well. Firstly a simple flat top shape defined as,

Figure 3.9. Numerical solution for the pump and Stokes componentes when a gaussian dependence in space and time is assumed for the pump pulse. The curves are given in terms of pulse energy as a function of the Raman exponential gain. under several situations.

(□) pump,

(×) S1,

(+) S2,

(▽) S3,

(△) S4.

(a_1) Raman oscillator with only cascade terms,

(a_2) Raman amplifier with only cascade terms,

(b_1) Raman oscillator with cascade terms, same as a_1 but vertically expanded and without the curve for the pump component,

(b_2) Raman oscillator with cascade and parametric terms at 30 atmospheres pressure,

(b_3) Raman oscillator with cascade and parametric terms at 10 atmospheres pressure,

(c_1) Raman amplifier with only cascade terms, same as a_2 but vertically expanded and without the curve for the pump component,

(c_2) Raman amplifier with cascade and parametric terms at 30atmospheres pressure,

(c_3) Raman amplifer with cascade and parametric terms at 10 atmospheres pressure.

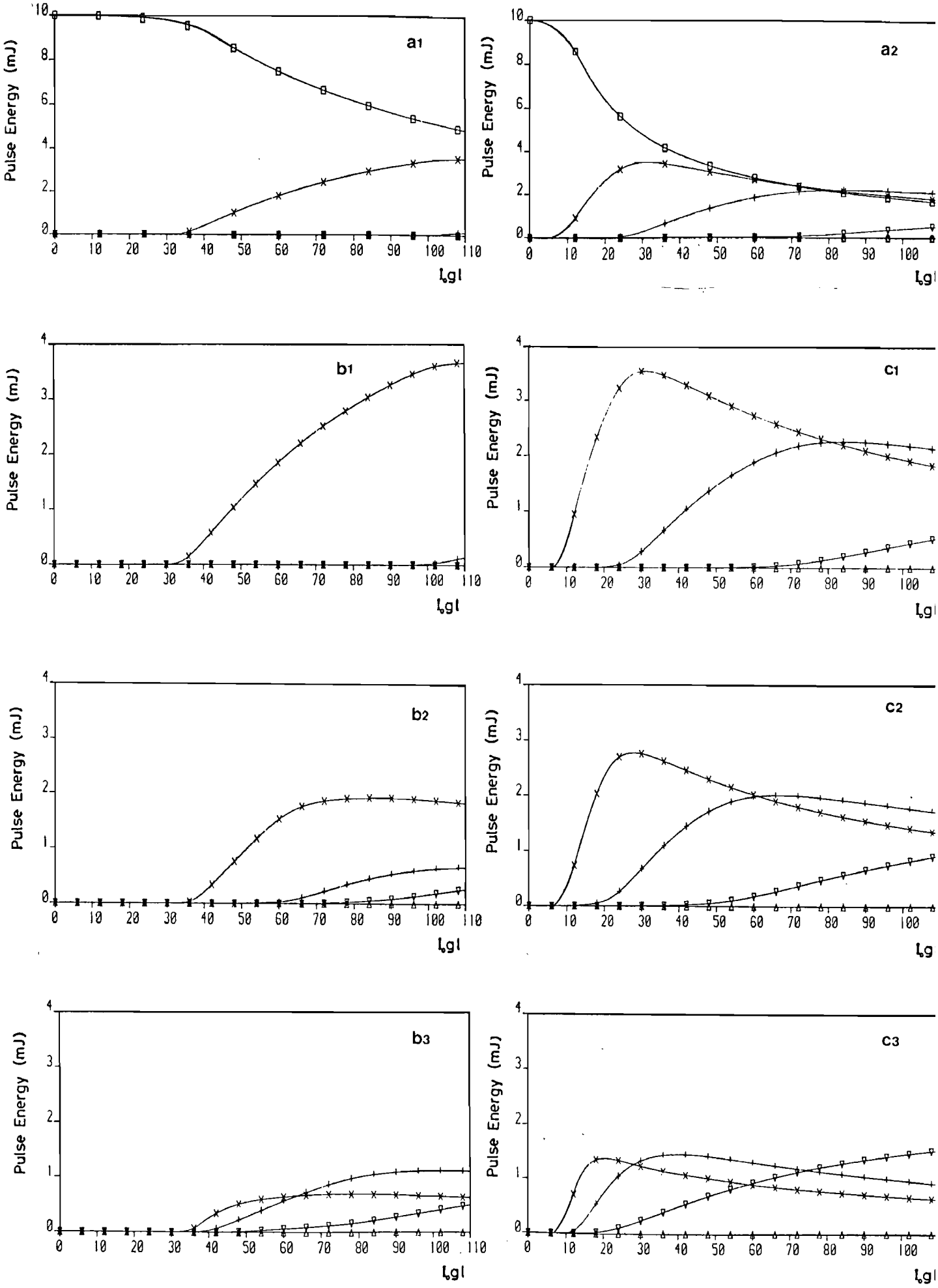

Figure 3.9

$$P_0^0(t) = P_M \qquad 0 < t < \tau_0 \qquad 3.121$$

$$P_0^0(t) = 0 \qquad 0 > t > \tau_0$$

$$T_{FWHM} = \tau_0$$

and a linearized pulse shape, where the raise and fall intensity variation time were aproximated by straight lines,

$$P_0^0(t) = (P_M/T_1).t \qquad 0 < t < T_1 \qquad 3.122$$

$$P_0^0(t) = P_M \qquad T_1 < t < T_2$$

$$P_0^0(t) = -P_M.t/(T_3-T_2) + P_M.T_3/(T_3-T_2) \qquad T_2 < t < T_3$$

$$P_0^0(t) = 0 \qquad 0 > t > T_3$$

and $T_{FWHM} = (T_3+T_2-T_1)/2$

Following the same procedure used to get 3.120 we can have the pulse energy for a general component as a function of ζ for these pulse shapes. The table I summarizes the results.

The figure 3.9 shows the solution for the set of equations with the intensity variation along the beam radius and accounting for the pulse shape as well. As we may notice we do not get a single Stokes component at any region of the Raman exponential gain and the maximum value each component can reach is greatly reduced.

The main conclusion from these numerical solutions are that nonuniforme spatial profile, the time behaviour and the inclusion of parametric terms lead to: (1) At one gain plane more than one Stokes component can be present with significant intensity. (2) Energy conversion efficiency to a particular Stokes component is reduced

Table I	Energy in the i_{th} component	Energy of the undepleted pump	Normalized energy for the i_{th} component
Gaussian profile	$(0.6.T_{TWHM}/S)\int_0^{\zeta} R_i(\zeta')/\sqrt{\ln(\zeta/\zeta')}.d\zeta'$	$1.06T_{FWHM}\ P_M$	$(0.56/\zeta)\int_0^{\zeta} R_i(\zeta')/\sqrt{\ln(\zeta/\zeta')}.d\zeta'$
Flat top	$T_{FWHM}.P_M.R_i(\zeta)$	$T_{FWHM}.P_M$	$R_i(\zeta)$
Linearized profile	$(T_1+T_3-T_2)P_M/\zeta^2.\int_0^{\zeta} R_i(\zeta')\zeta'd\zeta' + R_i(\zeta)P_M.(T_2-T_1)$	$T_{FWHM}.P_M$	$(T_1+T_3-T_2)/(T_{FWHM}.\zeta^2).\int_0^{\zeta} R_i(\zeta')\zeta'd\zeta' + R_i(\zeta).(T_2-T_1)/T_{FWHM}$

CHAPTER FOUR

Tunable SRS in Unguided and Guided Systems

4.1 Introduction

In this chapter we present the experimental results of SRS in high pressure cells (unguided system) and in capillary waveguides using the dye laser described in chapter two of this work as a pump source. The tunability and the power threshold for the Stokes components were investigated under several experimental conditions, aiming to characterize the perfomance of this tunable pump source both for guided and unguided cells and to find the influence of the spatial quality of the pump beam on the conversion efficiency and on the power threshold for SRS.

In most of the arrangements discussed in this chapter the pump source for the dye laser was the XeCl 308 nm wavelength excimer laser. However, for the experiments using the dye laser with phase conjugation we used the second harmonic of the Nd:YAG laser as the pump source. The characteristics of the output pulse of the dye laser do not change very much under the two different pumping systems, the pulse width becoming slightly larger for excimer laser pumping and the output radiation wavelength shifted to the red region.

	λ_p=308 nm	λ_p=532 nm
τ(FWHM)	14 nsec	12 nsec
λ_{peak}	580 nm	560 nm

Apart from these differences all the other parameters remain essentially the same, noteably dye laser pulse energy, ASE level and spatial quality of the dye output beam.

The basic experimental arrangement is the dye laser oscillator followed by amplifier stages. The spatial characteristics

of the output beam are controlled by using pinholes placed between the dye cells.

In figure 4.1 we show schematically the dye laser arrangement to produce SRS in an unguided medium. The scheme shown in figure 4.1a produces a dye output energy of 12 mJ in a 14 nsec FWHM pulse. A significant amount of this pulse energy is ASE generated inside the last dye amplifier stage and amplification of the ASE generated in the previous stage. The output beam has a roughly triangular shape, typical of the transversely pumped dye laser. In this set up no further attempt was made to improve the spatial quality of the output beam or to reduce the ASE level, apart from a careful dye oscillator design and the shaping of the excited pump region. The dye amplifier cells were put as far as possible from each other but we still observed a strong ASE signal due to the high gain in the second dye amplifier stage. This scheme will be referred to as scheme I

To improve the characteristics of this arrangement we need some additional devices like inter-stage pinholes as was discussed in chapter two. The scheme shown in figure 4.1b has a very much better output beam in terms of spatial intensity profile. No saturatable absorber was used in this arrangement because the power required to reach SRS threshold in an unguided medium is relatively high and the ASE pulse energy level is not enough to reach this value by itself. The dye laser output pulse energy is 5.7 mJ for this arrangement and this scheme will be referred to in the discussion of the experimental results as scheme II.

In figure 4.2 we have the schemes used to generate SRS in a guided system. Due to the necessity of a reasonably good coupling into the capillary waveguide we need to use pinholes in order to improve the dye output beam spatial quality. The scheme shown in figure 4.2a produces the lowest pulse energy of all the arrangements because in this set up we are looking for a very good spatial beam quality. With a 1.2 mm diameter aperture placed after the last amplifier stage we obtained a diffraction limited beam.

The arrangement shown in figure 4.2b is similar to the one which produced a diffraction limited beam but in this case we used a larger aperture diameter to get more output energy in the dye laser pulse. The beam still looks very spatially symmetrical with a Gaussian-like intensity profile, but it is not diffraction limited

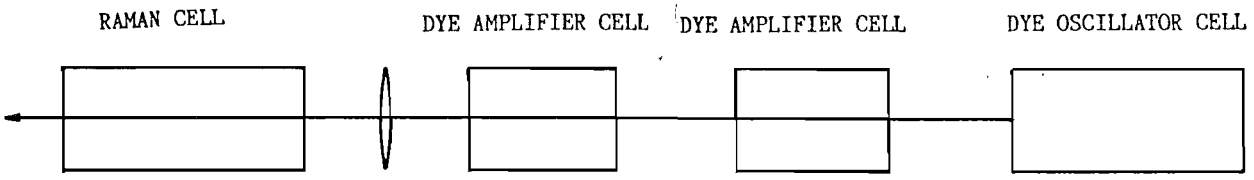

(a)

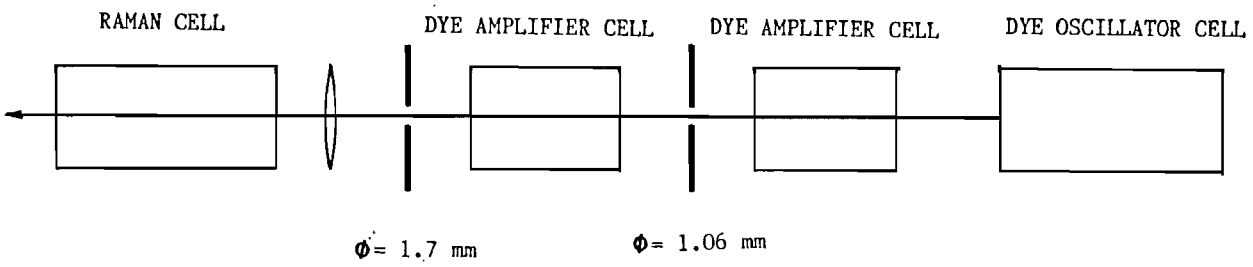

(b)

Figure 4.1. Experimental arrangement to generate Stimulated Raman Scattering in an unguided medium. (a) Scheme I, dye laser producing maximum output pulse energy, (b) Scheme II, dye laser producing a beam with a symmetrical spatial intensity profile over the cross section.

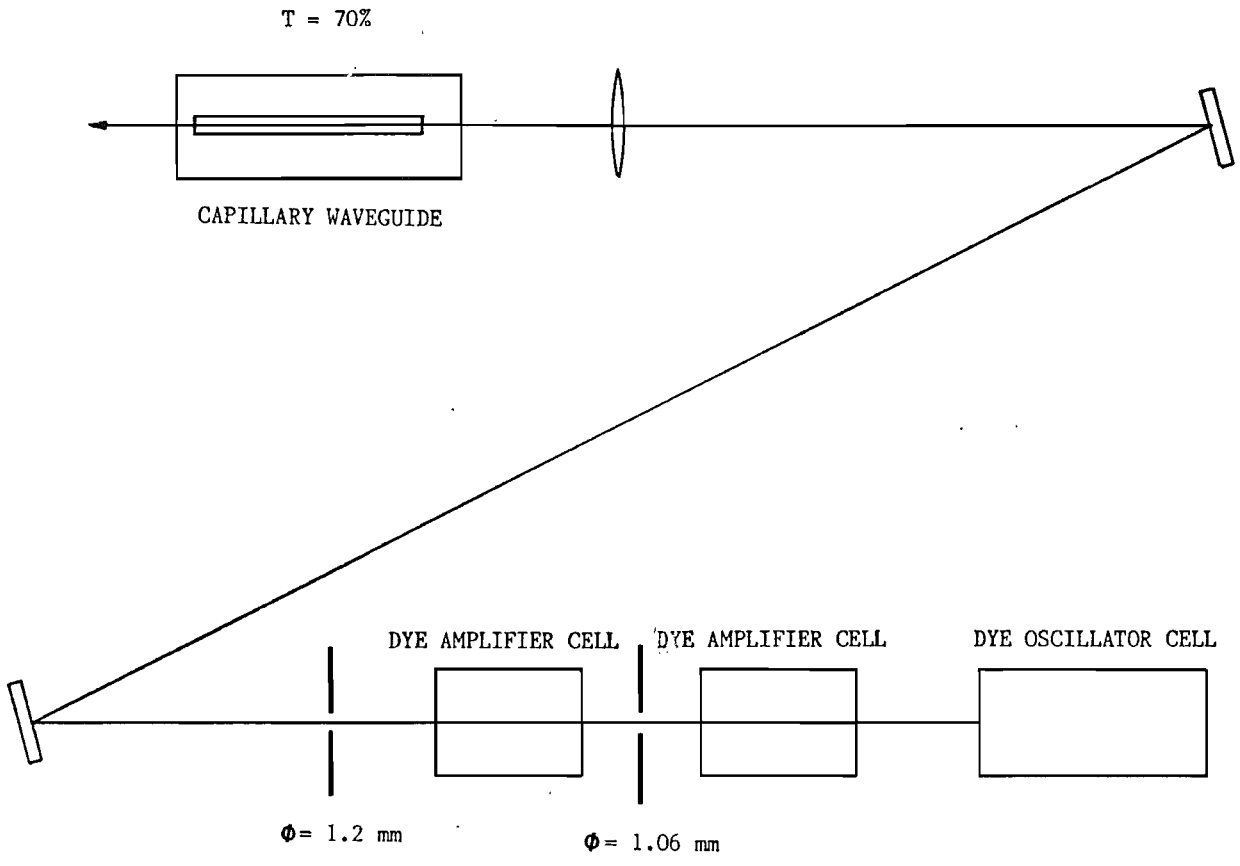

(a)

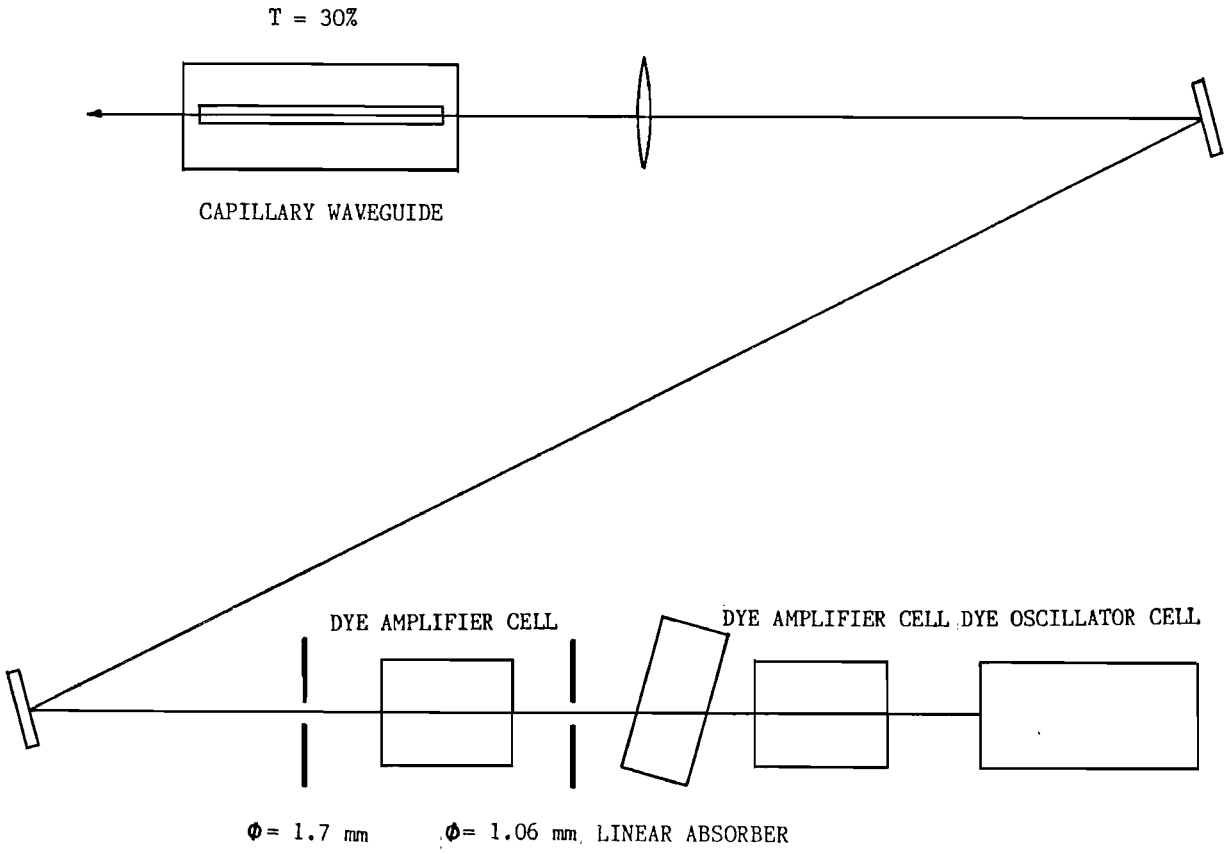

(b)

Figure 4.2. Experimental arrangement to generate Stimulated Raman Scattering in capillary waveguide.(a) Scheme III, dye laser producing a diffraction limited beam, (b) scheme IV, dye laser producing a nearly diffraction limited beam.

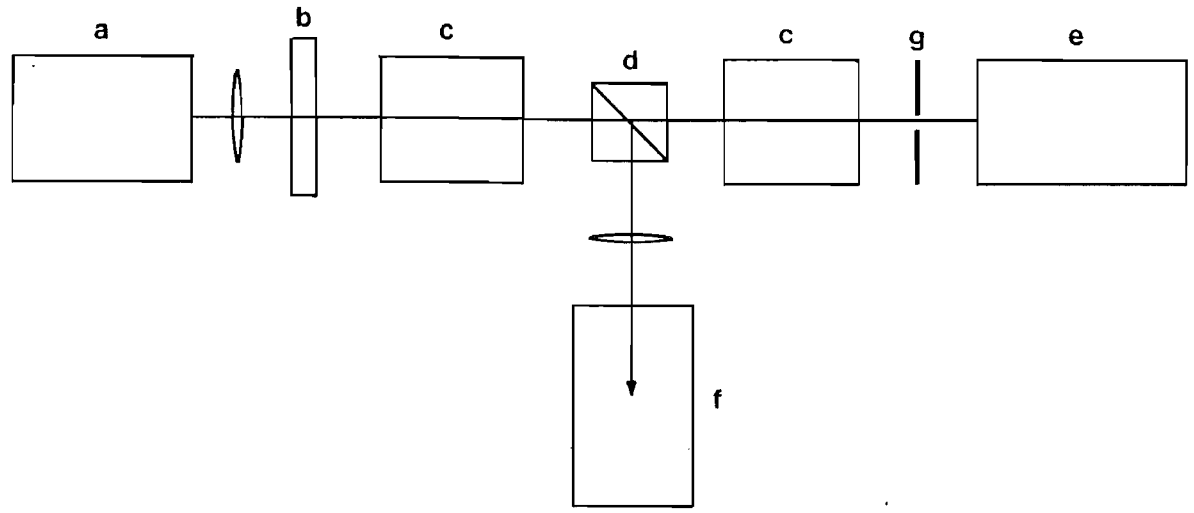

(a)

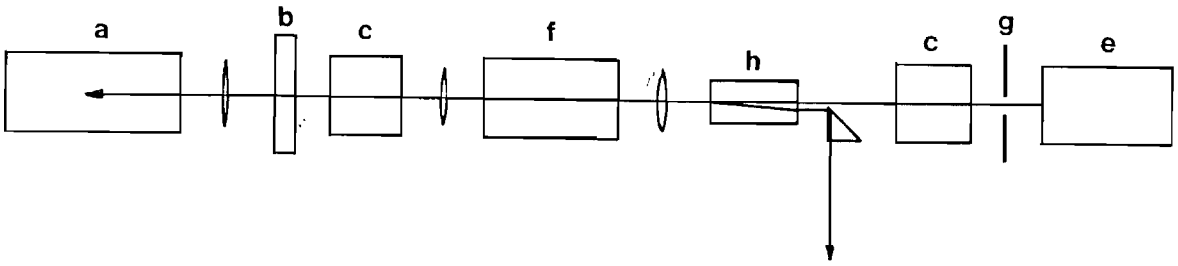

(b)

Figure 4.3. Experimental arrangement to generate Stimulated Raman Scattering using a dye laser with phase conjugation. (A) Raman cell placed outside the dye laser–phase conjugation system, (B) Raman cell placed inside the dye laser–phase conjugation system.

(a) phase conjugation cell,

(b) quarter wave plate,

(c) dye amplifier cell,

(d) polarizer,

(e) dye oscillator,

(f) Raman cell,

(g) aperture ϕ=400μm

(h) calcite.

any more. In both arrangements shown in figure 4.2 we use the linear and saturated absorbers because the pulse power necessary to reach SRS threshold is quite low due to the long interaction length provided by the guiding structure and in this case the ASE pulse energy, without the absorbers, is enough to generate its own SRS. This is especially important when the dye laser is being operated at an extreme of the dye tuning range when the molecules in the second amplifier stage are not depleted by the incoming beam from the first amplifier and dye oscillator and consequently the ASE level becomes even stronger than the dye laser pulse itself. These two schemes shown in figure 4.2a and 4.2b will be referred to as scheme III and scheme IV respectively.

Finally in figure 4.3 we show schematically the arrangement for the dye laser with phase conjugation. One of the advantages of this set up is the low ASE level. Only the laser signal is phase conjugated since the ASE signal has a very broad linewidth and consequently this component does not reach the threshold for SBS in acetone. The scheme shown in figure 4.3a has been used with a slight modification, that is when the Raman cell is placed inbetween the dye amplifier cells (fig 4.3b), where the pulse energy is higher than the pulse energy at the output of the usual arrangement. Experiments done with this modification showed very good results for SRS generation in terms of a higher number of anti-Stokes and Stokes components observed at the output. The perfomance of this set up was particularly good when a capillary waveguide was used as a Raman cell. Because the low gain in the first dye amplifier guarantees a good spatial beam quality and consequently a good transmission is obtainned in the capillary waveguide. Then, the beam coming back from the Brillouin cell is refocused inside the capillary, reproducing the good transmission of the forward beam. However, due to the the difficulties in measuring the actual energy going into the Raman cell when one uses this scheme we report only the results obtained with the set up shown in figure 4.3a. This scheme will be referred to as scheme V.

4.2 SRS pulse power in guided and unguided media

The term "threshold" used in this section and throughout this work does not indicate the usual situation in a resonator when

the gain provided by the active medium should balance the round trip losses for a given oscillator mode. For the stimulated Raman scattering process the term corresponds to an output energy for the generated Stokes component which is just enough to produce detectable depletion of the pump pulse.

For a pump pulse width of the order of 10 nanoseconds the Stokes energy at threshold is about 1 to 10 microjoules per pulse. This happens for a Raman gain exponent (G_{th}) of between 20 and 30. The pump pulse energy threshold is given in terms of this Raman gain exponent necessary to reach that observable energy in the Stokes pulse.

If we consider the situation where the Stokes component is growing from the noise background, the initial pulse energy for this Stokes component can be worked out by using expression 3.75 for a pump pulse width τ.

$$E_n = \tau.h.\nu.d\nu \qquad 4.1$$

Thus the Raman exponential gain necessary in order to reach the SRS threshold will be,

$$G_{th} = \ln(E_{th}) - \ln(\tau h\nu d\nu) \qquad 4.2$$

Where E_{th} is the Stokes pulse energy at threshold.

Due to the logaritnmic dependence the value of G_{th} does not change very much when parameters like Stokes pulse energy at threshold or pump wavelength are changed. In table I we have the values for G_{th} under two different Stokes energies and a wide variation of the pump wavelength and we may observe that the maximum variation of G_{th} is less than 50%.

TABLE I – Values for G_{th}

	E_{th}= 1 μJ	E_{th}= 10 μJ
λ= 100 nm	22.1	24.4
λ= 500 nm	23.7	26.0
λ= 1.0 μm	24.4	26.7
λ= 10 μm	26.7	29.0

When we consider the situation of the noise background level for a guiding structure through expression 3.77, we observe that it leads to a modification smaller than 0.4 in the value of G_{th}.

The exact value of the bandwidth is not critical either, since from expression 4.2 we can see that a ten times variation in a 0.3 cm^{-1} bandwidth (value assumed for the figures shown on table I) produces a variation smaller than 10% in the value of G_{th}.

With our experimental conditions the pump wavelength is 575nm and we are going to take the value of G_{th} as 25 in all our calculations.

4.2.1 Expressions for threshold pump power in unguided medium

The Raman exponential gain (G_U) along the axis for an unguided system with a length L can be written as

$$G_U = g\int_{-L/2}^{+L/2} \frac{2P}{\pi w^2(z)}\,dz \qquad 4.3$$

Where g is the Raman gain coefficient , P is the pump pulse peak power and w(z) the pump beam spot size at a position z inside the cell. By using the expression for the spot size [Kogelnik and Li (1966)]

$$w^2(z) = w_0^2[1+(2z/b)^2] \qquad 4.4$$

$$b = 2\pi w_0^2/\lambda \qquad 4.5$$

where w_0 is the beam waist formed in the center of the cell, we have:

$$G_u = g(4P/\lambda)\tan^{-1}(L/b) \qquad 4.6$$

However, in the general case when a configuration approximating to the tight focusing one is considered, the expression 4.3 is not valid any longer, since in this case the Stokes radiation is going to have an average gain which includes the off-axis intensity and consequently the overall Raman exponential gain is smaller than the one predicted by expression 4.3. The Raman exponential gain for this case is given by [Cotter et al (1975)]

$$G_u = [(\lambda_s/\lambda_p).\tan^{-1}(L/b)].(\sqrt{4Pg/\lambda_s}).(\sqrt{4Pg/\lambda_s}-2) \qquad 4.7$$

Where λ_s and λ_p are the wavelength for first Stokes and pump radiation respectively.

For the case of a Raman amplifier expression 4.3 can still be used since the confocal parameter is usually a few times the cell length. The Stokes average can be well approximated by the maximum gain since the stokes spot size can be made very small relative to the pump spot size.

The pump pulse power necessary in order to reach the Raman exponential gain G_{th} is defined as the Raman threshold power for this pumping system.

$$P_{th} = (\lambda_s/4g).\{1 + [1 + G_{th}\lambda_p/(\lambda_s\tan^{-1}(L/b))]^{1/2}\}^2 \qquad 4.8$$

The minimum value for P_{th} is reached in the tight focussing situation, i.e. when the beam waist size is made very small giving a confocal parameter very much shorter than the cell length.

$$P_{th|min} = (\lambda_s/4g).\{1 + [1 + 2G_{th}\lambda_p/(\pi\lambda_s)]^{1/2}\}^2 \qquad 4.9$$

As can be observed from expression 4.9 the value for the

pump pulse power necessary to reach Raman threshold depends only on the pump laser wavelength and the Raman medium gain coefficient. The dependence on the beam waist size disappears when one assumes tight focussing.

From expression 4.8 one can see that there is no optimum value for the pump beam waist which minimizes the pump power threshold, since the whole expression decreases monotonically with $\tan^{-1}(L/b)$, consequently any value for the beam waist size which produces $b \ll L$ will lead to the minimum threshold pump power. This happens because an increase in the pump intensity due to a reduction in beam waist size is compensated by an increase in the diffraction of the beam which decreases the interaction length. The overall result is that P_{th} does not depend on the pump focussing geometry any more. The general behaviour of the threshold pump power is shown in figure 4.4.

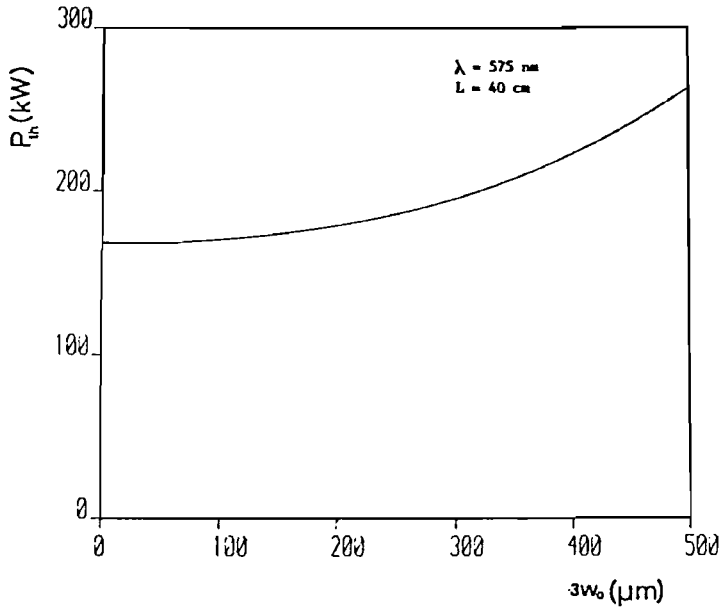

Figure 4.4. Calculated value for the SRS threshold pump pulse power as a function of the beam waist size inside the Raman cell.

4.2.2 Expression for threshold pump power in a guided medium

The Raman exponential gain for a guided structure can be written as

$$G_g = g \int_0^L \frac{P.\exp(-\alpha z)}{\pi w_0^2}.\, dz \qquad 4.10$$

Where g is the Raman gain coefficient, P is the pump pulse peak power at the input and w_0 is the beam waist formed at the capillary entrance. α is the energy transmission loss coefficient for the pump radiation and it is proportional to λ^2/a^3 where a is the capillary radius. In chapter 5 this parameter will be more completely defined. Solving the integral in expression 4.10 we have,

$$G_g = \frac{P}{\pi w_0^2}.g.L_{eff} \qquad 4.11$$

where

$$L_{eff} = [1 - \exp(-\alpha L)]/\alpha \qquad 4.12$$

Where L is the actual capillary length and L_{eff} the equivalent capillary length in which the pump radiation intensity can be regarded as a constant.

Unlike the usual tight focussing system, the guiding structure can prevent the beam from diffracting by reflecting it back into the Raman medium repeatedly. The overall Raman exponential gain now depends on the laser pulse power, the Raman gain coefficient and the cell geometry, i.e. the length of the waveguide and its internal diameter. By using this device we can make the spot size as small as we need to, increasing the beam intensity in the Raman medium without affecting the interaction length, since the diffraction losses are less important and the interaction length is defined basically by the attenuation of the propagating radiation.

From the capillary mode discussion carried out in chapter five of this work we can see that the EH_{11} mode will produce the lowest transmission loss coefficient. The condition for optimizing the coupling between a TEM_{00} mode and the EH_{11} mode is given by Abrams (1972), that is, the input radiation beam waist should be 2/3 of the capillary radius. With this condition satisfied we will have only 2% loss in the coupling $TEM_{00} \rightarrow EH_{11}$.

The pump pulse threshold power can be obtained from expression 4.11 by setting $G_g = G_{th}$ in that expression:

$$P_{th} = G_{th}\pi w_o^2/(gL_{eff}) \qquad 4.13$$

In this case, unlike the unguided case, the minimum pump pulse threshold power is not reached for a very small value of w_o. Since w_o is related to **a** , a small value of w_o will lead to a small capillary radius and consequently an increase in the beam propagating losses. As the transmission loss coefficient is proportional to w_o^{-3}, it will overcome the increase in the pump intensity due to the spot size reduction and the whole expression 4.13 will follow a w_o^{-1} law:

$$P_{th} = \pi\alpha G_{th} w_o^2/g = KG_{th}/(w_o g) \qquad 4.14$$

Where K is a constant which depends on the refractive index of the capillary waveguide.

At the other extreme, a large beam waist does not reduce the pump pulse threshold power in either the unguided or guided case, because the beam intensity drops down and the whole Raman exponential gain becomes very small. Expression 4.13 can be written in this situation as proportional to w_o^2.

$$P_{th} = \pi G_{th} w_o^2/(gL) \qquad 4.15$$

Thus we expect that for the capillary waveguide we will have a specific value of pump beam waist and capillary radius which give a minimum SRS threshold power.

Analytically, assuming $\alpha = K.\lambda^2/a^3$ and using expressions 4.11 and 4.12 with $w_o = (2/3)a$ we find the capillary radius which produces the maximum value of G_g for a fixed length L.

$$dG_g/da = 0$$

$$\exp(\alpha L) = [1 + 3\alpha L] \qquad 4.16$$

From 4.16, if L is chosen, we can determine the capillary diameter which produces the minimum threshold.The general variation of pump pulse threshold power with beam waist size for a guided medium is shown in figure 4.5. One can notice the minimum value reached and the reduction in the P_{th} value when compared with the

results for the unguided system shown in figure 4.4.

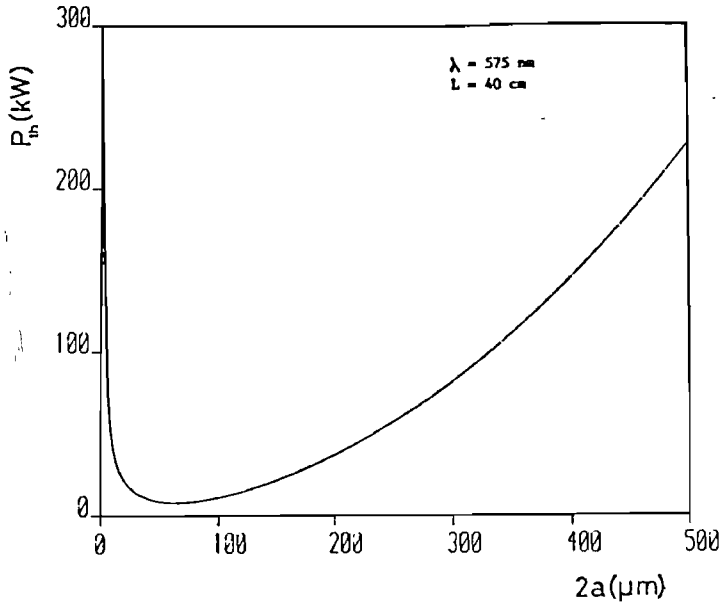

Figure 4.5. Calculated value for SRS threshold pump pulse power in hydrogen at 30 atmosphere pressure as a function of the capillary diameter.

Table II summarizes the pump pulse threshold power expressions for unguided and guided media under different beam waist and attenuation conditions.

Table II

	b≃L	b≪L	b≫L
Unguided	$\frac{\lambda_s}{4g}\cdot\frac{(1+(1+G_{th}(\lambda_p/\lambda_s))^{1/2})^2}{\tan^{-1}(L/b)}$	$\frac{\lambda_p G_{th}}{2\pi g}$	$\frac{\pi w_o^2 G_{th}}{2gL}$
Guided	$\frac{\pi w_o^2 G_{th}}{gL_{eff}}$	$\frac{\pi w_o^2 \alpha G_{th}}{g}$	$\frac{\pi w_o^2 G_{th}}{2gL}$

4.3 Experimental results

In figure 4.6 we have the plot of first Stokes pulse energy against pump pulse energy for scheme I shown in figure 4.1a. The gas pressure was kept at 30 atmospheres during all the measurements and a lens of 20 cm focal length focussed the pump beam inside the unguided medium. The beam waist formed inside the high pressure gas cell is smaller than 60 μm which for a 40 cm cell length will correspond to $b \ll L$ or $\tan^{-1}(L/b) \simeq \pi/2$ for the pump beam.

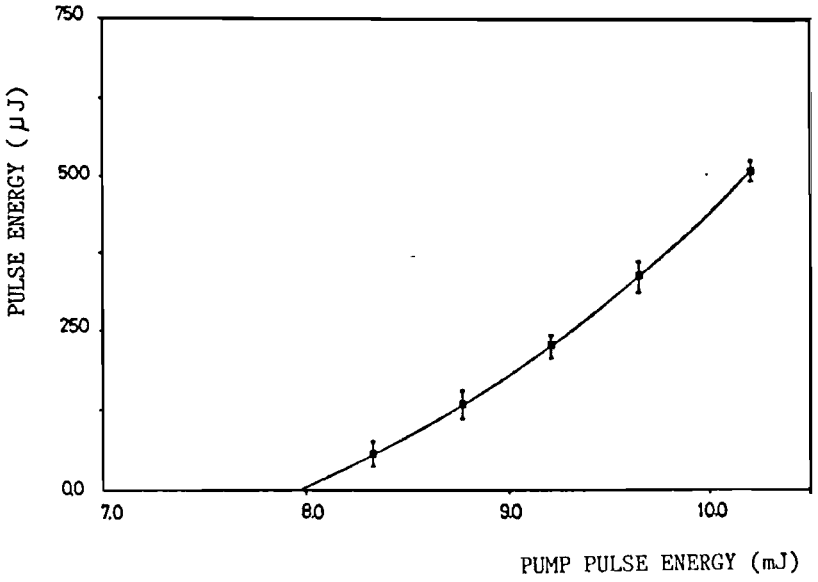

Figure 4.6. Experimental value for the first Stokes pulse energy in hydrogen at 30 atmosphere pressure in an unguided cell using scheme I.

The maximum conversion efficiency we had for this set up was 6.6% of pump photons into first Stokes photons for a pump pulse energy of 10.2 mJ inside the Raman cell.

All the Stokes and pump energy referred to in this section are values inside the cell. To make the correction from the measured values outside the cell we assumed a 4% transmission loss per surface for all the wavelengths.

The pump pulse threshold energy was measured to be 7.9 mJ which is about 3.5 times the theoretically predicted value for the pump pulse threshold energy for a diffraction limited beam of 2.3mJ.

The arrangement I does not have saturated or linear absorbers and the ASE pulse energy is 1 mJ at the extreme of the dye

laser tuning range. With the absorbers placed between the amplifier stages this energy is reduced to 200 μJ while the pump pulse energy at the peak of the tuning range is reduced from 12.0 mJ to 11.2 mJ at the output of the dye laser.

No second stokes was detected inside the range of the pyroelectric energy meter and a very faint first anti-Stokes was visually observed.

In order to improve the spatial characteristics of the dye laser beam a 1.06 mm diameter aperture was placed between the amplifier stages and a pin-hole with a 1.7 mm diameter was placed after the last amplifier, at the dye laser output. This is the scheme II shown in figure 4.1b. The output pulse energy was reduced to 5.7 mJ, 4.8 mJ inside the Raman cell.

The maximum conversion efficiency into the first Stokes component was 0.7% and the pump pulse threshold energy at 575 nm wavelength is 3.2 mJ. By reducing the diameter of the pinhole placed at the dye output from 1.7 to 1.2 mm, the pump pulse threshold energy is reduced to 2.4 mJ which agrees quite well with the theoretically predicted value.

The good agreement between the measured and estimated pump pulse threshold energy is due to the beam coming out of the dye laser being almost diffraction limited. However, the dye laser output pulse energy with this condition is 3.8 mJ, 3.2 inside the Raman cell, which is very close to the SRS threshold for the first stokes and a very small conversion efficiency was observed with this arrangement.

In figure 4.2 we show the schemes III and IV which were used to generate SRS in capillary waveguide. The dye laser pulse energy available inside the Raman cell was smaller in this case due to the 75% reflectivity mirror used to get the right distance between the dye laser output and the capillary entrance in order to match the two waists. However this was not a problem since in all situations we had a Raman exponential gain inside the guided medium enough to go beyond the peak of maximum conversion efficiency for the first Stokes radiation.

In figure 4.7 we show the output pulse energy for several stokes components against the input pump pulse energy, at 20 atmospheres gas pressure. For scheme IV up to the third Stokes shift was measured and three anti-Stokes components were observed. The

Figure 4.7. Experimental values of pulse energy for several Stokes components as a function of the input pump pulse energy in hydrogen at 20 atmosphere pressure using scheme IV.

(Δ) 1st Stokes

( ) 2nd Stokes

(+) 3rd Stokes

Figure 4.8. Calculated SRS threshold pump pulse energy versus pump wavelength.

(1) Unguided cell, scheme I,

(2) capillary waveguide with 70% transmission, scheme IV,

(3) capillary waveguide with 30% transmission, scheme III

(4) capillary waveguide with theorectical transmission 94%.

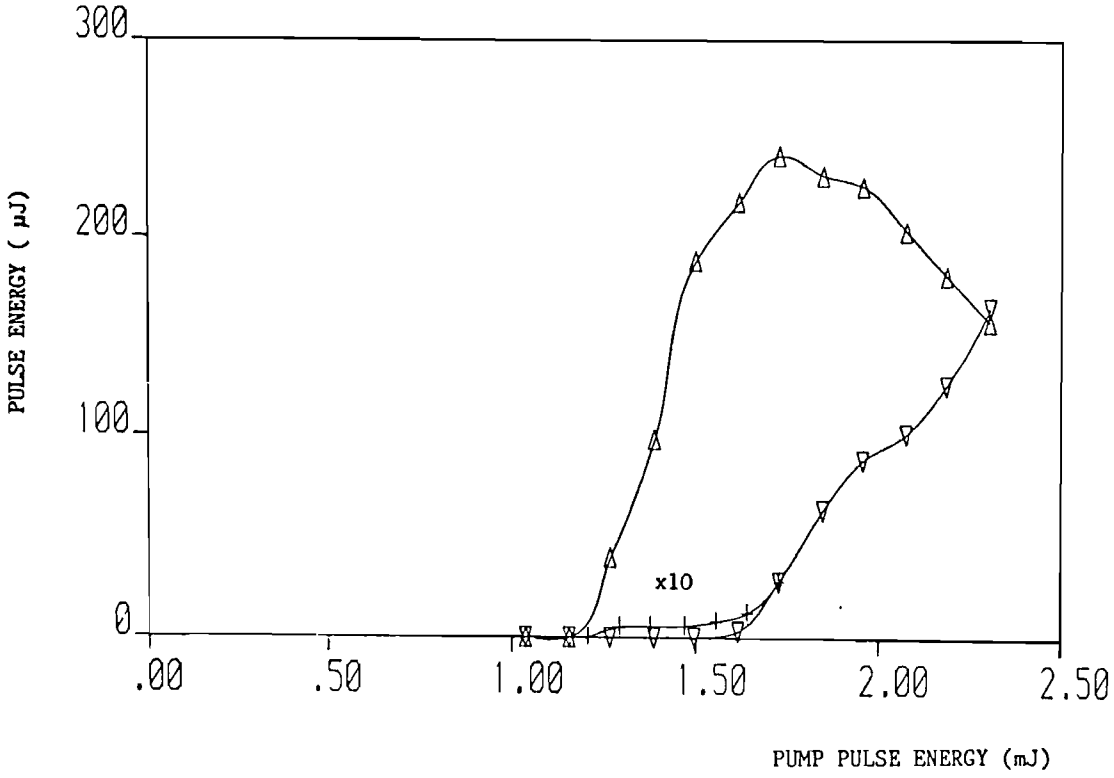

Figure 4.7

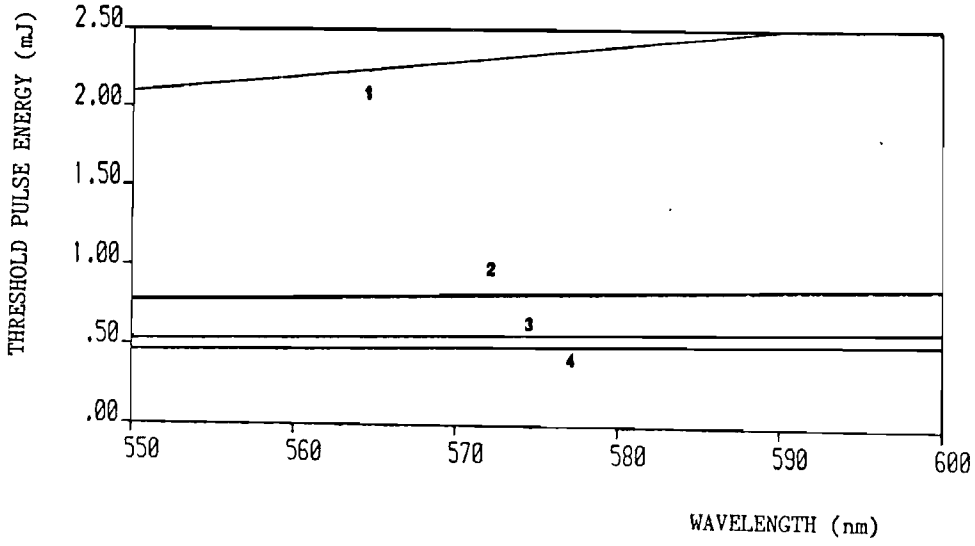

Figure 4.8

peak conversion efficiency for the first Stokes is 18% and it occurs for a pump pulse energy of 1.76 mJ. The maximum conversion efficiency for the second Stokes radiation is 13.7% at the maximum available pump pulse energy,that is 2.3 mJ. The pump energy transmission for this capillary is 30% and the energy threshold was measured to be 1.1 mJ, this value is higher than the theoretically predicted energy threshold 0.83 mJ.

Scheme III produce a SRS threshold pump pulse energy of 0.63 mJ, which is quite close the theoretically predicted value of 0.57 mJ for a 70% capillary transmission. The conversion efficiencies for all the Stokes components were higher than for scheme IV. The experimental results are summarized in table III, together with the pump energy at which they occurred.

Finally in figure 4.3 we have scheme V which shows the dye laser using phase conjugation. The maximum pump energy available inside the unguided Raman cell was 3.4 mJ in a 5 nsec FWHM pulse. The conversion efficiency for the first Stokes radiation at this pump energy was 8.4% and the pump pulse threshold energy 2.7 mJ, which is about 3 times the theoretically predicted value.

Table III summarizes the results obtained for each arrangement in terms of Stokes pulse energy.

The values indicated inside brackets correspond to the input pump pulse energy expressed in mJ at which the Stokes pulse conversion was measured. The schemes I, II and V refer to experiments with unguided systems and III and IV with capillary a waveguide.

We may observe that for a guided system the peak of the conversion efficiency is reached for a relatively small value of pump pulse energy due to the increse of the Raman exponential gain by the capillary waveguide. However, the amount of pump energy transfered into the Stokes components is not very high, even at the peak of the conversion efficiency. This happens due to the effect of the parametric processes occurring inside the Raman medium which tend to distribute the pump energy among various Stokes components simultaneously rather than concentrate this energy in a single Stokes component. This effect will be discussed in detail in the next chapter.

One conclusion about the results shown in table III is that the capillary waveguide is able to generate high order stokes shifts

Table III

Stokes pulse energy and conversion efficiency

Scheme	1st Stokes Energy(μj) η(%)	2nd Stokes Energy(μJ) η(%)	3rd Stokes Energy(μJ) η(%)
I	511 (10.2) 6.6	-	-
II	25 (4.8) 0.7	-	-
III	150 (0.8) 25	160 (2.0) 15.3	8.5 (2.0) 1.5
IV	240 (1.74) 18	165 (2.3) 13.7	2.7 (1.76) 0.5
V	218 (3.4) 8.4	-	-

Table IV

Pump pulse threshold energy for 1st Stokes

Scheme	Experimental value (mJ)	Theory (mJO
I	7.9	2.3
II	3.2	2.3
III	0.63	0.57
IV	1.1	0.83
V	2.7 (5ns pulse)	0.83 (5ns pulse)

requiring a relatively low pump pulse energy but the energy in each Stokes pulse is not so high as the one obtained for an unguided cell. From figure 4.6 we can illustrate this point, with a pump pulse energy of 10.2 mJ the first Stokes pulse energy is still going up.

The pump pulse threshold energy results for the first Stokes component are summarized in table IV.

For the unguided system the experimental pump pulse threshold energy drops down as we improve the beam spatial profile, as we can see when a 1.2mm diameteraperture is used (scheme III) giving an experimental value for the threshold energy very close to the predicted one.

For the capillary waveguide we have a similar result since a non diffraction limited beam implies a higher transmission loss. Besides that there is another factor to explain the increase of the pump pulse threshold energy,in that the non symmetry of the pump beam profile leads to a bad coupling to the EH_{11} mode. The actual energy being injected inside the capillary is smaller than the value we considered available to produce the SRS inside the cell.

The pump pulse energy threshold is plotted against the pump wavelength in figure 4.8. Expression 4.8 was used to work out the threshold energy for an unguided system and expression 4.13 was used for a capillary waveguide. For the guided system the calculation was carried out for three diferent capillary transmissions, 30% and 70% and the theoretical one, 94%.

4.3 **SRS tuning range - experimental results**

Figure 4.9 shows schematically the arrangement used to measure the SRS tuning range. The Stokes components and the unused pump that come out at the the end of the Raman cell are separated spatially through a set of dispersion prisms. The pulse energy for each component was measured using a pyroelectric energy meter and each energy value presented in this section is an average of ten pulses. A beam splitter sent part of the beam energy into a monochromator and the relative pulse energy at a particular wavelength is measured with a photodiode and a set of neutral density filters. The electrical signal from the photodiode is sent to a box-car averager where the relative value of the pulse energy is

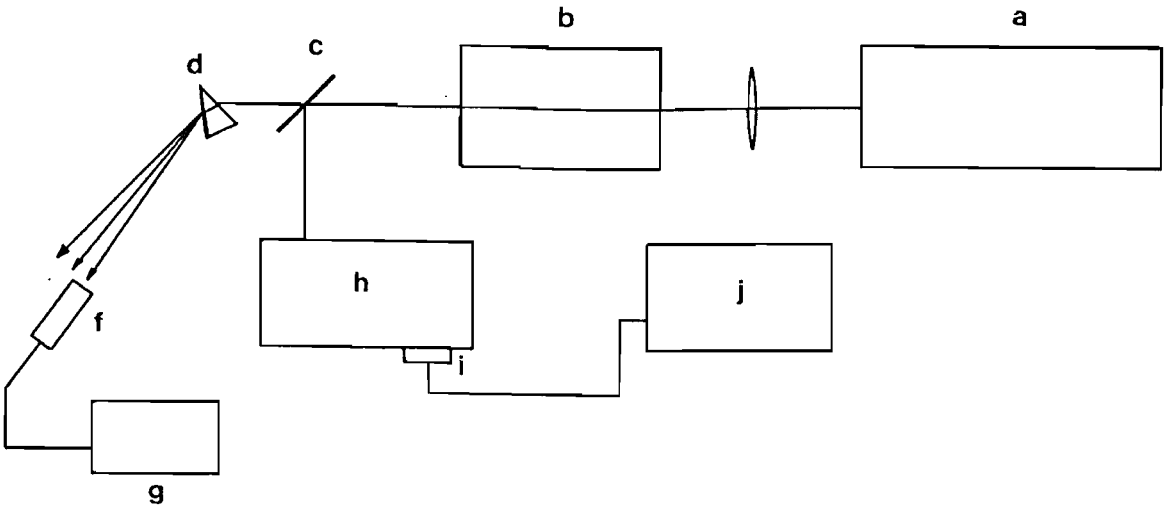

Figure 4.9. Experimental set up to measure the tuning range for Stokes components.(a) Dye laser, (b) Raman cell, (c) Beam spliter, (d) dispersion prism, (f) pyroelectric detector,(g) energy meter, (h) monochromator, (i) detector and (j) box car averager.

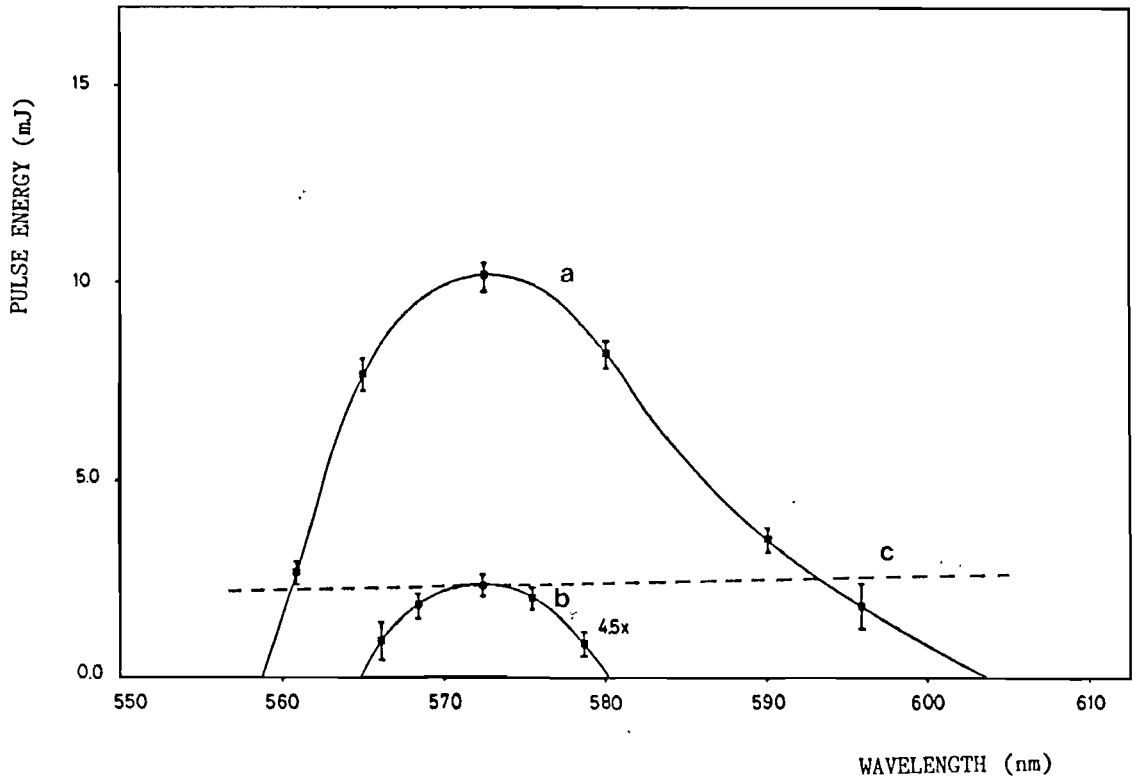

Figure4.10. Tuning range for dye laser and first Stokes component, scheme I. (a) dye laser tunig range, (b) first Stokes tuning range and (c) calculation for the SRS threshold pulse energy.

measured for each value of the pump wavelength. The wavelengths for the Stokes and anti-Stokes components were calculated using the Raman frequency shift for hydrogen.

With scheme I we have available a large amount of pulse energy, but due to the non uniformity of the pulse intensity profile a very high pump pulse energy was necessary to reach the threshold for the first Stokes. This fact leads to a narrow SRS tuning range for this scheme as we may observe from figure 4.10. The first Stokes radiation was obtained only near the center of the dye laser tuning range and its tuning range was from 739 nm to 764 nm with the maximum conversion effciency at 751 nm, a tuning range of 443 cm^{-1} in terms of wavenumbers. This arrangement has an ASE pulse energy of 1 mJ outside the Raman cell, no attempt was made to reduce this value since it is not enough to reach the SRS threshold in a unguided system.

In figure 4.11 we have the tuning range for the arrangement II. In this case the pump energy inside the Raman cell is 4.8 mJ due to apertures used between the amplifier stages. The tuning range for the first Stokes is smaller than the previous one, 343 cm^{-1}, from a wavelength of 743 nm to 762 nm. The difference in the tuning range is not very big in spite of the pulse energy in this case being almost half of the pulse energy produced in the arrangement I. This is due mainly to the reduction in the pump pulse threshold energy for the scheme II.

With these two schemes no high order Stokes shift was observed inside the range of sensitivy of the pyroelectric energy meter and first anti-Stokes was detected visually only.

The SRS tuning range for the capillary waveguide is shown in figure 4.12. Scheme IV is used and the pump transmission in the capillary is 30%. By the time this experiment was done the dye pump pulse energy was about 4.0 mJ, corresponding to 1.9 mJ inside the Raman cell, just before the capillary entrance. The tuning range for first Stokes component is shown in figure 4.13a and it goes from 741.4 nm to 769.4 nm wavelength, or 490 cm^{-1}. The shape of the tuning range curve is quite flat at the center due to first Stokes energy depletion in this region of the tuning range curve when the cascade transference of energy S1 → S2 becomes more efficient. The output pulse energy for the first stokes radiation remains around 200μJ during most of the tuning range.

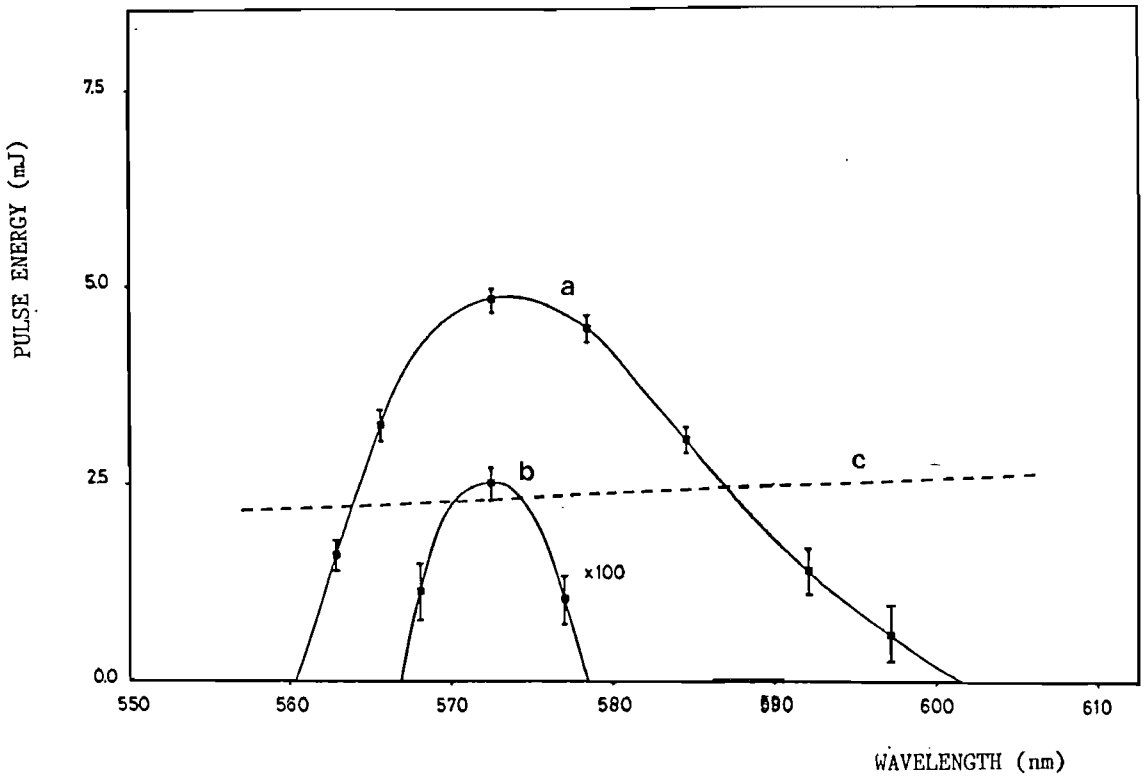

Figure 4.11. Tuning range for dye laser and first Stokes component, scheme II.

(a) dye laser tuning range,

(b) first Stokes tuning range

(c) calculation for the SRS threshold pulse energy.

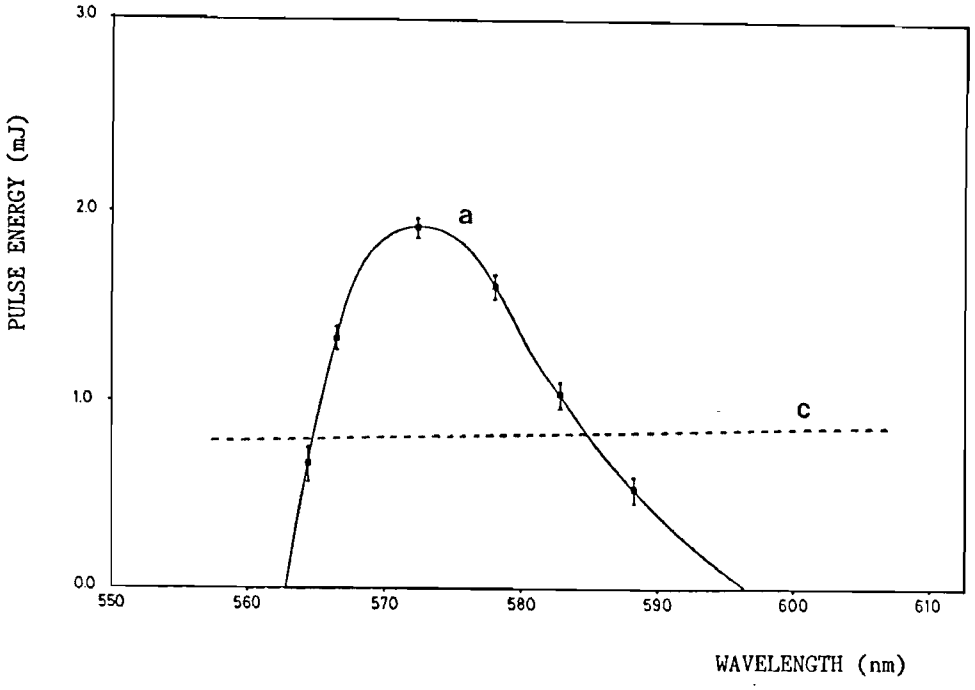

Figure 4.12. Experimental value for the dye laser tunig range, scheme IV.

(a) dye laser tuning range

(b) calculated SRS threshold pump pulse energy for a waveguide , scheme IV.

The curve for the tuning range of the second stokes shift is shown in figure 4.13b. The tuning range goes from 1.080 μm to 1.127μm, which corresponds to 386 cm^{-1} in terms of wavenumbers. The maximum conversion efficiency occurs at 1.1 μm. The error bars shown in these tuning range plots represent the maximum deviation of pulse energy from the averaged ten pulses.

The curve for the third Stokes is shown in figure 4.13c. As the pulse energy for this component was too weak we decided to remove the saturated absorber at the dye output in order to get some more pulse pump pulse energy. The pump pulse energy was then 2.3 mJ inside the Raman cell with an ASE level of 400 μJ. The tuning range for the third Stokes shift is from 1.98 μm to 2.064 μm, or 200 cm^{-1} and the peak of conversion efficiency occurs at 2.2μm.

Finally in figure 4.14 we have the tuning range for the first and second anti-Stokes. The AS1 tuning range goes from 459.5nm to 469.6nm, which corresponds to 468 cm^{-1} with the peak for conversion effciency at 463.5nm. For the second anti-Stokes the tuning range is from 386.5nm to 392 nm, 363 cm^{-1} in wavenumbers.

In all the tuning range plots for the dye laser radiation we added the curve for the first Stokes threshold pump pulse energy against the pump wavelength so that we can work out the maximum expected tuning range for the Stokes component in term of wavenumbers. The tuning range of the stokes components gets close to the maximum value when the experimental pump pulse energy threshold for the first Stokes gets close to the predicted value. Table V shows the value of Δ_{max} for configuration I,II and IV and the actual value for the tuning range obtained in the experiments.

TABLE V

Tuning range in wavenumbers (cm^{-1})

	Δ_{max}	Δ_{S1}	Δ_{S2}	Δ_{S3}	Δ_{AS1}	Δ_{AS2}
I	945	443	-	-	-	-
II	691	343	-	-	-	-
IV	589	490	386	200	468	363

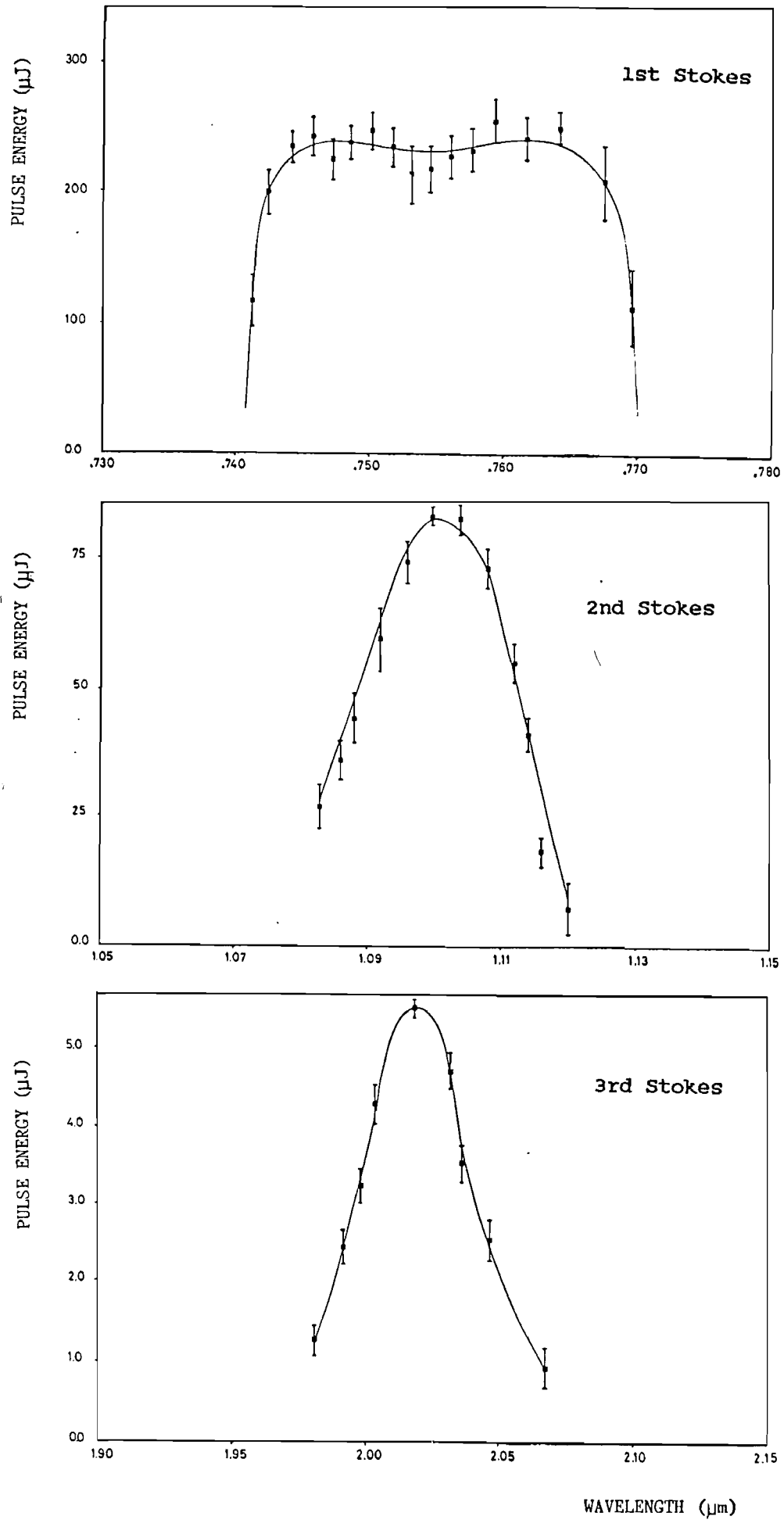

Figure 4.13. Tuning range for Stokes components, scheme IV.

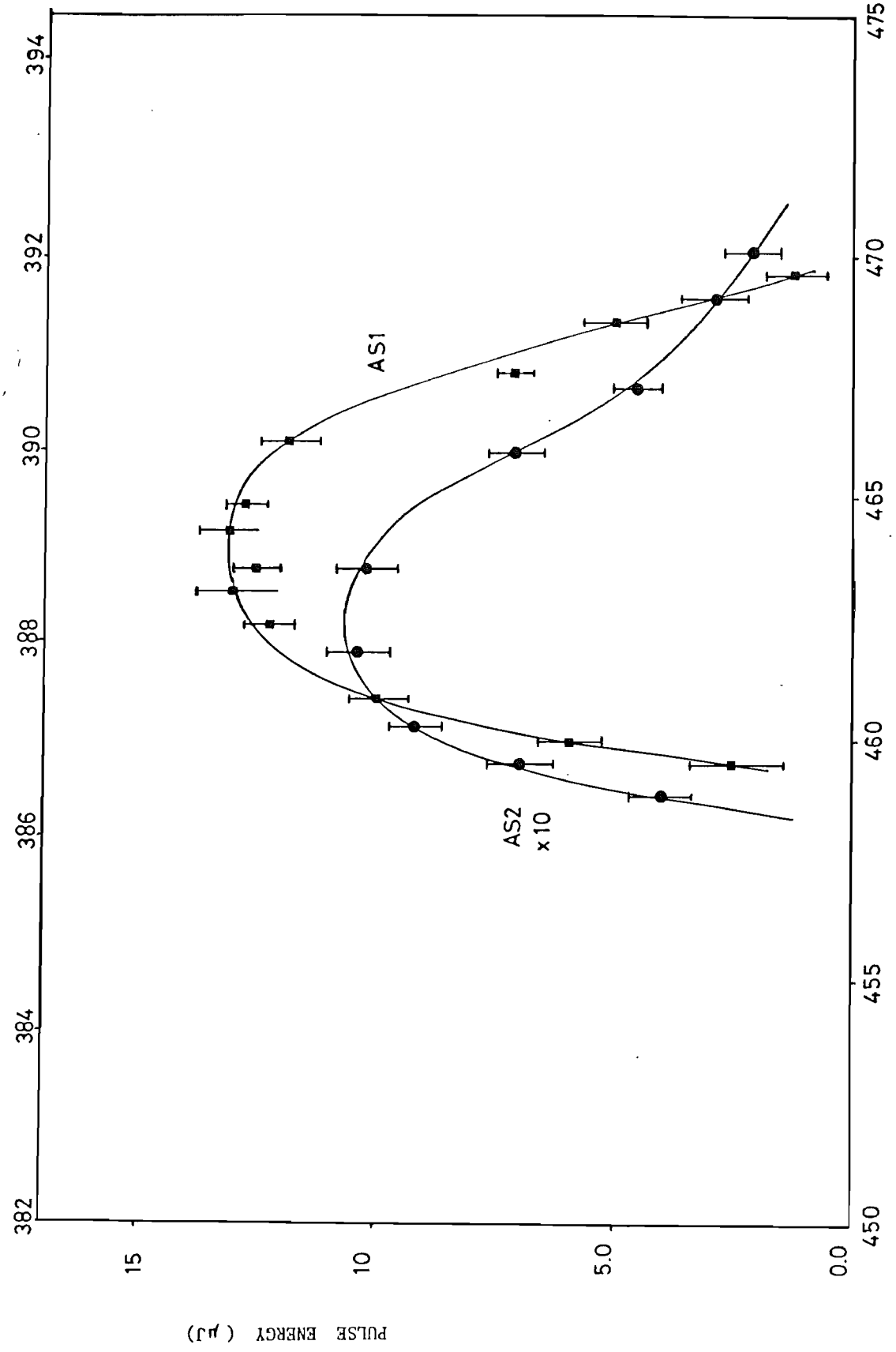

Figure 4.14. Tuning range for anti -Stokes components, scheme IV.

The wide tuning range expected from scheme I is due to the high pump pulse energy available in this arrangement, however in a transversly pumped dye laser a high gain in the amplifier stage leads to a spatially distorted beam and it raises the SRS threshold energy, so that the observed tuning range for this case is very much narrower than the expected one. In order to increase this tuning range we need to get a better beam in terms of spatial intensity profile, to reduce the SRS threshold. Unfortunately, by doing that we reduce the pump pulse energy and consequently the expected tuning range, as we can see in table V for Δ_{max} in the arrangement II. However, in this case the obtained tuning range is much closer to the expected one, although narrower than the one obtained with the arrangement I. A good solution for this problem seems to be a capillary waveguide, since a good beam will increase the pump transmission through the capillary and the long interaction length will provide a high value for the Raman exponential gain.

As we may see from the figures given in table V the tuning range for scheme IV which uses a guided structure is quite close to the maximum theoretically predicted one and even wider than the one obtained with scheme I where the dye laser pulse energy is more than twice as great.

There still remains the question about the improvement provided by the capillary in relation to the original unguided set up (arrangement I) since the final tuning range is not dramatically higher than the one obtained for the high pump pulse energy in scheme I, due to the reduction of the pump pulse energy in the attempt to improve the beam spatial quality.The obtaining of high order Stokes radiation seems to be the more striking point for the guiding system, since with the energy available in scheme I even if the beam were diffraction limited we could not get third Stokes generation in an unguided system. Thus, with scheme IV, the tuning range obtained in the 750 nm, 1.1 μm and 2.0 μm regions is a good result for a 5 mJ pump pulse dye laser with a pulse duration of 12 nanoseconds.

The pulse profile of the pump and the Stokes components at the output of the capillary waveguide in scheme IV are shown in figure 4.15. The temporal behaviour of the pulses was detected by using a vacuum photodiode. The figures 4.15a and 4.15b show the pump pulse before and after the guided medium, one may observe the strong

depletion suffered by the pulse. Figures 4.15c and 4.15d show the first Stokes and first anti-Stokes pulse profiles. The time scale in all photographs is 5 nsec per division. We may observe that Stokes and anti-Stokes have a very similar pulse width and both are slightly shorter than the pump pulse width, ~ 13 nsec. Finally, in figure 4.15e and 4.15f we have the pulse behaviour for the second Stokes and second anti-Stokes components. We may point out the shorter pulse width of both components compared with the previous one, less than 10 nsec. The pulse profile for the third Stokes could not be measured because its wavelength is beyond the limit of sensitivity of our detector.

Figure 4.15. Stimulated Raman Scattering in a capillary filled with hydrogen at 20 atmosphere pressures.

(a) dye laser pulse at capillary input,

(b) dye laser pulse after go through the Raman medium,

(c) 1st Stokes pulse,

(d) 1st anti-Stokes pulse,

(e) 2nd Stokes pulse,

(f) 2nd anti-Stokes pulse.

CHAPTER FIVE

PARAMETRIC PROCESSES - FOUR WAVE MIXING

The parametric terms are represented in equation 3.30 by the terms where $\Delta k_{i,j}$ does not vanish. The conversion efficiency for the parametric process is considerably smaller than the Raman conversion efficiency. The intensity of a component generated via four-wave mixing (parametric process) is proportional to the intensities of the components involved in the specific process, it does not follow an exponential growth with intensity as happens in the cascade process (Raman process). However, in spite of their relatively low conversion efficiency the parametric processes play an important role in determining the generation efficiency for a given component.

This fact is due to the possibility of all components interacting simultaneously in the Raman medium, producing an energy redistribution effect among the Stokes, anti-Stokes and pump radiations.This is the opposite effect to the cascade process which tends to concentrate the whole energy in one single component.

Another situation where the presence of parametric processes becomes important is when the Raman exponential gain (gIL) is not enough to excite a certain n_{th} component by a cascade process. In this case the parametric interaction provides a means by which this component can receive a significant amount of energy which can be very much higher than the energy it contains from the noise background. This fact reduces the necessary Raman exponential gain threshold.

5.1 The mismatch factor

A specific parametric process can be represented by the vector diagram showed in figure 5.1.

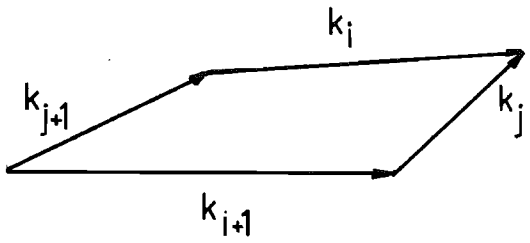

Figure 5.1. Vector diagram for a parametric process at exact phase match.

In this figure k denotes the wavevector of the interacting radiations. The optical frequencies of each component are in resonance with the Raman medium.

$$\omega_{j+1}-\omega_j=\omega_{i+1}-\omega_i=\omega_r$$

ω_r denotes the Raman frequency shift in rad/sec.

The factor which characterizes the dephasing among the waves is called phase mismatch factor, Δk. It is a measure of the phase velocity difference among the components. For the wavevectors along the axis of the interaction medium we define Δk as the scalar:

$$\Delta k= k_j-k_{j+1}-k_i+k_{i+1} \qquad 5.1$$

The coherence length for a parametric process along the axis of a Raman medium is defined as the distance for which the phase Δkl is 180°.

$$l_c=|\pi/\Delta k| \qquad 5.2$$

The value of Δk and l_c may be worked out for hydrogen by using the expression for the absolute refractiveindex as a function of the wavelength given by Peck and Huang (1977):

$$10^6(n-1)= 14895.6/(180.7-\sigma^2)+4903.7/(92-\sigma^2) \qquad 5.3$$

Where σ is the vacuum wave number in μm^{-1}. To reduce the refractive index to the experimental conditions we use the correction factor FC

$$FC= (Z_o/Z_m).P_mT_o/(P_oT_m) \qquad 5.4$$

The subscript o stands for the standard conditions (273 K and 1 atm.) and m for the experimental conditions. P is the pressure in atmospheres and T the absolute temperature. Z is the compressibility given by:

$$Z = 1 + (0.255/T - 23.9/T^2).P \qquad 5.5$$

In table I we have the values of Δk at 30 atmospheres and 298°K for fifteen parametric processes in Hydrogen and a pumping wavelength of 575 nm. The notation V(i,j,s,l) indicates the process

$$k_i - k_j = k_s - k_l \qquad 5.6$$

Table I

Mismatch factor for 15 four wave mixing process in H_2 with a 575 nm pumping wavelength at 30 atm.

Process	mismatch factor(cm^{-1})
V(-1,0,-2,-1)	4.51
V(0,1,-2,-1)	7.97
V(1,2,-2,-1)	10.51
V(2,3,-2,-1)	12.21
V(3,4,-2,-1)	13.12
V(0,1,-1,0)	3.47
V(1,2,-1,0)	6.01
V(2,3,-1,0)	7.71
V(3,4,-1,0)	8.61
V(0,1,1,2)	2.54
V(0,1,2,3)	4.24
V(0,1,3,4)	5.15
V(1,2,2,3)	1.70
V(2,3,3,4)	0.91
V(1,2,3,4)	2.60

5.2 Anti-Stokes generation

The mismatch factor for the parametric interaction involving AS1 and S1 component cannot be worked out from the medium dispersion and radiation wavelengths only. This happens due to the strong coupling between these components, using the pump energy as the coupling element. We are going to analyse this coupling under

the assumption of an undepleted pump signal which makes this coupling particularly strong.

When the energy conversion to the first Stokes component is small, i.e. when the factor gIL is small, all the components have a pulse energy very much smaller than the energy in the pump pulse and the expression 3.83 can be simplified by neglecting all the terms which do not contain the pump electric field modulus.

If we set i=1 and i=-1 in the simplified equation 3.83 and retain only the terms which contains $|E_0|^2$ we have a system of equations coupling the first Stokes and first anti-Stokes components under the assumption of low energy conversion from the pump radiation into any other component.

$$d|E_{-1}|/dz=[-3\omega_{-1}/(4cn_{-1})].[\chi(-1,-1).|E_0|^2.|E_{-1}| + \chi(-1,0).|E_0|^2.|E_1|.\cos(\Delta k_{-1,0}.z+\phi_0-\phi_{-1}-\phi_1+\phi_0)] \quad 5.7$$

$$d|E_1|/dz=[3\omega_1/(4cn_1)].[\chi(0,0).|E_0|^2.|E_1| + \chi(0,-1).|E_0|^2.|E_{-1}|.\cos(-\Delta k_{0,1}.z+\phi_0-\phi_1+\phi_0-\phi_{-1})] \quad 5.8$$

These equations can be further simplified by the approximation that:

$$\chi(-1,-1)=\chi(-1,0)=\chi(0,-1)=\chi(0,0) \quad 5.9$$

$$d|E_{-1}|/dz=-C_{-1}[|E_{-1}|+|E_1|\cos(\Delta k_{-1,0}.z+\phi_0-\phi_{-1}-\phi_1+\phi_0)] \quad 5.10$$

$$d|E_1|/dz=C_1[|E_1|+|E_{-1}|\cos(-\Delta k_{0,-1}.z+\phi_0-\phi_1+\phi_0-\phi_{-1})] \quad 5.11$$

where $$C_{-1}= [3\omega_{-1}/(4cn_{-1})].|E_0|^2 \quad 5.12$$

$$C_1= [3\omega_1/(4cn_1)].|E_0|^2 \quad 5.13$$

Under the condition of exact phase matching and $\Sigma\phi=0$ we have:

$$d|E_{-1}|/dz=-C_{-1}[|E_{-1}|+|E_1|] \quad 5.14$$

$$d|E_1|/dz=C_1[|E_1|+|E_{-1}|] \quad 5.15$$

By dividing equation 5.14 by equation 5.15 and integrating over z we obtain:

$$|E_{-1}|=-K|E_1|+K|E_1|^0-|E_{-1}|^0 \qquad 5.16$$

$$K=C_{-1}/C_1$$

Where $|E^1|^0$ and $|E^{-1}|^0$ are the initial values for the first Stokes and anti-Stokes electric fields respectively. By substituting expression 5.16 into equation 5.15 we obtain an equation for the first Stokes electric field variation without the anti-stokes component.

$$d|E_1|/dz=C_1[(1-K)|E_1|+A^0] \qquad 5.17$$

$$A^0=|E_{-1}|^0+K|E_1|^0 \qquad 5.18$$

As we may notice from expression 5.17 the expected exponential behaviour for the first Stokes component depends strongly on the value of K and as $K\simeq 1.0$ this exponential growth is completely removed and a linear growth is obtained for the S1 component. This result does not agree with the well known experimental results which show a clear exponential variation for the S1 pulse energy in the region where the pump pulse is not very much depleted.Shen and Bloembergen (1965) adressed this problem. It comes about because the positive work done on one part of the normal mode near ω_1 is exactly compensated by the negative work done on the other part near ω_{-1}. This situation is well know in parametric amplifiers in RF region, where no gain can be obtained at $\omega_1=\omega_0-\Delta\omega_r$ if the other side band at $\omega_{-1}=\omega_0+\Delta\omega_r$ is not supressed. It was shown that the solution is to assume a detuning of the AS1 frequency [Shen and Bloemberger (1965),figures 6 and 7] so that $\Delta k= 2gI_0$, where g is the Raman gain coefficient for the S1 component defined in equation 3.42 and I_0 the pump pulse intensity. Then the assumption of exact phase matching breaks down and the exponential growth is restored for the S1 component.

In our experiment for a pumping wavelength in the visible region of the spectrum and the typical intensities produced by the dye laser we have $\Delta k\simeq 6cm^{-1}$. In this work such detuning will be assumed in all our numerical calculations.

5.3 Phase Locking

Two mechanisms can give rise to higher order stokes components: Parametric and Raman processes. As we mentioned before the first mechanism is not very efficient for Stokes generation due to the linear dependence on the intensities of the components and to the mismatch factor which limits the interaction length for the interacting radiations. Now we shall look into the case where phase-locking occurs among the components and its influence on high order Stokes generation.

From equation 3.83 we may define a generalised phase Θ which includes the mismatch factor and the sum of the phases of each component.

$$\Theta(l,j)=\Delta k_{i,j}.z+\phi_{i+1}-\phi_i-\phi_{j+1}+\phi_j \qquad 5.19$$

If the phases ϕ in equation 5.19 are zero then the generalised phase Θ varies linearly with z, and the variation rate is given by the mismatch factor. The effect of the phases ϕ can be to lock the phase Θ at a particular value. This can allow gain to continue for greater distances in the interaction region than might be considered likely from $\Delta k_{i,j}.z$.

In order to make the analysis clear we are going to choose a specific Stokes component, without losing the generality of the conclusion. Let us consider the second stokes and the parametric process which includes the pump and first Stokes intensitites, V(0,1,1,2). From equations 3.83 and 3.84 we have:

$$d|E_2|/dz=[3\omega_2/(4cn_2)].[\chi(1,1).|E_1|^2.|E_2|-\chi(2,2)|E_3|.|E_2|+\chi(0,1).|E_1|^2.|E_0|.\cos\Theta(0,1)] \qquad 5.20$$

$$d|E_1|/dz=[3/(4cn_1)].[\chi(0,0).|E_0|^2.|E_1|-\chi(1,1).|E_2|^2.|E_1|] \qquad 5.21$$

$$d|E_0|/dz=[3\omega_0/(4cn_0)].[\chi(-1,-1).|E_{-1}|^2.|E_0|-\chi(0,0)|E_1|^2.|E_0|-\chi(0,1).|E_1|^2.|E_2|.\cos\Theta(0,1)] \qquad 5.22$$

$$d\phi_2/dz=[3\omega_2/(4cn_2)].\chi(0,0).(|E_0|/|E_2|).|E_1|^2.\sin\Theta(0,1) \qquad 5.23$$

$$d\phi_0/dz=[-3\omega_0/(4cn_0)].\chi(0,1).(|E_2|/|E_0|).|E_1|^2.\sin\Theta(0,1) \quad 5.24$$

$$d\phi_1/dz=0 \quad 5.25$$

Where we have used the fact that:

$$\Delta k_{0,1}=-\Delta k_{1,0}$$

$$\chi(0,1)=\chi(1,0)$$

For the parametric process the generalised phase can be written as:

$$\Theta(0,1)=\Delta k_{0,1}.z-\phi_2+\phi_1+\phi_1-\phi_0 \quad 5.26$$

The variation of Θ in relation to z can be obtained by differentiating expression 5.26 with respect to z:

$$d\Theta(0,1)/dz=\Delta k_{1,0}-d\phi_2/dz+d\phi_1/dz+d\phi_1/dz-d\phi_0/dz \quad 5.27$$

By substituting equations 5.23, 5.24 and 5.25 into equation 5.27 we have:

$$d\Theta(0,1)/dz= \Delta k_{0,1} + W.\sin\Theta(0,1) \quad 5.28$$

for

$$W=(3/4).|E_1|^2.[\chi(0,1)/c].(\omega_0.|E_2|/|E_0|-\omega_2.|E_0|/|E_2|) \quad 5.29$$

Where we have assumed $n_i\simeq 1.0$. Equation 5.28 can be written as:

$$d\Theta(0,1)/dz= W.[\Delta k_{0,1}/W + \sin\Theta(0,1)] \quad 5.30$$

Thus if $\Delta k_{0,1}/W \ll 1$, equation 5.30 has a steady-state solution.

$$\Theta=\Delta k_{0,1}/|W| \text{ for } W<0 \quad 5.31$$

$$\Theta=\pi+\Delta k_{0,1}/|W| \text{ for } W>0 \quad 5.32$$

Initially the pump electric field will be very much stronger than the electric field of the second Stokes component, W

will be negative and the phase Φ will be close to zero and so the second Stokes electric field will grow with $\cos\Phi\sim 1$ (equation 5.20). This process will go on until the energy in the S2 component is comparable to the remaining pump energy. At this point W changes sign and the generalised phase changes from ~ 0 to $\sim\pi$, so now we have $\cos\Phi\sim -1$.

This analysis, based on that of Butylkin and co-workers (1976/1977), has shown that a phase near zero is initially established and when the field starts to grow this phase locking is destroyed and reestablished several times as $\cos\Phi$ oscillates between 1 and -1. A final state is reached when the energy in the two beams I_0 and I_2 are the same. Using this equilibrium condition in equation 5.29 we obtain:

$$W=(6/4).|E1|^2.[\chi(0,1)/c].\omega_r \qquad 5.33$$

Where we have used the expression

$$\omega_0-\omega_2=2\omega_r$$

Comparing equation 3.33 with equation 5.33 we find that W may be expressed in terms of the Raman gain coefficient for the second Stokes beam and the intensity of the first Stokes radiation. The Raman gain coefficient for the second Stokes is defined via

$$I_2=I_2{}^0.\exp(g_1.I_1.z)$$

where

$$g_1=3.\omega_2.\chi(1,1)/(c^2.\varepsilon_0) \qquad 5.34$$

Since $\chi(0,1)\simeq\chi(1,1)$ which is well satisfied for small frequency shifts in a gas, we may write 5.33 as:

$$W=Ag_1I_1 \qquad 5.35$$

$$\text{for} \quad A=2\omega_r/\omega_0$$

Assuming the S2 component has an exponential growth, we may define a length l_0 as the length necessary for the energy of the second Stokes component to reach a reasonable value above the noise background via the cascade process,

$$l_0 = G_1/(g_1 . I_1) \qquad 5.36$$

and using 5.35 we can write

$$l_0 = AG_1/W \qquad 5.37$$

Using equation 5.37 and equation 5.2 which define the coherence length for a parametric process and using the condition for phase-locking $\frac{\Delta k_{0,1}}{W} \ll 1$ we have:

$$\Delta k_{0,1}/W = \pi l_0/(l_c AG_1) \ll 1$$

However, as $A = 2\omega_r/\omega_0 \sim 0.5$ and $G_1 \sim 10$ we have the factor $\pi/(AG_1) \sim 1$ and the inequality can be written as

$$\pi l_0/(l_c AG_1) \sim l_0/l_c$$

$$\Rightarrow \quad l_0/l_c \ll 1 \qquad 5.38$$

Thus the condition to reach phase locking for a given parametric process is that the Raman gain coefficient and the intensity of the $(n-1)_{th}$ component should be enough to produce a reasonable amount of energy in the n_{th} component via the cascade process in an interaction length smaller than the coherence length for this parametric process.

For our experimental conditions the coherence length for the parametric process V(0,1,1,2) is 1.24 cm at a gas pressure of 30 atmospheres. The product of the Raman gain coefficient (expression 5.34) and the pulse intensity of the S1 component has a maximum value of 1.6 cm^{-1} when one assumes a photon conversion of 100% from the pump into the first Stokes beam. As the value of A is approximately equal to one for hydrogen,($A \simeq 0.92$) the Raman exponential gain for the second Stokes component in a length equal to the coherence length is only 1.82, which is not enough to produce a pulse with observable energy.

Thus the phase locking process does not seem to be a very important effect in our experiment. Even at pressures as low as 4

atmospheres the growth of the S2 radiation in a length equal to the coherence length for the V(0,1,1,2) is still too small to produce any significant variation of the Raman exponential gain necessary to reach the SRS threshold for the S2 component.

However, what we have observed experimentally and confirmed through the numerical calculations is that the pump threshold energy for the second Stokes is very much smaller the the one expected when one considers only the cascade Raman interaction. The second Stokes threshold level is reached at a pump pulse energy for which the conversion into the first stokes is far below the maximum. Indeed, for some experiments, S1 and S2 seem to reach SRS threshold for almost the same value of pump pulse energy and after that they grow at different rates.

The explanation we propose for these facts involves an interaction via a parametric process but without assuming any phase locking for the interacting components and consequently without expecting the first Stokes radiation to reach a high energy level.

The growth of the second Stokes pulse energy in the region where the pump pulse remains undepleted can be enough to enormously reduce the pump pulse energy necessary to produce S2 at threshold level when account is taken of the energy generated by the parametric process V(0,1,1,2) itself along the whole length where the pump keeps a very high pulse energy. The difference between this explanation and the one using the phase locking effect is the kind of growth allowed for the S2 component. In the phase locking case we have an exponential growth, cascade process,which depends on the S1 pulse intensity. In the case we propose there is a linear growth, due only to the parametric process and the S2 energy increase is due mainly to the pump pulse energy not to the first Stokes energy level. So this explains why both components appear for almost the same pump pulse energy and why the first Stokes maximum conversion efficiency is strongly reduced when the parametric interaction is enhanced in any way. Because the S2 pulse intensity will be proportional to $I_0 I_1^2$ in the region where the pump pulse is undepleted. The mismatch factor will reduce the growth rate for the S2 component but will still be strong enough to start growing very efficiently at the point where the first Stokes reached threshold. From beyond this point the cascade transference of energy from S1 to S2 becomes very efficient and as the energy in the S2 component is

already reasonably high the Stokes component becomes depleted for a interaction length shorter than the one it needs to reach its maximum conversion efficiency.

5.4 First reduction of parametric terms

The usual way to treat this problem is by neglecting all the parametric terms which do not contain the pump component among the interacting waves. We are not going to follow this procedure in this work because we are interested in studying the Stokes components behaviour for a very wide range of Raman exponential gain and not only in the region where the pump has the highest energy level among all components.

The reduction of terms carried out in this section will neglect all the components which cannot reach a reasonably high energy level and as the cascade process is the only process which can efficiently generate Stokes components we will neglect all the components which cannot grow via the cascade process, i.e. anti-Stokes waves.

For the experimental conditions described in section 3.4.2, when a dye laser is used to produce SRS in molecular hydrogen, we will have two anti-Stokes components, pump and four Stokes components. Therefore any parametric process including one of these two anti-Stokes components will be neglected and consequently we will not have any influence of anti-Stokes intensities on the Stokes components, except for the first Stokes. The only parametric process including anti-Stokes components to be kept is the one linking first anti-Stokes to first Stokes wave, due to the strong coupling between these two components produced by the pump radiation.

The approximation described in this section reduces the number of parametric processes from 15 to 7. The general reduction is shown in table II

Table II

Reduction of terms for the Raman equations

	I	II	III
Number of equations	14	14	10
Number of cascade terms	12	12	8
Number of parametric terms	100	44	40
Number of parametric processes	15	9	7

I. No reduction of terms.

II.Usual reduction of terms.

III.reduction of terms in this work.

Figure 5.2 shows the solution for the set of equations 3.86 and 3.87 for three situations: no reduction of terms, reduction by keeping terms with the pump intensity only and the reduction described in this section.

5.5 Parametric process in an unguided medium

The importance of a specific parametric process is determined by two factors: the intensity of the interacting components and the phase mismatch factor. In a Raman medium the cascade process is going to try to concentrate the available energy in a single component. Thus the parametric processes which contain this component will be the most important ones in a certain region defined by the Raman exponential gain ζ. We may divide the Raman medium into several regions, each region being defined by the component which is growing more efficiently via the cascade proces. For example, the region **i** is the region where the components **i-1** and **i** have the highest energy level, as shown in the scheme below.

Figure 5.2. Numerical solution for the set of coupled equation. (a) No reduction of parametric terms, (b) reduction by keeping only terms which contain the pump intensity and (c) reduction described in section 5.4.

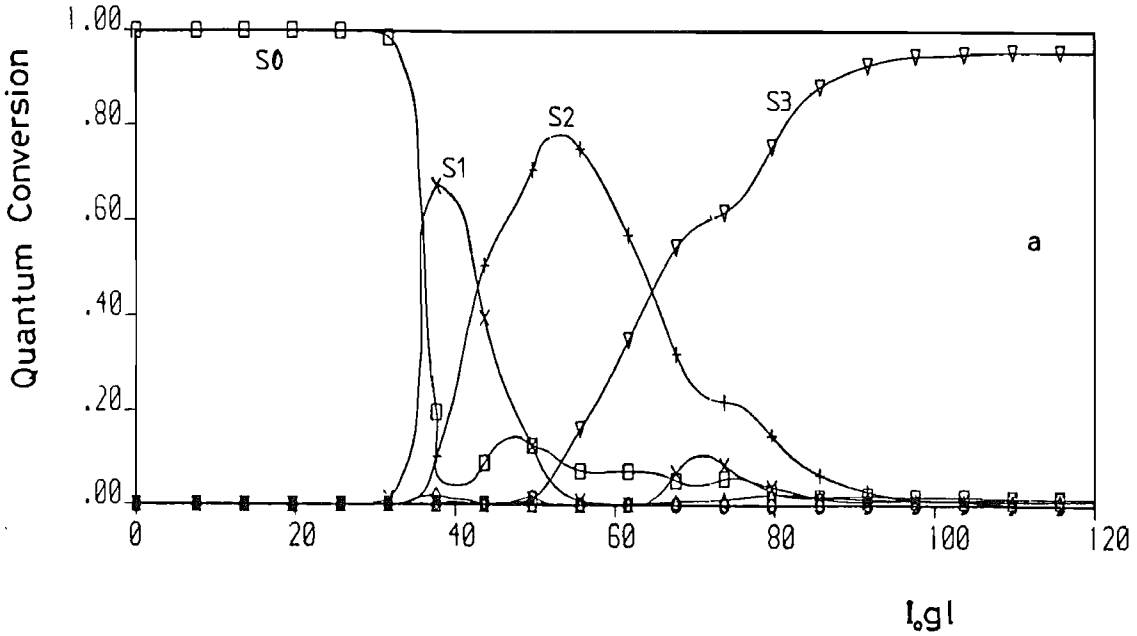
Quantum Conversion
1.00
.80
.60
.40
.20
.00
S0
S1
S2
S3
a
0
20
40
60
80
100
120
l,gl

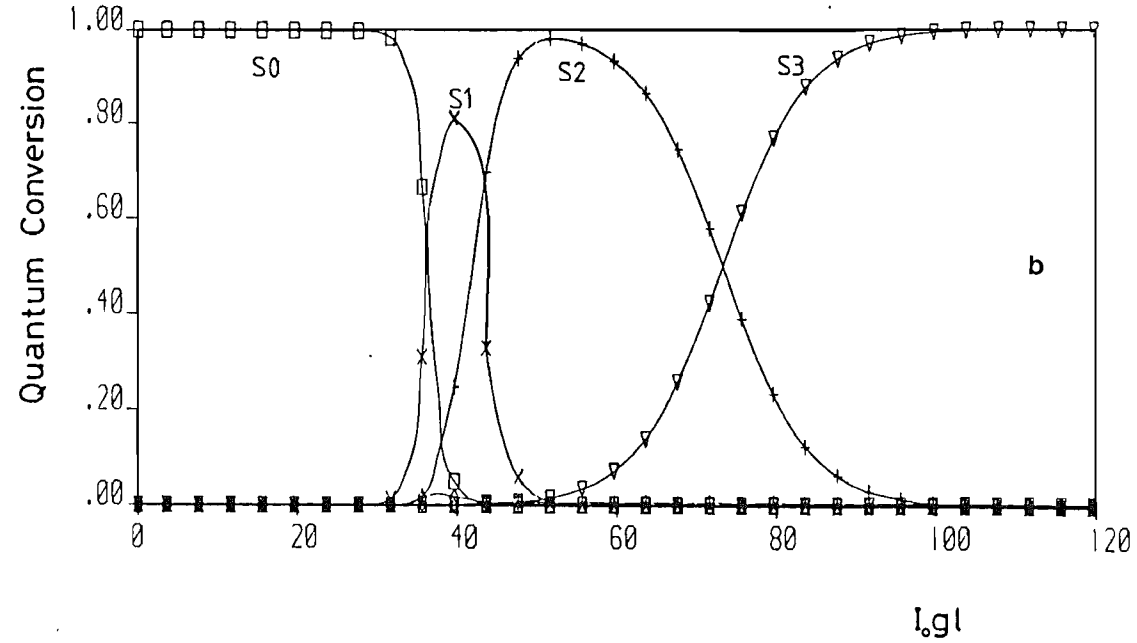
Quantum Conversion
1.00
.80
.60
.40
.20
.00
S0
S1
S2
S3
b
0
20
40
60
80
100
120
l,gl

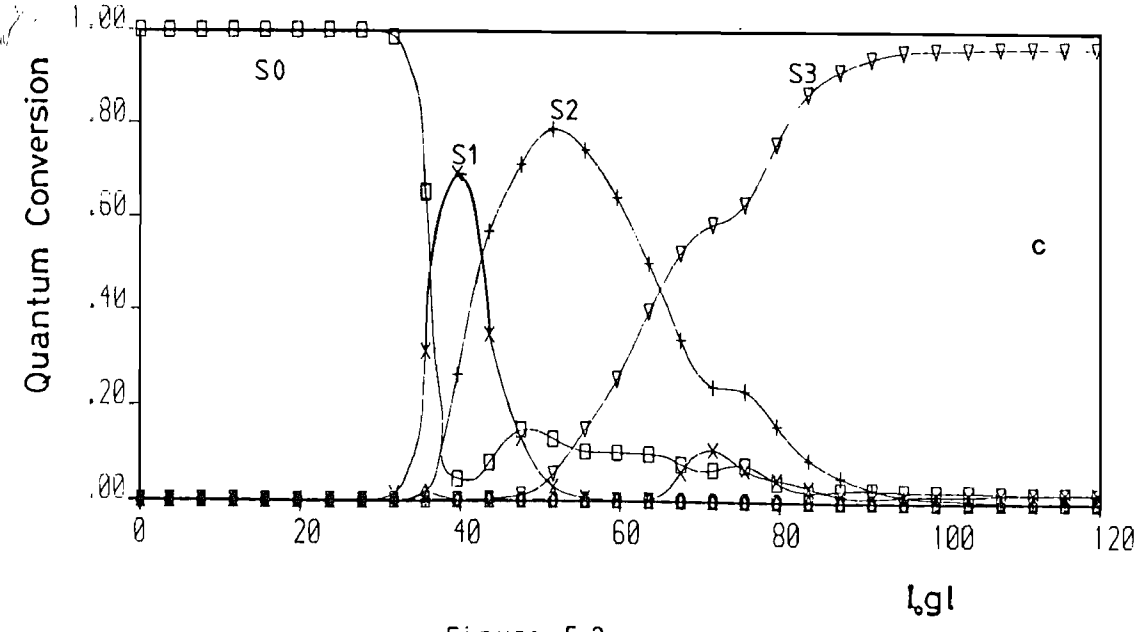
Quantum Conversion
1.00
.80
.60
.40
.20
.00
S0
S1
S2
S3
c
0
20
40
60
80
100
120
l,gl

Figure 5.2

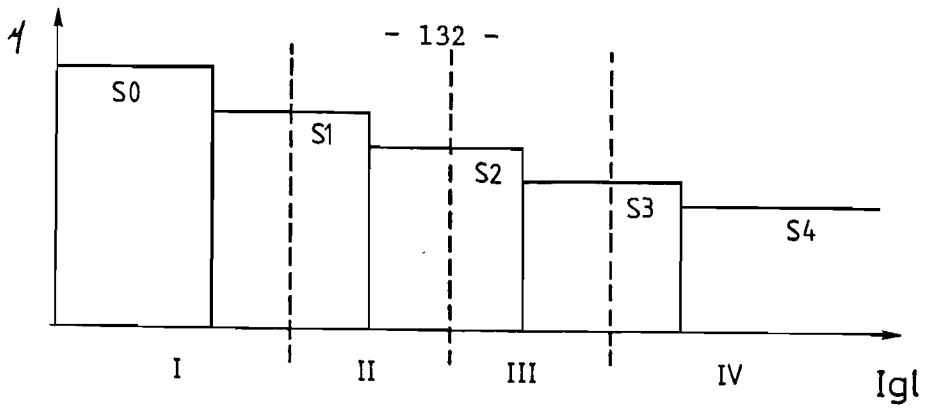

The region 1 is the region where the pump and the S1 component have their maximum energy levels. In this region we have the generation of S2 via the parametric process through the process V(0,1,1,2)

$$k_1 - k_2 = k_0 - k_1$$

The generation of S3 and S4 are carried out using energy from the pump and S1 as well.

S2 generation → V(0,1,1,2) $\quad I_2 \alpha I_1^2 I_0$ 5.39

S3 generation → V(0,1,2,3) $\quad I_3 \alpha I_1 I_0 I_2$ 5.40

S4 generation → V(0,1,3,4) $\quad I_4 \alpha I_1 I_0 I_3$ 5.41

The most effective parametric process in this region is V(0,1,1,2). This is not only because it involves the highest intensity beams but also because of the small phase mismatch factor as we can see in table I. Besides that, the S2 component is the only component which can start to grow very efficiently via the cascade process in this region, so even if the processes V(0,1,2,3) and V(0,1,3,4) were very efficient, the components S3 and S4 would not be able to reach high energy levels since the energies inthe S2 and S3 components are too small to start any efficient exponential growth.

In region 2 we have the first and second Stokes waves with the highest energy level.

S3 generation → V(1,2,2,3) $\quad I_3 \alpha I_2^2 I_1$ 5.42

S4 generation → V(1,2,3,4) $\quad I_4 \alpha I_2 I_1 I_3$ 5.43

In this region the process V(1,2,2,3) is the most important one. because it involves the highest intensities and it has the lowest mismatch factor. Similarly to region 1, the S4 would not reach a high energy level even if the process V(1,2,3,4) were a very efficient one. Finally in region 3 we have only one parametric process involving the highest beam intensities and generating components able to grow via the cascade process:

$$S4 \text{ generation} \rightarrow V(2,3,3,4) \qquad I_4 \propto I_3^2 I_2 \qquad 5.44$$

The parametric process V(2,3,3,4) has the smallest mismatch factor among all the four wave mixing processes. This happens because all the radiation wavelengths lie in the infrared region of the spectrum where the dispersion for H_2 is very small.

5.5.1 Wavevector angles to produce exact phase matching

The wavevector diagrams for the more important parametric processes mentioned in the previous section are shown in figure 5.3.

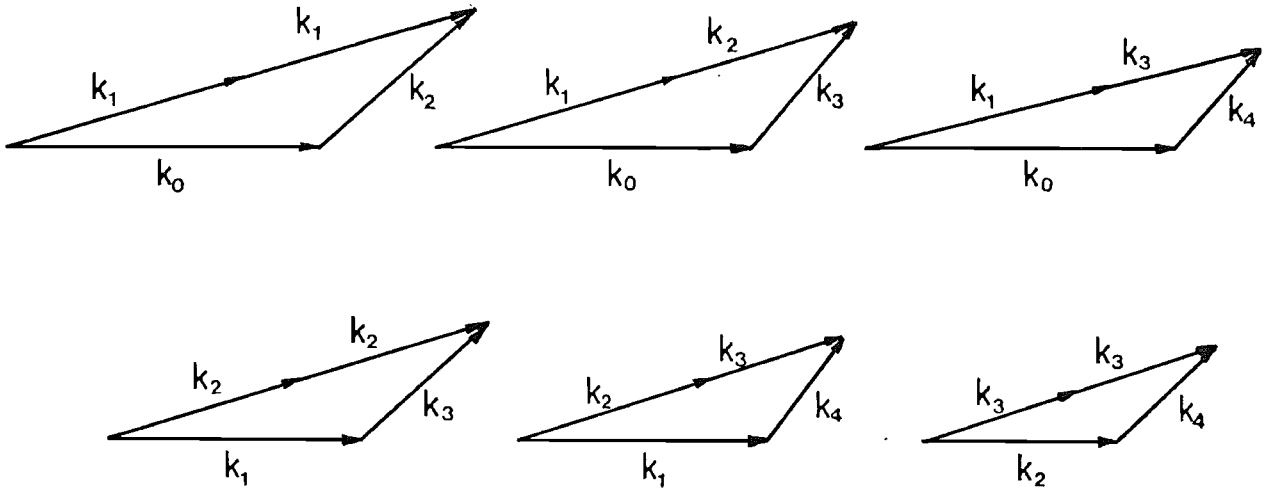

Figure 5.3. Wavevectors diagrams at exact phase matching for the more efficient parametric processes.

The configurations shown in figure 5.3 have the wavevector of the component with the strongest pulse energy in a certain region of the Raman medium along the axis of the interaction length. In region 1 where the pump pulse has the highest energy level among all the Stokes components, the wavevector k_0 lies on the horizontal axis

for all relevant parametric processes in this region. In region 2 the pulse energy for S1 component is the strongest one and the wavevector k_1 is on the horizontal axis for the processes V(1,2,2,3) and V(1,2,3,4).

In a practical arrangement the finite beam dimensions limit the interaction length. Then, to optimize the parametric interaction one must keep the wavevector angle as small as possible. That is the reason why we have the wavevectors in a collinear configuration in the wavevector diagrams for all parametric processes [B.V.Zhdanov et al (1976)].

Figure 5.4 shows the variation of the angle subtended by the wavevectors at exact phase matching, when the gas pressure is changed, for all the parametric processes discussed in this section. One can observe that in the region where a given component can grow efficiently via the cascade process the parametric process generating this component in this region produces the smallest phase matching angle of all the phase matching angles produced by the others parametric processes generating this component. For example the parametric process which generates fourth Stokes with the smallest phase matching angle is V(2,3,3,4) and this process is the more important process in region 3.

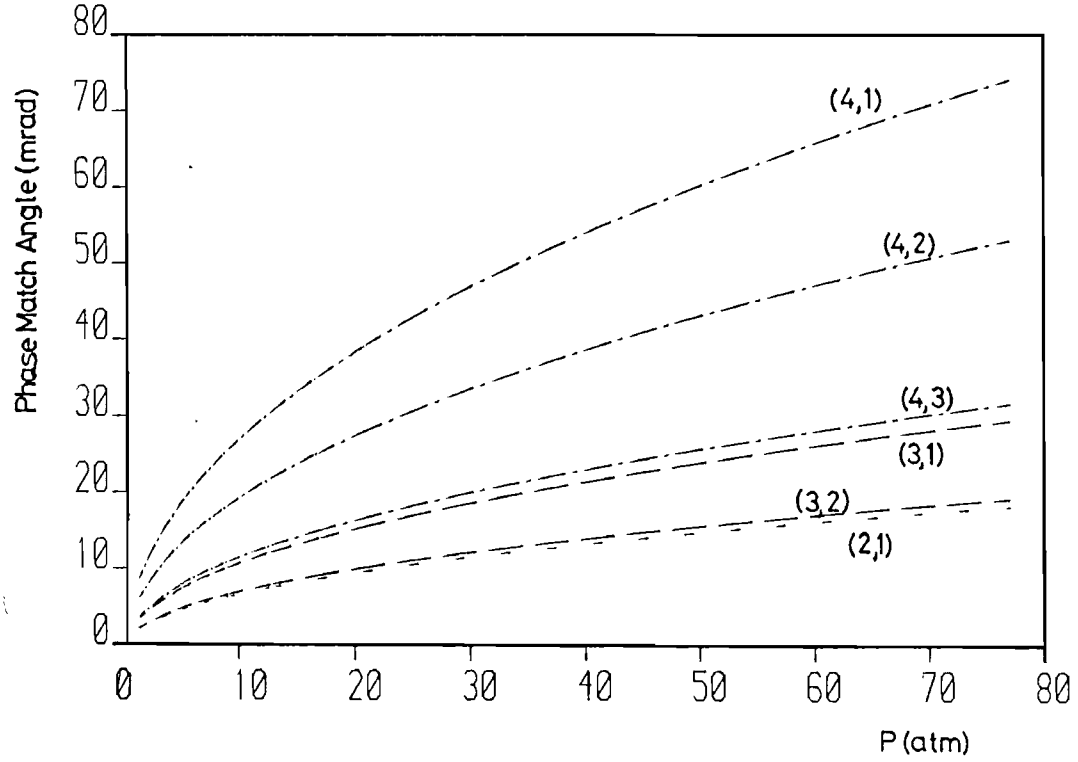

Figure 5.4. Calculation of phase matching angle for the parametric processes discussed in section 5.5.1. **(i,j)**: **i** indicates the Stokes component and **j** the ζ-region where it is been generated more efficiently.

The parametric processes are not very efficient and even at these angles for exact phase matching, the energy produced via four wave interaction is small when compared with the energy produced via cascade process. Besides, that the reasonably large angles depicted in figure 5.4 suggest that the parametrically generated radiation will escape from the excited region (walk off) in a very short distance, unless a tight focused beam is used and a wide range of angles will be provided.

5.5.2 **Anti-Stokes generation via the parametric process**

The parametric processes however, are very important for those components for which interaction with other components relies strongly on the four wave interaction only. That is the case for anti-Stokes waves which usually have a ring-like shape, characteristic of the parametric interaction.

The specific parametric process which will be used depends on which region in terms of Raman exponential gain we are observing the anti-Stokes component. Because the importance of the parametric process changes when we move from one region to another in the ζ range we have the anti-Stokes radiation being generated (more efficiently) by a sequency of different parametric processes when we move along the ζ range.

A direct consequence of this is the variation in the size of the anti-Stokes rings, since different parametric processes will have different phase matching angles.

The parametric processes generating first and second anti-Stokes radiations in each region are the following:

Region 1

AS1 generation	V(0,1,-1,0)	$I_{-1} \alpha I_0^2 I_1$	5.45
AS2 generation	V(0,1,-2,-1)	$I_{-2} \alpha I_0 I_1 I_{-1}$	5.46

Region 2

AS1 generation	V(1,2,-1,0)	$I_{-1} \alpha I_0 I_1 I_2$	5.47
AS2 generation	V(1,2,-2,-1)	$I_{-2} \alpha I_1 I_2 I_{-1}$	5.48

Region 3

AS1 generation	V(2,3,-1,0)	$I_{-1} \alpha I_0 I_2 I_3$	5.49
AS2 generation	V(2,3,-2,-1)	$I_{-2} \alpha I_2 I_3 I_{-1}$	5.50

Region 4

AS1 generation	V(3,4,-1,0)	$I_{-1} \alpha I_0 I_3 I_4$	5.51
AS2 generation	V(3,4,-2,-1)	$I_{-2} \alpha I_3 I_4 I_{-1}$	5.52

The wavevector diagrams for the parametric processes generating first anti-Stokes radiation are shown in figure 5.5.

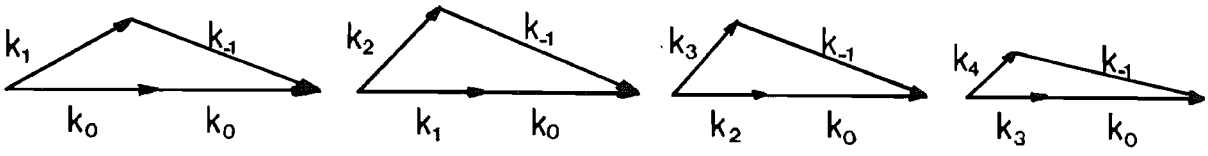

Figure 5.5. Diagrams for the radiation wavevectors at exact phase match at the four regions or the ζ range.

As we may observe for the process V(1,2,-1,0) the wavevector for the pump radiation, k_0, was kept along the interaction axis although this process has its maximum efficiency in region 2 where the S1 and S2 radiations are the strongest ones rather than S0 and S1. However, this configuration provides the smallest angle for the AS1 wavevector at phase matching. This proceeding was followed in all four processes, the pump wavevector was kept on the axis to allow the wavevector of the emergent component be as close as possible of the interaction axis.

Figure 5.6 shows the calculated results for the phase matching angle against pressure for the first and second anti-Stokes

5.5.3 **Experiment**

The beam coming from the Nd:YAG oscillator/amplifier laser is sent through an optical telescope and injected into a KD*P II frequency doubling crystal. The output radiation at λ=532nm is focused by a 100 cm focal length lens inside a cell filled with hydrogen at high pressure. The confocal parameter for the pumping

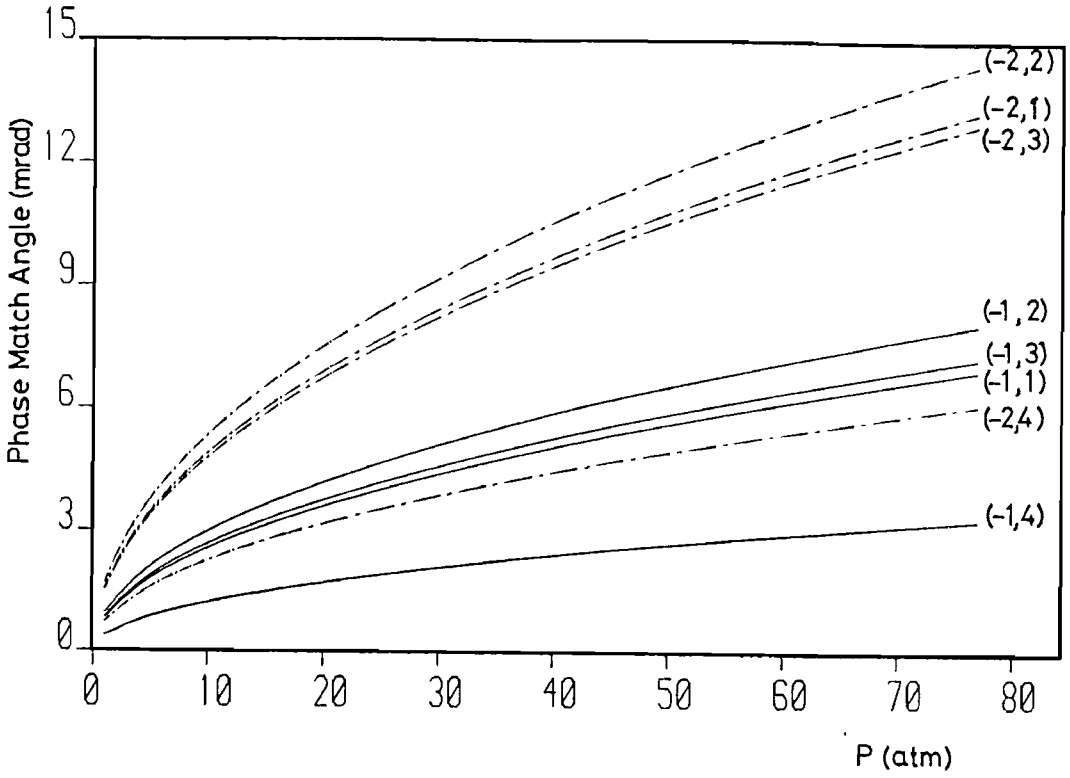

Figure 5.6. Calculation of phase matche angle for first and second anti-Stokes. **(i,j)**: **i** indicates the Stokes or anti-Stokes component and **j** the ζ-region.

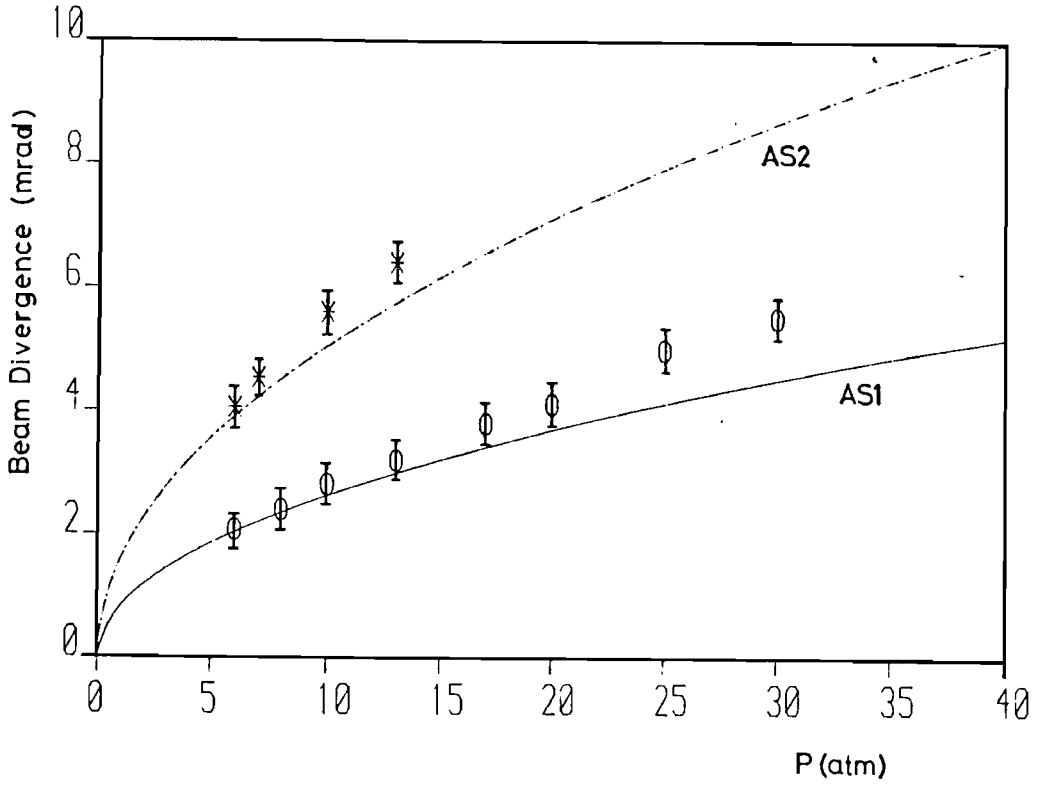

Figure 5.7. Experimental and theorectical (lines) values for beam divergence of AS1 and AS2 components under the experimental conditions described in section 5.5.3.

radiation is 31.4 cm and the cell length is 80 cm.

The experimental observations were concentrated in anti-Stokes components only, due to the fact that those components are mainly generated via parametric processes and consequently they may furnish a more clear idea of what is happening during the parametric interactions.

Two different sets of measurements were carried out. In the first set of measurements the diameter of the rings formed by the anti-Stokes beams were measured using a photographic plate placed at cell output. from these measurements we worked out the divergence angle for each component for several pressures in the Raman cell. In a second set of measuments the energy of the anti-Stokes components were measured using a pyroelectric energy meter.

5.5.3.1 **Measurement of the ring divergence-discussion**

Figure 5. 7 shows the values of the ring divergence against the pressure in the Raman cell for the first and second anti-Stokes components. The solid and the dashed lines correspond to the values of the AS1 and AS2 ring divergences worked out using the expressions presented in section 5.51. As we may observe from this figure the experimental values agree well with the theoretically predicted values for the ring divergence.

5.5.3.2 **Conversion efficiency for anti-Stokes**

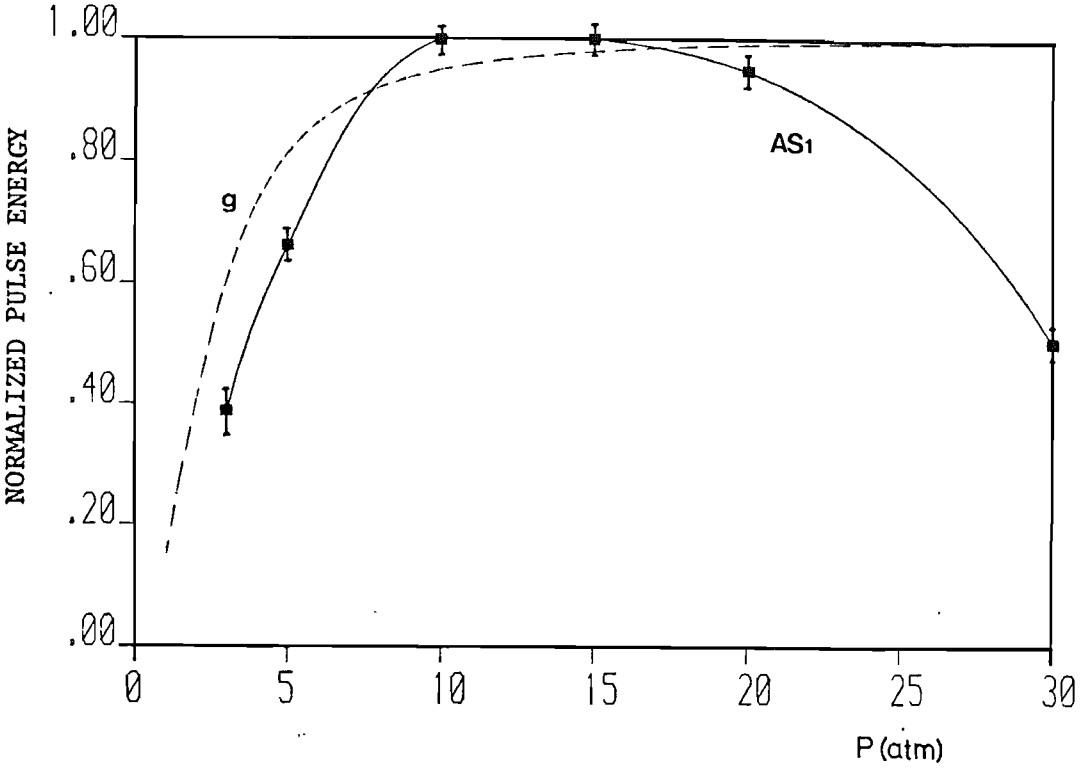

Figure 5.8. Conversion efficiency for AS1 component in an unguided cell and calculated value for the Raman gain coefficient (g) normalized to its value at high pressure

In figure 5.8 we show the efficiency of first anti-Stokes at different gas pressures. The normalized Raman gain coefficient is given as a function of pressure as well by the dashed line. As the pressure is reduced the overall efficiency is reduced too, although the interaction length gets bigger, that is due to the reduction in Raman gain coefficent. When the pressure is increased the energy of the anti-Stokes beam starts to decrease again. This happens due to the large angle necessary for phase matching at high pressures.

So the maximum conversion efficiency for the anti-Stokes radiation in an unguided medium should be found at low pressures,where the small angle required to phase match the parametric process provides: a long interaction length, a maximum value for the factor sinc(x) and allows the parametric process to sample the portion of the interacting beams with high intensity. The minimum value for the gas pressure will be very close to zero regarding only these aspects, however in a practical case it will be determined by the dependence of the Raman gain coefficient on the gas pressure.

5.6 Parametric processes in a guided medium

For a guided medium phase matching can be reached for a given parametric process by compensating the medium dispersion using different propagation modes for the interacting beams inside the waveguide. The method used in a waveguide to phase match a given parametric process does not differ very much from the one used for an unguided medium. Again a suitable configuration is chosen for the wavevectors in a way to overcome the variation of the medium refractive index with wavelength. However, in a waveguide this method leads to a very efficient interaction of the radiation via parametric processes, because the condition of exact phase match can be kept along the whole interaction length, unlike the unguided case where a large phase match angle leads to the walk off of the generated wave from the excited region. On the other hand phase matching for parametric processes in a waveguide is more critically dependent on pressure than it is in an unguided medium. In the guided medium the interacting waves must match a specific set of propagation modes to be phase matched, consequently only one value of gas pressure produces phase matching for a given set of propagation modes. Any variation from this value of pressure changes the refractive index for each component and the set of propagating modes is not able to phase match the process any more. As the pressure continues to change a new set of propagating modes will eventually reestablish the phase matched situation, but inbetween these specific values of pressure the intensity of a component produced only via a parametric process will be reduced.

5.6.1 Mismatch factor for a guided medium

The mismatch factor (defined by expression 5.1) may be written for a waveguide as,

$$\Delta k=2\pi[n_{eff}(\lambda_j)/\lambda_j - n_{eff}(\lambda_{j+1})/\lambda_{j+1} - n_{eff}(\lambda_i)/\lambda_i + n_{eff}(\lambda_{i+1})/\lambda_{i+1}] \qquad 5.53$$

n_{eff} is the effective refractive index,it includes the mode and medium dispersions and is defined as:

$$n_{eff}=\beta/k \qquad 5.54$$

Where β is the propagation constant for a given waveguide mode and k the wavevector in the vacuum. For a dielectric waveguide β is given by [Marcatilli and Schmeltzer (1964)]:

$$\beta=kn[1-(\mu\lambda/(2\pi an))^2/2] \qquad 5.55$$

Where a is the radius of the cylindrical waveguide and μ the the Bessel function root. From expressions 5.54 and 5.55 we may write the expression for the mismatch factor for a guided medium as,

$$\Delta k = M + G \qquad 5.56$$

Where

$$M=2\pi[n(\lambda_j)/\lambda_j - n(\lambda_{j+1})/\lambda_{j+1} - n(\lambda_i)/\lambda_i + n(\lambda_{i+1})/\lambda_{i+1}] \qquad 5.57$$

$$G=[1/(4\pi a^2)].[-(\mu_{nm})^2\lambda_j/n(\lambda_j) + (\mu_{nm})^2\lambda_{j+1}/n(\lambda_{j+1}) + (\mu_{nm})^2\lambda_i/n(\lambda_i) - (\mu_{nm})^2\lambda_{i+1}/n(\lambda_{i+1})] \qquad 5.58$$

μ_{nm} is the m_{th} root of the equation $J_{-1}(\mu_{nm})=0$, n and m are integers which characterize the propagating mode. The term M is the mismatch factor for the unguided medium. The term G is the mismatch factor due to the propagation of the components in several waveguide modes.

5.6.2 **Waveguide modes**

For each parametric process we need to find a set of waveguide modes which promote phase matching among the wavevectors of the interacting radiations. To find this set of modes we need to consider the most important characteristics of a given mode, which are: a good coupling of the interacting radiation into the waveguide (regarding the polarization of the beams) and low propagation loss. So, we may say that the mode polarization and attenuation coefficient will define the most likely modes to be used efficiently in a four wave interaction.

For vibrational Raman scattering the polarization of the i_{th} component generated via the cascade process will be same as the polarization of the $(i-1)_{th}$ component. Then the pump polarization will be kept in all Stokes waves and as we used a linearly polarized

laser we need to look for waveguide mode which can propagate this sort of polarized wave.

In a dielectric waveguide where the refractive index of the guide walls are bigger than the refractive index of the core, the two more important linearly polarizedmodes are the hybrid modes EH_{11} and EH_{12}. However the non linearly polarized hybrid mode $EH_{-n,m}$ is degenerate with the mode $EH_{n+2,m}$ (they have the same propagation constant) and if the field components of these modes are added we obtain new composite modes whose electric and magnetic field lines project as straight lines on a plane perpendicular to the z axis [Marcatili and Schmeltzer (1964)]

Then, the hybrid modes EH_{11}, EH_{12} and the combination of degenerate modes will produces a set of modes with a linear polarization.

The attenuation coefficient for hybrid mode and their combination is given by [Marcatili and Schmeltzer(1964)]

$$T_{nm}= \exp(-\alpha_{nm}L) \qquad 5.59$$

where, T_{nm} is the energy transmission for the nm mode, L is the waveguide length and α_{nm} is the attenuation coefficient for the nm mode which is given by:

$$\alpha_{nm}=[\mu_{nm}/(2\pi)]^2.(\lambda^2/a^3).(n^2+1)/\sqrt{n^2-1} \qquad 5.60$$

This attenuation coefficient is for a straight capillary.

From expression 5.60 we observe that a large value of μ_{nm} will produce a highly attenuated mode. Thus the transmission losses criterion does not produce a set of specific modes as the polarization criterion does. We must try to keep the value of μ_{nm} as small as possible for a set of linealy polarized modes. In table III we list the first seven polarized capillary modes in a increased order of μ_{nm}.

TABLE III

The first seven linealy polarized modes in capillary waveguide

	Mode denomination	Configuration	μ_{nm}
1	EH_{11}		2.405
2	$EH_{-11}+EH_{31}$		5.313
3	EH_{12}		5.520
4	$EH_{-21}+EH_{41}$		6.380
5	$EH_{-31}+EH_{51}$		7.588
6	$EH_{-12}+EH_{32}$		8.417
7	$EH_{-22}+EH_{42}$		9.761

5.6.3 Capillary mode angle

As the propagation along a guided medium can be regarded as a beam being reflected repeatedly by the waveguide walls, we may define the angle θ between the beam axis and the capillary walls in terms of the propagation constant.

$$\beta=(2\pi/\lambda).[1-(\mu_{nm}\lambda/(2\pi a))^2/2] \qquad 5.61$$

$$\cos\theta= \beta/k= 1 - (\mu_{nm}\lambda/(2\pi a))^2/2 \qquad 5.62$$

as the angle θ is usually very small we have the approximation:

$$\cos^2\theta=[1 -(\mu_{nm}\lambda/(2\pi a)^2/2]^2\simeq 1-(\mu_{nm}\lambda/(2\pi a))^2 \qquad 5.63$$

or $$\sin^2\theta=[\mu_{nm}\lambda/(2\pi a)] \rightarrow \theta\simeq\mu_{nm}\lambda/(2\pi a) \qquad 5.64$$

From expression 5.64 we may conclude that a high order capillary mode or combination mode has a large angle which implies a high transmission loss for these modes due to the larger fraction of pulse energy escaping from the waveguide core through the waveguide walls.

5.6.4 Pressure dependence of parametric processes in a guided medium

In the unguided medium the importance of a specific parametric process is defined by the region we are in terms of Raman exponential gain, ζ-region. It does not differ very much for the capillary waveguide, however, there is one fundamental difference for the Stokes components, because a parametric process can be phase matched along the whole interaction length. It means that a parametric process can start to drive energy into a specific component even if the intensities of the interacting waves for this parametric process are very small and this component will keep most of this energy generated parametrically until the point where it can start to grow via the cascade process. However for anti-Stokes components the situation is quite similar to the one for an unguided medium,i.e. although the parametric process can still be phase matched along the whole interaction medium, its importance depends on which ζ-region we are observing.

In a capillary waveguide we cannot just pick up the parametric process involving the i_{th} and $(i-1)_{th}$ component in the ζ-region i to generate the $(i+1)_{th}$ component as we have done for the unguided case, rather we need to take into account any parametric process generating the $(i+1)_{th}$ component. Because of the allowed phase matching along the whole capillary length, when the $(i+1)_{th}$ component reaches the point where it starts to grow viathe cascade process, a parametric interaction, which started several ζ-regions behind, has accummulated enough energy into the $(i+1)_{th}$ to be more important for the threshold reduction of this component than a parametric process which started in a near by ζ-region.

As an example we may take the generation of fourth stokes radiation via four wave mixing, what can occur through the following parametric processes:

Region 1	V(0,1,3,4)	$k_0-k_1=k_3-k_4$
Region 2	V(1,2,3,4)	$k_1-k_2=k_3-k_4$
Region 3	V(2,3,3,4)	$k_2-k_3=k_3-k_4$

In an unguided medium the process in region 3 was shown to be the more important because it is going to generate S4 using S2 and S3 component pulse energies, which are very strong in region 3. Besides that in this region the S4 wave starts to grow via cascade and so this parametric process produces a seed radiation to be amplified exponentially via the cascade process. The processes in region 1 and 2 are not important since the energy produced in the S4 component will walk off from the excited region before it reaches the region 3. But in a capillary waveguide the processes 1 and 2 can produce energy in the S4 component and provided the propagation loss is not too high for this component, it will reach region 3 with an energy level higher than the one due to the process 3, since the involved intensities for this process S2 and S3 have not yet reached the maximum value.

Thus, in a waveguide structure we need to consider any parametric process which is able to generate a given component due to the confinement of the beams. But we can still do some simplifications in the parametric terms for a capillary waveguide. Unlike the unguided cell, a capillary waveguide cannot efficiently phase match several parametric processes simultaneously. When we change the gas pressure in a unguided cell we can always find a set of angles for the wavevectors of the interacting waves which phase match the process. In a capillary these wavevectors should match a capillary propagating mode and as they are discrete, only specific values of gas pressure will phase match the same parametric process for different capillary propagating mode combinations and these values will not necessarily coincide with the values necessary for a different parametric process generating the same component.

For a capillary waveguide the most important parametric process is defined by the gas pressure and it can be any process generating the component inside the medium. The phase match is reached when $\Delta k=0$, or in terms of expression 5.56,

$$\Delta k=0 \Rightarrow M=-G \qquad 5.65$$

The value of G is given by a set of waveguide modes and it is a function of the waveguide parameters, i.e. bore diameter and the refractive index of the walls. To reach phase matching for a given parametric process we must find a value of gas pressure to produce a medium dispersion to satisfy expression 5.65.

To work out what pressure is going to provide phase matching for a specific parametric process we need to have the value of G, this means we need to know the set of propagating modes which is being used. However, to cover the whole number of possible mode combinations for a given four wave mixing process is not practical. Some assumption must be made in order to reduce the number of waveguide mode combinations. As the EH_{11} hybrid mode has a profile with its maximum along the axis of the cell and the smallest attenuation coefficient among all the other capillary modes, we are going to consider this mode as the propagating mode for the component with the highest energy level in each ζ-region.

A set of phase match pressures is given in appendix 4, where we considered two pump wavelengths 532 nm and 575nm and four different values for capillary bore diameter: 100μm, 200μm, 350μm and 600μm.

5.6.5 Stokes and anti-Stokes generation

As we may conclude from appendix 4, the pressure necessary to match a parametric process in a capillary waveguide for a given pump wavelength increases for three different reasons: for increasing Stokes order, for higher order ζ-region or for decreasing the capillary bore diameter.

Let us analyse some of the characteristics of the parametric process in a 200 micron diameter capillary. The tables shown in appendix 4 show that there is no way to phase match the parametric process V(0,1,1,2) using only the EH_{11} mode. Thus, the S2 generation in a Gaussian-like shape in region 1 is not possible with a pump wavelength in the visible region of the spectrum. This is an important point, because it is in region 1 where the S2 wave starts to grow via the cascade process, that, the possibility of a Gaussian-like seed radiation being generated via the parametric process is quite unlikely.

The S3 component has the same problem although less critically. The required gas pressure to phase match the process V(1,2,2,3) is 4.7 atmospheres for a pump wavelength of 575 nm.

For the generation of the S4 component the situation is very peculiar, because of the long wavelengths involved, the factor **M**, which characterizes the medium dispersion, is very small and simultaneously the factor G becomes very large. The result of this is a very high gas pressure if one wants to phase match a parametric process. It leaves the EH_{11} mode combination as almost the only pratical possibility.

The diameter of the capillary plays a very important role in determining the efficiency of the parametric process. For example, in a capillary with a diameter of 350μm the pressure necessary to phase match any parametric processes using a combination of the first seven capillary modes is very small. The process V(0,1,-1,0) which generates AS1 in region 1, cannot reach phase matching at all for any capillary mode combination, when the gas pressure in the Raman cell is above 30 atmospheres. This happens due to the high medium dispersion at short wavelengths and so the pressure needed to phase match the parametric process using a given capillary mode combination is not as high as for the Stokes generation. The generation of AS2 makes the thing even worse, but in both cases, AS1 and AS2 generation, we can reach phase match at a reasonably high gas pressure by using low order capillary mode combination and moving to high order ζ-regions. The longer wavelength of the interacting radiations in these regions allows phase matching to be reached at higher pressures.

Thus, the anti-Stokes radiation is generated more efficiently in region 3 and 4 where a combination of EH_{11} mode provides a reasonable value for the phase match pressure. A way to have efficient generation of anti-Stokes components is by using a small bore capillary. In this case the AS generation in regions 1 and 2 is more likely and the high propagation losses for this guide are not very critical due to the short wavelengths involved.

In short, we may say that a good way to inhibit anti-Stokes generation is to use a high gas pressure and/or a large capillary diameter. On the other hand, to enhance the anti-Stokes generation one must keep the gas pressure as low as the Raman gain coefficient allows and/or use a small capillary diameter. For a 200 micron

diameter capillary the efficiency of anti-Stokes generation increases when one moves to high order ζ-region and consequently most of the anti-Stokes energy coming out of the capillary waveguide is being generated in the region close to the output of the interacting medium.

In the next section we present the experimental observations of SRS and parametric processes in a capillary waveguide. Two pump sources were used: a dye laser and the 2nd harmonic of a Nd:YAG; two capillary bore diameters were used.

5.6.6 Experiment

5.6.6.1 Energy measurements for anti-Stokes components

Pump source: Dye laser

Capillary diameter: 200 μm

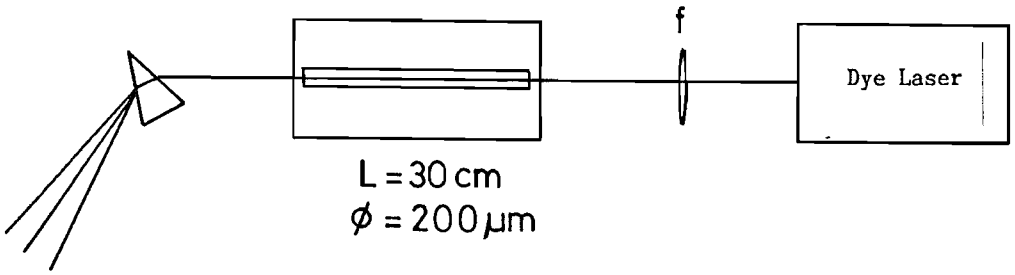

Figure 5.9. Schem of the arrangement used to investigate parametric process in an unguided cell.

In figure 5.9 we show schematically the arrangement used to investigate the component energies when the pressure is changed in the Raman cell containing a capillary waveguide. The dye laser is being used as the pump source, it includes two amplifier stages and saturated and linear absorbers. The maximum energy available inside the Raman cell is 2.3 mJ in a 12 nsec pulse. The capillary waveguide has a length of 30 cm and a bore diameter of 200 microns. The energy measurements were carried out by using a pyroelectric energy meter and a calibrated photodiode.

Figure 5.10 shows the relative output pulse energy for the first anti-Stokes against pressure. The pulse energy grows until it reaches a maximum value around 20 atmospheres and is reduced when the pressure is increased in the Raman cell beyond that value.

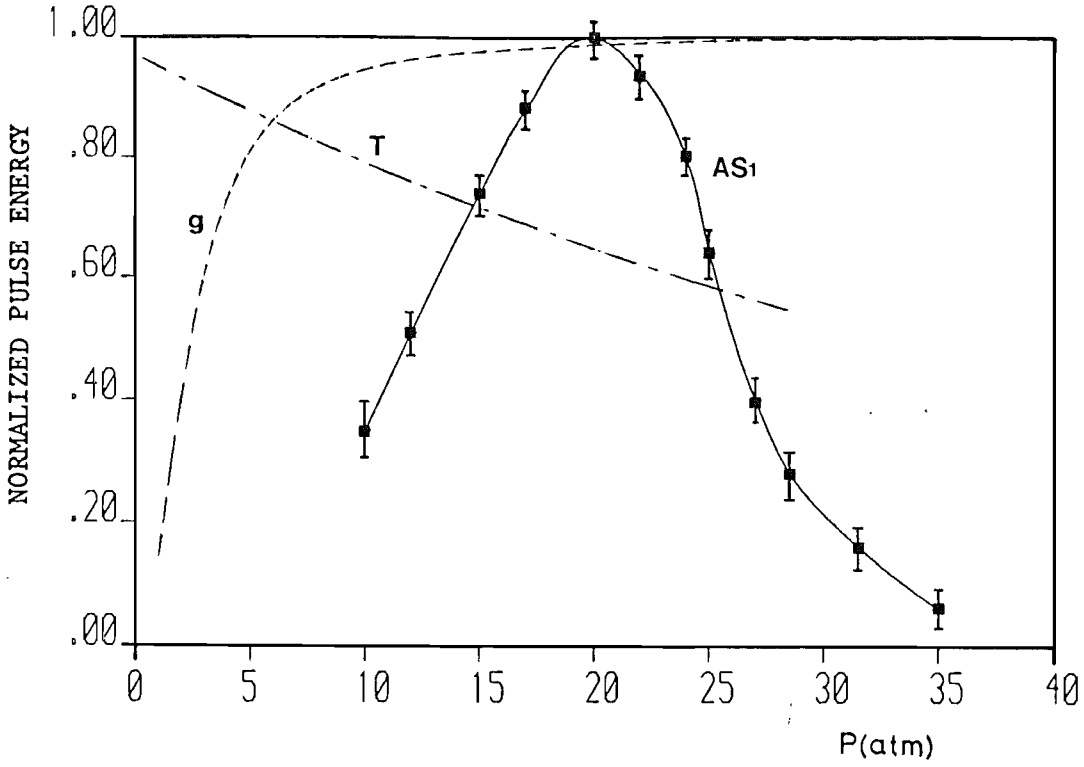

Figure 5.10. Relative output energy for AS1 component in a capillary waveguide. (T) capillary transmission. (g) Raman gain coefficient normalized to its value at high pressure.

5.6.6.2 **Energy measurements for Stokes components**

Pump source: Dye laser

Capillary diameter: 200 μm

In figure 5.11 we have a sequence of plots of Stokes pulse energy against pump pulse energy. Each plot corresponds to a set of measurements at a different gas pressure and we measured the pulse energy for the S1, S2 and S3 components. At 35 atmospheres a very low conversion efficiency is observed for the S1 component, which at the maximum pump energy has a pulse energy smaller than the energy for the S2 component. The small conversion efficiency for the first Stokes component efficiency remains until the gas pressure is reduced to values below 20 atmospheres.

One explanation for these diagrams can be given in terms of parametric processes. By using table I in appendix 4 we may observe the pressures necessary to phase match the process V(0,1,1,2), that is the parametric process which generates second Stokes radiation in region 1, using the pump and first Stokes pulse energy. This process requires very low pressure to reach the phase match when a

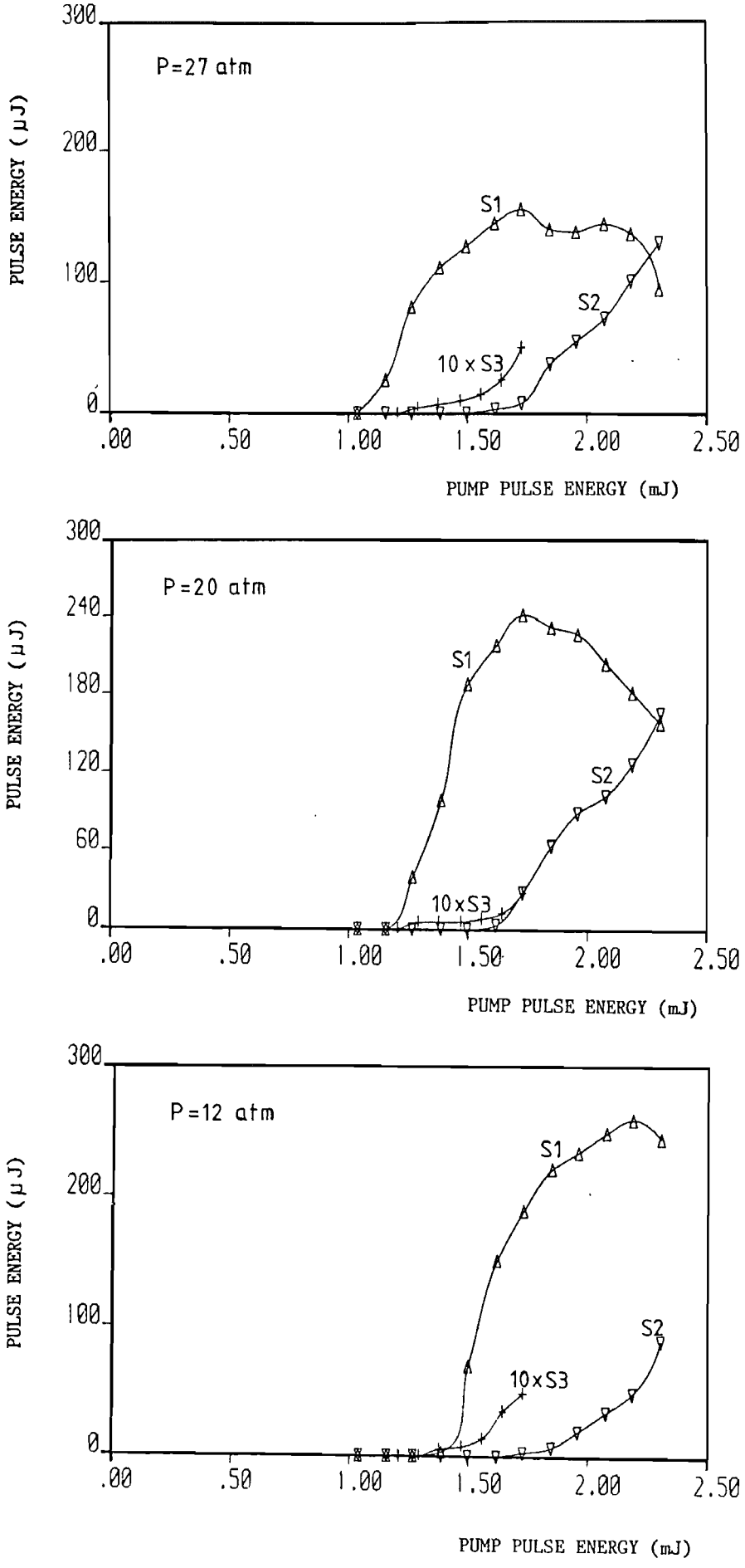

Figure 5.11. Pulse energy for S1, S2 and S3 agains pump pulse energy in a capillary waveguide for several gas pressures.

combination of EH_{11} capillary modes are used ~ 1 atm and at this pressure the Raman gain coefficient is too small and this process does not have any influence on the Stokes energies.For the next mode combination the phase match pressure jumps to 24 atmospheres and this value increases rapidly when we chose high order capillary modes as can be seen from table I in appendix 4. Then, when we have the Raman cell at high gas pressure this process can be matched exactly and a strong seed radiation is generated for the S2 component using the pump and S1 pulse energies. This explains the high energy level for the S2 component at high pressure and the strong depletion on the S1 component. As the pressure is reduced below 20 atmospheres there is no more capillary mode combination to phase match this process and the mismatch factor increases as we decrease the pressure in the cell, this can be seen by the increase in the conversion efficieny for the S1 component since the competition effect with the S2 component gets weaker.

We may observe that the pump pulse energy necessary to reach the SRS threshold increases as we reduce the gas pressure. This happens due to the reduction in the Raman gain coefficient which we discussed in chapter 3 of this work. At low pressure we are close to the pressure where the Dicke narrowing occurs and the Raman gain coefficient starts to be a function of the gas pressure.

Since the phase match condition for the S2 component can be reached only using high order capillary modes, we should expect a ring-like shape for this component at any practical value of gas pressure. In this experiment we did not measure the beam shape for the stokes components but in chapter 6 we will see that the S2 component actually has ring shape at the capillary output and this is the main difficulty in reaching a high conversion efficiency for this component using a capillary waveguide as a Raman oscillator and an unguided cell as an amplifier.

5.6.6.3 Energy measurements for anti-Stokes components
Pump source:2nd harmonic of Nd:YAG laser
Capillary diameter:200 μm

In figures 5.12 we show the relative output pulse energy for the first anti-Stokes radiation. The set up used for this measurement is different from the previous one. The pump source is

the second harmonic of a Nd:YAG laser, 532nm wavelength and the pulse energy available at the capillary entrance is 20 mJ in a 20 nanosecond pulse. The capillary is 34 cm long and it has a 200 micron bore diameter.

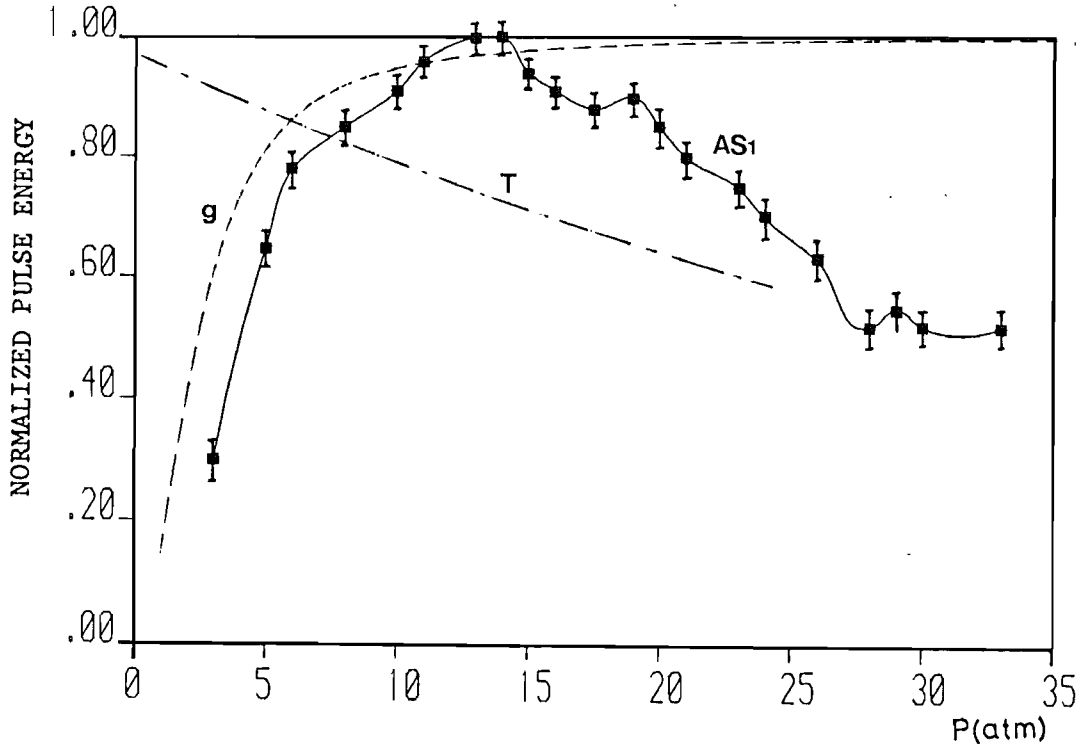

Figure 5.12. Relative output energy for AS1 component in a capillary waveguide. (T) capillary transmission. (g) Raman gain coefficient normalized to its value at high pressure.

In figure 5.12 we show the Raman gain coefficient and the capillary transmission as well. The Raman gain coefficient is normalized to 2.7 cm/GW, which is the value of g in the pressure broadening region. The capillary transmission was obtained by considering the transmission for each capillary mode assumed by the anti-Stokes radiation when the pressure is changed and the AS1 or AS2 components needed to find a new mode to reach the phase match. The curve is shown as a continuous line which passes through the discretes value obtained in the calculation.

One can observe that figure 5.12 shows a relative pulse energy dependence on pressure very similar to the one shown in figure 5.10. The difference between these curves is the shift of the maximum conversion efficiency to lower pressure values. This is because the reduction in the pump wavelength leads to a small factor G and consequently a small pressure is necessary to phase match the process.

5.6.6.4 Beam shape observations for anti-Stokes components
Pump source:2nd harmonic of Nd:YAG laser
Capillary diameter:200 μm

At very low pressures, 2 to 4 atmospheres, we observe a spot-like shape and a very low conversion efficiency for the first and second anti-Stokes components. For the first anti-Stokes as the pressure is increased a very diffuse ring appears surrounding the central spot. As the pressure is increased above 11 atmospheres the central spot becomes smaller and fickle from shot to shot while the ring surrounding it becomes very well defined.For the AS2 component the central spot disappears at very low pressure and a ring -like shape appears at pressure as low as 5 atmospheres.

In figure 5.13 we show a sequence of photographs taken using a scanning photo diode array which is placed after a set of ultraviolet filters in order to detect only the AS1 and AS2 radiation. The first photo was taken at a pressure of 5 atm in the Raman cell, the central spot corresponds to the AS1 beam and the ring surrounding it is the AS2 component. As the pressure is increased the central spot changes to a well defined ring shape and no central spot is observed for higher pressures.

5.6.6.5 Comments

From these experimental observations we may conclude that the decreasing of the pulse energy for anti-Stokes components shown in figures 5.10 and 5.12 at lower pressures are determined basically by the reduction of Raman gain coefficient at low pressures. At higher pressures another effect takes over, the component needs to use a high order capillary mode to reach phase matching. These high order modes reduce the efficiency of the process mainly in two ways: The first is the high propagation loss for the high order capillary modes and the second is the shape mismatch. While the pump and first Stokes use the EH_{11} hybrid mode, the anti-Stokes components use a high order capillary mode which has an intensity profile quite different from the EH_{11} intensity profile, making the transference of energy among the components very inefficient.

5.6.5.6 Energy measurements for anti-Stokes components
Pump source:2nd harmonic of Nd:YAG laser
Capillary diameter:350 μm

The last set of measurements was made using a large bore capillary. The experimental set up is similar to the others used in this section, the pump radiation is the second harmonic of a Nd:YAG laser and the capillary waveguide has a 40 cm length and 350 μm diameter.

In figure 5.14 we show the relative pulse energy for the AS1 component. The two main differences from this figure and the one for the output energy using a 200 μm diameter capillary are: The low output pulse energy for the anti-Stokes component and the shift of the maximum conversion to lower pressures when one use a large capillary diameter. One possible explanation for these facts may be taken from table II shown in appendix 4. From this table we can see that the phase match pressure for most of the mode combinations is very small, so for pressures in the experimental range of 10 to 30 atmospheres only very high order capillary modes can be used. Consequently we have a strong propagation loss for the anti-Stokes radiation generated in this mode besides the already mentioned fact of the mismatch between the EH_{11} intensity profile and the intensity profile for these high order capillary modes. At low pressures, where phase matching can be reached with low order capillary modes the reduction in the Raman gain coefficient reduces the efficiency for the whole process.

5.6.5.7 Beam shape observations for anti-Stokes components
Pump source:2nd harmonic of Nd:YAG laser
Capillary diameter:350 μm

In figure 5.15 we show the results of the measurement of the ring diameter for AS1 and AS2 components. The measurements were done at a distance of 2.5 meters from the capillary output. The line joinning the points is only a guide for the eyes. The first six points shown in the figure whithout error bars correspond to a calculation for the AS1 angle using the expression 5.64. As we may observe from the figure the minimum pressure used in the experiment to measure the AS1 ring diameter already corresponds to a phase

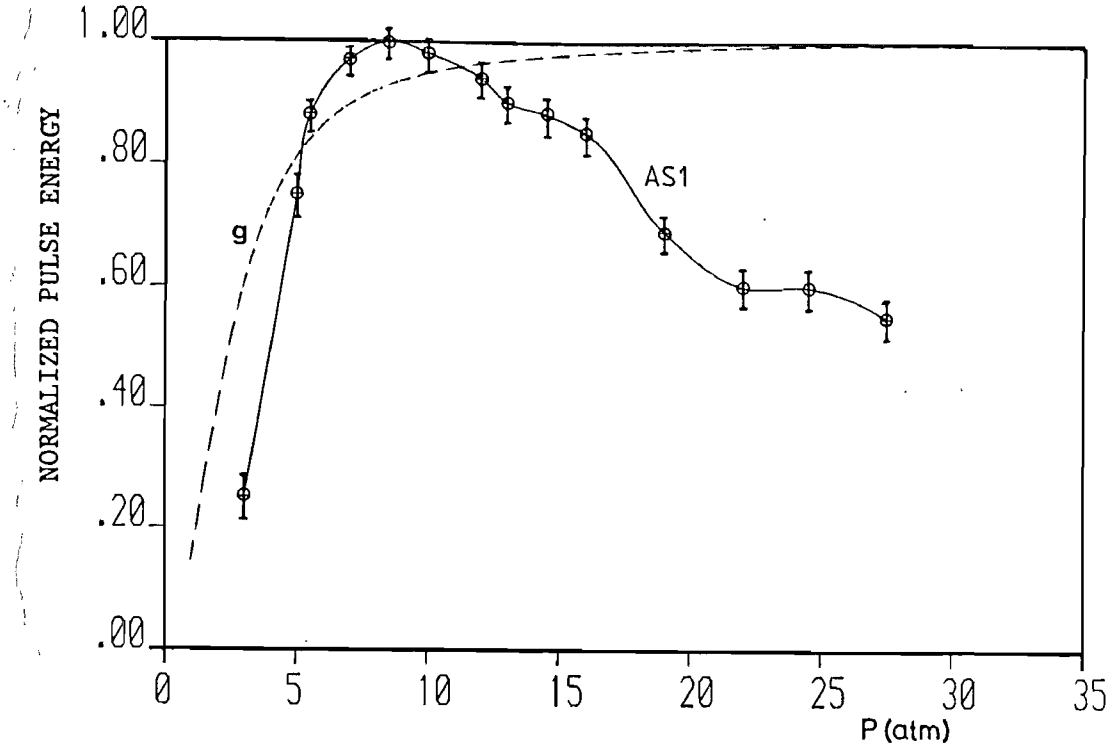

Figure 5.14. Relative output energy for anti-Stokes components in a capillary waveguide. (a) first anti-Stokes, (b) second anti-Stokes. The Raman gain coefficient (g) is ploted normalized to its value at high pressure.

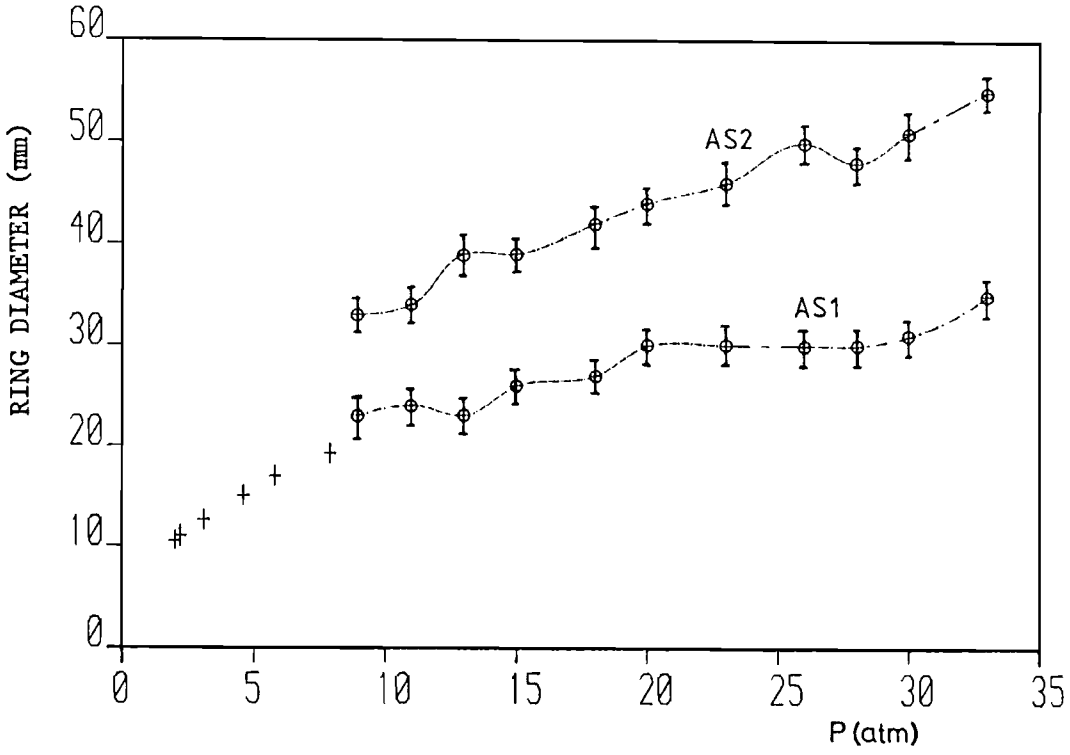

Figure 5.15. Ring diameter for AS1 and AS2 beams at 2.5 meters from capillary output. The line joint the points is only a guide for the eyes. The first six points without error bars correspond to the expected ring diameter using the first six capillary modes.

likely and a long coherence length and central spot are provided, allowing an exponential growth. However, as the parametric processes involving the EH_{11} mode and the cascade processes generate the same sort of spot-like beam, it is not easy to decide which process is producing the beam.

5.7 Final reduction of parametric terms

In section 5.4 we had the first reduction of parametric terms, in which we negleted all the four-wave interactions which include an anti-Stokes component among the interacting waves. In this section we discuss a new criterion for a further simplification of the parametric terms, based on the explanation given in section 5.5 and the experimental results.

From section 5.5 we have that the most important parametric process in the ζ-region 1 is V(0,1,1,2). Because the other processes in this region, V(0,1,2,3) and V(0,1,3,4), have a larger mismatch factor along the interaction axis and the components they generate, S3 and S4, cannot grow so efficiently via the cascade process in this region as the second Stokes wave.

From equation 3.83 and 3.84 we find that the intensity for the S2 component when mainly generated parametrically is proportional to $I_1^2 I_0$. So, even when the mismatch factor is high, the energy going into this component is still very much above the background noise level. The consequence of this amount of energy generated in the S2 component is that when the S1 component starts to grow exponentially above the threshold level, the S2 component does not need a Raman exponential gain equivalent to the one needed by the first Stokes in order to reach the SRS theshold. As a matter of fact S2 reaches the SRS threshold before the S1 component reaches its maximum conversion efficiency and from this value of ζ the S2 component starts to drain energy out of the S1 component via the cascade process, reducing in this way the maximum conversion efficiency of the S1 radiation. Thus the V(0,1,1,2) plays a very important role in determining the efficiency for the first Stokes radiation.

In ζ-region 2 the component S3 starts to be generated via the process V(1,2,2,3) and the same effect mentioned in the previous paragraphs of this section will occur. However the process is not so

efficient as in ζ–region 1 because the intensity of the parametrically generated S3 component is proportional to $I_2^2 I_1$ and the value of I_1 is not very high due to the S2 influence in ζ–region 1. But this process willstill produce enough energy in the S3 component so that the SRS threshold for the S3 component is reduced. Then. the conversion efficiency for the second Stokes is reduced in the same way that the conversion for the first Stokes wave was reduced.

Finally in ζ–region 3 the process V(2,3,3,4) generates the fourth Stokes radiation.

For the final reduction of terms we are going to keep only the parametric processes V(0,1,1,2), V(1,2,2,3) and V(2,3,3,4). In a general way we may say that if we are at ζ–region **j**, the strongest components will be S_{j-1} and S_j and the more important parametric process is V(j-1,j,j,j+1).

In figure 5.17 we compare the solution for equations 3.83 and 3.84 when all the parametric processes are considered and when only the three processes mentioned above are taken into account.

Table IV shows the overall reduction carried out in the Raman equations. In the final reduction we neglect the process V(0,1,-1,0) which was discussed in section 5.2, since when one uses the correct value for the mismatch factor, this process does not have any big influence on the first Stokes conversion efficiency.

TABLE IV

Final reduction of terms

	I	II	III
Number of equations	14	14	10
Number of cascade terms	12	12	8
Number of parametric terms	100	44	12
Number of parametric processes	15	9	3

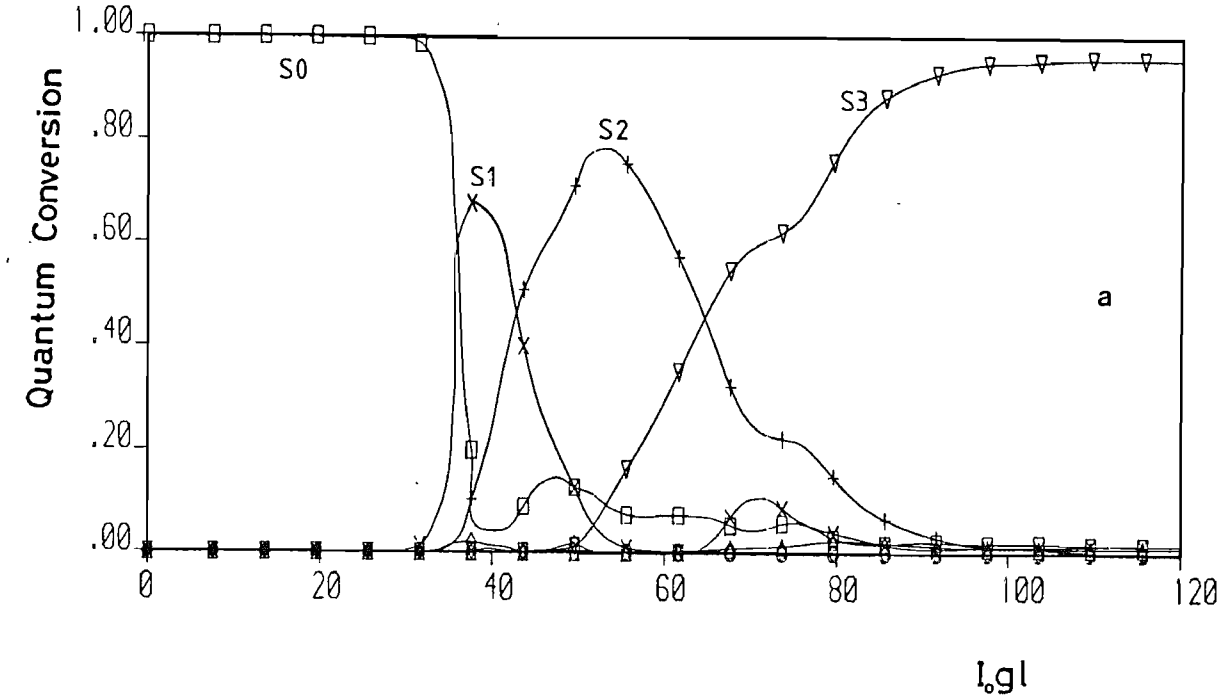

(a)

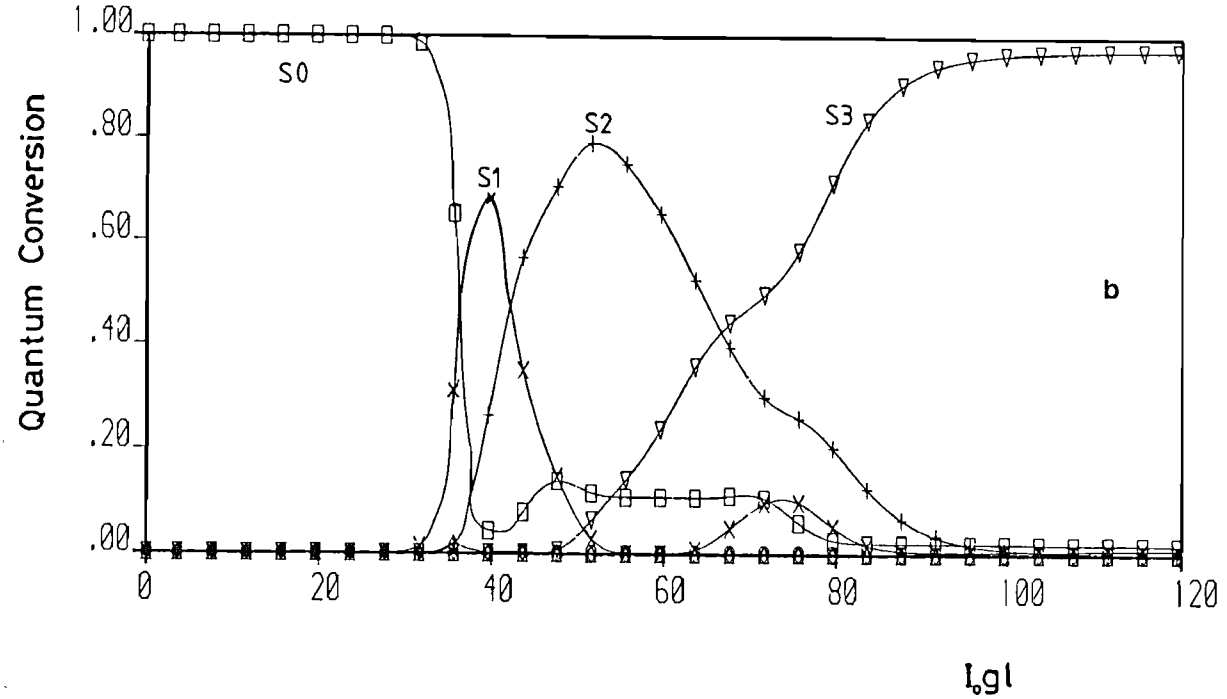

(b)

Figure 5.17. Numerical solution for the set of coupled equations. (a) solution with no reduction of terms, (b) solution with the reduction proposed in this chapter.

I. No reduction of terms.

II. Reduction by keeping terms with the pump intensity.

III. The final reduction described in this section.

All the considerations about reduction in the number of parametric terms are valid only for an unguided medium, in which we can define the more important parametric processes based on the exponential growth and the walk off for the radiations. In a waveguide structure we cannot neglect the other parametric processes because any radiation generated in any region in the waveguide will remain inside the active medium for the whole interaction length. For the capillary waveguide any parametric process can become important in so far as the gas pressure provides phase matching for a parametric process with a given set of capillary propagation modes. Consequently no general simplification is possible for a guided medium, however, for a given value of pressure and capillary diameter some simplification can still be done regarding the Stokes conversion efficiency.

5.8 **Biharmonic pumping**

As an extension of the discussion about parametric processes carried out in this chapter, we are going to analyse the case where the components interacting in a specific parametric process do not come from a unique pump source.

As a result of stimulated Raman scatering (SRS) in a medium, a high power wave of coherent molecular vibrations is produced from which a probe light wave can be scattered. Since this process does not require an intensity threshold, a weak radiation can be down shifted in frequency with good efficiency. For example, tunable radiation from an optical parametrical oscillator can be used and the shifted signal can be tuned continuously over a wide infrared range. This process was proposed by Brosnan et al (1977) and is know as coherent Raman mixing.

Usually the theory of coherent Raman mixing assumes that the probe wave is scattered by vibrations excited by the pump and first Stokes components,i.e. it assumes the Raman cell in the ζ-region 1. However, for a high value of Raman exponential gain the higher order scattering components may play an important role in

ther mixing process. Nikitin (1982) showed that the second Stokes together with the first stokes component can excite the medium vibration and produce more efficient infrared generation due to the longer wavelengths involved.

The case discussed in this section is a more general one, where strong radiation is injected in an already excited medium and this radiation can produce medium excitation by itself. Then we analyse the parametric interaction among the Stokes components produced by each pump. This situation where we have a molecular vibration driven by two different sources, we will call biharmonic pumping.

The complex amplitude of the molecular vibration in the case where the pump intensity is enough to generate several Stokes waves can be written in a short form as, [Nikitin (1982)]

$$Q= E_0E_1^* - \Sigma_{j\neq 1}E_{j-1}E_j^*.\exp(i\Delta k_j.z) \qquad 5.66$$

where $$\Delta k_j= (k_0-k_1)-(k_{j-1}-k_j) \qquad 5.67$$

E_0, E_1 and E_j are the complex amplitudes for the pump, first Stokes and a j_{th} Stokes or anti-Stokes electrical field. Δk_j is the mismatch factor and j may assume any value different from j=1, in order to include all the Stokes and anti-Stokes components.

We are going to consider the case where the pump (E_0) is in the visible region and can generate up to four Stokes waves, two anti-Stokes waves will be considered too.

The other pump is in the infrared region and its photon energy can produce only two Stokes shifts, for this pump one anti-Stokes will be considered. The first pump may well be a dye laser or second harmonic of a Nd:YAG laser while the second pump can be the radiation of a Nd:YAG laser.

The amplitude of the molecular vibrations for the infrared pump may be written as:

$$V = Y_0Y_1^* - Y_{-1}Y_0^*.\exp(i\delta_1 z) - Y_1Y_2^*.\exp(i\delta_2 z) \qquad 5.68$$

where $$\delta_1=(S_0-S_1)-(S_{-1}-S_0) \qquad 5.69$$

$$\delta_2=(S_0-S_1)-(S_1-S_2) \qquad 5.70$$

Where Y_j and S_j are the complex amplitude of electrical field and wavevector for the j component.

For the pump in the visible region we have:

$$Q=A_0A_1^*\text{-}A_{-2}A_{-1}^*.\exp(i\Delta_1.z)\text{-}A_{-1}A_0^*.\exp(i\Delta_2.z)\text{-}A_1A_2^*.\exp(i\Delta_3.z)\text{-}A_2A_3^*.\exp(i\Delta_4.z)\text{-}A_3A_4^*.\exp(i\Delta_5.z) \quad 5.71$$

where

$$\Delta_1=(k_0\text{-}k_1)\text{-}(k_{-2}\text{-}k_{-1}) \quad 5.72$$

$$\Delta_2=(k_0\text{-}k_1)\text{-}(k_{-1}\text{-}k_0) \quad 5.73$$

$$\Delta_3=(k_0\text{-}k_1)\text{-}(k_1\text{-}k_2) \quad 5.74$$

$$\Delta_4=(k_0\text{-}k_1)\text{-}(k_2\text{-}k_3) \quad 5.75$$

$$\Delta_5=(k_0\text{-}k_1)\text{-}(k_3\text{-}k_4) \quad 5.76$$

Then if we allow:
1. Cascade and parametric processes among the components generated by Y_0,
2. Cascade and parametric processes among the components generated by A_0,
3. Parametric processes among the components generated by A_0 and Y_0,

we obtain the following set of Raman equations:

$$dY_{-1}/dz=(\gamma_{-1}/2).[Y_0V.\exp(-i\delta_1z)+Y_0Q.\exp(-i\theta_1z) \quad 5.77$$

$$dY_0/dz=(-\gamma_0/2).\{Y_1[V+Q.\exp(-i\theta_2z)]+Y_{-1}[V^*.\exp(i\delta_1z)+Q^*\exp(i\theta_1z)]\} \quad 5.78$$

$$dY_1/dz=(\gamma_1/2).\{Y_2[V.\exp(-i\delta_2z)+Q.\exp(-i\theta_3z)]+Y_0[V^*+Q^*\exp(i\theta_2z)]\} \quad 5.79$$

$$dY_2/dz=(-\gamma_2/2).\{Y_1[V^*\exp(i\delta_2z)+Q^*\exp(i\theta_3z)]\} \quad 5.80$$

$$dA_{-2}/dz=(g_{-2}/2).\{A_{-1}[Q.\exp(-i\Delta_1z)+V.\exp(-iT_1z)]\} \quad 5.81$$

$$dA_{-1}/dz=(g_{-1}/2).\{A_0[Q.\exp(-i\Delta_2 z)+V.\exp(-iT_2 z)]-A_{-2}[Q^*\exp(i\Delta_3 z)+V^*\exp(iT_1 z)]\} \quad 5.82$$

$$dA_0/dz=(-g_0/2).\{A_1[Q+V.\exp(-iT_3 z)]+A_{-1}[Q^*\exp(i\Delta_2 z)+V^*\exp(iT_2 z)]\} \quad 5.83$$

$$dA_1/dz=(g_1/2).\{A_2[Q.\exp(-i\Delta_3 z)+V.\exp(-iT_4 z)]+A_0[Q^*+V^*\exp(iT_3 z]\} \quad 5.84$$

$$dA_2/dz=(-g_2/2).\{-A_3[Q.\exp(-i\Delta_2 z)+V.\exp(-iT_5 z)]+A_1[Q^*\exp(i\Delta_3 z)+V^*\exp(iT_4 z)]\} \quad 5.85$$

$$dA_3/dz=(g_3/2).\{A_4[Q.\exp(-i\Delta_6 z)+V.\exp(-iT_6 z)]-A_2[Q^*\exp(i\Delta_4 z)+V^*\exp(iT_5 z)]\} \quad 5.86$$

$$dA_4/dz=(-g_4/2).\{A_3[Q^*\exp(i\Delta_6 z)+V^*\exp(iT_6 z)]\} \quad 5.87$$

Where γ and g are the Raman gain coefficient for the medium excited by Y_0 and A_0 respectively. θ and T are the mismatch factor for the parametric processes using components generated by the two pump sources. They are defined as:

$$\theta_1=(k_0-k_1)-(S_{-1}-S_0) \qquad T_1=(S_0-S_1)-(k_{-2}-k_{-1})$$

$$\theta_2=(k_0-k_1)-(S_0-S_1) \qquad T_2=(S_0-S_1)-(k_{-1}-k_0)$$

$$\theta_3=(k_0-k_1)-(S_1-S_2) \qquad T_3=(S_0-S_1)-(k_0-k_1)$$

$$T_4=(S_0-S_1)-(k_1-k_2)$$

$$T_5=(S_0-S_1)-(k_2-k_3)$$

$$T_6=(S_0-S_1)-(k_3-k_4) \quad 5.88$$

The equations 5.78 to 5.88 describe most of the processes involving Stimulated Raman scattering and four-wave mixing. If V is set to zero in those equations we have the typical equations for coherent Raman mixing. When Y_i is set equal to zero we have the

usual equations for the SRS and parametric processes discussed in section 5.2 and 5.7 of this work.

Due to the wide range of processes included these equations are too extensive in their complete form and an analysis must be done for each particular case. For example, a pump source in the visible is able to generate third Stokes radiation in hydrogen and we want to increase the pulse energy of this component by using radiation from a Nd:YAG laser. To carry out the analysis we need to answer two questions:1. What is the most important parametric process for this energy transference? 2. In which ζ-region should the Raman medium be for each pump? In the case of pumping with 532nm and 1064μm radiation we may say that the beginning of the region 3 is the best for the pump radiation at 532 nm. At this point the second Stokes component (E_2) is very strong and provides an efficient exponential growth for the seed radiation for the third Stokes (E_3). E_3 is generated parametrically involving components of the two pump system (parametric process T_5). For the pump in the infrared region the Raman medium should be in ζ-region 1 , because the involved wavelengths are in a region of low gas dispersion and due to the small Raman coefficient for the second Stokes wave (Y_2) , most of the energy can be concentrated in the pump (Y_0) and first Stokes (Y_1) beams. However, if the pulse energy of the infrared source is too powerful when compared with the pulse energy of the 532nm pump source, the ζ-region for the Raman medium at this wavelength is not important since in this case most of the energy going into the S3 component is coming from the parametric process T_5 itself,

$$T_5=(S_0-S_1)-(k_2-k_3)$$

and the intensity of the E_3 component is proportional to the product involving the infrared pump pulse intensity and its first Stokes component and the second Stokes generated by the visible pump source,

$$E_3 \propto Y_0 Y_1 A_2$$

In chapter 6 we will present the experimental arrangement and the results of the experiment for biharmonic pumping in hydrogen using a Nd:YAG laser and its second harmonic as pump sources.

CHAPTER SIX

HIGH EFFICIENCY RAMAN CONVERSION

In this chapter we analyse the methods for obtaining a high conversion efficiency for a specific Stokes shift. The experimental set up to reach this good perfomance for first and third Stokes is described.

Among the factors which limit the transference of energy into a Stokes component are: Medium saturation, backward stimulated Raman scattering, four-wave mixing and high order Stokes generation.

The first factor, the medium saturation, is a problem only when one needs to run the Raman cell at very low gas pressures, but at the usual pressures, 20 to 50 atmospheres, this effect is not observed.The same happens with backward stimulated Raman scattering, the high pressure in the Raman cell and the laser linewidth, 0.3 cm^{-1}, make the coherence length for the Raman medium too short for this sort of interaction.

The third and fourth factors, however, play a very important role in the determination of the conversion efficiency for a given Stokes shift. As was discussed in chapter five, the parametric interaction among any set of four components leads to a redistribution of the available energy among the components, preventing in this way any single component reaching a very high conversion efficiency. Most of the techniques described in this chapter will deal with methods to minimize this redistribution of energy.

The fourth factor, in spite of its importance in determining the conversion efficiency of a given Stokes component, cannot easily be minimized, especially when one uses pump wavelengths in the visible region of the spectrum where the Raman gain coefficient is particularly high. Thus, the methods described in this chapter try to give a maximum conversion efficiency for a given Stokes component for a value of Raman exponential gain (ζ) which is small compared with the value of ζ necessary to generate the next Stokes component efficiently.

6.1 Oscillator and amplifier analysis

Regarding the conversion efficiency of the Stokes components we may say that the parametric processes produce two effects which are related. The first effect is the redistribution of energy among the Stokes components due to a pure parametric interaction among these components. The second effect, which also affects the Raman conversion efficiency, is the reduction of the expected value of Raman exponential gain for a given Stokes component to reach the SRS threshold.

The second effect is more important than the first one in determining the conversion efficiency of the Stokes component. Due to the (usually) short interaction length and the linear dependence of generated intensity on each of the interacting intensities, the parametric processes have a small influence on the intensity of a Stokes component in a ζ-region where it is growing viathe cascade process. However, in the second effect we have a combination of parametric and Raman cascade processes occurring which reduce the conversion efficiency of a given Stokes component. This effect was described in the last chapter, where we saw that only a few parametric processes need to be considered. These parametric processes were defined in section 5.7 and they depend on which ζ-region we are observing.

$$\text{Region } j \quad \Rightarrow \quad \text{Process} \quad V(j,j-1,j+1,j) \tag{6.1}$$

The process $V(j,j-1,j+1,j)$ generates energy in the component S_{j+1} in a part of the ζ-region where only the S_{j-1} component has high pulse energy. Then, when the S_j component reaches the SRS threshold, the energy into the S_{j+1} component is very much above the background level and so it needs a small value of ζ in order to reach the Raman threshold. As a consequence of this one needs a very small amount of energy in the S_j component in order to reach SRS threshold for the S_{j+1} component. Thus, after S_{j+1} reaches the SRS threshold the two components become strongly coupled through the usual Raman interaction and the conversion efficiency for S_j is reduced. The equations coupling the S_j and S_{j+1} components involving only cascade terms can be written as:

$$dE_j/dz=(-3\omega_j/4cn_j).\chi(j,j).E_j.|E_{j+1}|^2 \qquad 6.2$$

$$dE_{j+1}/dz=(3\omega_{j+1}/4cn_{j+1}).\chi(j,j).E_{j+1}.|E_j|^2 \qquad 6.3$$

Thus, this example of energy redistribution is a unique case where parametric and cascade processes are directly related to each other.

The main approach for overcoming the energy redistribution effect and for obtaining a high conversion efficiency for an S_j component is to inject seed radiation at the wavelength λ_j in the Raman cell, so that the maximum conversion efficiency for the S_j component will occur for a small value of Raman exponential gain.

In figure 6.1 we show the result of the numerical calculation when the first Stokes component starts from noise background and when a small signal, at S1 wavelength, is injected in the amplifer. In this calculation we assumed a loosely focused pump beam, so that the confocal parameter is equivalent to the cell length. The more important conclusion about this calculation is that, the first Stokes component can reach a much higher conversion efficiency when a seed radiation is used than when this component starts from noise background. The exact value of the energy in the seed radiation is not fundamentally important to determine the final Stokes conversion efficiency. We noted that a variation of 10 times in the initial pulse energy produces a increase of less than 10% in the overall conversion efficiency.

6.1.1 The oscillator-amplifier tandem configuration

The seed radiation for an S_{j+1} component in ζ-region 1 is obtained in a primary Raman cell, in which we do not need a high conversion efficiency. However the beam generated in this Raman cell should have very good spatial characteristics since it will define the spatial characteristics of the amplified beam. This primary Raman cell is basically a superfluorescent Raman amplifier, i.e. a Raman cell where the desired Stokes component grows from the noise background level in a single pass of the pump beam through the Raman medium. This superfluorescent Raman amplifier will be referred simply asthe Raman oscillator throughout this chapter.

The pump beam is focused inside the Raman oscillator where the seed radiation for the S_{j+1} component is generated. This seed radiation and the pump left after the Raman oscillator are focused

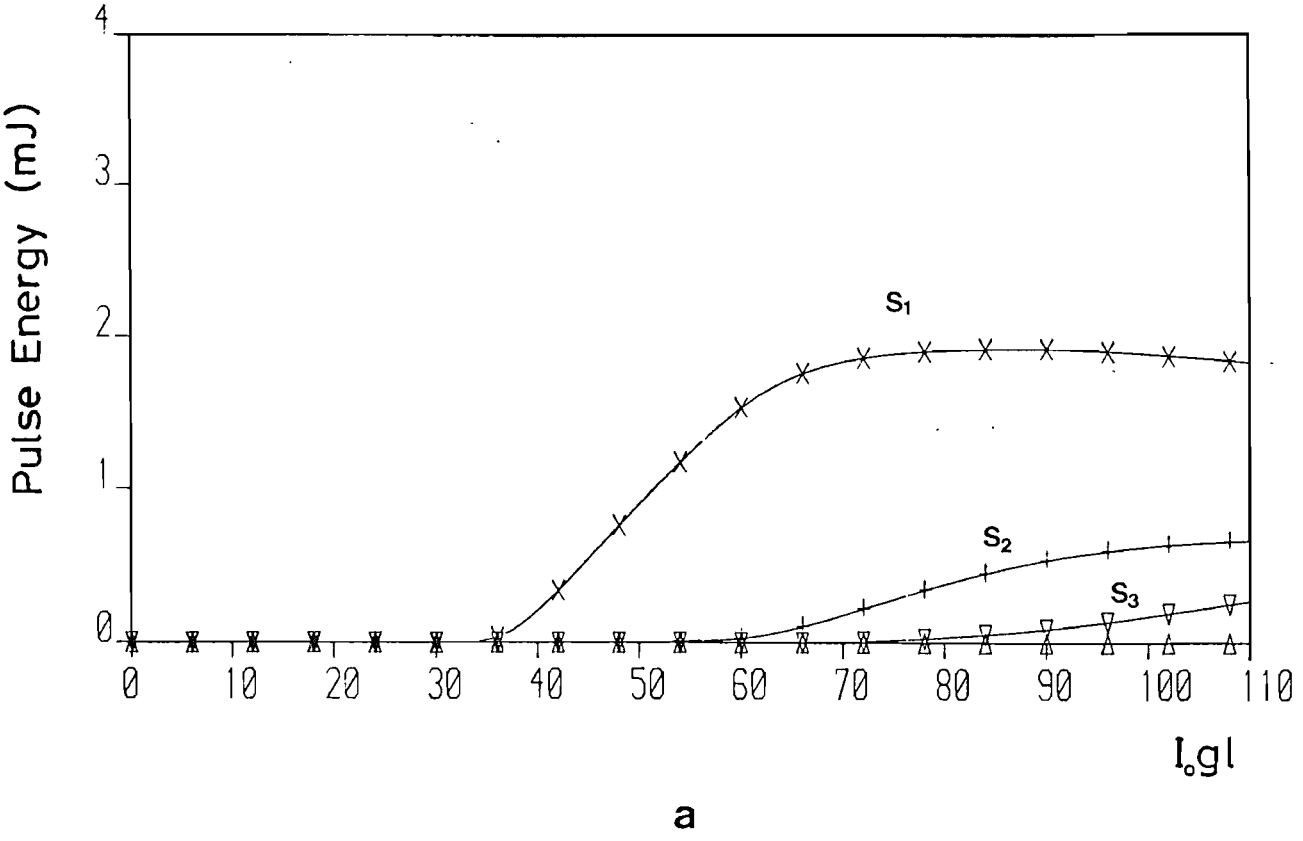

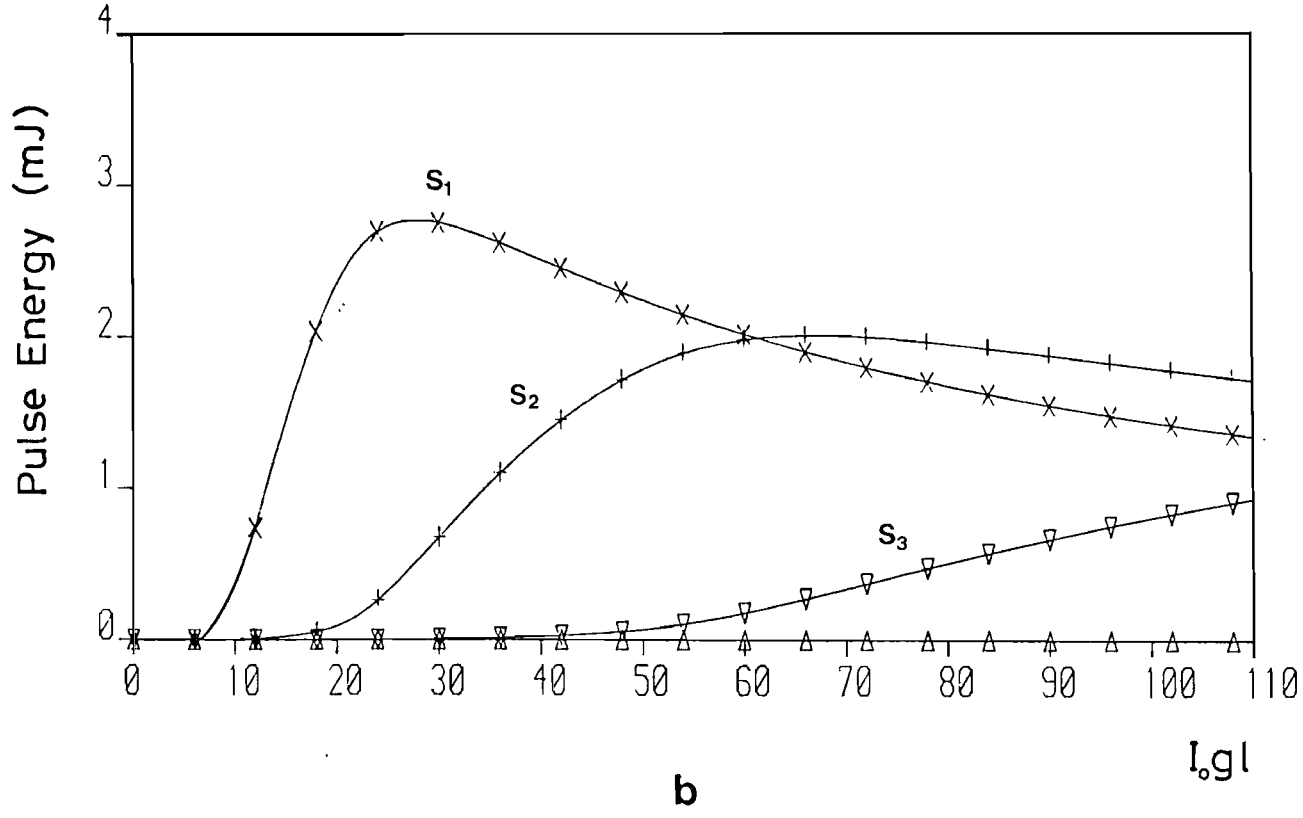

Figure 6.1. Numerical solution for the Raman equations including parametric terms, gaussian profile for intensity distribution and a Gaussian structure in time.

Pump pulse energy= 10mJ,

Stokes initial pulse energy= noise (figure 6.1a)

1 μJ (figure 6.1b)

inside the Raman amplifier,figure 6.2.

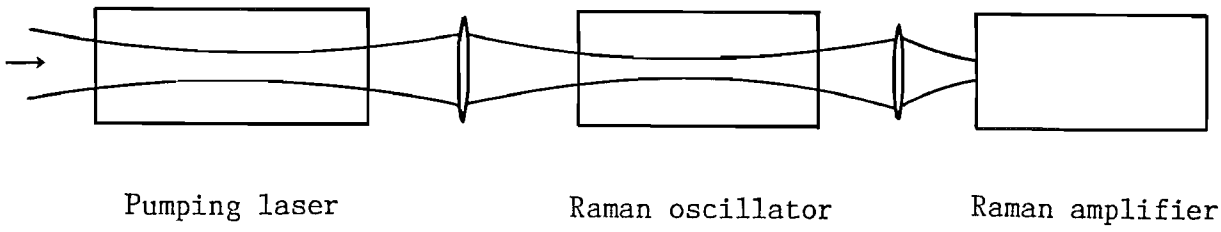

Figure 6.2. Raman oscillator and Raman amplifier in a tandem configuration.

This configuration brings several advantages from the experimental point of view. It does not need any delay line to make the pump and the seed radiation arrive at the same time inside the Raman amplifier and it provides automatic alignment for the two beams. The alignment of these two beams is not a trivial task, due to the difference in spot sizes and wavelengths. Komine and Stappaerts (1982) reported that an overlap to within 0.2 mradwas needed (using several external positioning mirrors) but this can still be too great a misalignment for a long Raman amplifier cell. In the tandem configuration shown in figure 6.2 the seed radiation is generated by the pump itself and they both travel along the same path and consequently they are exactly collinear inside the Raman amplifier, which guarantees the maximum transference of energy from one beam to the other.

The oscillator-amplifier configuration should fulfil certain requirements in order to produce the maximum conversion for a specific Stokes shift:

Raman oscillator: 1. This stage should be able to generate a reasonable amount of energy into the S_{j+1} component using as little energy as possible from the pump beam.

2. The generated beam in this stage should ideally be diffracted limited, because the spatial characterisics of the seed radiation will determine the spatial characteristics and/or the output energy of the amplified beam.

Raman amplifier: The Raman exponential gain in this stage should be that necessary to produce a maximum conversion efficiency for the S_j component.

The requirements for the Raman oscillator are difficult to satisfy simultaneously in some cases. For example, for the case of the generation of first Stokes seed radiation in an unguided cell without depleting the pump very much, we need to use a large spot size in the Raman oscillator in order to keep the pump intensity at low levels and to have a Raman exponential gain just enough to produce a pulse energy for a first Stokes slightly above the threshold level. But a large spot size will allow generation of first Stokes beam at wide angles, producing a non-diffraction limited beam.

The maximum value for the spot size inside the Raman oscillator can be given approximatly by imposing the condition that the maximum angle at which the radiation can be generated is smaller than the beam diffraction angle. For a beam waist w_0 formed by the pump beam at the center of the Raman cell with length L, the maximum angle for an output beam which makes use of the whole interaction length in the cell is given by $2w_0/L$, when one assumes a long confocal parameter relative to the cell length. This angle must be kept smaller than the diffraction angle for a TEM_{00} profile for the first Stokes beam $\lambda_s/\pi w_s$. This condition leads to a minimum cell length given by:

$$L_{min}=2\pi w_0 w_s/\lambda_s \qquad 6.4$$

We may say that the cell length should be bigger than roughly the pump beam confocal parameter.

We overcame this problem by using an interstage configuration for the dye laser and the Raman oscillator in such a way that only a small part of the pump pulse energy went into the Raman oscillator cell. This arrangement will be explained in detail in the next section.

The requirement for the Raman amplifier is not difficult to reach, at least for low Stokes orders. It may be achieved mainly by choosing a convenient length for the Raman amplifer cell, so that

the Raman exponential gain willbe the one needed to produce a maximum conversion efficiency for a specific Stokes shift. As the spatial characteristics of the amplified beam are defined by the injected seed radiation one can afford to use a very large spot size for the pump beam in the Raman cell which minimises the redistributionof energy due to parametric processes only, increasing even further the conversion efficiency in the amplifier stage.

6.2 High conversion efficiency for the first Stokes wave

The experimental arrangement is shown schematically in figure 6.3. The dye laser was described in chapter two of this work and consists of a dye oscillator followed by two dye amplifiers. The dye cells are optically pumped by a Lambda Physik XeCl excimer laser, which produces 100 mJ in a 20 ns pulse. Rhodamine 6G laser dye is used throughout the experiment. A four-prism beam expander and a 2,800 lines/mm holographic grating are used in the dye oscillator cavity, which results in a $0.2cm^{-1}$ bandwidth for the tunable output radiation. With a pump pulse energy of 3 mJ from the excimer laser we obtain 40 μJ in a diffraction limited beam coming from the dye oscillator and 14 nsec FWHM.This dye laser pulse is amplified in the first dye amplifier stage which has a gain length of 1 cm, pumped by a 10 mJ pulse energy. The last dye amplifier cell has a 2 cm gain length and is pumped by the remaining energy from the excimer laser.

Between the first and second dye amplifiers there is a 200 μm bore diameter, 72 cm length quartz capillary waveguide as the Raman oscillator. The capillary is placed inside a stainless steel cell filled with hydrogen at 25 atmospheres pressure. Uncoated flat BK-7 glass windows were used at both ends of the cell. Due to the low laser threshold power required for SRS in a capillary waveguide [Berry et al (1982)] a dye laser pulse energy of 0.68 mJ sent into the capillary generates 60 μJ of first Stokes radiation.

Both the first Stokes and the unused pump beam emerging from the output end of the capillary are sent through the second dye laser amplifier. The unused dye laser beam is strongly amplified whereas the first Stokes is slightly attenuated. Thus, this seed Stokes beam is locked together with the amplified dye laser beam both spatially and temporally. The beams are focused at the centre of a 35 cm long Raman amplifier cell.

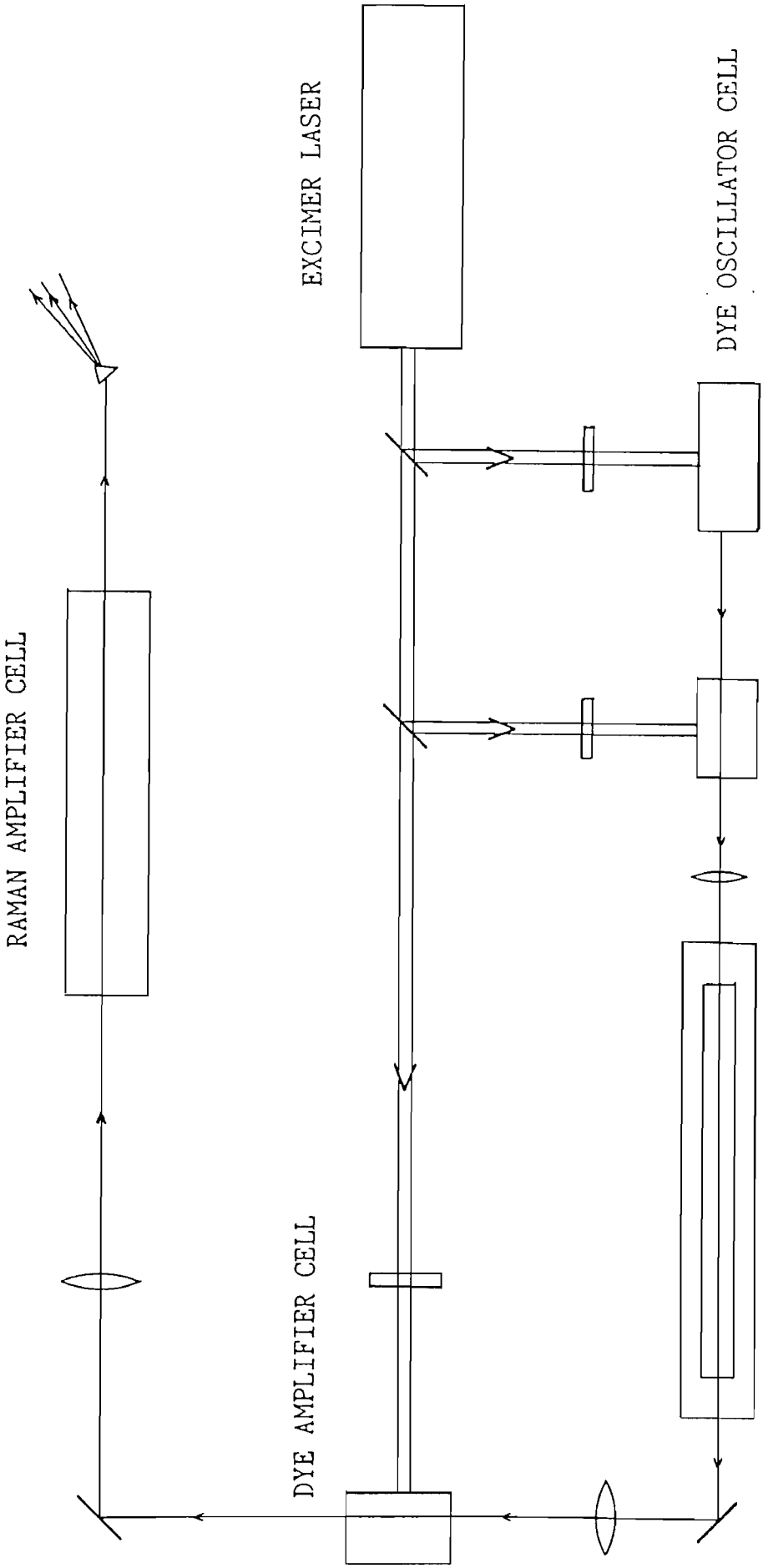

Figure 6.3. Experimental configuration of the dye-laser pumped Raman oscillator-amplifier.

The amplified first Stokes beam and remaining pump pulse beam are separated spatially after the Raman amplifier cell through a set of dispersive prisms and their energies were measured with a Laser Precision Corp. model RK3230 pyroelectric energy meter. The temporal profiles of the dye laser and Stokes pulses were recorded with a vacuum photodetector at various points along the optical set up and displayed using a Tektronix model R7912 transient digitizer and display unit, which have a combined bandwidth of about 500MHz. The spatial profile of the amplified Stokes is monitored with a scanning photo-diode array.

6.2.1 **The capillary waveguide as a Raman oscillator**

The utilization of a capillary waveguide as Raman oscillator is a very convenient way to meet the specifications for the oscillator stage given in section 6.1.1.

The positioning of the capillary waveguide after the first dye amplifier cell is quite a fundamental point in determining the perfomance of the whole system. Due to the low amplification in the first dye amplifier cell, the diffraction limited beam generated in the dye oscillator is not very much distorted, allowing consequently good coupling of the dye laser beam into the EH_{11} mode inside the capillary. This provides a low propagation loss for the pump beam and a Gaussian-like shape for the first Stokes beam. Good beam quality at this stage is quite important in our scheme as it determines the beam quality of the amplified Stokes and hence the ultimate Stokes brightness. This low propagation loss allied with a long interaction length provides a Raman exponential gain which is enough to generate a reasonable amount of first Stokes radiation using less than 10% of the total dye laser output pulse energy, which is a very important requirement for a Raman oscillator.

The theoretically predicted transmission for this waveguide is 90% at the dye laser wavelength of 575 nm. During the experiments however, a typical transmission was 50%. The lower transmission is believed to be due to bend and non-uniformity of the quartz capillary waveguide [Berry et al (1982)] and imperfect coupling of the pump beam inside the guide due to the position and size of the pump beam waist at the capillary entrance.

6.2.2 Stokes amplification in the Raman amplifier

The unused dye laser pump beam emerging from the capillary waveguide is amplified in the second dye amplifier cell and a 7 mJ pulse energy is obtained. The first Stokes seed radiation is attenuated from 60 μJ down to 40 μJ by the dye solution (methanol solvent). Both the dye laser and Stokes beams are focused inside the Raman amplifier by a 50 cm focal length lens. The hydrogen pressure was kept at 20 atmospheres during this experiment. The longer wavelength of the Stokes radiation produces a slightly bigger spot size inside the Raman amplifier cell than the dye laser beam. This is an advantage for the Raman conversion process, since all the dye laser beam is engulfed by the seed Stokes beam and an efficient depletion of the dye laser pump pulse is ensured. For this arrangement a 3.5 mJ pulse energy for the Stokes beam is obtained after the Raman amplification, which corresponds to a quantum conversion efficiency in excess of 90%.

The length of the Raman amplifier cell was chosen to give a maximum conversion efficiency for the first Stokes component. The Raman exponential gain for a 350 μm spot size inside the cell is approximately 20.

The beam profile for the amplified Stokes wave has quite a symmetrical Gaussian-like shape and in order to quantify this spatial characteristic we carried out some measurement on the beam profile. To do this measurement we focused the amplified Stokes beam down to a waist w_o, at a known position outside the Raman amplifier cell. With another lens (f_o) we imaged the waist w_o onto the scanning photo diode array (SPA) surface. The size of the spot on the SPA is related to the waist w_o via the known expression:

$$w_o=[f_o/(d-f_o)].w_{spa} \qquad 6.5$$

where d is the distance from the image to the lens f_o. Then we took out the lens f_o and measured the spot size with the SPA at several distances in order to determine the beam divergence δ_m, from the waist w_o. The ratio **M** between this measured divergence δ_m and the divergence expected for an waist w_o with a exact Gaussian profile δ_o, gives the factor by which the beam divergence exceeds the diffraction limited value.

$$M = \delta_m/\delta_0 \qquad 6.6$$

where $$\delta_0=\lambda_s/\pi w_0 \qquad 6.7$$

This was the method used to investigate the spatial characteristics of the amplified Stokes beam and we found M~1, which indicates a diffraction-limited beam.

6.2.3 Experimental results

The sequential temporal profile of the dye laser pulse as it goes through the several stages are depicted in figure 6.4. In figure 6.4a and 6.4b we have the pulse before and after the capillary waveguide, respectively. The pulse depletion shown in figure 6.4b is a result of the generation of first Stokes radiation inside the Raman oscillator. The Stokes pulse is shown in figure 6.5a.

Figure 6.4c shows the dye laser pulse after being amplified in the second dye amplifier cell. We can mention that the initial spike shown in this pulse temporal profile comes from the amplification of the undepleted part of the pulse coming from the Raman oscillator. However, most of the pulse energy is contained in the later part of this pulse. At this point we emphasize an important feature of this arrangement, which is the temporal match between the Stokes pulse and the portion of the dye laser pulse which contains most of the pump pulse energy, since this is the pulse region from which the Stokes wave was generated during the Raman interaction inside the capillary waveguide. Since we have spatial overlap as well due to the beams collinearity, we end up with very good matching for the two beam inside the Raman amplifier cell.

The temporal profile for the dye laser pulse is shown in figure 6.4d. As can be seen from the high degree of depletion in this pulse very efficient Raman conversion of the dye laser pulse into the first Stokes beam might occur in the Raman amplifier. The spatial profile of the amplified Stokes radiation is shown in figure 6.5b.

Using expression 3.67 which gives the intensity for the first Stokes beam as a function of the input dye laser pulse intensity, we can compare the experimental result with the expected

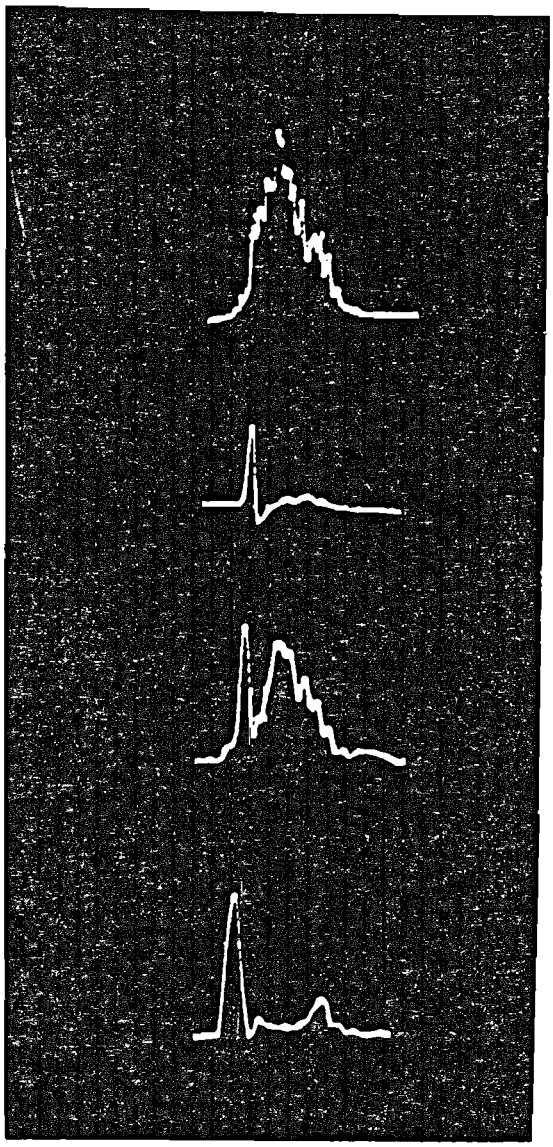

Figure 6.4. The temporal profiles of the dye laser at various stages in the configuration shown in figure 6.3: (a) at the input of the capillary, (b) at the output of the capillary, (c) after the second stage dye amplifier, (d) after the Raman amplifier.

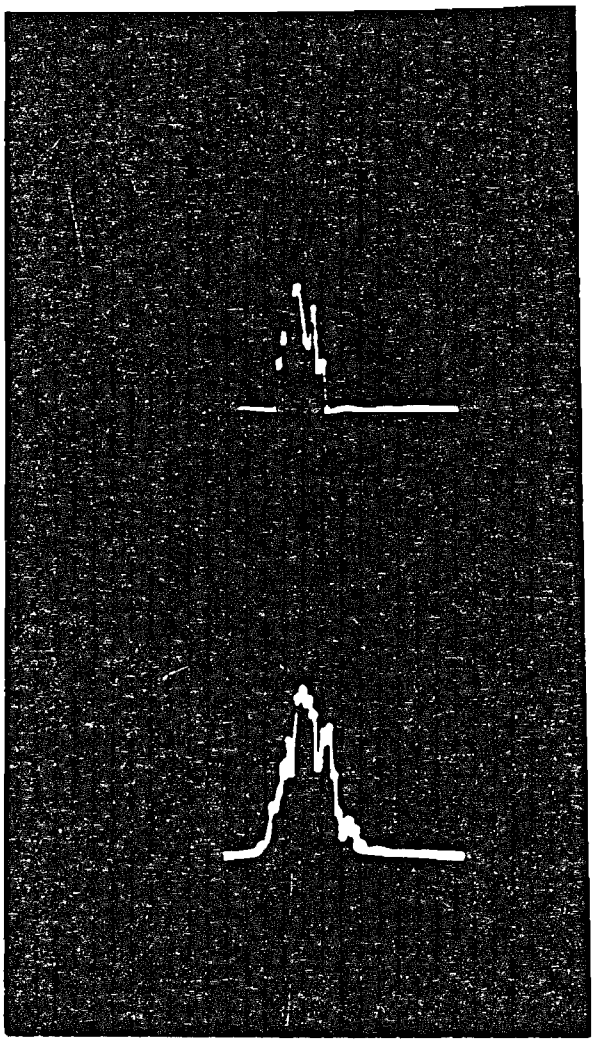

Figure 6.5. The temporal profiles of the first Stokes radiation: (a) after the capillary weaveguide, (b) after the Raman amplifier.

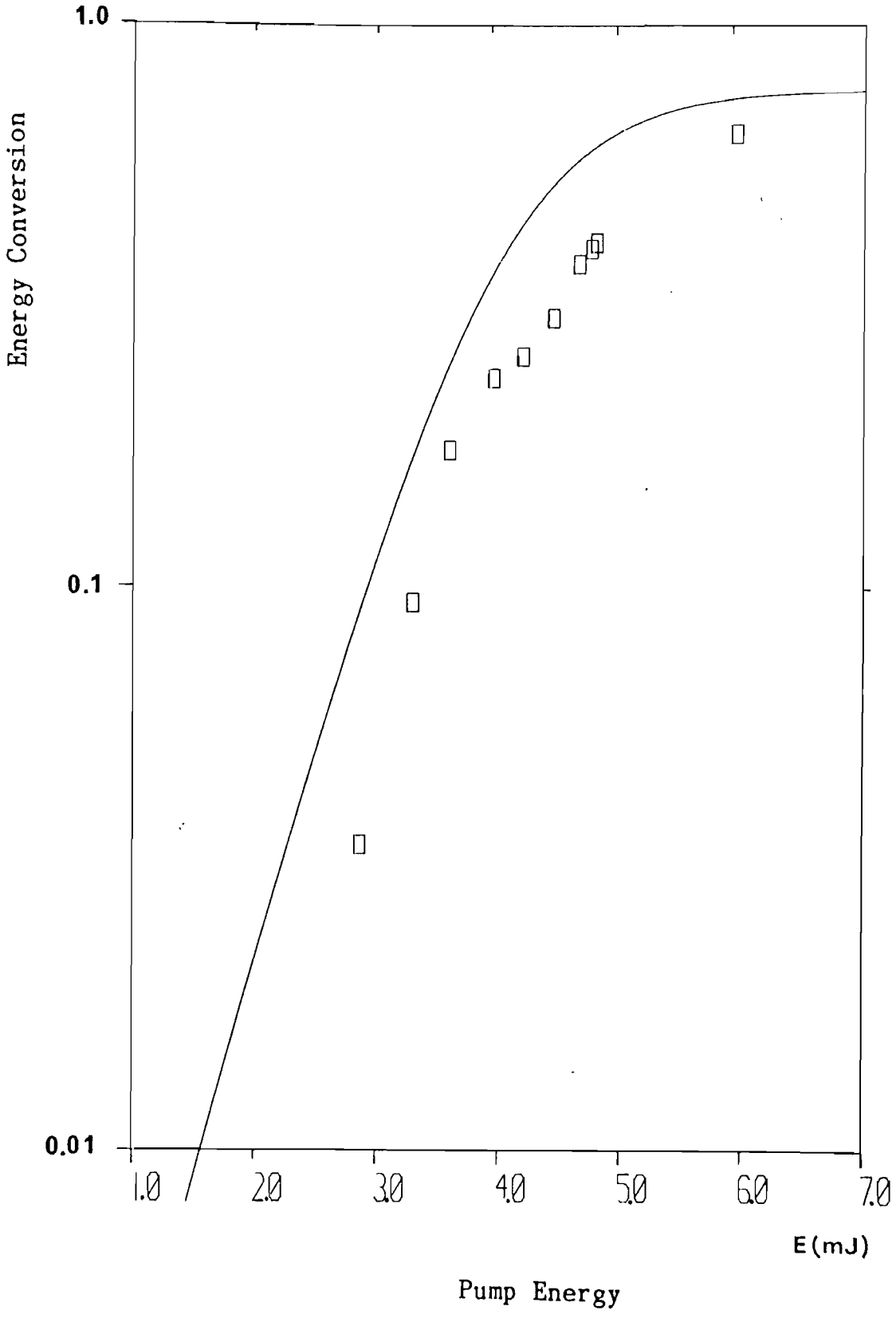

Figure 6.6. Raman energy conversion efficiency into first Stokes as a function of the input dye laser energy. The squares indicate the experimental results, the solid line corresponds to the calculation using expression 3.67.

commercially available dye laser systems and for laser pulses in the psec region, since the pulse synchronization between the interacting beams is automatically satisfied in this arrangement.

6.2.4 high order Stokes generation

The simplicity of the scheme described in the previous section allied with the high conversion efficiency obtained for a diffraction limited beam, led us to try the same set up to generate high order Stokes shifts, in this case the second Stokes wave.

The first dye amplifier cell was pumped with more excimer pulse energy and 1.1 of mJ dye laser pulse energy was injected into the capillary waveguide. The S2 radiation was observed at the capillary output with 20 μJ pulse energy.

Following the same procedure as for the first Stokes wave the second Stokes and the unused dye laser pulse energy were sent through the second dye amplifier where the dye laser beam was amplified. The two beams were focused inside the Raman amplifer cell.

A strong dependence of the amplified second Stokes beam with gas pressure was observed in this case. In the previous arrangement for the first Stokes beam, only when the gas pressure was reduced to values below 10 atmospheres did we notice a decrease in the Raman conversion efficiency. However for the second Stokes amplification we observed a maximum conversion efficiency at 10 atmospheres, while the energy in the first Stokes component did not change very much when the pressure was varied from 7 to 15 atmospheres. For gas pressures higher than 15 atmospheres the first Stokes pulse energy started to increase until it reached a plateau at 20 atmospheres while the pulse energy for the second Stokes was reduced almost to the value of the input seed radiation pulse energy.

This experimental observation suggest a strong parametric interaction inside the Raman amplifier. Measurements of the intensity profile over the cross section for the second Stokes beam showed a ring shape at the capillary output for a gas pressure of 7 atmospheres in the Raman oscillator, for lower gas pressures a spot and ring structure was observed.

The maximum conversion efficiency for the second Stokes component was 30%, after the Raman amplifier cell in a spot– ring

shape. One possible solution for this problem is to reduce the gas pressure in the Raman oscillator in order to generatethe second Stokes beam in a spot-like shape. The difficulty is, for pressures below 7 atmospheres in the capillary waveguide, we need more than 1.1 mJ in the dye laser pulse to generate any measurable energy for the second Stokes component. Then the seed generation starts to require a large amount of pump energy to be generated, leaving a very small amount of pump energy for the Raman amplifier, resulting in a low conversion efficiency for the whole system.

The system presented in this section, in spite of a reasonable conversion efficiency, fails to produce a spot-like output beam. In the next section we present a variation of the arrangement for the first Stokes generation which satisfies both requirements of a reasonable conversion efficiency and a spot-like beam for a high order Stokes wave.

6.3 Efficient SRS conversion into high order Stokes waves.

The main idea behind reaching a high conversion efficiency for the first Stokes still holds when one wants to have good conversion efficiency for a higher Stokes order. We need seed radiation for the S_i component and a reasonable intensity for the S_{i-1} Stokes component inside the Raman amplifier, so that we have an efficient conversion $S_{i-1} \rightarrow S_i$ via the cascade process. The problem is, how to generate seed radiation for the S_i component without depleting the pump strongly. The arrangement used to get high conversion for the S1 component cannot be used straight away because the single stage Raman oscillator is not able to generate high order Stokes with good efficiency due to the effect of energy redistribution caused by the parametric processes inside the capillary waveguide.

The set up described in section 6.2 can still be used if we have a pair of Raman cells for each Stokes shift. This solution, however, implies that we need to use several cells to reach a specific high order Stokes, which is not practical in some cases. We will try to keep the arrangement as simple as possible and in this section we describe a scheme using only two Raman cells in order to generate any high order Stokes with a reasonable conversion efficiency in a spot-like shaped beam.

An arrangement giving a good conversion efficiency for a

high order Stokes S_i component is not trivial, because, in principle, we need to have a high conversion efficiency for all the previous Stokes shifts as well, from S_1 to S_{i-1}, and this is quite difficult to reach with a single oscillator-amplifier configuration. An experimental set-up reported by Komine and Stappaerts (1982) quoted a conversion efficiency of 18% for the third Stokes shift with an oscillator-amplifier arrangement. This good conversion efficiency is due mainly to the pump wavelength in the ultraviolet region (308 nm) providing a large Raman gain coefficient and high medium dispersion. The High Raman gain coefficient leads to a large ζ value and then the S3 component can be generated with reasonable values of pump pulse power and cell length. The high medium dispersion at these wavelengths helps to reduce the effect of the four-wave interaction, since the wavevectors of the interacting beams require a wide angle to reach the phase match and consequently they do not interfere very much with the intensity of the growth via the cascade process, whichis mainly along the axis of the Raman cell.

In our case the pump is in the visible region of the spectrum and consequently the third Stokes component is in the near infrared region of the spectrum which makes the Raman gain coefficient and the medium dispersion very small.

The basic problem we have is to find a way to generate a reasonable amount of seed radiation at the desired Stokes shift without considerably depleting the pump pulse. One solution for this problem is found by analysing the interacting mechanisms inside the Raman cell. All we need is a mechanism able to generate any Stokes component without needing to go through the previous Stokes shift and this mechanism need not be very efficient because we need only a small amount of energy in the seed radiation and the pump pulse must be as little depleted as possible. There is only one mechanism having these specifications: four-wave mixing.

Using this principle we will consider two Raman cells. In the first one, the Raman oscillator, seed radiation for an S_i Stokes component is produced via the parametric process. this seed radiation is amplified in the second Raman cell, Raman amplifer, mainly by cascade processes.

With this arrangement we found a way to make the parametric processes increase the conversion efficiency for Stokes radiation. The pump beam is focused inside the Raman oscillator cell to provide

a wide range of angles, so that the desired parametric process can be phase matched properly. The gas pressure in this cell must be kept as low as possible, not only to enhance the conversion efficiency of the parametric process, but to reduce the Raman gain coefficient. The reason for this is to avoid the enhancing the cascade Raman generation in this stage, since the parametric process produce quite efficient generation of S2 radiation via the process

$$k_0 - k_1 = k_1 - k_2$$

This limits the conversion efficiency for the S1 component to very low levels, as was discussed in Chapter Five and this is not very convenient because we need a strong first Stokes component in the Raman amplifier to carry on the cascade transference of energy from the pump to the desired seed input radiation.

As a Raman amplifier we use a capillary waveguide because we need a high Raman exponential gain in order to amplify the S_i component via the cascade process. The guiding structure brings out two problems: the coupling of the radiation generated in the Raman oscillator into the Raman amplifier cell and the enhancement of parametric processes due to the confinement of the radiation as we have discussed in section 5.6.5. These will be analysed later in this chapter.

6.3.1 **Experimental results**

The experimen tal arrangement is shown schematically in figure 6.8. A Nd:YAG laser (described in chapter 2) and a KD*P type II doubling crystal produce an energy of 15.7 mJ in a 22 nsec FWHM pulse inside the Raman oscillator at 532 nm wavelength. A broad band infrared filter was used to block the infra red radiation going through the doubling crystal. The 50 cm long Raman oscillator was a stainless steel cell filled with hydrogen at 10 atmosphere pressure. Uncoated flat BK-7 glass windows were used at both ends of the cell. The beam generated by the Nd:YAG laser was not diffraction limited because we used a large aperture (5.5mm) inside the laser cavity in order to get more energy per pulse and consequently high order transverse modes were allowed too. The pump beam was focused inside the cell by a 70 cm focal length lens.A 240μm beam waist size was formed at the centre of the Raman oscillator cell for a 2.5 times

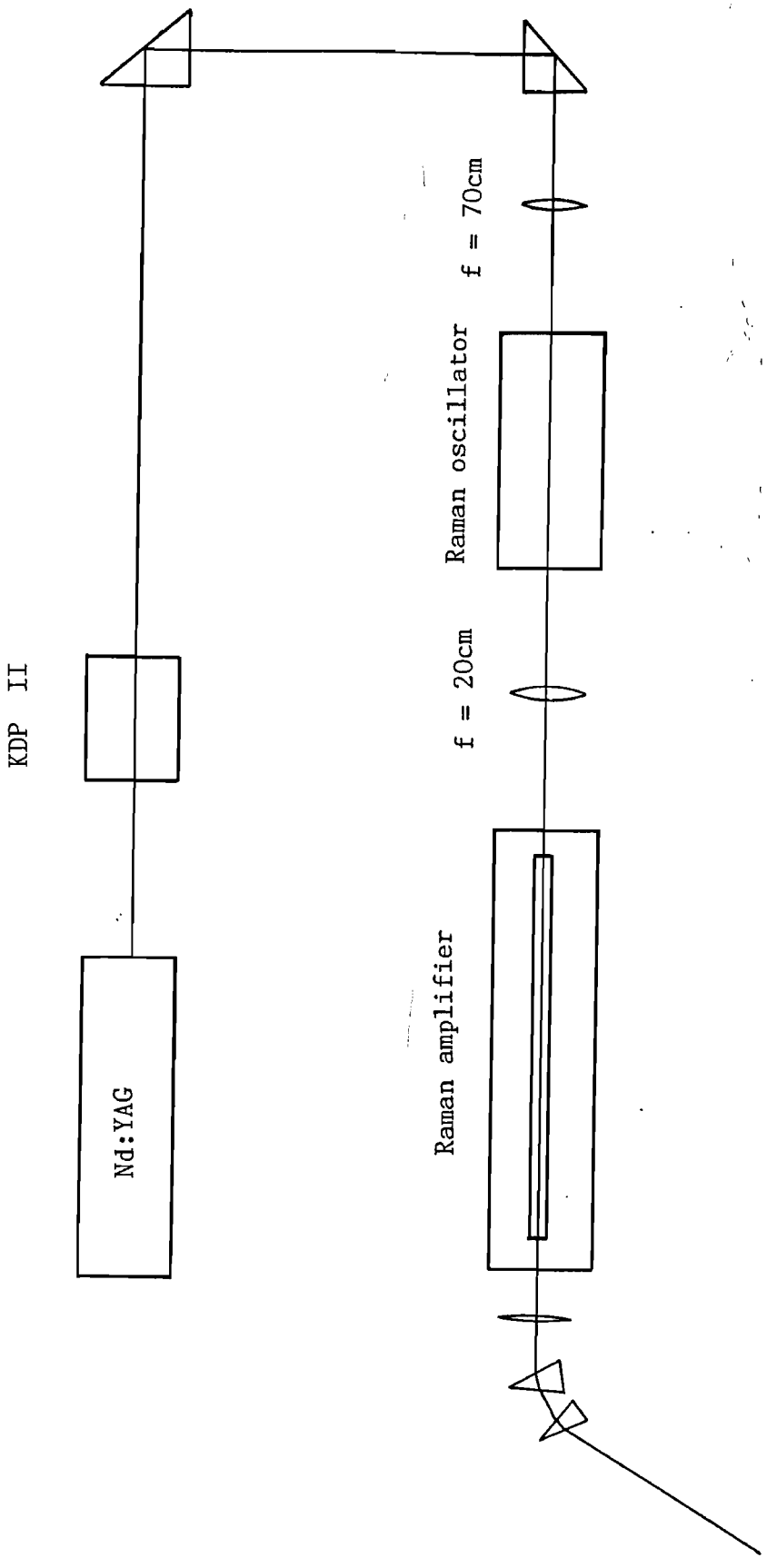

Figure 6.8. Raman oscillator-amplifier arrangement using a capillary waveguide as a Raman amplifier.

diffraction limited beam.

The energies for the components generated inside the Raman oscillator were measured using a pyroelectric energy meter, table I.

Table I

Pulse energy for the components generated in the Raman oscillator cell

component	pulse energy
pump (532nm)	9.1 mJ
1st Stokes (683nm)	2.2 mJ
2nd Stokes (954nm)	0.45 mJ
3rd Stokes (1.58μm)	0.045 mJ
4th Stokes (4.60μm)	not measurable
1st anti-Stokes(436nm)	0.28 mJ
2nd anti-Stokes(369nm)	0.022 mJ
3rd anti-Stokes(320nm)	<1μJ

Several anti-Stokes components were observed, although only the two first ones have a pulse energy above 1 μjoule.

All the radiations produced in the Raman oscillator cell were focused with the remaining pump at the entrance of a 71 cm long and 350μm diameter pyrex made capillary waveguide by a 20 cm focal length lens. The coupling into the capillary was optimized for the pump beam. In table II we show the measured transmission for the Stokes components in the capillary. The transmission for the pump beam was measured with no gas in the cells. For the Stokes components only the Raman oscillator was filled (at 10 atmospheres) while the Raman amplifier cell was kept empty.

Table II

Capillary transmission for the Stokes components

Component	Transmission
pump (532nm)	50%
1st Stokes (683nm)	37%
2nd Stokes (954nm)	30%
3rd Stokes (1.58μm)	<20%

The gas pressure in the Raman amplifier was 28 atmospheres and a set of dispersion prisms were used to separate the components. The pulse energies were measured using a pyroelectric energy meter and the values corrected for inside the Raman cell assuming a 92 % transmission for the cell windowns at all wavelengths. Table III shows the final result.

TABLE III

Pulse energies for Stokes components at the output of the Raman amplifier

Component	Input energy	Output energy
Pump (532nm)	7.7 mJ	0.67 mJ
1st Stokes (683nm)	1.86 mJ	0.67 mJ
2nd Stokes (954nm)	0.38 mJ	1.34 mJ
3rd Stokes (1.58μm)	0.038 mJ	0.58 mJ

6.3.2 Raman exponential gain in the Raman oscillator

An unguided cell was used as the Raman oscillator because in this arrangement all the pump pulse power went through the first Raman cell and we could not afford to lose any fraction of this pump energy due to propagation losses or a non-optimum coupling, as usually happens in a capillary waveguide. Besides that the main advantage of a guiding structure is the large Raman exponential gain, but for this arrangement this is exactly what we do not want, since the Raman exponential gain should be kept as small as possible in the Ramam oscillator so that the parametric processes are the main way which the components can interact.

The Raman exponential gain in the Raman oscillator must be kept between 35 and 45. These limits were obtained from numerical calculations for the equations involving cascade and parametric processes. For a value of Raman exponential gain (ζ) bigger than 45 the effect of the second stokes wave on the first Stokes becomes very strong, which makes the whole process very inefficient.

For our experimental conditions we have the following parameters:

Pump peak power= 671 KW

Raman gain coefficient= 2.55 cm/GW

Pump wavelength= 532 nm

Cell length= 50 cm

Beam waist size= 240 μM

No.times diffrac. limt.(M)= 2.5

and the Raman exponential gain for the Raman oscillator is

$$G=38$$

This value for G is convenient for producing fairly efficient generation of first Stokes radiation and simultaneously producing third Stokes via the parametric process.

Besides the choice of the Raman exponential gain the parametric processes can be enhanced by changing the pump focusing condition inside the Raman oscillator as well as the gas pressure.

6.3.2.1 **Pressure and focusing conditions in the Raman oscillator**

The seed radiation for the S3 components can be generated via the parametric process V(1,0,3,2), which is the more efficient process generating S3 in ζ-region 1.

$$k_0-k_1=k_2-k_3 \qquad 6.8$$

The phase matching condition for this process can be satisfied for a long interaction length if the pump beam is conveniently focused inside the Raman cell in such a way as to provide a wide range of angles for the interacting radiations. This avoids the generated beam escaping from the excited region in a very short length inside the excited region.

The phase matching angle and the beam divergence are related through the expression:

$$d= 2w_0/\sqrt{\theta^2-\delta^2} \qquad 6.9$$

$$d_{MAX}= \text{cell length}$$

and

$$\text{if } \delta \geq \theta \Rightarrow d=\text{cell length}$$

Where δ is the beam divergence angle, defined basically by the focusing condition, the beam wavelength and the spatial profile of the pulse intensity over the beam cross section. The phase matching angle is denoted by θ, w_0 is the pump beam waist size and **d** the actual interaction length for the parametric process.

For our experimental conditions the divergence for the pump beam inside the Raman oscillator cell is 1.76 mrad (for a 2.5x diffraction limited beam). The phase match angle for the parametric process V(1,0,3,2) can be worked out by using figure 5.7 shown in chapter five of this work, at 10 amosphere pressure it is 10 mrad. Then, the interaction length (d) for a 240 μm beam waist is 4.9 cm.

This value of **d** can be increased by decreasing the gas pressure or by focusing the pump beam to a smaller waist size. However, the pulse energy produced into the S3 component, 45 μJ, is quite satisfactory and we kept this pressure and focusing condition throughout the experiment.

6.3.3 **Raman amplifier**

The components generated in the Raman oscillator are focused at the entrance of the capillary waveguide, which is acting as the Raman amplifier. The choice of a capillary waveguide as the Raman amplifier is due basically to two factors:The spatial quality of the beams generated in the Raman oscillator and the large Raman exponential gain needed to reach amplification, via the cascade process, of the S3 component.

The spatial quality of the beam is quite a decisive factor in the capillary choice, the seed radiation coming from the Raman oscillator cell does not have a Gaussian profile, but a ring-like shape due to its generation mainly via parametric process. We want to have a Gaussian-like profile at the amplifier output. A capillary waveguide can provide a suitable solution for this problem since it acts as a spatial filter for the input beams, due to the high propagation loss for high order modes.

The requirement of a large Raman exponential gain is usually fulfilled by the guided structure, however in this case, where the pump beam is not diffraction limited, the utilization of a capillary waveguide is even more essential, since the diffraction losses make the Raman exponential gain too small in an unguided cell

when a tight focusing configuration is used.

In the following sub-sections we explain these assertions in more detail.

6.3.3.1 Non diffraction limited beam in unguided and guided media

The Raman exponential gain for an unguided system with a length **L** is given by expression 4.7 in chapter four.

$$G_u=[(\lambda_s/\lambda_p).tg^{-1}(L/b)].(\sqrt{4Pg/\lambda_s}).(\sqrt{4Pg/\lambda_s}\ -2)$$

Where λ_s and λ_p are the first Stokes and pump wavelengths respectively.

Let us now consider a beam whose divergence is **M** times the divergence for a diffraction limited beam with a beam waist size w_0.

$$\delta'=M\lambda/\pi w_0 \qquad 6.10$$

Since the confocal parameter is a measure of how much the beam diffracts we can write:

$$b'=b/M \qquad 6.11$$

Where **b** is the confocal parameter for the diffraction limited beam. The expression for the Raman exponential gain then becomes (Appendix 5):

$$G_u'=[(\lambda_s/\lambda_p').tg^{-1}(L/b')].\sqrt{4Pg/\lambda_s}\ .(\sqrt{4Pg/\lambda_s}\ -2) \qquad 6.12$$

where $\lambda_s'=M\lambda_s$

$\lambda_p'=M\lambda_p$

$b'=b/M$

As we may notice, the Raman exponential gain for a tight focusing configuration,i.e. maximum possible value for G_u', given by

$$G_u'=[\pi\lambda_s/(2\lambda_p')].\sqrt{4Pg/(\lambda_s)}.[\sqrt{4Pg/(\lambda_s)}\ -2] \qquad 6.13$$

still depends only on the Raman medium and the pump laser characteristics, i.e. pulse power, wavelength and the factor by which the beam divergence exceed the diffraction limit.This happens because an increase in the pump intensity due to a reduction in the beam waist size is compensated by an increase in the diffraction of the beam which decreases the interaction length. The overall result is that G_U' does not depend on the pump focusing geometry anymore, figure 4.4.

However, when one uses a capillary waveguide as the Raman cell the pump beam can be focused to a small waist size without reducing the interaction length much, since the guiding structure can prevent the beam from diffracting by reflecting it back into the Raman medium repeatedly.

The Raman exponential gain for a guided medium is given by expression 4.11 in chapter four

$$G_g = [P/(\pi w_0^2)].g.L_{eff} \qquad 6.14$$

where

$$L_{eff} = [1 - \exp(-\alpha L)]/\alpha \qquad 6.15$$

Where w_0 is the beam waist formed at the capillary entrance and for optimum launch is **(2/3)a** where a is the capillary radius [Abrams (1972)], L is the capillary length and α the attenuation coefficient given by expression 5.77 in chapter five, it is proportional to the ratio λ^2/a^3,

$$\alpha = A.\lambda^2/a^3 \qquad 6.16$$

where

$$A = 3.68x10^{-2}.(\mu_{nm})^2 \qquad 6.17$$

For an M times diffraction limited beam the attenuation coefficient can be written as [Hanna (1984)]

$$\alpha' = A.\lambda'^2/a^3 \qquad 6.18$$

where

$$\lambda' = M\lambda$$

By substituting α' into expression 6.15 we have the Raman exponential gain for a non diffraction limited beam in a guided medium.

$$G_g' = [P_g/(\pi w_o^2)].L_{eff}' \qquad 6.19$$

where

$$L_{eff}' = [1 - \exp(-\alpha' L)]/\alpha \qquad 6.20$$

Figure 6.9 shows the capillary transmission against pump wavelength for several values of **M**.

The effect of the non diffraction limited beam in both guided and unguided systems is equivalent to an "increase"in the radiation wavelength and its effect can be taken into account in all the expressions for the Raman exponential gain by performing the transformation:

$$\lambda \Rightarrow M\lambda \qquad 6.21$$

It is important to point out that there is no real change in the radiation wavelength, and what the transformation does is to assume that the increase in the beam diffraction is not due to any peculiarity of the beam spatial profile but is due to a virtual increase in the radiation wavelength of a beam with an exact gaussian profile.

The enhancement of the Raman exponential gain produced by the guided structure relative to the gain in the unguided situation can be defined in a very general way as

$$S = G_g'/G_u' \qquad 6.22$$

Where G_g' and G_u' are the Raman exponential gains for the guided and unguided systems respectively, for a non diffraction limited beam and a general value of beam waist size. By substituting expressions 6.12 and 6.19 into expression 6.22 we have

$$S = gP\lambda_p' L_{eff}'/\{\pi\lambda_s w_o^2 tg^{-1}(L/b')[\sqrt{4P_g/\lambda_s}\,(\sqrt{4P_g/\lambda_s}-2)]\} \qquad 6.23$$

In figure 6.10 we show the plot of the **S** values against the capillary radius for the wavelength 532nm for hydrogen. As we may observe from these diagrams the optimum value for the capillary radius increases when the value of **M** is increased and the **S** peak value decreases simultaneously.

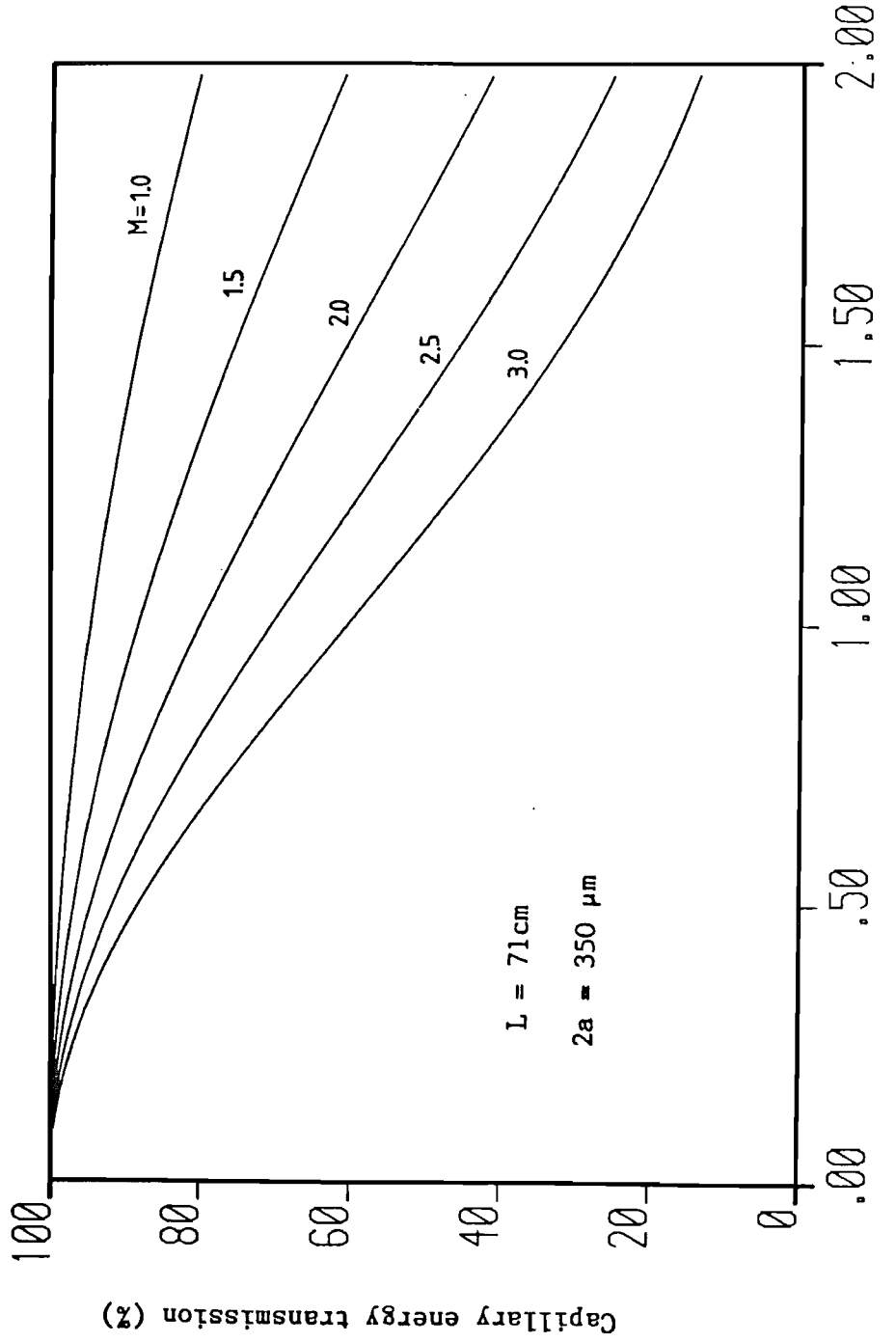

Figure 6.9. Calculation of the capillary energy transmission for the EH_{11} propagating mode.

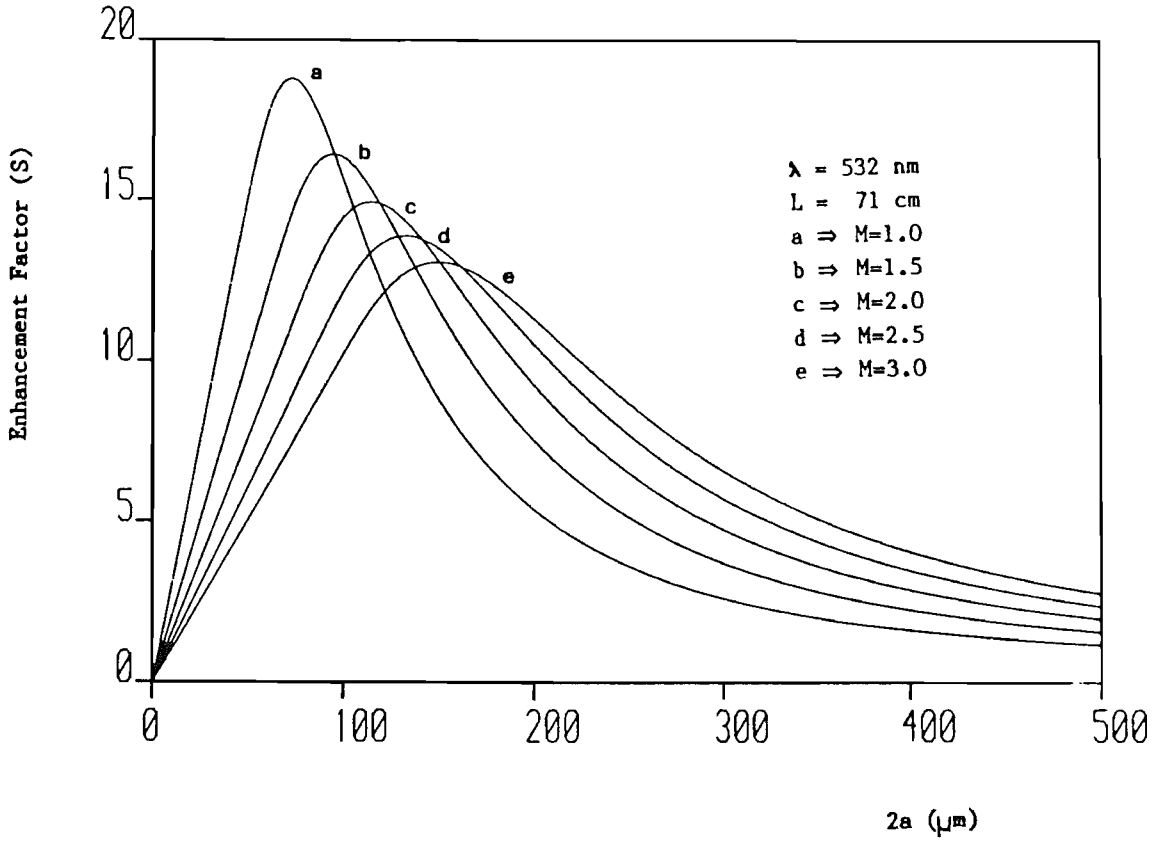

Figure 6.10. Calculation of the ration of the raman exponential gain in capillary waveguide to the Raman exponential gain in an unguided cell with the same length and a pump pulse power of 700kW.

As can be seen the capillary waveguide can provide a maximum enhancement in the Raman exponential gain by a factor of almost 14 for a beam 2.5 times diffraction limited when a 132 micron bore diameter capillary is used. An important point to note is that the enhancement provided by the capillary is improved for a non diffraction limited beam when the capillary bore diameter is not the optimum valeu. For a non diffraction limited beam it is even more worthwhile to use a capillary waveguide than for a diffraction limited beam. For example, for a 350 micron bore diameter the enhancement factor is 2.0 times for a diffraction limited beam and 4.4 times for a 2.5 times diffraction limited beam.

6.3.3.2 **Capillary as a spatial filter**

Apart from the increase in the Raman exponential gain relative to the values expected for the unguided cell and a non diffraction limited beam, the use of a capillary waveguide plays a very important role in the arrangement to obtain a good conversion and a good beam profile for the third Stokes component. As we have mentioned before, the seed radiation has a ring-like shape which would make the cascade process very inefficient inside the Raman amplifier cell, besides the fact that a beam with an annular profile is quite inconvenient for some applications.

The radiations generated in the Raman oscillator cell are focused at the capillary entrance, but due to their ring-like profile they do not couple efficiently into the EH_{11} capillary hybrid mode, rather their energies are distributed among several capillary modes but, only that fraction of energy coupled into low order capillary modes will participate efficiently in the interacting processes, since the other modes will be strongly attenuated as they propagate along the interaction medium.

Beside this mode selection due to the propagation loss, further mode selection is provide by the Raman process itself. This happens because as the pump and first stokes beams come out of the Raman oscillator cell in a spot like shape and the focal length of the lens used to focus the radiations inside the capillary waveguide was chosen in a way to optimize the coupling of the pump wavelenth, we have most of the pump and first stokes energy coupled into EH_{11} mode. Consequently the Raman cascade interaction in the ζ-region where these two components are the strongest ones will be very

efficient for capillary modes which have a intensity profile with a maximum along the axis, since it makes the exchange of energy with the EH_{11} mode more efficient.

Considering both ways of selection we are left with two more important capillary modes

Mode denomination	Configuration	μ_{nm}
EH_{11}		2.405
EH_{12}		5.520

and the output beam will be mostly a combination of these two modes.

It is important to observe the role of the input seed radiation in the spatial quality and efficiency of the output beam. Mode selection, either by attenuation of high order capillary modes or by cascade exponential growth, is possible only because we have energy in several capillary modes, including EH_{11}. This is the importance of the set-up as a complete unit, Raman oscillator-Raman amplifier. If we do not have seed radiation injected into the capillary the energy in the S_i high order Stokes component is generated initially only viathe parametric process and, as a consequence of that, the high order capillary mode which is being used by the parametrically generated component will have much more energy than the low order capillary mode which is starting from the the noise background energy level.

Thus, without seed radiation being injected, the high order capillary modes would come out with most of the energy in the third Stokes wave, because the confinement of the radiation inside the guiding structure would provide exponential growth for these modes. The whole process would be less efficient than the usual Raman amplification using the EH_{11} mode, not only because of the high transmission losses for the high order capillary modes, but because of the profile mismatch between the pump beam and the beam growing exponentially.

This generation of a high order Stokes component in a ring-like shape was experimentally observed and it was described in section 6.2.4. A capillary waveguide was used as a Raman oscillator, i.e. all the components started from the noise level and the second Stokes wave was generated in a ring-like shape.

For this Raman oscillator–amplifier arrangement the ideal conditions for the generation of the S_i component are:

Raman oscillator output:

S_0 → as little depleted as possible
S_1 → just above the threshold level
S_i → seed radiation as strong as possible
S_j → noise level
$(j \neq i,1,0)$

Raman amplifier bore diameter and length:

1. Enough to produce a peak for the conversion efficiency into the S_i component at the capillary output.
2. Enough to considerably attenuate high order capillary modes, especially EH_{12}.

These conditions are not very different from the ones given in section 6.1.1. The only difference is the inclusion of the second requirement for the Raman amplifier cell. Basically the capillary length provides the elimination of high order modes through the propagation loss and the pump powerprovides the enhancement of the Gaussian–like shaped modes. Thus the correct capillary length and bore diameter will be determined by the degree of mode selection required while the pump power will be related to the energies of the first Stokes and the seed radiation.

6.3.3.3 Gas pressure in the Raman amplifier cell

Another way to prevent high order modes from extracting energy from the EH_{11} capillary is by acting on the parametric processes themselves. The way to do this, as was explained in the last chapter, is by a suitable choice of the capillary bore diameter and the pressure in the Raman cell. Our calculations showed that parametric processes like V(1,0,3,2) and V(2,1,3,2) which are quite important in generating third Stokes radiation in ζ–region 1 and 2 respectively, will be very far from the phase matching condition for a gas pressure above 20 atmospheres in a 350 μm diameter capillary,

unless high order capillary modes be used, but in that case the propagation loss will be a very efficient mechanism of mode selection. For example, the energy transmission for the fourth capillary mode is less than 1% for a 350 μm diameter and 71 cm long capillary and this mode is still of too low an order to provide phase matching for these parametric processes at 28 atmospheres pressure.

6.3.4 **Experimental results**

In table IV we show our experimental results compared with other authors' published results. The conversion efficiency for our experiment was worked out using the pump pulse energy before the first lens used in the arrangement,(used to focus the beam into the Raman oscillator cell) and the third Stokes pulse energy after the amplifier cell. Thus the efficiency we quote for our experiment is based on the actual available pumping energy at the laser output and the energy in the high order Stokes component outside the Raman cell.

All the transmission losses for uncoated optics are included in our calculation. For example, the actual pump pulse energy at the laser output is 18.6 mJ while the pulse energy available inside the Raman oscillator cell is 15.7 mJ. The third Stokes pulse energy used in our conversion efficiency calculation is 537 mJ which is 92% of the actual value generated inside the Raman amplifier cell. So, the figures we quote for the conversion could be improved if AR coated optics were used, especially for the optics between the Raman oscillator and Raman amplifier since a smaller transmission loss will lead to a bigger value for the seed radiation energy.

For the second Stokes generation we quoted the results obtained simultaneously with the third Stokes energy measurements. No attempt was made to optimize the second Stokes pulse energy since the main aim of this experiment was to generate as much energy as possible at a 1.58μm wavelength. In spite of this the conversion efficiency we obtained for the S2 component was not very much different from the ones obtained by other authors where the experimental conditions were optimized to produce this Stokes wave. As we can see from the analysis carried out in the previous section the second stokes pulse energy can be increased if we use a shorter

capillary length and eliminate the seed radiation for the third Stokes beam, using a seed input radiation for the S2 component instead.

All the conversion efficiencies that we quote in table IV are for the whole system, including Raman oscillator and Raman amplifier conversion efficiency. The conversion for the Ramam amplifier alone is not quoted, because in certain cases there is so much energy in the first and second Stokes beams that the conversion efficiency relative to the pump beam does not have much meaning, since the third Stokes wave obtains energy from all the components.

The factor GI indicated in table IV is defined as the product of the Raman gain coefficient for the Stokes component being generated and the pump pulse power. In this way we can compare all the experimental results for a given Stokes component on the same ground. This is because some experiments were carried out using a pump wavelength in the ultraviolet region [(Komine and Stappaerts (1979,1982)] while others used a pump peak power four times bigger than ours [Hartig and Schmidt (1979)]. We quote the normalized value for GI, the value of GI for our experiment being used as the normalization factor.

Table IV

2nd Stokes Generation

	Exp.1	Exp.2	Exp.3	This work
Pulse energy	1.9 mJ	2.97 mJ	2.5 mJ	1.2 mJ
Conv. Effic.	18.1%	11.4%	16%	12%
$(GI)_n$ factor	5.2	12	3.3	1.0

3rd Stokes Generation

	Exp.1	Exp.2	Exp.3	This work
Pulse energy	-	2.03 mJ	400 μJ	537 μJ
Conv. Effic.	-	9.4%	4.4%	8.6%
$(GI)_n$ factor	-	16.5	3.1	1.0

Exp.1 Komine and Stappaerts (1979)

Exp.2 Komine and Stappaerts (1982)

Exp.3 Hartig and Schmidt (1979)

The parameters used to calculate the numbers given in table IV are shown in table V.

Table V

	Exp.1	Exp.2	Exp.3	This work
Pump energy (mJ)	14.9	35.0	30.0	18.6
Pulse width (FWHM, nsec)	6.5	8.0	10	22
Pump wavelength (nm)	355	308	560	532
S2 wavelength (microns)	0.504	0.414	1.05	0.95
S3 wavelength (microns)	0.64	0.50	1.85	1.58

The pulse energy for the pump beam given for the Komine and

Stappaerts (1979) experiment is not the pulse energy available at the laser output but the value just before the cell entrance.

6.3.4.1 Spatial profile for the amplified beam

The quality of the third Stokes beam spatial profile was verified by using a scanning slit and a pyroelectric energy meter. The beam waist at the capillary output and its divergence were measured.

The capillary output was imaged on the scanning slit surface and a 4.95 mm spot diameter was measured at this point.

The focal length of the lens used to image the beam is 15 cm in the visible region (measured at 632.8nm), this value was corrected to the focal length in the near infrared and we found a focal length of 15.3 cm for the lens in the 1.58 μm region. Thus we had a beam magnification of 19 times and a beam waist diameter at the capillary output of 261 μm.

For a diffraction limited beam the divergence for this waist size is 3.86 mrad. Measurement of the beam spot size directly at 35 cm from the the capillary output showed a 5.05 mm beam diameter which corresponds to a beam divergence of 7.21 mrad, i.e. 1.9 times the divergence expected for a diffraction limited beam.

One reason for this large beam divergence is probably the effect of the EH_{12} mode in the output beam profile. In this case the attenuation and cascade process were not enough to eliminate this mode completely. This might be seen from the measured spot size at the capillary output, 130 micron. If the EH_{11} modealone was propagating, the spot size at the capillary output would be 117 microns (2a/3). So, a fraction of the output beam energy is in the EH_{12} mode and the bigger spot is due to the ring-like shape for the spatial profile of this mode.

6.3.5 Conclusion

The Raman oscillator/amplifier configuration described in this section produces a conversion efficiency of 8.6% into the third Stokes component, with more than halfa millijoule available outside the cell at a 1.58 microns wavelength. This value is comparable with the ones obtained by other authors who have used more powerful pump sources and pump wavelengths in the ultraviolet region of the

spectrum and it is better than the results obtained using a tunable source to pump the Raman medium producing radiation in the near infrared region. Besides that the capillary waveguide as a Raman amplifier produces a central spot at the amplifier cell output, in spite of the ring-like shape of the input radiation caused by the parametric generation in the Raman oscillator. Yet it shows an improvement of the generated beam spatial profile relative to the original pump beam: 2.5 ⇒ 1.9 times diffraction limited. Thus it has been experimentally shown that a two cell system can generate high order Stokes radiation in the infrared region with a relatively high conversion efficiency.

6.4 **Biharmonic pump - Experimental results**

As we showed in section 5.8 in chapter five, when the Raman medium is being excited by two pump waves simultaneously, the Stokes components generated by each pump can interact among themselves by means of parametic processes. For the case of third Stokes wave amplification using the set up described in section 6.3 in this chapter, when one allows another pump beam into the Raman amplifier, the most important parametric process is

$$T_5=(S_0-S_1)-(k_2-k_3)$$

Where k2 and k3 are the wavevectors for the second and third Stokes generated by the pump at 532nm wavelength respectively, while S_0 and S_1 are the wavevectors for the new pump and the new Stokes beams in the Raman amplifier cell.

To verify the influence of biharmonic pumping on the third Stokes output pulse energy we used basically the scheme already described in figure 6.9. We allowed the 1.064μm radiation to enter the Raman oscillator and Raman amplifer cell simultaneously with the 532nm beam. The pulse energy for the infrared beam is 35 mJ.

The energy obtained for the third Stokes pulse after the capillary waveguide was 900 μJ, which corresponds to 980 μJ inside the Raman cell. An external conversion efficiency of 12% was measured relative to the 532nm wavelength pump. Table VI shows the results obtained for scheme 6.9 when one uses single pump and biharmonic pumping in terms of third Stokes component pulse energy.

Table VI

	Single pump λ=532nm	Biharmonic pumping λ=532nm/λ=1.064μm
Pump energy (mJ	18.6	22 (532nm) 35 (1.064μm)
S3 energy (μJ)	537	900
Conversion	8.6%	12%

The main effect of the biharmonic in the pump set up is the increase of the seed radiation energy for the S3 component generated in the Raman oscillator, its energy is 80% bigger than the value obtained for a single pump. On the other hand, in spite of the higher pulse energy for the 532nm radiation entering the Raman oscillator cell, we observe the same pulse energy as for the single pump case at the Raman oscillator output. This is problably due to transference of energy from the 532nm beam to the first Stokes component generated by the the 1.064μm radiation through the process

$$\theta_2=(k_0-k_1)-(S_0-S_1)$$

The effect of biharmonic pumping is not very significant in the Raman amplifier. This is due to the large bore diameter capillary and the relatively high gas pressure, which make the parametric process between the two sets of components very inefficient.

The spatial profile for the Third stokes was measured and we found a beam divergence 1.4 larger than the expected beam divergence for a diffraction limited beam.

CHAPTER SEVEN

Generation of 1.5μm wavelength radiation by SRS

7.1 Introduction

Stimulated Raman Scattering radiation has been observed in liquids and gases in the near infra red region [Meadors and Poiries (1972)] thus providing a practical technique for generating "eye -safe"laser radiation at significant power levels. Interest in such a source of "eye-safe" radiation (λ~1.5μm) arises from the need for a military range finder.

Another important application for 1.5μm radiation is in optical fiber communication, since these devices present a low transmission loss for radiation at this wavelength. This is a fundamental parameter when one wants to transmit a signal in long fiber lengths without needing to use too many repeaters. Or, due to these optical fiber characteristic the 1.5μm radiation can be used in a reflectometer in order to detect faults in a long optical fiber[Senior (1985)].

In the last Chapter we showed a practical set up to generate 1.5μm radiation from a pump source in the visible region of the spectrum (532nm). This is important because that is the region where the most efficient dye lasers are and one can obtain tunable high order Stokes radiation with a reasonable conversion efficiency. The main problem with this sort of arrangement is that to generate a component at 1.5μm, one needs go through three Stokes shifts, which reduces the overall conversion efficiency into the infrared component.

In this chapter we investigate 1.5μm generation using a single Stokes shift. A Nd:YAG laser is used as pump source for several Raman media which allows us to produce first Stokes radiation in the 1.5 μm region.

Several liquids and a gas, methane, were used as Raman media. A repetitively Q-switched Nd:YAG and a Q-switched and mode locked laser were used to establish the characteristics of the Raman

medium under long (nsec) and short (psec) pump pulse widths.

7.2 SRS in liquids with a Q-switched pump source

The use of liquids as Raman media brings out several advantages over gases. The first advantage isin the Raman cell itself which can have its design simplified since it is not required to support high gas pressure anymore. So, the output and input windows are used only to avoid evaporation or contamination of the Raman medium and consequently their thickness can be very small, the minimum thickness is limited only by practical reasons (handling and gluing). Besides that the whole Raman cell body can be made of a very light material, which might be convenient for a system being used outside the laboratory.

The Raman gain coefficient for some liquids is comparable with most gases used at high pressure. For example, for methanol the Raman gain coefficient (g) is 2.27 cm/GW at 532nm pump wavelength (table I) which is comparable to the value for hydrogen at high pressure, 2.7 cm/GW and it is bigger than the value of g for methane at 30 atmosphere pressure, 0.83 cm/GW.

To have efficient Stokes conversion one must consider the parametric processes as well, because as we have shown in chapter five, the energy redistribution effect can reduce the Stokes conversion efficiency to very low values. In this case the liquids show an enormous advantage relative to gases, because of their high dispersion the parametric processes require very large angles to reach the phase matching condition, of the order of 5 to 10 degrees. Consequently the parametric processes in liquids do not extract a significant amount of energy from the radiations growing via the cascade process. The liquid's high dispersion provides an efficient discrimination against the four-wave interaction.

Relative to parametric processes we still need to consider Δk, the mismatch factor along the Raman medium axis. As was discussed in chapter five, the parametric process along the axis of the Raman medium can generate a reasonable amount of energy at the second Stokes wavelength, reducing in this way the expected first Stokes pulse power necessary to reach the SRS threshold for the S2 component. This is the main process which limits the conversion efficiency from the pump into first Stokes beam. For a Raman medium with a high dispersion we should expect a very large value for Δk.

However, the large Raman gain coefficient shown by some liquids can compensate for this fact and the growth of the second Stokes component might limit the conversion efficiency for first Stokes. It would be a problem if the most important liquids used to generate radiation in the 1.5 μm regiondid not possess characteristics which overcome this problem, that is, the strong absorption by the medium for any radiation with wavelength longer than 1.7μm. It prevents any second Stokes radiation reaching a high energy level.Figure 7.1 shows the transmission spectrum for DMSO (dimethyl-sulphoxide) and cyclohexane. When the medium is being pumped by 1.064μm radiation, the second Stokes wavelength will be longer than 2.0μm and we should not expect any interference of this component with the first Stokes, since the S2 power will be kept at very low values during the whole interaction length.

At the same time this absorption represents the main disadvantage of the liquids since their significant absorption at 1.064μm and 1.5μm wavelengths.

The medium absorption at 1.064μm affects the generation of the first Stokes component. It increases the pump pulse power necessary to reach the SRS threshold, while the absorption at 1.5μm affects the conversion efficiency for the component.

Other disavantages are: Stimulated Brillouin Scattering, self focussing and heating of the Raman medium by the non radiative relaxation of the excited molecules. These effects, unlike the medium absorption, can be minimized by means of a suitable choice of the pump source parameters.For example, the SBS effect is a problem because the Brillouin gain coefficient is considerably bigger than the Raman gain coefficient for most of the liquids, however this problem might be overcome by using a pump pulse short enough to be in the transient region for the Brillouin effect and reduce the effective Brillouin gain coefficient [Carr (1985)]. The short pump pulse does not affect the Raman gain coefficient since the medium can still be regarded as in the steady state forthe Raman transition due to the large Raman linewidth presented by most of liquids, typically 10 cm^{-1} (T_p=1.0 picosec). Then a 100 picosecond FWHM pump pulse width can still be considered in the steady state region for a liquid, even at gain saturation.

The other effects are due to the non linear dependence of the refractive index on the pump electric field. The change in the refractive index will modify the pump pulse intensity inside the

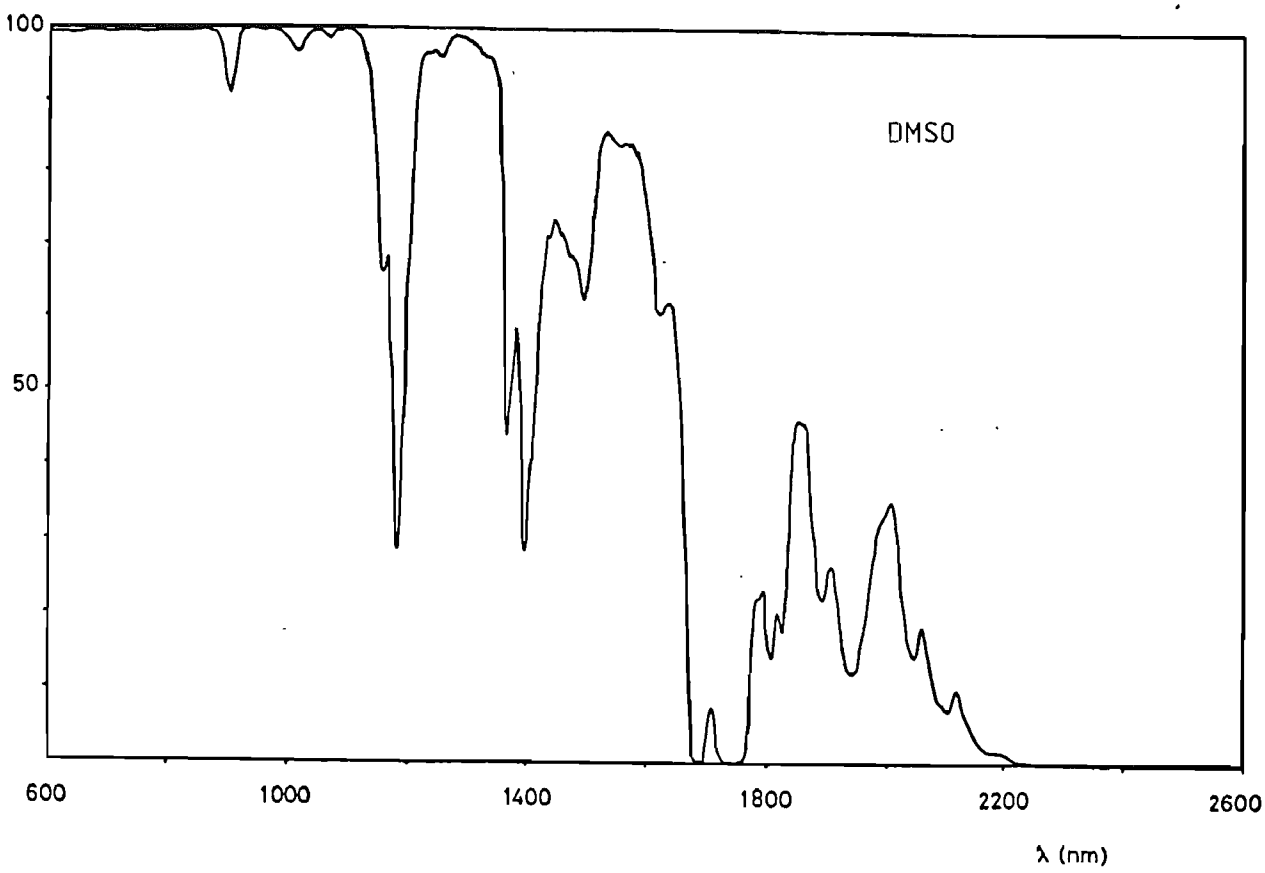

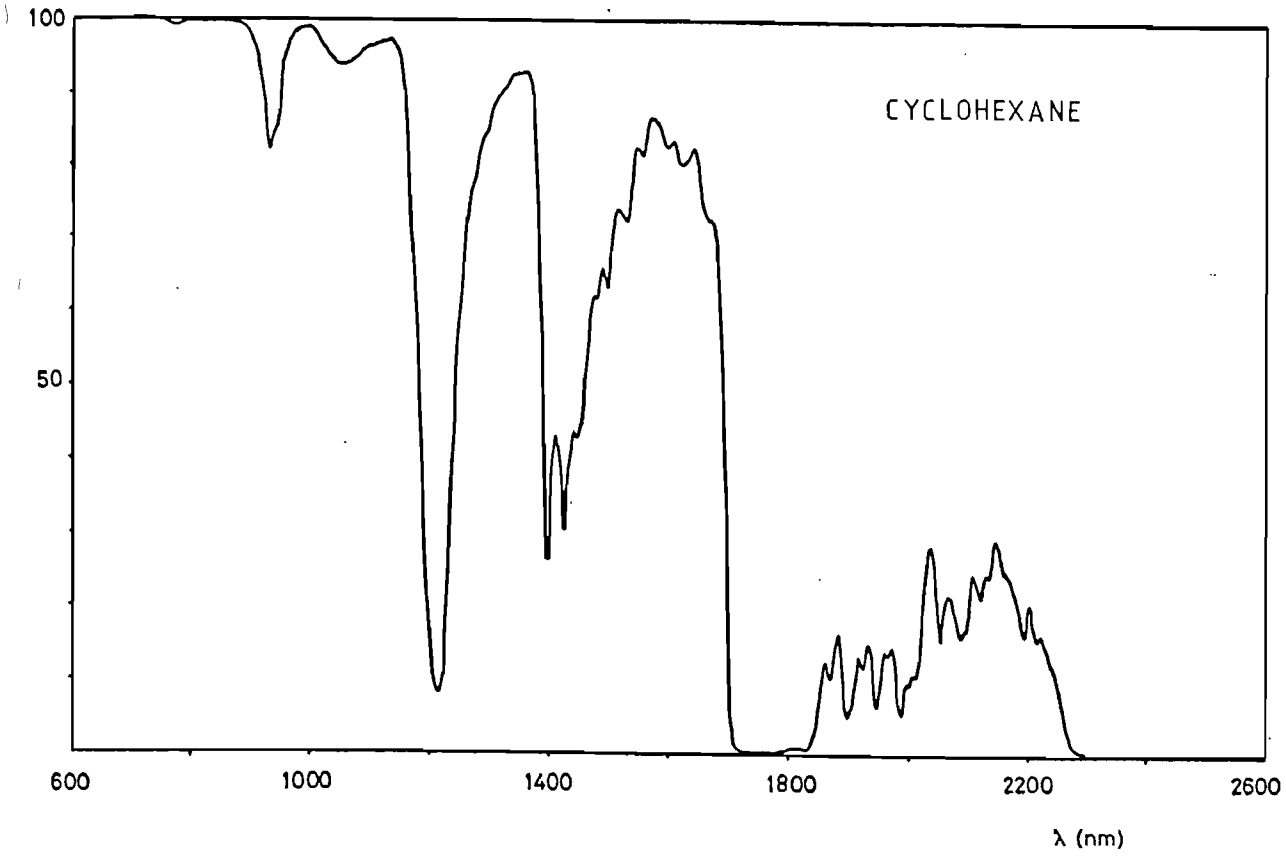

Figure 7.1. Transmission curve for dimethyl sulphoxide and cyclohexane in the range 600nm to 2.6μm, for a 1cm long cell.

medium and consequently the whole Raman scattering process is greatly affected.

7.2.1 Refractive index variation

The heating of the Raman medium can have a cumulative effect on the medium parameters, i.e. the parameter changes become noticeable only after a certain number of pump pulses have arrived in the cell. It can also change the medium characteristics within the duration of a single pump pulse (nsec). We refer to these two effects as slow and fast processes.

For the slow process the heating problem can be solved by using the pump laser at low pulse repetition rate so that the heat generated by one pulse is removed from the pumped volume before the next pump pulse arrives.

These effects can be summarized through the non-linear dependence of the refractive index on the electrical field of the pump radiation.

$$n = n_0 + n_2E^2 + n_{2h} \qquad 7.1$$

Where n_0 is the linear refractive index. n_2E^2 is the non-linear term which leads to the focusing of the pump beam due to the Kerr effect. The third term takes into account the change in refractive index due to heating in the Raman medium, n_{2h} is proportional to dn/dT, where T is the temperature in the medium. This term is usually negative since the rate of refractive index variation with respect to temperature is negative for the medium we are working with [Alfano and Shapiro (1970)] and consequently it leads to a defocusing of the pump beam.

The Raman medium can be be heated basically by two processes: The first process is related with Stimulated Raman Scattering itself. The excited molecules in the first vibrational level relax to the ground state and convert their energy to heat. This process depends on how efficiently the Raman medium can be excited and consequently it is a function of the pump pulse intensity. The second process which increases the medium temperature is the linear absorption of the pump beam energy. This process depends essentially on the pump beam energy. The refractive index variation can be summarized in the following way:

Increasing in $n \rightarrow 1$. Self focusing (Kerr effect)
intensity dependent

Decreasing in $n \rightarrow 1$. SRS relaxation – intensity dependent
2. Linear absorption – energy dependent

7.2.2 SRS threshold in liquids

Let us consider that the medium dispersion is large enough to prevent a significant amount of energy going into a Stokes component viathe parametric process and that high order Stokes components do not reach high energy levels due to linear absorption in the medium. Then, we may write equation 3.59 in terms of the intensities of interacting radiations as:

$$dI_0/dz=-g_0'I_0I_1-\alpha_0I_0 \qquad 7.2$$

$$dI_1/dz= g_1I_1I_0 -\alpha_1I_1 \qquad 7.3$$

Where I_0 and I_1 are the pump and first Stokes intensities, α_i is the medium absorption coefficient for the i_{th} component. The Raman gain coefficient g_1 is defined by expression 3.42 and g_0' is related to g_1 through expressions 3.60 and 3.61:

$$g_0'= (\chi_1''/\chi_0'').g_0 \qquad 7.4$$

where

$$g_0= (\chi_0''/\chi_1'').(\omega_0^2.k_1/\omega_1^2.k_0) \qquad 7.5$$

By substituting 7.5 into 7.4 and the value of g_0' into equation 7.2 we have:

$$dI_0/dz=-(\omega_0/\omega_1).g_1I_0I_1-\alpha_0I_0 \qquad 7.6$$

$$dI_1/dz= g_1I_0I_1-\alpha_1I_1 \qquad 7.7$$

At the SRS threshold we may assume that the pump pulse is not depleted by the first Stokes intensity and since

$$(\omega_0/\omega_1)g_1I_1/\alpha_0 \ll 1 \qquad 7.8$$

equation 7.6 becomes:

$$dI_0/dz=-\alpha_0 I_0 \qquad 7.9$$

or

$$I_0=I_0^0.\exp(-\alpha_0 z) \qquad 7.10$$

Where I_0^0 is the pump intensity at the entrance of the cell.

By substituting expression 7.10 into 7.7 we have:

$$dI_1/dz=[g_1 I_0^0.\exp(-\alpha_0 z) - \alpha_1].I_1 \qquad 7.11$$

The integration of this expression along a cell with length **l** produces:

$$\ln(I_1/I_1^0)=(g_1 I_0^0/\alpha_0).[1-\exp(-\alpha_0 l)] - \alpha_1 l \qquad 7.12$$

I_1^0 is the noise intensity for the Stokes components, it is calculated through expression 3.76.

Equation 7.12 can be expressed in terms of Raman exponential gain, $G=\ln(I_1/I_1^0)$

$$G= [G_0/(\alpha_0 l)].[1-\exp(-\alpha_0 l)] - \alpha_1 l \qquad 7.13$$

Where $G_0=g_1 I_0^0 l$ is the Raman exponential gain for a lossless medium.

The SRS threshold is defined in the same sense as in chapter 4 and the value of G_{th}, i.e. the Raman exponential gain necessary to reach the threshold for the first Stokes component, is in between 20 and 25 depending on the pump wavelength and Raman medium linewidth.

As one may observe from expression 7.13 a large value of l will require a large pump intensity to reach the SRS threshold due to the medium absorption. On the other hand a short cell length gives rise to a small exponential gain and a large pump intensity is required again.

$$I_0^0 g_1=\alpha_0(G_{th}+\alpha_1 l)/[1-\exp(-\alpha_0 l)] \qquad 7.14$$

By taking the first derivative of expression 7.13 with respect to l and equating the result to zero we have an equation which give us

the optimum value for the cell length:

$$\exp(\alpha_0 l_0) - 1 = (\alpha_0/\alpha_1)G_{th} + \alpha_0 l_0 \qquad 7.15$$

Where l_0 is the cell length which requires the lowest value of pump intensity to reach the SRS threshold. For example, for a medium absorption coefficient at the Stokes and pump wavelengths of $0.11cm^{-1}$ and $0.02cm^{-1}$ respectively and considering $G_{th}=21$, the optimum value for the cell length is 95 cm.

The medium absorption at the Stokes wavelength (α_1) has less influence than the medium absorption at the pump wavelength (α_0) on the first Stokes threshold. The long cell length obtained is basically defined by the medium absorption at the pump wavelength (α_0).

The analysis made so far assumes that the pump beam is not focused into the Raman medium. When this case is considered the beam diffraction must be included in the threshold calculation as well. Cotter et al (1975) analysed that case in a lossless medium and the SRS threshold pump pulse power is:

$$P_{th}= [\lambda_1/(4g_1 n)].\{1+[1+G_{th}\lambda_0/(\lambda_1 tg^{-1}(1/b)]^{1/2}\}^2 \qquad 7.16$$

Where b is the confocal parameter, $b=2\pi w_0^2/\lambda_0$.

However, when we take into account the absorption loss and the beam diffraction simultaneously, there is no straightfoward analytical solution for the set of coupled equations involving the pulse intensity for the pump and first Stokes.

An approximate analytical expression was obtained using numerical calculation, that is:

$$P_{th}= [\lambda_1/(4g_1 An)].\{1+[1+(G_{th}+\alpha_1 l)\lambda_0/(\lambda_1 tg^{-1}(1/b)]^{1/2}\}^2 \qquad 7.17$$

where $A=[1-\exp(-\alpha_0 l)]/\alpha_0 l$

In order to compare the SRS threshold power calculation under the various discussed conditions let us consider the following parameters:

$\alpha_0 = 0.02 cm^{-1}$ $w_0 = 170 \mu m$

$\alpha_1 = 0.11 cm^{-1}$ $l = 48 cm$

$\lambda_0 = 1.064 \mu m$ $b = 24 cm$

$\lambda_1 = 1.58 \mu m$ $g_1 = 1.17$ cm/GW

$G_{th} = 21$ $n = 1.4$

1. No absorption losses, no beam diffraction

$$P_{th} = G_{th}\pi w_0^2/(2g_1 ln) \Rightarrow P_{th} = 121 \text{ KW}$$

2. With absorption losses, no beam diffraction

$$P_{th}=[\pi w_0^2/(2g_1 ln)].(G_{th}+\alpha_1 l)\alpha_0 l/[1-\exp(-\alpha_0 l)]$$

$$\Rightarrow P_{th} = 236 \text{ KW}$$

3. No absorption losses, with beam diffraction

$$P_{th}=[\lambda_1/(4g_1 n)].\{1+[1+ G_{th}\lambda_0/(\lambda_1 tg^{-1}(l/b))]^{1/2}\}^2$$

$$\Rightarrow P_{th} = 535 \text{ KW}$$

4. With absorption losses and beam diffraction

$$P_{th}=[\lambda_1/(4g_1 nA)].\{1+[1+(G_{th}+\alpha_1 l)\lambda_0/(\lambda_1 tg^{-1}(l/b)]^{1/2}\}^2$$

$$A= [1-\exp(-\alpha_0 l)]/\alpha_0 l \Rightarrow P_{th} = 984 \text{ KW}$$

One can observe that all the expressions used to work out the SRS threshold pump pulse power can be obtained from expression 7.17.

7.2.3 Experimental results for SRS in liquids using a Q-switched pump in the visible region of the spectrum.

In the visible region of the spectrum the absorption coefficient for most of the liquids we analysed is quite small. It gives us the opportunity to investigate the perfomance of these materials in a condition free of heating by linear absorption.

The second harmonic of a Nd:YAG laser was used as pump

source. The 532nm wavelength is in a region of the spectrum where the absorption coefficients for the pump and first Stokes radiation are very small compared with their values in the near infrared region. Thus any observed change in the refractive index of the medium must be due either to the Kerr effect or heating due to relaxation of the excited molecules produced by SRS. Both processes are intensity dependent.

The arrangement used to measure the SRS threshold is shown schematically in figure 7.2. Eight different liquids were investigated and their main parameters are given in table I.

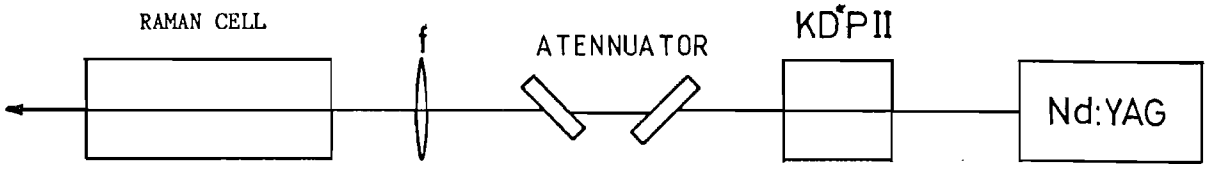

Figure 7.2 Experimental arrangement to generate SRS in liquids.

We may observe from this table a wide range of Raman shift frequencies, though we know that in order to generate radiation at 1.5μm wavelength we need to use materials with a Raman shift around 2800cm^{-1}, when the Nd:YAG laser is being used as the pump source. The reason for including materials witha Raman shift frequency quite different from the one we need is to investigate the possibility of using these liquids as a frequency shifter for pump sources in the visible region,like dye lasers, to the red or near infrared region of the spectrum.

The experimental results are summarized in table II. The focusing condition and cell length were different for each experiment and they are characterized by the ratio **l/b** quoted in the third column of table II.

7.2.4 Discussion

The threshold pump pulse power quoted in table II was worked out using expression 7.16. The confocal paramater was calculated through the expression

$$b=2\pi n w_0^2/\lambda_0 \qquad 7.18$$

Table I

Paramters used to work out the SRS threshold pump pulse power at 532nm

Medium	Raman linewidth (cm^{-1})	Raman shift (cm^{-1})	Raman gain coefficient (cm/GW)	Refractive index
CS_2	0.5[a]	686[a]	12.5[a]	1.64[b]
Acetone	17.4[a]	2925[c]	1.2[a]	1.36[d]
Benzene	2.3[a]	992[a]	5.2[a]	1.50[d]
DMSO	—	2916[h]	—	1.48[d]
Toluene	1.9[e]	1004[f]	1.2[e]	1.49[d]
Methanol	18.7[a]	2834[a]	2.3[a]	1.33[d]
Acetonitrile	—	2917[h]	1.7[h]	1.34[d]
Cyclohexane	—	2852[f]	2.4[g]	1.44[d]

a. Colles (1969)
b. Ippen (1970)
c. Krumin'sh et al (1984)
d. BDH catalogue 1985/1986
e. Kaiser et al (1972)
f. Eckhardt (1966)
g. Colles et al (1972)
h. Pointer et al (1985)

Table II

Experimental results for a pump wavelength of 532nm

Medium	$P_{th}(E)$ (KW)	$P_{th}(T)$ (KW)	l (cm)	w_o (μm)	l/b	λ_1 (nm)
CS_2	160	19	10	47	2.34	552
Acetone	60	269	15	73	1.78	630
Benzene	25	65	10	73	1.07	562
DMSO	53	—	15	73	1.63	630
Toluene	29	384	10	95	0.64	562
Methanol	159	118	15	47	4.32	626
Acetonitrile	39	209	10	73	1.20	630
Cyclohexane	17	125	15	73	1.69	627

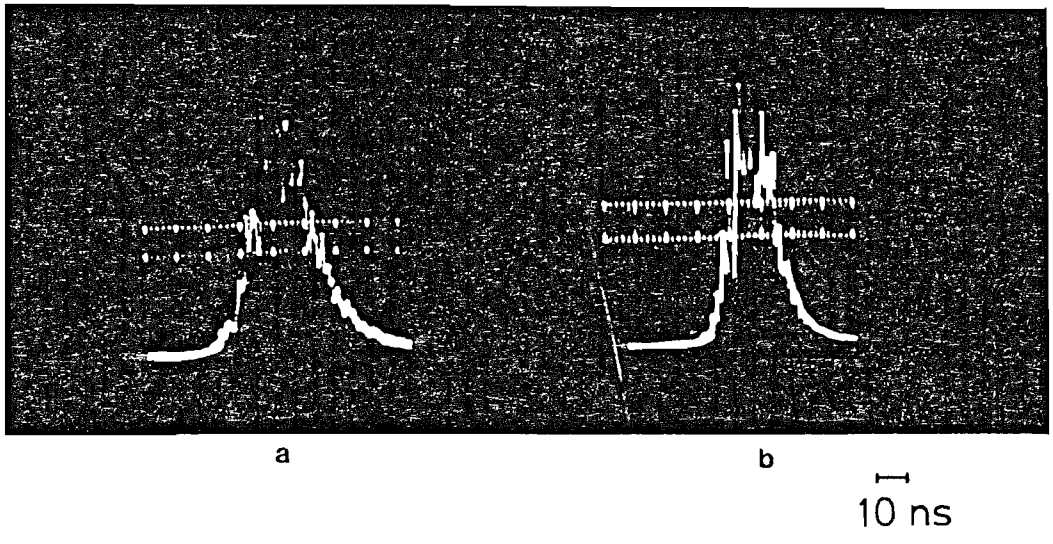

Figure 7.3. Temporal profile for the fundamental (a) and second harmonic(b) pulses of Nd:YAG laser.

Where **n** is the refractive index of the medium.

The experimentally observed value for the SRS threshold pump pulse power is generally smaller than the predicted one. One reason for that is the multi longitudinal mode characteristic of the pump pulse. CS_2 and methanol showed higher threshold, but the reason for this behaviour is not understood.

As can be seen in figure 7.3, the temporal profiles for the 1.064μm and 532nm wavelength pulses show a sequence of short pulses inside the main pulse envelope. These pulses result from beating between longitudinal modes inside the laser cavity and their width is very narrow, leading to a very high peak power. As the Raman medium, due to the large Raman linewidth of liquids, can still be considered as in the steady state, the actual Raman exponential gain is higher than that calculated as the gain of a monochromatic pump.

The observed SBS threshold pump pulse power was higher than the SRS pump pulse power, in spite of the SBS gain coefficient being bigger than the SRS gain coefficient for these liquids. This is expected because the Brillouin Scattering process is in the transient regime for the short pulses and the medium responds effectively to the pulse envelope rather than to the short spikes.

Medium breakdown was observed for toluene for beam waists smaller than 94μm. For acetone and acetonitrile the medium breakdown was reached for waist sizes smaller than 73μm and 47μm respectively. Dimethyl sulphoxide, methanol and cyclohexane did not show medium breakdown under our experimental conditions.

The maximum conversion efficiency was obtained with cyclohexane when a 15 cm cell was pumped with 110 KW peak power focused down to a 75μm waist size. We measured for first Stokes component (627nm) a pulse energy of 462μJ. This energy corresponds to a 33% conversion efficiency.

7.2.5 Experimental results for SRS in liquids using a Q-Switched pump in the near infrared region of the spectrum.

The two main differences shown by the medium when pumped by radiation in the infrared region are the medium absorption of the pump and Stokes pulse energies and the smaller Raman gain coefficient. In table III we have the values of the absorption coefficients calculated from the transmission curve obtained for

these liquids in the spectrophotometer.

Table III

Absorption coefficient

Medium	$\alpha_0(cm^{-1})$	$\alpha_1(cm^{-1})$
Acetone	0.005	0.160
DMSO	0.020	0.170
Acetonitrile	0.018	0.104
Cyclohexane	0.062	0.290

As may be observed from table III the absorption coeffcient is bigger for the first Stokes than for the pump beam and from the transmission curves we noticed that the transmission dropped almost to zero for wavelengths longer than 1.7μm.

The SRS threshold pump pulse power was measured using an experimental set up similar to the one shown in figure 7.2, but without the doubling crystal, we focused the fundamental beam of the Nd:YAG laser directly into the Raman medium. The waist size inside the cell was 95μm and the cell length was 15cm. The results are summarized in table IV together with the theoretical value for the SRS threshold pump pulse power, worked out using expression 7.16 and the attenuation coefficients shown on table III.

We tried to observe SRS in cyclohexane at several different focusing conditions and a pump pulse power up to 2.0MW, but no first Stokes components reached the SRS threshold. It suggests that the medium is being heated and the pump beam defocused in a time scale of the same order of the pulse duration. Thus cyclohexane is not a suitable medium for generating 1.5 μm radiation using a 1.064μm wavelength Q-switched pump.

In order to investigate the slow thermal effect on DMSO and acetonitrile, we increased the pump pulse energy and measured the first Stokes pulse energy at two different pump pulse repetition rates. The results are shown in table V.

Table IV

SRS threshold pump pulse power in liquids for a pump wavelength of 1.064μm

Medium	$P_{th}(E)$ (MW)	$P_{th}(T)$ (MW)	l/b	λ_1 (μm)
DMSO	0.61	–	1.92	1.54
Acetonitrile	0.45	1.21	2.12	1.54
Cyclohexane	not reached	1.20	1.99	1.53

Table V

First Stokes pulse energy at two pump pulse repetition rates

	DMSO		Acetonitrile	
	2.0 Hz	0.3 Hz	2.0 Hz	0.3 Hz
Output energy	110μJ	533μJ	1.25mJ	1.43mJ
Conversion eff.	0.5%	2.4%	5.6%	6.4%

Pump pulse energy: 32.5mJ

Pulse width (FWHM): 30ns

Beam waist size: 95μm

Table VI

First Stokes pulse energy in acetonitrile pumped by 1.064 μm

	w_0=190μm	w_0=95μm	w_0=73μm
Output energy	0.76mJ	1.7mJ	1.2mJ
Conversion eff.	2.5%	5.6%	3.9%

As can be seen in table V the first Stokes pulse energy for DMSO changes by almost a factor of five, when the repetition rate is reduced from 2 to 0.3 pulses per second. However acetonitrile showed a reasonable conversion efficiency and the Stokes pulse energy did not change too much when the pump rate was increased.

To investigate the maximum Stokes pulse energy that we could reach with our pumping system, the acetonitrile was used as Raman medium for three different focusing conditions. It is important to mention that just before this experiment was done the Pockel's cell in the Nd:YAG laser was replaced by a new one and the laser output pulse energy increased to 44mJ while a reduction in the pulse width was observed. Table VI shows the results for a pump pulse rate of 2pps.

7.2.6 Raman Oscillator-amplifier configuration for liquids

When one uses a liquid as a Raman medium the high order Stokeswaves in the spectral region above 1.7μm are kept at very low energy levels and besides that the parametric processes are quite inefficient due to the large medium dispersion. These were the main problems we tried to avoid with gas by using an oscillator amplifier configuration. However, a new problem appears: the medium absorption for radiations at the Stokes and pump wavelengths.

To overcome this new problem an oscillator-amplifier arrangement can be used again. From expression 7.14 one can work out the optimum value for the cell length in order to reach the SRS threshold using a minimum amount of pump pulse energy. In this case we must have a relatively long cell, defined mainly by the pump absorption coefficient. This cell acts as the Raman oscillator.

In a second cell acting as the Raman amplifier we have the amplification of the Stokes signal generated in the Raman oscillator cell. This cell must have a very short length due to the typically high absorption coefficient at Stokes wavelength. Consenquently the available Raman exponential gain is small and one way to reach a reasonable conversion efficiency into the first Stokes component is by injecting a seed radiation into the Raman amplifier.

Two oscillator-amplifier configurations were tried during the experiments. The Raman medium was acetonitrile which showed the best characteristics in the near infrared region. The first

arrangement is similar to the one used in section 6.3, i.e. the whole pump energy goes through the Raman oscillator (l=40cm) in a losely focused configuration (f=100cm), where it generates a seed radiation for the first Stokes beam. The remaining pump pulse and this seed radiation are focused inside the Raman amplifier (l=10cm) to an 87μm beam waist size. This arrangement produced a pulse energy of 420μJ when a pump pulse energy of 20mJ was available just before the Raman oscillator entrance. This 3% conversion efficiency is well below the value predicted by the numerical simulation, 12%. One problem with this arrangement is the attenuation of the pump pulse when it goes through the Raman oscillator and besides that this arrangement does not guarantee that the two waists (pump and Stokes) are formed exactly at the same position inside the Raman amplifier cell due to the dispersion in the medium.

The second oscillator–amplifier arrangement is shown in figure 7.4. A fraction of the beam energy (16mJ) is used to generate a seed radiation in a Raman oscillator cell, while the large portion of the pulse energy (42mj) is directed to pump the Raman oscillator cell.

A pulse energy of 68μJ is generated in the Raman oscillator stage at 1.54μm wavelength, it corresponds to 53μJ at the entrance of the amplifier cell. Table VII shows the results for the output Stokes pulse for several Raman amplifier cell lengths.

Table VII

Raman oscillator–amplifier results for liquids

cell length	Output energy with no pumping	Output energy with amplifier being pumped
4 cm	32.5μJ	76μJ
8 cm	19.1μJ	268μJ
10 cm	17.2μJ	306μJ
15 cm	8.8μJ	1.300μJ

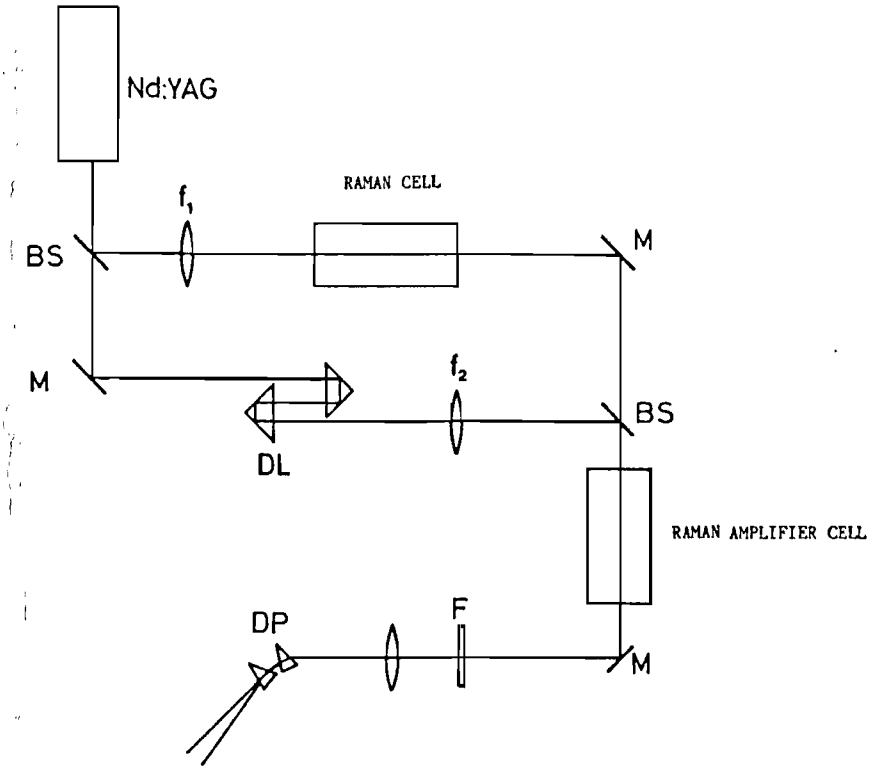

Figure 7.4. Oscillator-amplifier arrangement to generate 1.5μm radiation via SRS in acetonitrile pumped by 1.064μm wavelength radiation.

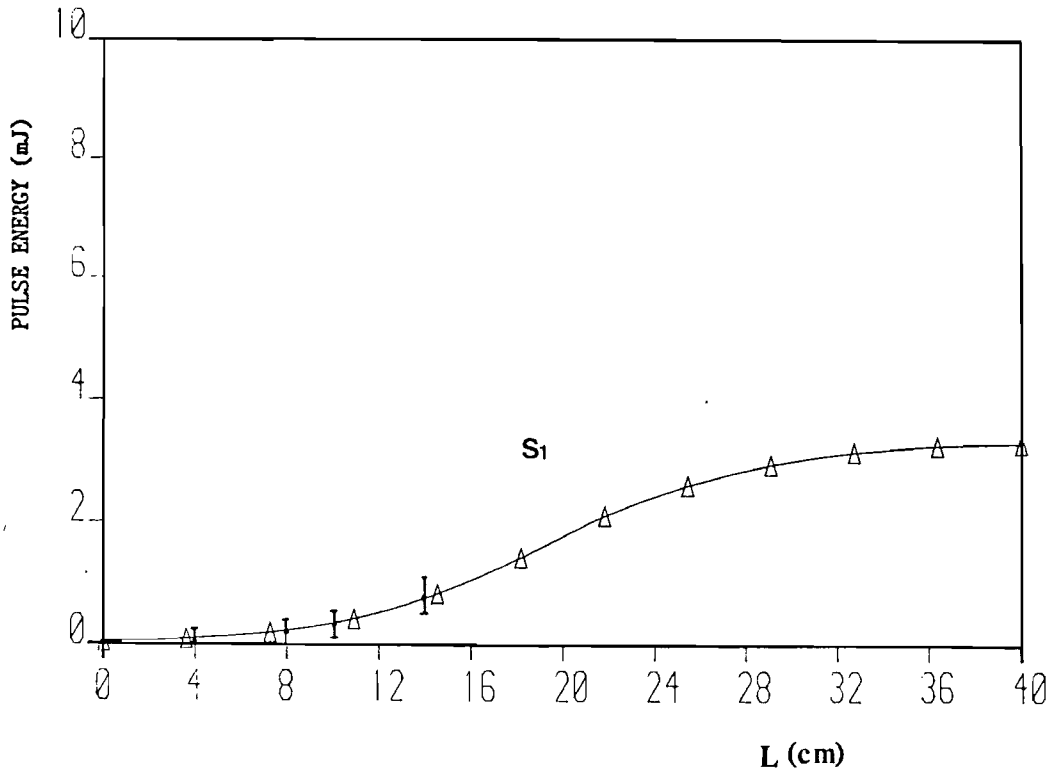

Figure 7.5. Numerical calculation and experimental results for first Stokes generation in acetonitrile using the scheme shown in figure 7.4.

Figure 7.5 shows the numerical simulation for the Raman amplifier cell. The experimental results are plotted together and one can see that they agree quite well with the predicted values.The best result we have is with a 15 cm long amplifier cell, when 1.3mJ is been generated at first Stokes pulse.

7.2.7 Conclusion

For pump radiation with wavelength in the visible region of the spectrum where the medium absorption coefficient is quite small, the best result was obtained with cyclohexane, 33% conversion efficiency into first Stokes beam when pumped by 532nm wavelength radiation. In the near infrared region region, 1.064μm wavelength, the best result was obtained with acetonitrile in a single cell configuration, 6% into first Stokes beam at 1.54μm wavelength. The use of an oscillator–amplifier configuration does not lead to any improvement due to the medium absorption at the pump wavelength.

7.3 SRS in liquids with a Q–switched and mode locked laser

One possible solution for overcoming the thermal problems due to the medium absorption that we mentioned in the last section is to use pump pulses with short duration, so that the energy required in each pulse to reach the necessary pulse power is very much reduced. The large Raman linewidth presented by the liquids assures that the system is able to respond to the fast power variation inside the Raman medium.

A Nd:YAG active mode locked laser was used to generate these short pulses [(Pratt (1986)]. The 850μm beam waist is at the output mirror and the output is magnified by a factor of three by a telescope placed 80cm away from the laser output. The pulse width is 95 ns after the laser cavity and becomes 85 ns after going through the amplifier stage.

The energy in the Q–switched pulse envelope just before the laser amplifier is 1.0mJ. This corresponds to a mode locked pulse energy of 76μJ for a 65.24MHz frequency modulation. After having been amplified the energy in the Q–switched pulse is 10mJ, which corresponds to an energy of 868μJ for a individual mode–locked pulse.

7.3.1 Single pass SRS threshold – experimental results

We concentrated our investigations on cyclohexane and acetonitrile. A beam waist of 92.5μm was formed inside a 10 cm long cell, giving a confocal parameter of 7.2 cm for cyclohexane and 6.8cm for acetonitrile. The maximum energy available in a mode locked pulse inside the Raman cell was 583μJ , which corresponds to a pulse peak power of 6.1MW.

However for cyclohexane the SRS threshold was not reached, in spite of its calculated SRS threshold pump pulse power being only 0.97MW. No medium breakdown was observed and the radiation emerging from the Raman cell showed a diffuse pattern with a very large angle divergence. No damage was noticed on the input window, even for pump intensity as high as 20GW/cm^2.

A completely different result was observed for acetonitrile. With this liquid the SRS threshold pump pulse power does not differ very much from the theoretically predicted value. The SRS threshold was reached for a energy of 150μJ in a 90ps mode locked pulse, which corresponds to a peak power of 1.56MW, while the theoretical value is 1.2MW.

7.3.2 Synchronously pumped oscillator SRS threshold

When a train of mode locked pulses is available an efficient way to generate Raman scattering is by using a configuration which allows each pulse in this train of pulses to amplify the Stokes radiation generated by the previous pulse. The Stokes component generated in a single pass by one pulse is reflected back to the Raman cell entrance to provide an initial value for the Stokes component pulse energy above the noise background level for the next mode locked pulse.

The basic arangement for this synchronously pumped oscillator is shown schematically in figure 7.6.

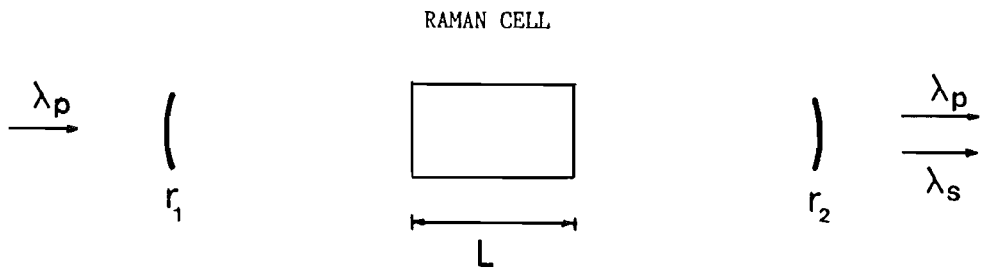

Figure 7.6. Scheme for a synchronously pumped oscillator

The input and output mirrors have a reflectivities r_2 and r_1 for the Stokes radiations respectively. The transmission losses for both the pump and Stokes signal are characterized by the extinction coefficients α_0 and α_1. If the single pass Raman exponential gain is denoted by G and the initial value for the first Stokes intensity by I_0, the amplification for the Stokes in a single pass can be written as:

$$I=I_0.\exp(-\alpha_1 L).\exp(G) \qquad 7.19$$

The pump radiation transmission loss was included in the single pass Raman exponential gain factor G.

After n pump pulses go through the Raman cell the Stokes pulse intensity is given by:

$$I=I_0.(r_1 r_2)^{n-1}.\exp[-(2n-1)\alpha_1 L+nG] \qquad 7.20$$

At SRS threshold the Stokes pulse intensity is given by:

$$I_{th}=I_0.\exp(G_{th}) \qquad 7.21$$

Where G_{th} is the Raman exponential gain necessary for a specific pulse in the train of mode locked pulse to reach the threshold energy level. In terms of synchronously pumped oscillator parameters we have

$$G_{th}=(n-1)\ln(r_1 r_2)-(2n-1)\alpha_1 L+nG_0 \qquad 7.22$$

Where G_0 is the single pass Raman exponential gain necessary in order that the Stokes component reach the SRS threshold level.

$$G_0=[G_{th}+(2n-1)\alpha_1 L-(n-1)\ln(r_1 r_2)]/n \qquad 7.23$$

The minimum value for this single pass Raman exponential gain is obtained by imposing the condition that, after a complete round trip in the cavity, the Stokes intensity must remain equal to its initial value at the Raman cell entrance.

$$I=I_0(r_1 r_2)\exp(-2\alpha_1 L+G) \qquad 7.24$$

Then by imposing the condition $I=I_0$ we have

$$G_{0min}= 2\alpha_1 L-\ln(r_1 r_2) \qquad 7.25$$

G_{0min} determines the minimum value for the single pass Raman exponential gain we need; it gives the ultimate value for the Raman threshold reduction in a SPO (synchronously pumped oscillator) arrangement, i.e. G_{0min} is the minimum single pass gain necessary to produce SRS threshold in a SPO system with a pump system containing an infinite number of pulse in the train of mode locked pulses.

$$\lim_{n\to\infty} G_0= G_{min} \qquad 7.26$$

7.3.2.1 **Experimental results**

The experimental arrangement is shown schematically in figure 7.7. The Raman SPO cavity is formed by two flat windows and two lenses. The lens next to the input window focuses the pump radiation to a 92.5μm waist size inside a 15 cm long Raman cell. The input window has a reflectivity of 60% for the Stokes signal (1.54μm) and a transmissivity of 70% for the pump radiation (1.064μm). The wedged and uncoated output window reflects 4% of the Stokes radiation back to the Raman SPO. The spot size for the Stokes beam at the centre of the cavity is determined by the separation (**a**) of the uncoated lens from each window.

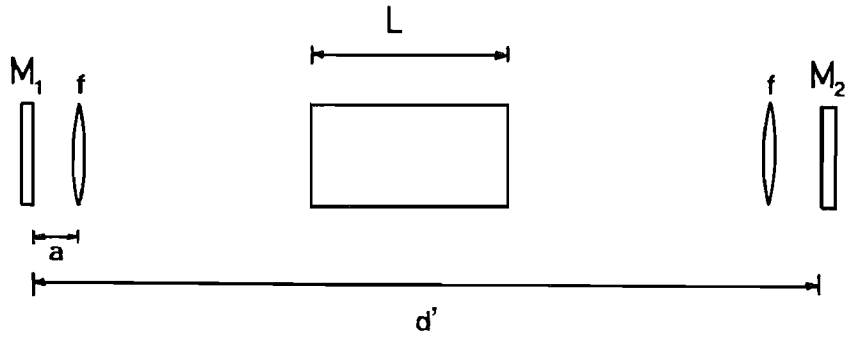

Figure 7.7. Experimental arrangement for the Raman synchronously pumped oscillator using a liquid as the Raman medium.

The cavity length is chosen so that the Stokes beam is reflected back to the Raman cell entrance at the same time the pump pulse arrives at this point. Thus, the time for a complete round trip of the Stokes wave inside the cavity should be an integer multiple of the time between two consecutive mode locked pulses. For our arrangement the mode locking frequency is 65.24 MHz, which gives a time separation of 7.66 ns between two consecutive mode locked pulses. For a cavity with a refractive index equal to unity the distance required between the two windows to have synchronization between the pump and Stokes pulses is 115 cm, however, in our arrangement the liquid in the Raman cell has a refractive index of 1.34 and the cavity length should be corrected through the expression

$$d' = d - L.(n-1) \qquad 7.27$$

Where d is the cavity length without the Raman cell inserted. For acetonitrile in a 15 cm long cell the cavity length d' is 109.4cm.

The minimum single pass Raman exponential gain is worked out using expression 7.25 and the parameters of this arrangement.

$$r_1=3.39\% \quad r_2=50.78\% \quad L=15cm \quad \alpha_1=0.104cm^{-1}$$

$$G_{0min} = 7.18$$

Considering that the Raman exponential gain necessary to reach SRS threshold in a single pass is 25, the maximum SRS threshold pump pulse power reduction we can expected for this

arrangement is 3.48 times.

From expression 7.23 we can work out the actual expected SRS threshold reduction for a 90 ns Q-switched envelope pulse width:

$$G_0 = 8.8$$

Which corresponds to a theoretical reduction in the SRS threshold pump pulse power of 2.8 times.

Experimentally the SRS threshold was reached with 97μJ energy in a mode locked pump pulse, corresponding to a peak power of 1MW. Table VIII summarizes the experimental results and theoretical predictions for SRS threshold in the Raman SPO using acetonitrile as the Raman medium.

Table VIII

Calculated values for SRS threshold in the Raman SPO

	G_{th}	P_{th}	No. times reduction
single pulse	25.0	1.20MW	1.0
SPO	8.8	0.40MW	2.8
SPO(limit)	7.2	0.35MW	3.5

Experimental values for acetonitrile and Raman SPO

	P_{th}	E_{th}	No. times reduction
single pulse	1.56MW	150μJ	1.00
SPO	1.00MW	97μJ	1.54

The temporal profile of the pump pulse after going through the SPO is shown in figure 7.8. One can see the reason for the discrepancy between the theoretical and experimental values for the

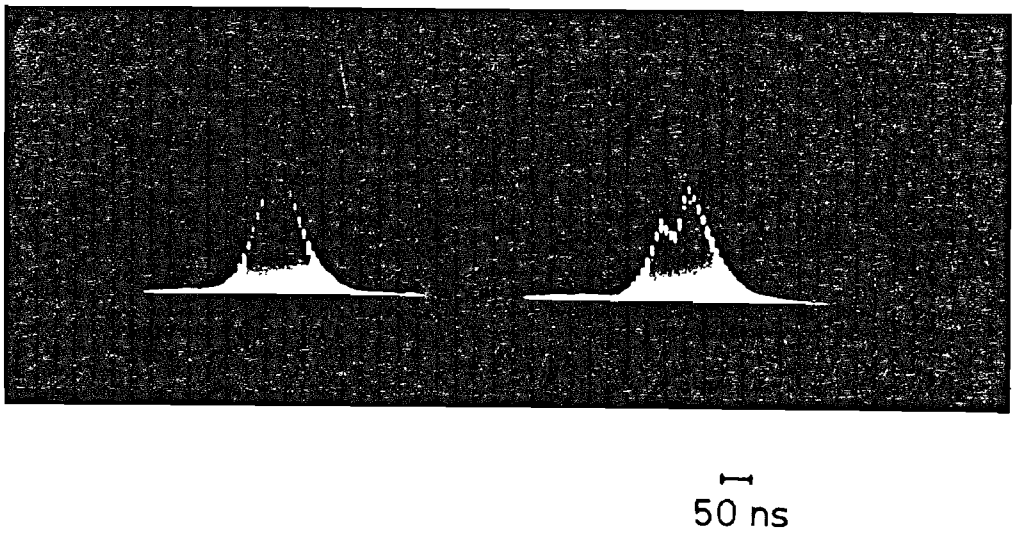

Figure 7.8. Temporal profile of the pump pulse before (a) and after (b) it goes through the Raman cell. For acetonitrile pumped by 1.064μm radiation.

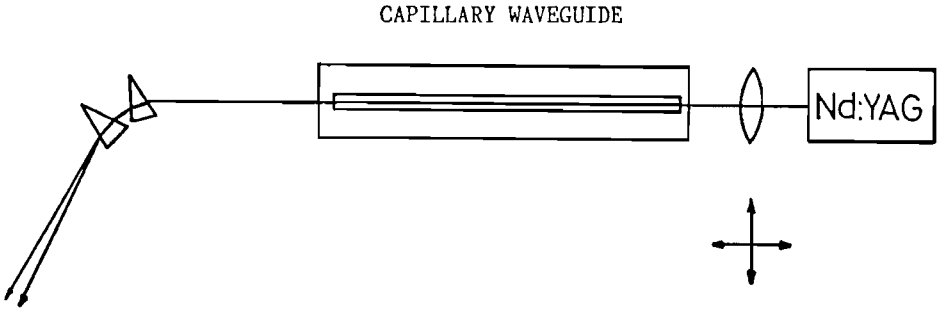

Figure 7.9. Experimental arrangement to generate 1.5μm radiation using a capillary waveguide and a Q-switched and mode locked laser.

SRS threshold pump pulse power. Although mode locked pulses which come before the center of the Q-switch envelope show some depletion, the mode locked pulses near the center of the train of pulses, where the peak power is higher, do not show any depletion. It suggests that the initial pulses are heating the medium and causing defocusing of the pump beam, thus the actual number of pulses participating of the SRS threshold reduction is smaller than the one we assume in our calculations.

7.4 SRS in gas with a Q-switched and mode locked laser

As has been seen in the previous section of this chapter although liquids show a high Raman gain coefficient and some important properties like high medium dispersion and attenuation of high order Stokes components, they have a strong thermal effect which leads to a defocusing of the pump beam inside the Raman medium, preventing a better Raman conversion into the first Stokes beam.

One possible solution to overcome this problem is to use a gas as the Raman medium, for which the self focusing and thermal defocusing are not the main problem.

Methane was chosen because its Raman shift is suitable for generating 1.5μm radiation via a single Stokes shift when this medium is pumped by the fundamental beam of a Nd:YAG laser. Although no gas absorption should occur in this case, we have the problem of a small Raman gain coefficient and a small transient effect since the Raman linewidth for methane is in the 1 cm^{-1} region.

The small Raman gain coefficient can be compensated by using a long interaction length. A capillary waveguide is used and the experimental arrangement is shown schematically in figure 7.9.

In this set up a 77cm long and 200μm diameter capillary has been used. The lens used to focus the pump beam at the capillary entrance has a fine positioning control which allowed us to get a good transmission for the pump signal in the capillary, 60% (the theoretical value is 68%).

Figure 7.10 shows the pump pulse at the output of the capillary waveguide, before and after SRS threshold is reached, for a 60 atmosphere pressure in the Raman cell.

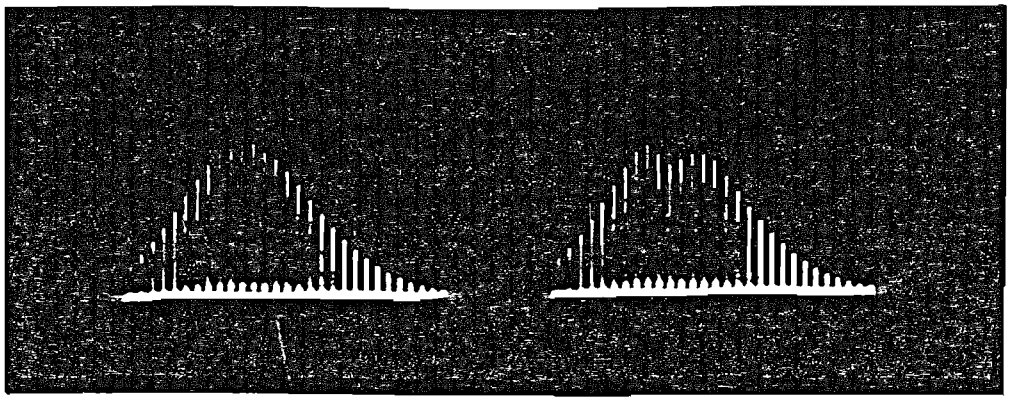

Figure 7.10. Pump pulse before (a) and after (b) the SRS threshold (E=35μJ) in a capillary waveguide filled with CH_4.

The energy in the whole train of mode lock pulses at SRS threshold was 475μJ which corresponds to a mode locked pulse energy of 32μJ at SRS threshold.

The expected SRS threshold pump pulse power can be derived from expression

$$g.I.L_{eff}=G_{th}$$

For our experimental conditions we have:

$$L_{eff}=60cm \quad \text{and} \quad g=0.45cm/GW$$

Assuming $G_{th}=25$ and a factor F=1.6 [Hanna et al (1986)] to account for the transience in the Raman medium, we have for a 90ps pulse width a pump mode locked pulse energy of 20μJ.

A similar arrangement was used for a Spectra Physics, Nd:YAG mode locked laser. In this case an 82cm long and 180μm diameter capillary was used at a gas pressure of 70 atmospheres. The transmission for the pump in the capillary was 38% (T_{theo}=58%). The mode locked pulse energy at SRS threshold was 29μJ and the theorectically predicted value for a 170ps mode lock pulse width is 24μJ.

As can be noticed there is a good agreement between the experimental and theorectical values for the pump pulse energy at SRS threshold for both laser systems.

7.4.1 Synchronously pumped oscillator

A similar arrangement used in section 7.3.2 for liquids can be used for a capillary waveguide with methane as the Raman medium. The experimental set up for this case is slightly different from the one discussed in the previous section regarding the way the Stokes beam is fed back. In this case the Stokes pulse is not fed back to the capillary entrance crossing the Raman medium a second time, but an external loop is established to do that, figure 7.11.

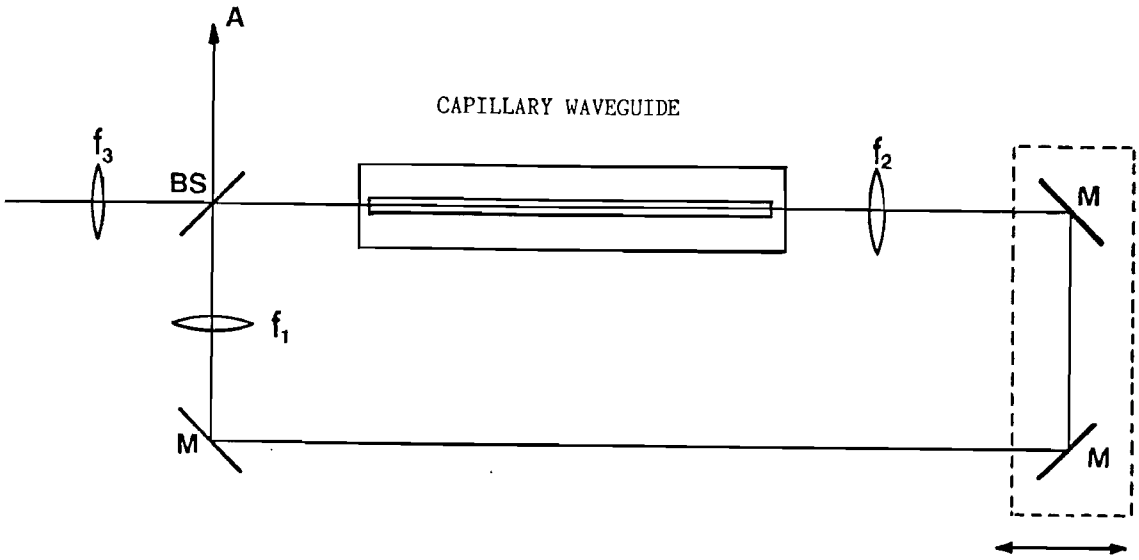

Figure 7.11. Experimental arrangement for Raman SPO using a capillary waveguide. Methane is the Raman medium.
R= Beam splitter (BS) reflectivity for 1st Stokes.
r= mirror (M) reflectivity for 1st Stokes.
c= coupling factor for 1st Stokes into the capillary.
T= capillary transmission for 1st Stokes.
G= single pass raman exponential gain.
t= transmission for the lenses (f_1 and f_2)

Using the paramters defined in figure 7.11 we have that the pulse intensity for the Stokes pulse at the point A is given by:

$$I=I_0.t^2.r^3.T.(1-R).\exp(G) \qquad 7.28$$

Thus the Stokes pulse intensity available at the capillary entrance at the arrival of the next pump pulse is:

$$I.I_0.t^2.r^3.T.R.c.\exp(G) \qquad 7.29$$

After the n_{th} pump pulse goes through the capillary waveguide the

stokes pulse intensity at the point A can be written as:

$$I=I_0.t^{2n}.r^{3n}.T^n.R^{(n-1)}.c^{(n-1)}.(1-R)^n.\exp(nG) \qquad 7.30$$

From expression 7.30 the accumulated Raman exponential gain for a specific stokes pulse at the n_{th} pump mode locked pulse is:

$$G^{spo}=(n-1)\ln(R.c)+n\ln(1-R)+2n\ln(t)+3n\ln(r)+n\ln(T)+nG \qquad 7.31$$

If we set $G^{spo}=G_{th}$ in expression 7.31 we can work out the single pass Raman exponential gain necessary to reach SRS threshold in a SPO configuration.

$$G_0=[G_{th}-(n-1)\ln(Rc)-n\ln(1-R)-2n\ln(t)-3n\ln(r)-n\ln(T)]/n \qquad 7.32$$

The minimum value for G_0 can be worked out from expression 7.29 by imposing the condition, $I=I_0$, or from expression 7.32 by letting $n\to\infty$.

$$G_{0min}=-\ln(Rc)-2\ln(t)-3\ln(r)-\ln(T) \qquad 7.33$$

For our experimental conditions we have:

R=0.30
c=1.00
t=0.81
r=0.67
T=0.38

→ $G_{0min}=3.8$

Thus, in our experiment the maximum allowed reduction in the pump pulse power relative to the single pass case is 6.5 times.

Figure 7.12 shows the pump pulse at the capillary output before and after SRS threshold been reached. The mode locked pump pulse energy at SRS threshold is 7.4μJ.

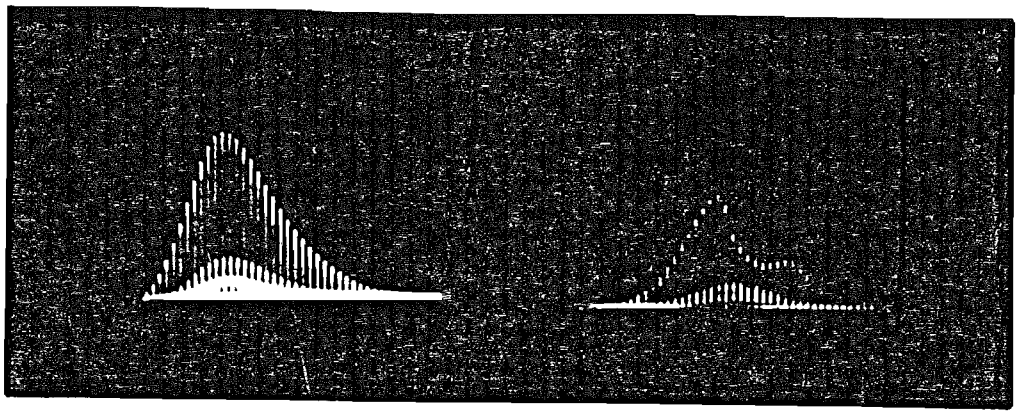

Figure 7.12. Pump pulse before(a) and after(b) SRS threshold is reached in a SPO configuration with a capillar waveguide and CH_4 as the Raman medium.

The predicted SRS threshold pump pulse energy using expression 7.32 for a number of pulses of 10 measured from the figure 7.12, is 6.4μJ for a coupling factor (c) equals to unity. The difference between this value and the experimental one is due to the fact that the coupling factor c, is not 100%, i.e., not all the generated energy at first Stokes component is feedback into the capillary waveguide.

Figure 7.13 shows the pump pulse after the capillary waveguide for a single pass configuration and for a SPO, at the same pump pulse energy. One may notice that in the first case the SRS threshold has not yet been reached while for the SPO case a large depletion is observed in the pump pulse.

These results now indicate that the scheme based on SRS in a methane filled capillary, using a 1.06μm mode-locked Q-switched Nd:YAG laser, can provide a convenient high power source of mode pulses at 1.5μm.

CHAPTER EIGHT

Conclusion

In this work it has been shown that Stimulated Raman Scattering is a convenient way to generate coherent radiation in a wide region of the spectrum, with high conversion efficiency and brightness.

For a medium with a small Raman gain coefficient a long interaction length is required in order to produce the Raman exponential gain necessary to reach the SRS threshold. In this case a capillary waveguide should be used since the confinement of the radiation inside the guide compensatesfor the diffraction loss and provides a large Raman exponential gain for the system. In the case of a train of mode locked pulses a synchronously pumped arrangement can increase the Raman exponential gain as well, as has been seen in Chapter Seven.

The use of a capillary waveguide as a Raman cell for a dye laser system is quite important, because as we have shown in Chapter Four, the tuning range for the Stokes components is increased when compared with the tuning that one can obtain by pumping an unguided Raman cell with the same pulse power. Besides that we observed generation of Stokes components up to the third Stokes shift and several anti-Stokes when we used a guided medium. Thus, the increase in the tuning range of the generated Stokes components allied with the generation of high order Stokes radiation at pump pulse power levels easily obtained with standard dye lasers, makes the capillary waveguide a very important device for extending the tuning range of these lasers to other regions of the spectrum.

The problem of a non diffraction limited beam produced by a transversely pumped dye laser can be solved by using the capillary waveguide in the configuration described in Chapter Six, where a Raman oscillator- amplifier configuration was used and a high conversion efficiency in a diffraction limited beam was obtained for the first Stokes beam

On the other hand a capillary waveguide enhances the parametric process since the capillary propagation modes can provide

phase matching for a wide range of four-wave mixing processes. Besides that, all the components generated via cascade or parametric processes in the Raman medium are confined inside the excited medium along the whole interaction length by the guiding structure. This makes any energy exchange among the components an important factor to be taken into account in determining the conversion efficiency of the Stokes components (Chapter Five).

A way to minimize this effect is through a suitable choice of the capillary bore diameter and gas pressure. The interacting component needs to usea high order capillary mode to be phase matched, which implies a very high propagation loss for the parametrically generated component. In this case the effect of this parametric process in the determination of a specific Stokes component can be neglected.

However, in certain cases the enhancement of the parametric processes provided by the guiding structure is not a problem, but rather an advantage. That is the case for anti-Stokes radiation generation. These components are generally generated more efficiently via the parametric process and in an unguided cell they have a ring-like shape, due to the angle required to phase match the process. This sort of beam profile is quite inconvenient for some applications.

In a capillary waveguide the parametric process which generates the required anti-Stokes component can be phase matched using only the EH_{11} hybrid capillary mode, which has a Gaussian-like profile. This phase matching can be reached at high pressures, i.e. in the pressure broadening region of the Raman medium where the value of the Raman gain coeffient is maximum, making the interaction more efficient than in the unguided medium.

8.1 Future experimental work

Several experiments can be suggested regarding generation of coherent radiation with high efficiency using Stimulated Raman Scattering.

An experimental arrangement to generate high power pulses at 1.5μm wavelength can be based on the results shown in Chapters Six and Seven.

As has been seen in Chapter Seven a very low SRS threshold can be reached in methane when one uses a capillary waveguide as

the Raman cell. However, the generated 1.5μm cannot reach high energy levels inside theguiding structure due to the propagation losses and parametric interactions. One solution is to use a scheme similar to the one shown in Chapter Six, figure 8.1.

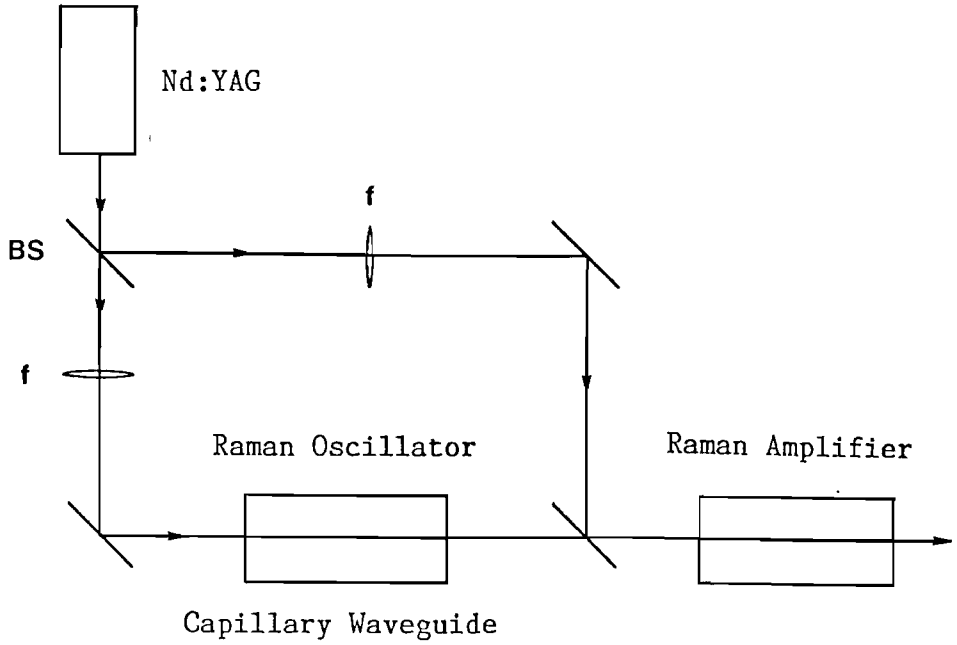

Figure 8.1. Experimental arrangement to generate 1.5μm with high efficiency and high brightness.

The Nd:YAG laser beam is split into two to pump two Raman cells. In the first cell a capillary waveguide is used to generate a seed radiation at 1.5μm in methane at high pressure. A small portion of the pump beam energy is required to pump this stage since the SRS threshold for this system is very low, as has been seen in Chapter Seven. The seed radiation and the pump beam energy are focused inside the unguided cell used as a Raman amplifier. This is an experimental arrangement similar to the one discussed in Chapter Six, when a dye laser was used to pump high pressure hydrogen in an oscillator-amplifer configuration and a conversion efficiency above 90% was reached in a diffracted limited beam.

Another technique we could suggest is related to the SRS in methane using the mode locked laser mentioned in Chapter Seven. At a high repetition rate (100Hz) of the Q-switched pulse, we observed burn marks on the cell window and capillary entrance after approximately 15 minutes of laser operation.These burns marks do not seem to depend on the pulse intensity since they appear at the cell window where the intensity is very low and even when the laser was operated cw-mode-locked only. Rather it is connected with the amount

of energy delivered to the medium during a certain interval of time. There are two possible solutions, one of them is to pump the Raman medium at a low repetition rate, the other one is to have a single mode-locked pulse rather than a train of pulses. A single mode lock pulse can still provide a large Raman exponential gain due to its high power level and thepulse energy delivered to the medium is very small, allowing an increase in the repetition rate of the pump system.

A third experimental possibility is the utilization of the Raman oscillator-amplifier configuration to obtain high conversion efficiency and high brightness in the ultraviolet region of the spectrum. This is a simple way to have a diffraction limited and high pulse power laser in the ultraviolet region of the spectrum.

This arrangement is based fundamentally on the fact mentioned in Chapter Five that anti-Stokes radiation can be generated in a spot-like shape in a capillary waveguide. The arrangement is shown schematically on figure 8.2.

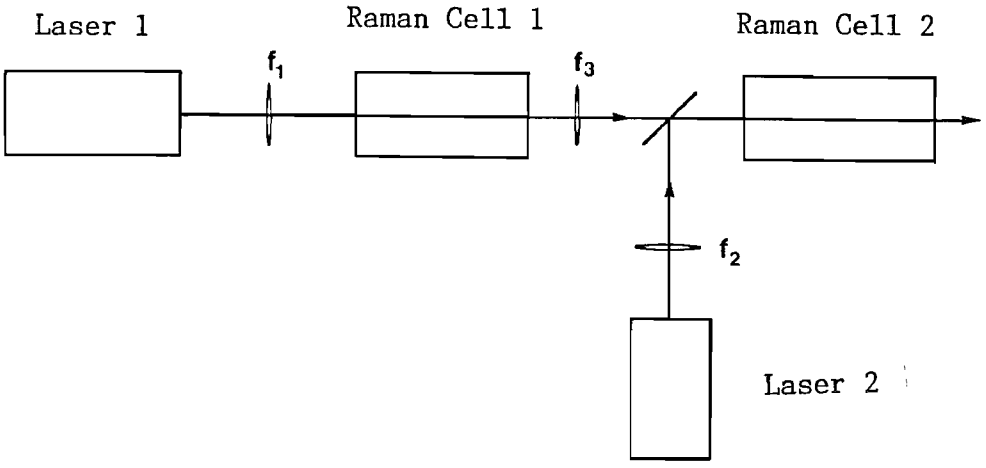

Figure 8.2. Experimental arrangement to have high pulse power and a diffraction limited beam in the ultraviolet region of the spectrum.

The Raman cell 1 contains a capillary waveguide and is pumped by the laser 1 to produce anti-Stokes radiation in a spot-like shape. The seed radiation at the anti-Stokes wavelength is focused inside an unguided Raman cell 2 which is pumped by the laser 2.

The laser 1 should have a diffraction limited beam in order to minimize the transmission loss in the capillary waveguide. the required pulse power for this laser is not very high, it should be

just enough to generate seed radiation in the capillary. As has been seen in Chapter Four of this work this pulse power is related to the spatial quality of the beam.

The capillary bore diameter and the gas pressure in the Raman cell 1 should provide phase matching conditions for a parametric process which generates the desired anti-Stokes radiation using onlythe EH_{11} mode. The tables given in Appendix 4 can be used to work out this pressure.

Laser 2 produces high pulse power but does not have a beam with good spatial distribution. The radiation generated in this laser should have a suitable wavelength, in order to generate an excitation in the Raman medium in the Raman cell 2 for which the first Stokes wavelength coincides with the anti-Stokes seed radiation wavelength.

The Raman cell 2 is an unguided cell filled with a Raman medium not necessarily the same as the one in the Raman cell 1. It must have a reasonably high Raman gain coefficient to guarantee a good conversion efficiency from the beam of the laser 2 into the seed radiation and provide, when pumped by laser 2, a first Stokes pulse at the same optical frequency of the anti-Stokes seed radiation.A small Raman shift is desired in this stage, in order that the wavelength of the amplified radiation is not too different from the wavelength of the beam generated in the laser 2.

With this arrangement a high pulse power and non diffraction limited beam in the ultraviolet region, as is the case for most commercially available excimer lasers,can be transformed into a laser with a similar pulse power and a diffraction limited beam.

APPENDIX 1

Determination of the Optimum Distance Between the Grating and the Dye Cell

The divergence angle at the grating surface can be written as:

$$\delta\theta=\lambda/\pi w_0 \qquad \text{A1.1}$$

where

$$w_0=w/\{1+[\pi w^2/(\lambda R)]^2\}^{\frac{1}{2}} \qquad \text{A1.2}$$

w is the beam spot size on the grating surface and R is the radius of curvature of the beam.

$$\partial(\delta\theta)/\partial w=[2\pi w^2/(\lambda R^2)].\{1+[\pi w^2/(\lambda R)]^2\}^{-\frac{1}{2}}-[\lambda/(\pi w^2)].\{1+[\pi w^2/(\lambda R)]^2\}^{\frac{1}{2}} \qquad \text{A1.3}$$

When $\partial(\delta\theta)/\partial w=0$ we have the minimum value for $\delta\theta$ and by solving this equation we find

$$R/w^2=\pi/\lambda \qquad \text{A1.4}$$

From Kogelnik and LI (1966) we have

$$\lambda z/(\pi w_0{}^2)=\pi w^2/\lambda R \qquad \text{A1.5}$$

and then we have:

$$Z_{opt}=\pi w_0{}^2/\lambda \qquad \text{A1.6}$$

By substituting A1.6 into expression A1.1 we have

$$\delta\theta_{min}=2\lambda/\pi w \qquad \text{A1.7}$$

APPENDIX 2

Total Internal Reflection

From figure 2.5 we can see that total internal reflection occurs when

$$\theta_3 \geq \arcsin(1/n) \qquad \text{A2.1}$$

and it does not occur when

$$\theta_3 < \arcsin(1/n) \qquad \text{A2.2}$$

Where n is the refractive index and the angles are defined in figure 2.5. From this figure we have that

$$\theta_2+\theta_3=\theta \qquad \text{A2.3}$$

and using Fresnel's law for beam refraction we can write:

$$\sin\theta_1=n\sin\theta_2 \qquad \text{A2.4}$$

In the region where no restriction is imposed on the value of θ_1, we may assume that θ_1 has its minimum possible value,i.e. $\theta_1=0$.

$$\theta_1=0 \quad \Rightarrow \quad \theta_2=0 \qquad \text{from A2.4}$$

and consequently from A2.2 we have $\theta_3=\theta$ and condition A2.2 becomes:

$$\theta < \arcsin(1/n) \qquad \text{A2.5}$$

In this region, defined by A2.5, there is no total internal reflection and any imput angle (θ_1) can be used.

On the other hand, if we set the minimum possible value of θ_1 as equal to 90, we have from A2.3 and A2.4:

$$\theta_3=\theta-\arcsin(1/n) \qquad \text{A2.6}$$

and by using condition A2.1 we have:

$$\theta \geq 2\arcsin(1/n) \qquad \text{A2.7}$$

In this region for any input angle (θ_1), the beam will be internally reflected.

APPENDIX 3

Beam Expander – Reflection Losses

For a single prism we may write the expressions for the reflection losses as:

$$R_A=tg^2(\theta_1-\theta_2)/tg^2(\theta_1+\theta_2) \qquad A3.1$$

$$R_B=tg^2(\theta_3-\theta_4)/tg^2(\theta_3+\theta_4) \qquad A3.2$$

Where R_A and R_B are the power reflection coefficients at the input and output surfaces of the prism and the angles θ_1, θ_2, θ_3 and θ_4 are defined in figure 2.5.

For a complete round trip of the beam inside the cavity, i,e. the beam passes twice through the prism, we can write:

$$T= T_A^2.T_B^2 \qquad A3.3$$

$$R= 1-T_A^2.T_B^2 \qquad A3.4$$

Where

$T_A=1-R_A$ → Transmission for the input surface A3.5

$T_B=1-R_B$ → Transmission for the output surface A3.6

T and R are the total transmission and reflection respectively.

Let us considerer now the case where more than one prim is being used.

The total reflection loss is given now by

$$R=1-T \qquad A3.7$$

where

$$T=\Pi_i(T_{Ai}.T_{Bi})^2 \qquad A3.8$$

Where Π_i indicates the product of i factors, T_{Ai} and T_{Bi} are the transmission for the input and output surface of the i_{th} prism.

$$T_{Ai} = 1 - R_{Ai} \qquad \text{A3.9}$$

$$R_{Ai} = tg^2(\theta_{i1}-\theta_{12})/tg^2(\theta_{i1}+\theta_{i2}) \qquad \text{A3.10}$$

$$T_{Bi} = 1 - R_{Bi} \qquad \text{A3.11}$$

$$R_{Bi} = tg^2(\theta_{i3}-\theta_{i4})/tg^2(\theta_{i3}-\theta_{i4}) \qquad \text{A3.12}$$

and using the angles defined in figure 2.5 for a case of a generic i_{th} prism we have the following geometric relationship:

$$\theta_{i2}=\arcsin(\sin\theta_{i1}/n) \qquad \text{A3.13}$$

$$\theta_{i3}=\arcsin(\sin\theta_i\ n^2-\sin^2\theta_{i1}\ -\cos\theta_i.\sin\theta_{i1}) \qquad \text{A3.14}$$

$$\theta_{i4}=\arcsin(\sin\theta_i\ 1-\sin^2\theta_{i1}/n^2\ -\cos\theta_i.\sin\theta_{i1}/n) \qquad \text{A3.15}$$

Where θ_i is the apex angle for the i_{th} prism.

When we consider no reflection loss for the second surface (normal incidence), expression A3.8 becomes:

$$T=\Pi_i T_{Ai}^2 \qquad \text{A3.16}$$

In figure A3.1 we have the plot of the transmission loss for a single prism and a set of four prism as a function of the input angle, for the two cases described by expressions A3.8 and A3.16.

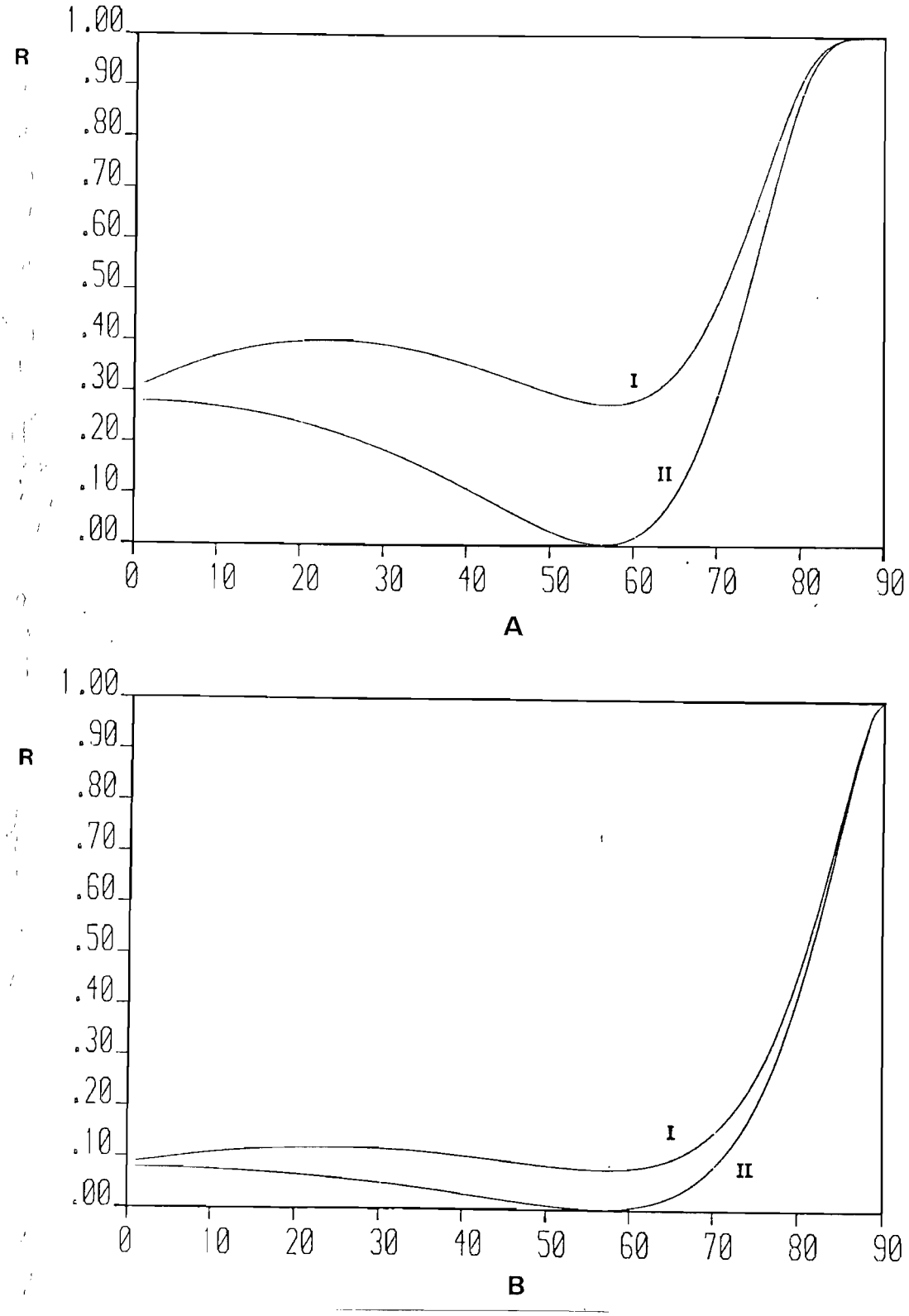

Figure A3.1. Relative transmission loss for one prism(a) and a set of four prisms (b) as a function of the input angle ($'_{i1}$). In these plots curve I corresponds to the case where the actual output angle is considered in the calculation while in curve II we assumed that the beam is normal to the output surface. The reflection losses due to the refractive index were not taken in account in these diagrams

APPENDIX 4

Gas Pressure for Phase Matching in Capillary Waveguide

In this appendix we calculate the value of gas pressure which provides phase matching for a parametric process inside a capillary waveguide filled with hydrogen.

Two pump wavelengths were considered 532nm, 575nm and four capillary diameters 100μm, 200μm, 350μm and 600μm.

To carry out the calculation we used expressions 5.74, 5.75 and 5.82 given in Chapter Five.

In each page of this appendix we have four tables of phase matching pressure values for each pump wavelength, each table corresponds to a different capillary diameter.

The propagating mode used by each component is indicated in the following way:

$$V(0,1,1,2) \rightarrow (I,V,V,H)$$

Mode	spatial configuration	μ_{mn}
I. EH_{11}		2.405
II. $EH_{-11}+EH_{31}$		5.313
III. EH_{12}		5.520
IV. $EH_{-21}+EH_{41}$		6.380
V. $EH_{-31}+EH_{51}$		7.588
VI. $EH_{-12}+EH_{32}$		8.417
VII. $EH_{-22}+EH_{42}$		9.761

Thus for the process V(0,1,1,2)

$$k_0 - k_1 = k_1 - k_2$$

the pump component (S0) uses the propagation mode I (EH_{11}), while the first Stokes (S1) and second Stokes (S2) can use any of the seven propagation modes (V: propagation modes change vertically in tables, H: propagation modes change horizontally in tables).

For example, the gas pressure to phase match the parametric process V(0,1,1,2) for a 200μm diameter capillary and a pump wavelength of 575nm when the first Stokes beam is using mode III (EH_{12}) and the second Stokes is using mode V (EH_{-31}+EH_{51}) is 19.1 atm.

When phase matching is not allowed at all we indicate that by NA and when the pressure necessary is higher than 100 atm we indicate that by HP.

TABLE I - V(0,1,1,2) ⇒ V(I,V,V,H)

λ=532nm

2a=100μm

2.3	73	80	HP	HP	HP	HP
NA	NA	NA	11	64	HP	HP
NA	NA	NA	NA	54	96	HP
NA	NA	NA	NA	7.9	45	HP
NA	NA	NA	NA	NA	NA	51
NA	NA	NA	NA	NA	NA	NA
NA	NA	NA	NA	NA	NA	NA

2a=200μm

NA	19	20	28	41	52	71
NA	NA	NA	2.8	16	27	46
NA	NA	NA	NA	14	24	43
NA	NA	NA	NA	2.0	12	32
NA	NA	NA	NA	NA	NA	13
NA	NA	NA	NA	NA	NA	NA
NA	NA	NA	NA	NA	NA	NA

2a=350μm

NA	6.0	6.5	9.2	14	17	23
NA	NA	NA	NA	5.2	8.6	15
NA	NA	NA	NA	4.4	7.8	14
NA	NA	NA	NA	NA	4.1	10
NA	NA	NA	NA	NA	NA	4.1
NA	NA	NA	NA	NA	NA	NA
NA	NA	NA	NA	NA	NA	NA

2a=600μm

NA	2.0	2.2	3.1	4.6	5.8	7.9
NA	NA	NA	NA	1.8	2.9	5.1
NA	NA	NA	NA	1.5	2.7	4.8
NA	NA	NA	NA	NA	1.4	3.5
NA	NA	NA	NA	NA	NA	1.4
NA	NA	NA	NA	NA	NA	NA
NA	NA	NA	NA	NA	NA	NA

λ=575nm

2a=100μm

3.5	95	HP	HP	HP	HP	HP
NA	NA	NA	20	89	HP	HP
NA	NA	NA	7.8	76	HP	HP
NA	NA	NA	NA	19	73	HP
NA	NA	NA	NA	NA	NA	79
NA	NA	NA	NA	NA	NA	NA
NA	NA	NA	NA	NA	NA	NA

2a=200μm

NA	24	26	36	54	67	92
NA	NA	NA	5.1	22	36	61
NA	NA	NA	1.9	19	33	57
NA	NA	NA	NA	4.8	18	43
NA	NA	NA	NA	NA	NA	20
NA	NA	NA	NA	NA	NA	1.1
NA	NA	NA	NA	NA	NA	NA

2a=350μm

NA	7.7	8.5	12	18	22	30
NA	NA	NA	1.7	7.3	12	20
NA	NA	NA	NA	6.2	11	19
NA	NA	NA	NA	1.6	6.0	14
NA	NA	NA	NA	NA	NA	6.4
NA	NA	NA	NA	NA	NA	NA
NA	NA	NA	NA	NA	NA	NA

2a=600μm

NA	2.6	2.9	4.0	5.9	7.4	10
NA	NA	NA	NA	2.5	4.0	6.7
NA	NA	NA	NA	2.1	3.6	6.4
NA	NA	NA	NA	NA	2.0	4.8
NA	NA	NA	NA	NA	NA	2.2
NA	NA	NA	NA	NA	NA	NA
NA	NA	NA	NA	NA	NA	NA

TABLE II – V(0,1,-1,0) ⇒ V(I,V,H,I)

λ=532nm

2a=100μm

NA	25	27	38	57	71	97
39	63	65	76	94	HP	HP
42	67	69	80	98	HP	HP
60	84	86	97	HP	HP	HP
88	HP	HP	HP	HP	HP	HP
HP	HP	HP	HP	HP	HP	HP
HP	HP	HP	HP	HP	HP	HP

2a=200μm

NA	6.2	6.8	9.6	14	18	24
9.7	16	16	19	24	27	34
11	17	17	20	24	28	35
15	21	22	24	29	32	39
22	28	29	31	36	40	46
28	34	34	37	42	45	52
38	44	45	47	52	55	62

2a=350μm

NA	2.0	2.2	3.1	4.6	5.8	7.9
3.2	5.1	5.3	6.2	7.7	8.9	11
3.5	5.4	5.6	6.5	8.0	9.2	11
4.9	6.8	7.0	7.9	9.4	11	13
7.2	9.2	9.4	10	12	13	15
9.0	11	11	12	14	15	17
12	14	15	15	17	18	20

2a=600μm

NA	NA	NA	1.1	1.6	2.0	2.7
1.1	1.7	1.8	2.1	2.6	3.0	3.7
1.2	1.8	1.9	2.2	2.7	3.1	3.9
1.7	2.3	2.4	2.7	3.2	3.6	4.3
2.4	3.1	3.2	3.5	4.0	4.4	5.1
3.1	3.7	3.8	4.1	4.6	5.0	5.7
4.2	4.9	5.0	5.3	5.8	6.2	6.9

λ=575nm

1.1	29	32	45	66	83	HP
47	75	78	91	HP	HP	HP
52	80	83	96	HP	HP	HP
73	HP	HP	HP	HP	HP	HP
HP	HP	HP	HP	HP	HP	HP
HP	HP	HP	HP	HP	HP	HP
HP	HP	HP	HP	HP	HP	HP

NA	7.3	8.0	11	17	21	28
12	19	20	23	28	32	40
13	20	21	24	29	33	41
18	25	26	29	34	39	46
27	34	35	38	43	47	55
34	41	41	45	50	54	61
46	53	54	57	62	67	74

NA	2.4	2.6	3.7	5.4	6.8	9.3
3.8	6.1	6.4	7.4	9.2	11	13
4.2	6.5	6.7	7.8	9.5	11	13
5.9	8.2	8.5	9.5	11	13	15
8.7	11	11	12	14	15	18
11	13	14	15	16	18	20
15	17	18	19	20	22	24

NA	NA	NA	1.2	1.8	2.3	3.2
1.3	2.1	2.2	2.5	3.1	3.6	4.4
1.4	2.2	2.3	2.7	3.2	3.7	4.6
2.0	2.8	2.9	3.2	3.8	4.3	5.1
3.0	3.8	3.8	4.2	4.8	5.2	6.1
3.7	4.5	4.6	4.9	5.5	6.0	6.9
5.1	5.9	6.0	6.3	6.9	7.4	8.2

APPENDIX 5

Raman Exponential Gain for a Non Diffraction Limited Beam

From expression A5.27 given by Cotter et al (1975) we have

$$(1/A)dA/dz = P_p/(2k_s w_p^2) - 1/R_s \qquad A5.1$$

where

$$R_s = k_s w_p^2/G_0 \qquad A5.2$$

$$P_p = G_0 k_s w_p^2 \qquad A5.3$$

$$w_p^2 = w_0^2(1+(2z/b)^2) \qquad A5.4$$

Where A is the amplitude of the electric field and all the other quantities have the meaning as defined by Cotter et al(1975).

For a non diffraction limited beam we have as defined in Chapter Six:

$$b' = b/M \qquad A5.5$$

By substituting expression A5.5 into A5.4 we have:

$$(1/A)dA/dz = [(P_p - 2P_p)/(2k_s w_0^2)].[1/(1+(2z/b')^2)] \qquad A5.6$$

Solving the diferential in A5.6 in this case of a non diffraction limited beam we find:

$$\ln[A(L)/A(0)] = [(P_p - 2P_p)/(2k_s w_0^2)]b'\tan^{-1}(L/b') \qquad A5.7$$

Since $b' = 2\pi w_0^2/(M\lambda_p)$

We can write:

$$\ln[A(L)/A(0)]=[(P_p-2\ P_p)/(2\kappa M)].\tan^{-1}(L/b') \qquad A5.8$$

where $\kappa=\lambda_p/\lambda_s$

From expression A5.8 the power exponential gain coefficient can be written as:

$$G=[(P_p-2\ P_p)/(\kappa M)].\tan^{-1}(L/b') \qquad A5.9$$

By writing P_p in terms of the Raman gain coeffcient and pump power we have:

$$P_p=4gP_p/\lambda_s$$

and expression A5.9 becomes;

$$G=[\lambda_s/(M\lambda_p)].\tan^{-1}(L/b').\sqrt{4P_p/\lambda_s}(\sqrt{4P_p/\lambda_s}-2) \qquad A5.10$$

APPENDIX 6

Volume 55, number 3 OPTICS COMMUNICATIONS 1 September 1985

HIGH EFFICIENCY AND HIGH BRIGHTNESS RAMAN CONVERSION OF DYE LASER RADIATION

D.C. HANNA, M.T.T. PACHECO and K.-H. WONG

Department of Physics, University of Southampton, Highfield, Southampton SO9 5NH, UK

Received 17 May 1985

A technique for efficient Raman conversion of an excimer pumped dye laser is described, based on the use of a Raman oscillator/amplifier combination. A photon conversion efficiency of 90% to first Stokes is demonstrated, with diffraction-limited beam quality.

Stimulated Raman scattering provides a simple means for extending the tuning range of dye laser radiation into regions where dye laser operation is inefficient or difficult to achieve. The simplest, and most widely used arrangement involves tight focussing of the pump beam into the Raman medium, with the Stokes radiation generated on a single pass through the medium. In practice however this arrangement gives poor control over the various processes which can occur, such as multiple Raman shifts, backward Raman scattering and generation of higher order Stokes and anti-Stokes radiation through four wave mixing. The results of such an uncontrolled mixture of processes can be poor conversion efficiency and a large angular spread of the generated radiation. By contrast, it has been shown that by arranging the Raman medium as an oscillator-amplifier combination [1–5] with a small fraction of the pump used for the oscillator and the main part of the pump used to drive the amplifier, good control can be obtained and high conversion efficiency to a selected Stokes order can be achieved. The main disadvantage of the oscillator-amplifier scheme is the extra complexity introduced and in particular the exacting requirement on spatial overlap of the pump beam and injected Stokes beam in the amplifier stage. Stappearts et al. [6] have also shown that where a broadband pump is used the gain in the amplifier is reduced unless the injected Stokes beam and pump beam at the amplifier are adjusted to travel over equal paths from the pump laser. This however introduces a further complexity (fig. 1 shows a schematic set up). In this letter we describe a scheme for stimulated Raman scattering from a dye laser in which the required spatial and temporal overlap of the pump and Stokes beams at the Raman amplifier are automatically achieved. The technique can be extended to multiple Raman shifting but we report here the results obtained where conversion to the 1st Stokes was optimised. With a XeCl excimer-pumped dye laser of ~7 mJ output, using H_2 gas as the Raman medium, we obtain 90% photon conversion efficiency into a diffraction-limited 1st Stokes beam.

The experimental arrangement is shown in fig. 2. The essential feature is that Raman oscillator stage is before the final dye amplifier stage. The Stokes radiation and the residual dye laser radiation from the Raman oscillator are collinear and this collinearity is preserved after passing through the final dye amplifier cell. Further more in this scheme the final dye amplifier also maintains the temporal coincidence, first established in the Raman oscillator between the Stokes intensity fluctuations and the dye oscillator intensity fluctuations.

Our dye laser system consists of an oscillator and two amplifiers, pumped by a XeCl excimer laser with a 20 ns, 100 mJ output. The dye oscillator incorporated a four-prism beam expander and 2800 line/mm holographic grating to narrow the linewidth to 0.3 cm^{-1}. A 400 μm diameter aperture was inserted in

Volume 55, number 3 OPTICS COMMUNICATIONS 1 September 1985

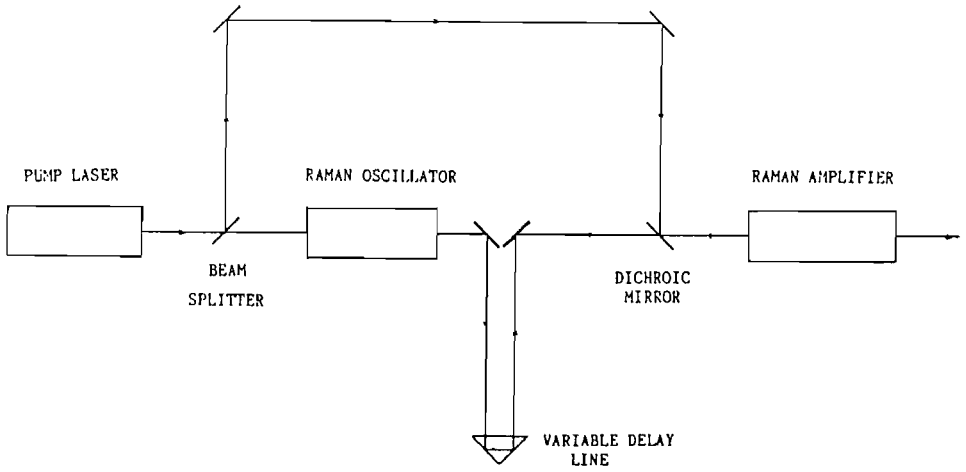

Fig. 1. Schematic of Raman oscillator/amplifier with provision for equalising paths from the pump laser to the Raman amplifier.

the dye oscillator to ensure a diffraction-limited output. With ~3 mJ pump energy into the dye oscillator, its output was 40 μJ in a 12 ns pulse and this was amplified to ~700 μJ in the first dye amplifier cell, pumped by ~10 mJ from the excimer laser. The Raman oscillator cell, filled with H_2 to a pressure of 25 atm., contained a fused silica capillary waveguide of 200 μm bore diameter and 72 cm length. The use of the capilllary offered two main advantages. The lower SRS threshold [7] meant that more pump energy was available for the second dye amplifier, hence improving the overall conversion efficiency. Also the output beams from the capillary (both the Stokes beam and the residual dye beam) were constrained to be diffraction-limited by the spatial filtering action of the guide. The measured transmission of the capillary with the dye laser beam optimally focussed into the capillary was 70%, somewhat lower than the calculated value [8] of 90% for a dye laser wavelength of 565 nm. With 680 μJ of dye laser input to the

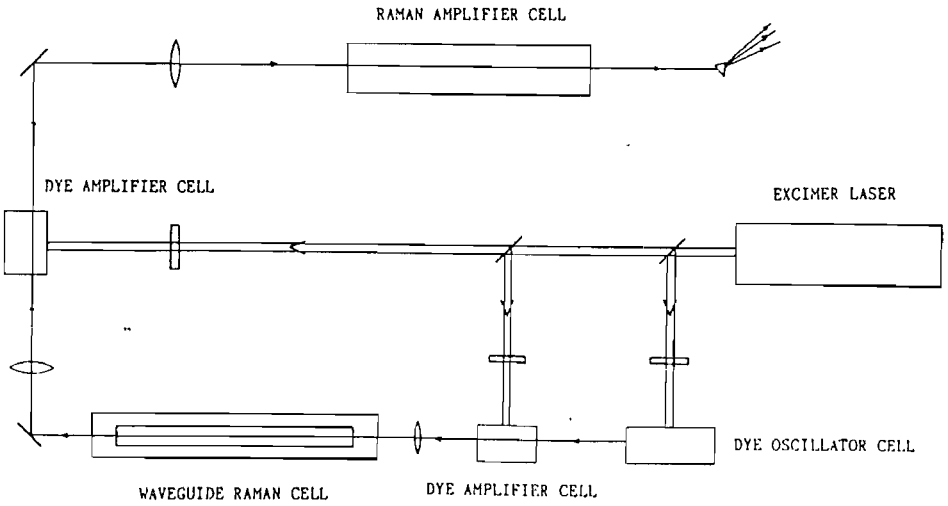

Fig. 2. Experimental configuration of the dye-laser-pumped Raman oscillator-amplifier.

Raman oscillator (i.e. about a factor of two above threshold), the 1st Stokes (738 nm) output energy was 60 μJ. In this experiment we deliberately kept the pump energy low enough to prevent significant second Stokes generation since our aim was to achieve maximum conversion to first Stokes in the Raman amplifier. The first Stokes and remaining dye laser beam from the capillary exit then pass through the second dye amplifier, a 2 cm long cell pumped by 70 mJ of excimer laser energy. The first Stokes beam suffered a small attenuation, from 60 μJ input to 40 μJ output, in the dye medium (Rhodamine 6G in methanol) whereas the dye laser beam was amplified to an energy of 7 mJ. The collinear dye and Stokes beams were then loosely focussed by a lens of 50 cm focal length, into the Raman amplifier cell. The cell length l was 35 cm and the dye beam waist, formed at the centre of the cell, had a spot size radius w_0 of 350 μm. Under these conditions the power gain e^G in the amplifier cell was insufficient for Stokes generation to occur without the injected Stokes beam. A rough calculation of G, showed that with the maximum dye input (5.5 mJ in 12 ns), the peak, on-axis Raman gain G was only approximately 20 confirming that self oscillation would not be expected. Typically around 30 μJ of Stokes radiation could be injected into the Raman amplifier cell and fig. 3 shows the measured energy conversion efficiency to 1st Stokes as a function of dye laser input energy. Energy measurements were made with a pyroelectric energy meter. The maximum energy efficiency was 70%, corresponding to a

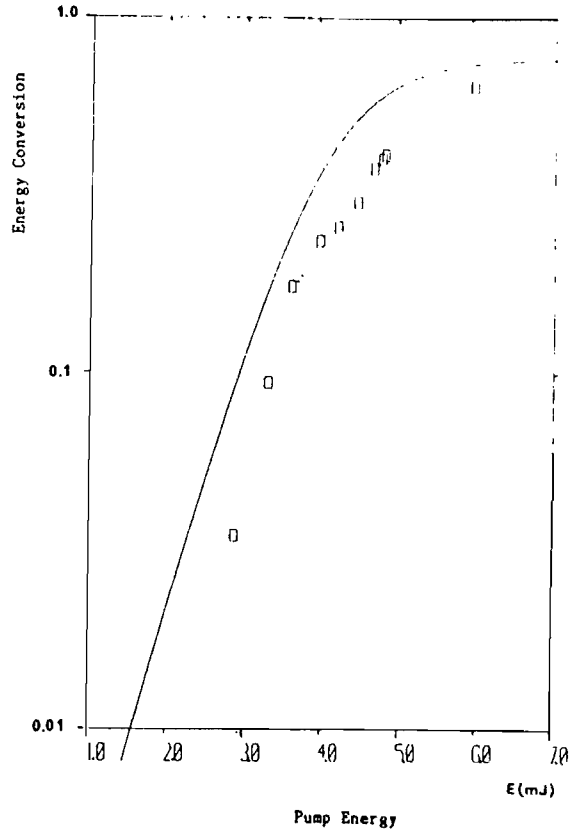

Fig. 3. Raman energy conversion efficiency into the first Stokes as a function of the input dye laser energy. The squares indicate the experimental results, the solid line corresponds to the calculation.

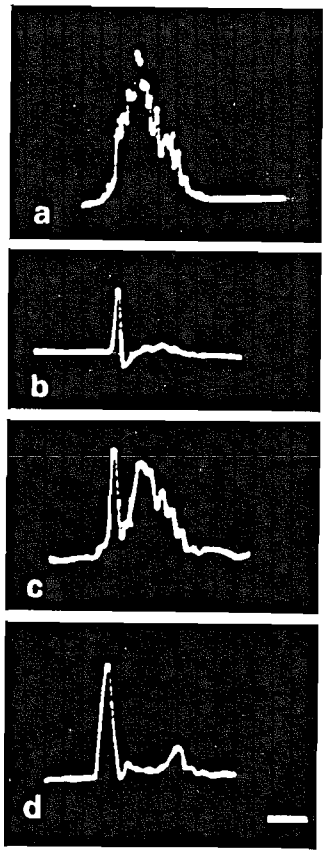

Fig. 4. The temporal profiles of the dye laser at various stages in the configuration shown in fig. 2: (a) at the input of the capillary, (b) at the output of the capillary, (c) after the second stage dye amplifier, (d) after the Raman amplifier. The bar in (d) represents 5 ns.

photon conversion efficiency of 90%. Also shown in fig. 3 is a calculation (solid line) of conversion efficiency, including the effect of pump depletion. The calculation is approximate since it makes the simplifying assumption that the pump beam of power P has a uniform transverse profile with intensity I_p given by $I_p = P/\pi w_0^2$. The Raman gain coefficient used in this calculation is $g_R = 2.4 \times 10^{-11}$ m/W ($g_R I_p l \equiv G$), corresponding to the more general expression

$$g_R = \frac{1.8 \times 10^{-11}\ \text{m/W}}{\lambda_S(\mu\text{m})},$$

where λ_S is the Stokes wavelength [9].

Figs. 4 and 5 show the temporal behaviour of the dye laser pulse and first Stokes pulse at various stages through the system. In fig. 4b it is seen that the dye pulse emerging from the capillary is heavily depleted except for a spike left at the beginning of the pulse. Fig. 4c shows the dye pulse leaving the second dye amplifier and it can be seen that most of the energy gain goes into the depleted portion of the dye pulse rather than the spike. This is an important feature for efficient Stokes conversion in the Raman amplifier since the injected Stokes radiation coincides with the depleted portion of the dye pulse. Fig. 4d shows the transmitted dye pulse after the Raman amplifier (vertical scale of 4d ten times less sensitive than fig. 4c). Figs. 5a and b show the Stokes pulse before and after the Raman amplifier, respectively, with 5b having a vertical scale ten times less sensitive than in 5a.

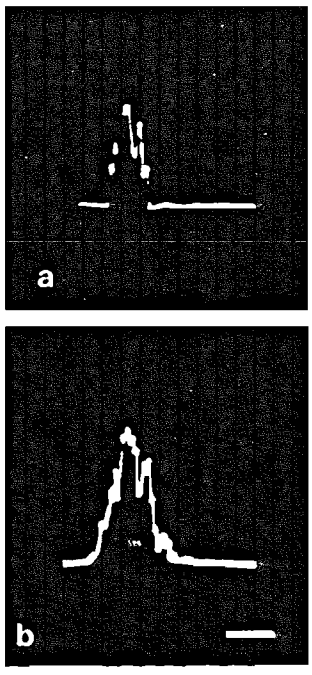

Fig. 5. The temporal profiles of the first Stokes radiation: (a) after the capillary waveguide, (b) after the Raman amplifier. The bar in (b) represents 5 ns.

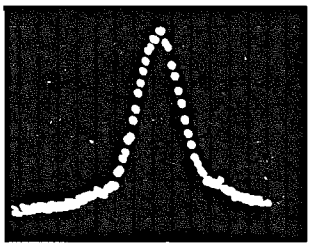

Fig. 6. Transverse intensity profile of the amplified first Stokes pulse, as monitored by a photodiode array.

The Stokes output beam quality was assessed by focussing the beam then measuring the waist-size and the beam divergence from this waist. This measurement showed that the beam was diffraction-limited and fig. 6, which shows the intensity profile recorded with a diode array confirmed the smooth profile that was noted visually.

Conclusions. We have demonstrated a stimulated Raman scattering arrangement involving a Raman oscillator/amplifier configuration which automatically ensures excellent spatial and temporal overlap between the pump beam from a dye laser and the injected Stokes beam. This results in a very high conversion efficiency and suggests that near infrared radiation may be generated more efficiently by this method rather than by direct pumping of near infrared dyes.

This work has been supported by the Science and Engineering Research Council. K.-H. Wong holds an SERC fellowhip and M.T.T. Pacheco acknowledges support from C.T.A. São Paulo, Brazil.

References

[1] A.Z. Grasyuk, Sov. J. Quant. Electron 4 (1974) 269.
[2] H. Komine and E.A. Stappearts, Optics Lett. 4 (1979) 398.
[3] A. De Martino, R. Frey and F. Pradière, IEEE J. Quantum. Electron., QE-16 (1980) 1184.
[4] H. Komine, E.A. Stappaerts, S.J. Brosnan and J.B. West, Appl. Phys. Lett. 40 (1982) 551.
[5] H. Komine and E.A. Stappaerts, Optics Lett 7 (1982) 157.
[6] E.A. Stappaerts, W.H. Long Jr. and H. Komine, Optics Lett. 5 (1980) 4.
[7] A.J. Berry, D.C. Hanna and D.B. Hearn, Optics Comm. 43 (1982) 229.
[8] E.A.J. Marcatili and R.A. Schmeltzer, Bell Syst. Techn. J. 43 (1964) 1783.
[9] D.C. Hanna, D.J. Pointer and D.J. Pratt, to be published.

Seventh National Quantum Electronics Conference

Efficient stimulated Raman scattering in gases and liquids

D C Hanna, D J Pointer, M T T Pacheco

Department of Physics
University of Southampton
Highfield
Southampton SO9 5NH

We report results on the development of high power mode-locked laser sources with tunability in the near-infrared via stimulated Raman scattering in various gases and liquids. The pump laser used in this work has been either an actively mode-locked, Q-switched NdYAG laser (8mJ, 100psec at 1.06μm) or a dye laser (~1mJ, 70psec, tunable around 570nm) synchronously pumped by the second harmonic of the NdYAG laser. An important feature has been the diffraction-limited and bandwidth limited performance of these pump lasers since this has contributed to the high efficiency, low threshold and good amplitude stability of the generated pulses. Particular attention has also been paid to achieving this same diffraction - and bandwidth-limited performance for the generated radiation. The use of a Raman oscillator/amplifier configuration is a central feature since (a) this provides control over the spatial coherence of the generated radiation and (b) it provides control over the extent to which higher order Stokes generation occurs.

Examples of the results achieved with this approach are as follows :

1. Using CH_4 gas at 30 atm as the Raman medium and the 1.06μm pump, 1st Stokes radiation at 1.54μm is generated with an energy efficiency of 25% (1.2mJ generated from 4.8mJ of 1.06μm). The duration of the 1.54μm pulse, measured by second harmonic auto-correlation is ~50psec, and energy stability (at 5Hz repetition rate) is ~6%, identical to the 1.06μm pump.

2. Using the Rhodamine 6G dye laser pump, third Stokes generation, tunable from 1.1μm to 1.2μm has been achieved with energy efficiency greater than 1% over this range and 10% efficiency at the centre of the range (100μJ generated from the 1mJ pump). The use of longer wavelength dyes, out of around 650nm, will extend the tuning range of third Stokes to ~ 1.5μm, a region of particular interest for nonlinear propagation studies in optical fibres.

In addition to CH_4 as a Raman medium we have investigated H_2, D_2 and a number of liquids. The results of careful measurements of the Raman gain for these liquids will be presented. A number of liquids look promising as they have shown high conversion efficiency (up to 90% photon conversion efficiency to 1st Stokes) without the appearance of competing nonlinear effects such as stimulated Brillouin scattering and self-focussing, and have significantly lower thresholds than the gases. Results from these liquid media will be presented.

AN ANALYSIS OF STIMULATED RAMAN SCATTERING IN GUIDED SYSTEMS

M.Tadeu Pacheco and D.C.Hanna

Department of Physics
University of Southampton
Highfield, Southampton, SO9 5NH

In this paper we compare the performance of a capillary waveguide and an unguided cell in terms of the pump power necessary to reach the threshold for Stimulated Raman Scattering (SRS) and the Raman exponential gain. The main characteristics of the capillary waveguide and their role in the SRS process are discussed. The case of a non diffraction limited beam is also considered and a general expression is derived for the overall enhancement provided by the capillary.

Neste trabalho e feita uma comparacao entre um guia de onda dieletrico e uma celula sem guiagem em termos da potencia necessaria para se alcancar o limiar de geracao Raman e do ganho exponencial. As principais caracteristicas dos capilares e o papel que representam no espalhamento Raman estimulado (ERE) sao discutidas. O caso de um feixe nao limitado por difracao e tambem considerado e uma expressao geral e apresentada para o incremento no ganho exponential devido a utilizacao de um sistema guiado.

1. Introduction

Stimulated Raman Scattering (SRS) provides a simple means for extending the characteristics of lasers in the visible region to the ultraviolet or infrared region of the spectrum. For example, the tuning range of the dye laser radiation can be extended into regions of the spectrum where dye laser operation is inefficient or difficult to achieve. Similarly the high repetition rate and high pulse power available with visible lasers can be transferred to different wavelengths.

However the SRS effect is a third order non linear process which generally implies that a high pulse intensity must be provided in order to reach threshold and make the whole process efficient. The problem becomes greater when one goes to the infrared region where the Raman gain coefficient for most of the materials is very much reduced. The most widely used arrangement involves tight focussing of the pump beam into the Raman medium and the Stokes radiation being generated on a single pass through the medium. In practice this arrangement gives poor control over the various processes which can occur, such as multiple Raman shifts, backward Raman scattering and generation of high order Stokes and anti-Stokes radiation through four-wave-mixing processes. The result of such an uncontrolled mixture of processes can be poor conversion efficiency and a large angular spread of the generated radiation. Besides, in this tight focussing arrangement the Raman exponential gain depends only on the pump laser characteristics, such as pump pulse power, wavelength and spatial quality of the pump beam.

Radiation in the near-and far-infrared is of great interest nowadays due to their applications in communication and photochemistry. However, in order to obtain efficient Raman conversion in these regions of the spectrum one needs a laser of high power with a very good beam quality, since these parameters will compensate for the small Raman gain coefficient in the infrared region of the spectrum. Nevertheless, if one uses a guiding structure containning the Raman medium, a new parameter is involved: the cell geometry.

Unlike the usual tight focussing system, the guiding structure can prevent the beam from diffracting by reflecting it back into the Raman medium repeatedly. The overall Raman exponential gain now

depends on the laser pulse power, the Raman gain coefficient and the cell geometry, i.e. the length of the waveguide and its internal diameter. By using this device we can make the spot size much smaller, increasing the beam intensity in the Raman medium while still maintaining a long interaction length, since the diffraction losses are less important and the interaction length is defined basically by the attenuation of the propagating radiation.

2. Raman threshold for unguided medium

The Raman exponential gain along the axis for an unguided system with a length L can be written as,

$$G_U = g\int_{-L/2}^{L/2} \frac{2P}{\pi w^2(z)}\, dz \qquad 1$$

where g is the Raman gain coefficient , P is the pump pulse peak power and w(z) the pump beam spot size at a position z inside the cell (Figure 1). By using the expression for the spot size [1] ,

$$w(z)^2 = w_0^2[1+(2z/b)^2] \qquad 2$$

$$b = 2\pi w_0^2/\lambda \qquad 3$$

where w_0 is the beam waist formed in the center of the cell, we have:

$$G_U = g(4P/\lambda).\tan^{-1}(L/b) \qquad 4$$

However, in the general case when a tight focussing configuration is considered, expression 1 does not correctly describe the gain experienced by the Stokes wave, since in this case the Stokes radiation have a gain which is averaged over the pump intensity profile and consequently the overall Raman exponential gain is smaller than the one predicted by expression 1.

The Raman exponential gain for this case is given by [2]

$$G = [(\lambda_s/\lambda_p).\tan^{-1}(L/b)].\sqrt{4Pg/\lambda_s}.(\sqrt{4Pg/\lambda_s} - 2) \qquad 5$$

For the case of a Raman amplifier expression 1 can still be used since then, tight focussing is not used used and the confocal parameter is usually a few times the cell length. The Stokes average can be well approximated by the maximum gain since the Stokes spot size can be made small relative to the pump spot size.

Let us assume G_{th} is the exponential gain necessary to reach the SRS threshold. The term "threshold" used in this section and throughout this paper does not indicate the usual condition in a resonator when the gain provided by the active medium should balance the round trip losses for a given oscillator mode. For the stimulated Raman scattering process the term describes a situation in which the output power for the generated Stokes pulse has reached a level which is just enough to start to deplete the pump pulse. The Stokes radiation pulse power grows exponentially from the noise background level or an input signal and when its energy is strong enough to extract an appreciable part of the pump pulse energy, we say that the Stokes component has reached threshold. For a pump pulse width of the order of 10 nanoseconds the Stokes energy at threshold is about 1 to 10 microjoules per pulse. This happens for a Raman exponential gain (G_{th}) of between 20 and 30.

The pump pulse needed to reach this Raman exponential gain is defined as the Raman threshold power for this pumping system,

$$P_{th} = (\lambda_s/4g).\{ 1 + [1 + G_{th}\lambda_p/(\lambda_s tg^{-1}(L/b))]^{1/2}\}^2 \qquad 6$$

The minimum value for P_{th} is reached in the tight focussing situation, i.e. when the beam waist size is made very small so that the confocal parameter is much shorter than the cell length.

$$P_{th}|_{min} = (\lambda_s/4g).[1 + (1 + 2G_{th}\lambda_p/\pi\lambda_s)^{1/2}]^2 \qquad 7$$

As can be observed from expression 7 the value for the pump pulse power necessary to reach Raman threshold depends only on the pump laser wavelength and the Raman medium gain coefficient. The dependence on the beam waist size disappears when one assumes tight focussing.

3. Raman threshold for a guided medium

From expression 6 one can see that there is no optimum value for the pump beam waist which minimizes the pump power threshold, since the whole expression decreases monotonically with $tg^{-1}(L/b)$, consequently any value for the beam waist size which produces $b \ll L$ will lead to the minimum threshold pump power. This happens because an increase in the pump intensity due to a reduction in the beam waist size is compensated by an increase in the diffraction of the beam which decreases the interaction length. The overall result is that P_{th} does not depend on the pump focussing geometry any more.

However, when one uses a capillary waveguide as the Raman cell the pump beam can be focused to a small waist size without reducing the interaction length, since the confinement of the radiation in the guided medium reduces the diffraction. However, due to the fact that the refractive index of the gas inside the guide is smaller than the refractive index of the guide walls, the propagating radiation has losses, unlike the lossless propagation which occurs in guided based on total internal reflection. The attenuation coefficient is given by [3]

$$\alpha_{nm} = (\mu_{nm}/2\pi)^2 \cdot \frac{\lambda^2}{a^3} \cdot \frac{\frac{1}{2}(\eta^2+1)}{\sqrt{\eta^2-1}} \qquad 8$$

where μ_{nm} is the m_{th} root of the equation,

$$J_{-1}(\mu_{nm}) = 0$$

and **n** and **m** are integers that characterize the propagating mode, **a** is the capillary radius and η is the capillary wall refractive index. This attenuation coefficient is for a straight capillary,but if the system is curved, an extra term should be added to the attenuation coefficient given in expression 8 [3]. Experimentally, however we observed that this bend effect is a minor problem compared with the transmission losses and the coupling losses. In table I we have the seven first capillary propagating modes in order of increasing μ_{nm}.

From the attenuation coefficient we have that a large value of μ_{nm} will produce a highly attenuated mode. Thus we must try to keep μ_{nm} as small as possible. From table I we can see that the hybrid mode EH_{11} has the smallest value for μ_{nm}, therefore this will be the pre-

ferred mode for the beam inside the capilllary since it will produce the smallest attenuation of all the propagating modes. The condition for optimizing the coupling between a TEM_{00} mode and the EH_{11} mode is given by [4]. That is, beam waist of the input radiation should be 2/3 of the capillarybore radius. With this condition satisfied calculations [4] predict only 2% loss in the coupling $TEM_{00} \rightarrow EH_{11}$.

The exponential gain for a guided structure can be written as

$$G_g = g \cdot \int_0^L \frac{P \cdot \exp(-2\alpha z) \cdot dz}{\pi w_0^2} \qquad 9$$

where all the quantities have the same meaning as defined previously for the unguided cell and w_0 is the beam waist size formed at the capillary entrance, which satisfies the condition for minimum coupling losses (Figure 2). Solving the integral in expression 9 we have,

$$G_g = \frac{P}{\pi w_0^2} \cdot g \cdot L_{eff} \qquad 10$$

where

$$L_{eff} = [1-\exp(-2\alpha L)]/2\alpha \qquad 11$$

where L is the actual capillary length and L_{eff} the equivalent capillary length over which the pump radiation intensity can be regarded as having a constant value.

From expression 10 we may observe that unlike the tight focussing arrangement, the capillary waveguide Raman exponential gain depends strongly on the cell characteristics,like cell length, bore diameter and the cell material refractive index.

The pump pulse threshold power can be obtained from expression 10 by setting $G_g = G_{th}$ in that expression:

$$P_{th} = \frac{G_{th} \cdot \pi w_0^2}{g L_{eff}} \qquad 12$$

In this case, unlike the unguided case, the minimum pump pulse threshold is not reached for a very small value of w_0. Let us assume a fixed length of cell and since w_0 is related to a, a small value of w_0 will lead to a very small capillary radius and conse-

quently an increase in the beam propagating losses. As the attenuation losses are proportional to w_0^{-3} they will overcome the increase in the pump intensity due to the spot size reduction and the whole expression 12 will follow a w_0^{-1} behaviour:

$$P_{th}|_{\lim_{w_0 \to 0}} \propto 1/w_0 \qquad 13$$

At the other extreme, a large beam waist does not reduce the pump pulse power threshold in either the, unguided or guided case, because the beam intensity drops down and the whole Raman exponential gain becomes very small. The expression 12 can be written in this situation as proportional to w_0^2:

$$P_{th}|_{\lim_{w_0 \to \infty}} \propto w_0^2 \qquad 14$$

Thus we expect that for a capillary waveguide of a given length we will have a specific value of pump beam waist and capillary radius which give a minimum SRS threshold power. This value can be obtained from the expression 11 and it is found to be a function of the pump wavelength and the capillary characteristics. The exact value of the optimum capillary radius is given through the implicit equation,

$$\exp(\alpha L)=(1+3\alpha L) \qquad 15$$

Figure 3 shows the pump pulse power threshold variation with the beam waist size for both arrangements, and we notice the minimum value reached for the guided structure and the enormous reduction in the P_{th} value when compared with the unguided system.

4. SRS with a non diffraction-limited beam

Let us now consider a beam whose divergence δ' is M times that for a diffraction limited beam with a beam waist size w_0,

$$\delta' = M.\lambda/\pi w_0 \qquad 16$$

Since the confocal parameter is a measure of how much the beam diffracts we can write:

$$b' = b/M \qquad 17$$

where b is the confocal parameter for a diffraction limited beam. The expression for the unguided Raman exponential gain then becomes [5],

$$G_u' = [(\lambda_s/M\lambda_p).tg^{-1}(L/b')].\sqrt{4Pg/(\lambda_s)}.(\sqrt{4Pg/\lambda_s} - 2) \qquad 18$$

where

$$b' = b/M$$

As we may notice, the Raman exponential gain for a tight focussing configuration still depends only on the Raman medium and the pump laser characteristics,i.e. pulse power, wavelength and number of times the beam is diffraction-limited.

$$L \gg b'$$

$$G_u' = [\pi\lambda_s/(2M\lambda_p)].\sqrt{4Pg/(\lambda_s)}.(\sqrt{4Pg/\lambda_s} - 2) \qquad 19$$

For the guided structure the non diffraction limited beam effect will appear in the attenuation coefficient, since it will produce a large beam diffraction angle inside the capillary and consequently will increase the leakage losses, and we have [5]

$$\alpha' = (\mu_{nm}/2\pi)^2.\frac{\lambda'^2}{a^3}.\frac{\frac{1}{2}(\eta^2+1)}{\sqrt{\eta^2-1}} \qquad 20$$

and

$$\lambda' = M\lambda$$

The effect of the non diffraction limited beam in both systems is to "increase" the radiation wavelength and its effect can be taken in account in any previous expression by performing the transformation:

$$\lambda \rightarrow M\lambda$$

it is important to point out that there is no real change in the radiation wavelength, and what the transformation does is to assume that the increase in the beam diffraction is not due to any peculiarity of the beam spatial profile but is due to a virtual increase in the radiation wavelength of a beam with a perfect Gaussian profile.

The enhancement of the Raman exponential gain produced by the guided structure relative to the gain in the unguided situation can be defined in a very general way as

$$S = G_g'/G_u' \qquad 21$$

where G_g' and G_u' are the Raman exponential gains for the guided and unguided systems respectively for a non diffraction limited beam and a general value of beam waist size. By substituting expressions 10, 18 and 20 into expression 21 we have

$$S=PgL_{eff}'M\lambda_p/[\pi w_o^2\lambda_s\tan^{-1}(L/b')\sqrt{4Pg/\lambda_s}(\sqrt{4Pg/\lambda_s}\ -2)] \qquad 22$$

where

$$L_{eff}'= [1-\exp(-2\alpha'L)]/2\alpha'$$

$$b'= b/M$$

In figure 4 we show the plot of the S values against the capillary radius for a wavelength of 532 nm and several values of M. As we may observe from these diagrams the optimum value for the capillary radius increases when the value of M is increased and the S peak value decreases simultaneously.

For a large beam waist size the Raman exponential gain can be approximated by the Stokes gain along the axis given by expression 4, and the factor S_o can be written as,

$$S_o = \lambda_p Mb'L_{eff}'/(4\pi w_o^2 L)$$

additionally the effective length can be approximated by the actual capillary length since a large spot size implies a large capillary bore diameter and consequently a low transmission loss (expression 8),

$$S_0 = \lambda_p M b'/(4\pi w_0^2) \qquad 23$$

and as

$$b' \propto 1/M$$

the final expression for the S_0 factor does not depend on the beam diffraction any longer.

$$S_0 = \lambda_p . b/(4\pi w_0^2) \qquad 24$$

5. Conclusion

The capillary waveguide provides a very convenient way of reducing the threshold pump pulse power since it can keep the interaction length relatively long while the pump pulse intensity is increased through the reduction of the capillary bore diameter. Besides this main feature of producing a large Raman exponential gain the capillary brings out another advantage which is the mode selection due to the spatial filter effect. This mode selection is particularly important when one has a large amount of available energy in the pump pulse but the beam intensity spatial distribution over the cross section does not resemble a Gaussian one. In this case the attenuation for the higher order capillary modes will select basically the EH_{11} mode and the output beam willhave a Gaussian-like shape. The Raman conversion efficiency for this situation is not expected to be very high since the effective input beam pulse energy is very small. However, from the enhancement factor S defined in the text we can see for example, that the capillary waveguide can provide a maximum enhancement in the Raman exponential gain by a factor of almost fourteen times for a beam 2.5 times diffraction limited when a 132 micron bore diameter capillary is used. An important point to note is that the enhancement provided by the capillary is improved for a non diffraction limited beam when the capillary bore diameter is not the optimum value, i.e. for a non diffraction limited beam it is even more worthwhile to use a capillary waveguide than for a diffraction limited pump beam. For example, for a 350 micron bore diameter the enhancement factor is 2.0 for a diffraction limited beam and 4.4 for a 2.5 times diffraction limited beam. Figure 5 shows a photograph taken of the beams coming out of the capillary waveguide used as a Raman amplifier.

There are two anti-Stokes and 3 Stokes components, the pump beam has a wavelength of 532 nm and it is non diffraction limited and the input radiations have a ring-like shape yet a reasonably symmetrical beam was generated as one can observe from the Stokes spot shape. The wavelength for the third Stokes component is in the 1.5 μm region and its pulse energy is ~ 500 microjoules in a 20 nanosecond pulse , approximately the same energy as the pump pulse seen in the photograph. This experiment will be described in more deitail in a later publication in this magazine.

6. Acknowledgment

This work has been suported by the Science and Engineering Research Council. M.Tadeu Pacheco acknowledges the support from Instituto de estudos Avancados/CTA, Brasil and finally we would like to thank Dr. I.D.Carr for his valuable comments.

FIGURE CAPTIONS

Figure 1. Scheme of SRS generation in an unguided medium.

Figure 2. Scheme of SRS generation in a capillary waveguide,

Figure 3. SRS threshold power for a guided and an unguided media.

Figure 4. Enhancement factor against capillary diameter for a beam 1, 1.5, 2.0, 2.5 and 3 times diffraction limited.

Figure 5. Photograph of the beams coming out the capillary waveguide. The wavelength of the pump radiation is 532 nm. Two anti-Stokes components can be observed at the left side of the pump spot and two Stokes components at the right side.

REFERENCES

1. Kogelnik H. and Li T., Appl. Optics, 5, (1966) 1550

2. Cotter D., Hanna D.C. and Wyatt R., Appl. Physics, 8, (1975), 333

3. Marcatili E.A.J. and Schmeltzer R.A., Bell Syst. Tech. Journal,43 (1964) 1783

4. Abrams R.L., IEEE J. of Quant. Electronics, QE8, 11 (1972), 838

5. Pacheco M.T., PhD thesis, Southampton (1986)

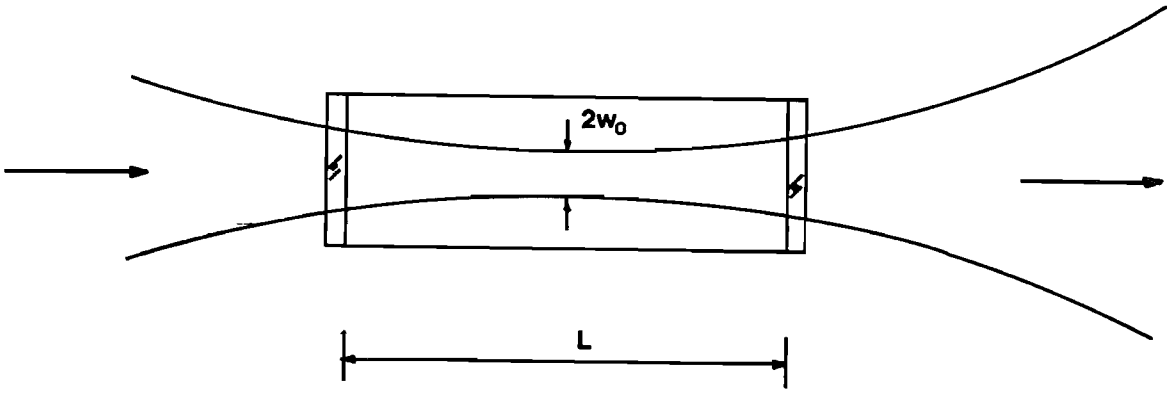

Figure 1

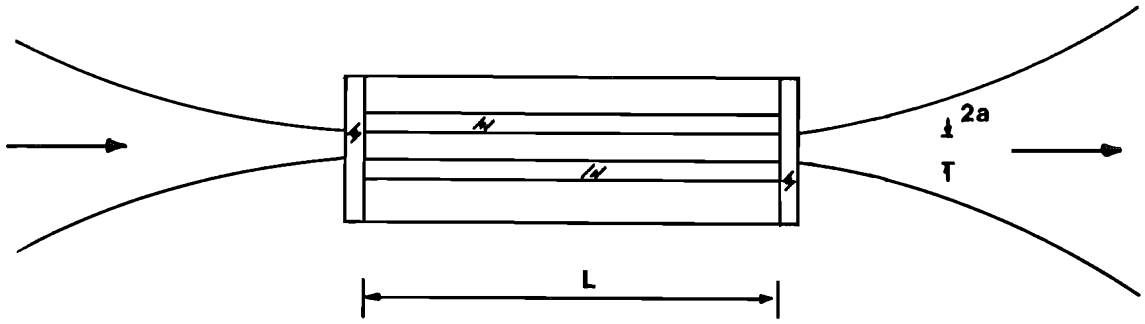

Figure 2

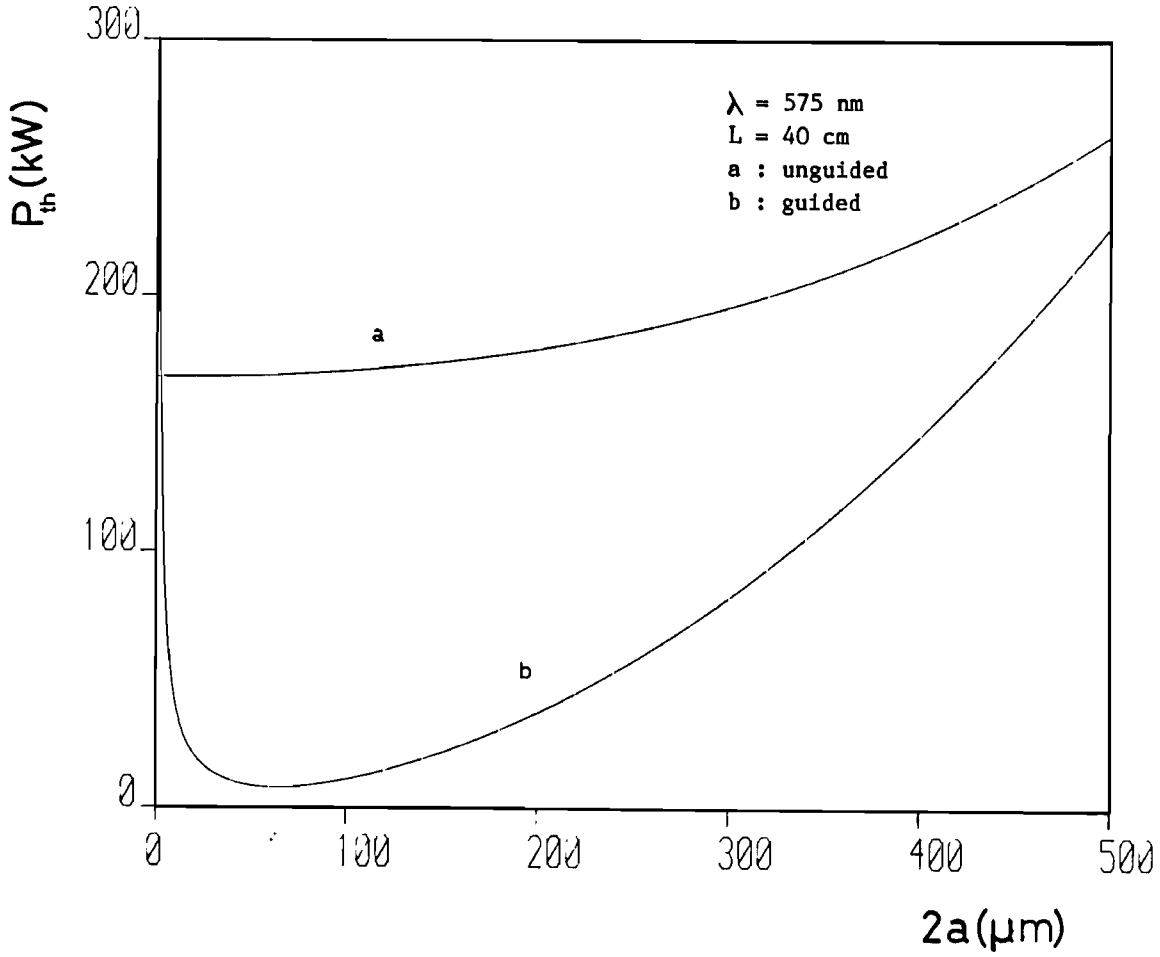
300
200
100
0
P_{th} (kW)
λ = 575 nm
L = 40 cm
a : unguided
b : guided
a
b
0
100
200
300
400
500
2a(μm)

Figure 3

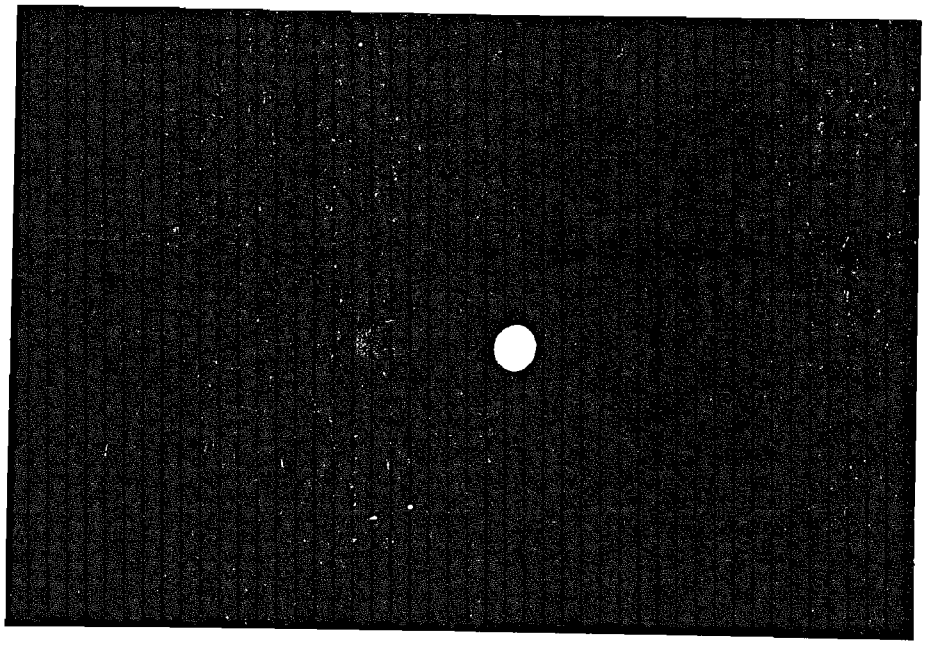

Figura 5

Low threshold operation of a capillary waveguide Raman laser: a convenient source of mode-locked pulses at 1.54μm

D C Hanna, M T T Pacheco and D Shepherd

Department of Physics

University of Southampton

Highfield, Southampton SO9 5NH

The spectral region around 1.5μm is currently receiving emphasis as a result of the requirement of optical communication systems. There is a continuing need for sources in this region and in particular for sources of mode-locked pulses of sufficient power to allow investigation of soliton behaviour and pulse compression. We report the development of such a source at 1.54μm, of pulse duration < 100psec, peak power > 30kw, based on stimulated Raman scattering (SRS) using a mode-locked, Q-switched cw NdYAG laser as pump. The Raman medium is CH_4, at a pressure of ~70 atmospheres, contained in a hollow glass capillary waveguide. The waveguide configuration reduces SRS threshold by more than an order of magnitude, to ~30μJ, well below the 70μJ energy available in the ~100psec pulses from the NdYAG laser. Besides reducing the threshold the waveguide ensures diffraction-limited performance for the Raman source. A further significant reduction of threshold, by a factor of 4, has been achieved by

operating the waveguide Raman laser as synchronously-pumped oscillator, by feeding back the Stokes radiation via a ring resonator configuration. Threshold energy is thereby reduced to ~7μJ per pulse ie. ~70kw. It is expected that the output at 1.54μm will be transform-limited and current measurements are aimed at checking this.

Low threshold operation of a capillary waveguide Raman laser: a convenient source of mode-locked pulses at 1.54μm

D C Hanna, M T T Pacheco and D Shepherd

Department of Physics

University of Southampton

Highfield, Southampton SO9 5NH

The spectral region around 1.5μm is currently receiving emphasis as a result of the requirements of optical communications systems. There is a continuing need for sources in this region and in particular for sources of mode-locked pulses of sufficient power to allow investigations of soliton behaviour and pulse compression. So far the colour centre laser has provided the only suitable source. In this paper we report the development of a source of mode locked pulses at 1.54μm based on stimulated Raman scattering (SRS) in CH_4 in a capillary waveguide using a commercial mode-locked Q-switched cw NdYAG laser as the pump. Since such a pump laser is widely used in optical communication research laboratories, and capable of high repetition rate operation(~1khz), the simple addition of a capillary Raman cell provides a potentially attractive and simple route to short pulse operation at 1.54μm.

Previous measurements of Raman gain in CH_4 in a capillary waveguide [1] had indicated that low enough threshold energies should in principle be achievable to permit oscillation with the ~70-80μJ energy available in ~100ps pulses from a mode locked Q-switched cw NdYAG laser. In practice a threshold energy of just 30μJ has been achieved, for a single pass Raman generator. The Q-switched envelope contains ~20 pulses of sufficient energy to exceed threshold and the Raman output consists of a train of ~10 pulses. A single pulse selector could be used if desired. On the other hand the train of pump pulses can be exploited to provide synchronous pumping of a Raman oscillator. In this way we have reduced the threshold by a factor of four, so that at threshold the energy of individual mode-locked pulses is just 7.4μJ, ie. an order of magnitude less than the pump laser is capable of providing.

The laser used in these experiments is a Spectra Physics 3000, cw NdYAG laser. It gives an output energy of ~1.4mJ in a 220nsec Q-switched envelope, containing mode-locked pulses of ~100psec duration at a repetition frequency of 82MHz, implying a peak pulse energy of ~70μJ. The output was TEM_{00} mode. The fused silica capillary waveguide, of length 81cm, internal diameter 180μm, outside diameter 300μm, was supported in thick walled capillary and this was held in a high pressure cell of ~1m length equipped with a fused silica window at each end [2]. The pump beam was focussed to a beam waist at the capillary entrance, with waist size w_0 chosen to be one third the capillary diameter. Careful alignment of the capillary ensured that coupling was predominantly to the EH_{11} mode and the

transmitted radiation leaving the capillary was in the form of a clean circular spot. An advantage of the capillary waveguide, besides providing a reduced threshold, is that the SRS output is in a diffraction limited beam.

The output energy of the Stokes radiation at 1.54μm, has been measured to be ~ 3μJ in a single mode locked pulse, when the input pump energy at 1.06μm was ~70μJ. Pulse duration of the Stokes output has not yet been measured, but, since it must be less than the 100psec of the pump pulse, the peak output power is at least 30kw. So far measurements have all been made at 5Hz repetition rate since early measurements at 1kHz suffered from problems of decomposition of the CH_4 gas forming a carbon deposit on the input window and the capillary input. The cause of this gas decomposition is not yet understood but it appears to be related to average input power, occurring even with fixed Q output from the NdYAG laser. Operation at 5Hz, with its reduced average power has eliminated the problem. Future tests will examine the maximum repetition rate at which operation can be maintained. A single pulse switchout will allow much higher repetition rate,~100Hz, for the same average power as used in our current experiments.

The synchronously pumped Raman oscillator should also permit higher repetition rate operation since the input power requirement is significantly reduced. The oscillator configuration was in the form of a ring having four reflectors, three being 90^0 total internal reflection prisms and one being an uncoated glass plate acting as a

beam splitter to transmit the pump and reflect the Stokes beam. Cavity length adjustment was provided to ensure synchronism and intracavity lenses provided matching of the Stokes beam from the output end of the capillary back into the input end. The observed threshold reduction of a factor of four is in good agreement with a simple model, as indeed are the absolute threshold values. Further measurements planned for the synchronously pumped oscillator include a measurement of pulse duration. Some pulse shortening can be anticipated. Pulse duration and bandwidth measurements will also be made on the single pass Raman generator to see whether, as expected the pulses are transform-limited. With the peak powers of > 30kw already produced by this source, more than enough power is now available for a number of nonlinear propagation studies in optical fibres.

References

1. D C Hanna, D J Pointer and D J Pratt, IEEE J.of Quantum Electronics, to be published (Feb 1986)

2. A J Berry, D C Hanna and D B Hearn. Optics Comm. 43, 229 (1982)

Optics Communications

Higher-Stokes order Raman conversion to the near infrared: High efficiency and brightness via a capillary waveguide amplifier.

D C Hanna and M T T Pacheco

Department of Physics

University of Southampton

Highfield

Southampton SO9 5NH

UK

Abstract

Efficient Raman conversion in H_2 gas from 0.53μm to third Stokes (S_3) at 1.58μm has been demonstrated using an oscillator/amplifier configuration. Seed radiation from the oscillator controls the divergence of the Stokes beams and a capillary amplifier configuration enhances the conversion. An overall 9% photon conversion efficiency to S_3 is achieved with the S_3 beam divergence twice the diffraction limit. Photon conversion efficiency within the amplifier is ~20%.

Stimulated Raman scattering of dye laser radiation in H_2 gas offers an attractively simple means of generating radiation with wide tunability. Multiple Stokes shifts can be produced simply by focussing the pump beam into the Raman medium. By using a capillary waveguide [1-3] the Raman gain can be considerably enhanced and this has allowed efficient conversion of dye laser radiation to third Stokes radiation in the infrared [2,4]. A problem generally encountered with such Raman generators, whether a guided or unguided geometry is used, is that the higher order Stokes radiation may be generated with a large angular spread. Potential uses of this Stokes radiation may be vitiated by this reduced spatial coherence and potential users are often unable to assess the potential utility since most reported results on such Raman generators do not include quantitative data on beam quality. Techniques for achieving efficient multiple Stokes generation with near diffraction-limited beam quality have been demonstrated [5-7]. The principle involves first generating the multiple Stokes radiation in a Raman oscillator and then injecting this radiation, after suitable spatial filtering, into a Raman amplifier where it acts as a seed from which each of the successive Stokes orders will grow. The generated Stokes radiation can then preserve the spatial coherence of the injected radiation. In their demonstration of this principle Komine and Stappaerts [5,6] used an ultraviolet pump laser, with 1st, 2nd and 3rd Stokes all in the visible region of the spectrum. In this paper we report an extension of this technique to infrared generation. Here the main difficulty to contend with is the reduced Raman gain at longer Stokes wavelengths.

To overcome this problem we have used a capillary waveguide configuration to enhance the gain in the amplifier. We report the result obtained from this scheme. To summarize the experimental results, we have converted 0.53μm pump radiation to 3rd Stokes radiation at 1.58μm with a photon conversion efficiency of 9%. The measured divergence of the 3rd Stokes beam corresponds to twice the diffraction limited value, somewhat better than the beam quality (2.5 x diffraction limit) of the pump laser itself. The conversion efficiency is better than that reported by Hartig and Schmidt [2] and comparable to that recently reported by Mannik and Brown [4] (both of whom used a capillary Raman generator alone) despite the fact that our pump power was around seven times smaller. This testifies to the advantage of the oscillator/amplifier configuration.

Since a dye laser of suitable power to act as the pump laser was not available for these measurements we used the second harmonic of a Q-switched Nd:YAG laser. The Nd:YAG laser was deliberately operated with a number of transverse modes, so that the second harmonic beam, with a measured divergence around 2.5 times the diffraction limit, simulated the beam quality of typical high power dye lasers, but the power (corresponding to a 20mJ pulse of 22nsec duration) was somewhat lower.

The arrangement of Raman oscillator and amplifier is shown in fig.1. This scheme is simple to use since the Stokes radiation generated in the oscillator is automatically aligned and temporally overlapped with the pump radiation as it enters the amplifier stage. A similar scheme

has been found to give very efficient operation where performance was optimised for 1st Stokes generation [8]. For the scheme in fig 1. the requirements are that 1st, 2nd and 3rd Stokes radiation be generated in the oscillator but without causing too great a depletion of the pump since this needs to be preserved for the amplifier stage. Suitable conditions for this to be achieved were found with a 10 atmosphere gas pressure and the pump beam focussed to a spot radius of ~240μm at the centre of the oscillator cell. The low gas pressure enhanced the production of higher order Stokes via four-wave mixing. With these conditions the generated energies from the oscillator were 2.2mJ (S_1), 0.45mJ (S_2), 45μJ (S_3) with ~9 mJ of pump radiation still remaining.

With our limited power we found it beneficial to enhance the gain in the amplifier stage by using a capillary waveguide. When an amplifier stage without waveguide was used, efficient generation of second Stokes (S_2) could be achieved (11% quantum efficiency) but the best efficiency for S_3 generation, after testing various focusing arrangements and gas pressures in the amplifier, was ~1.5%. This was increased by a factor of six when a capillary waveguide was used in the amplifier. The waveguide consisted of a fused silica capillary of 70cm length and 350μm bore diameter. Ideally a large bore diameter is desired to reduce four-wave mixing processes and thus allow domination by the cascade of Raman processes growing from the seed radiation [5,6]. A large bore in turn implies a long guide length to provide sufficient Raman gain. We have therefore used the maximum convenient length. However the bore diameter had to be chosen small enough for

the Raman gain to allow the cascade to proceed to the point where efficient S_3 generation was reached. A 350μm diameter was necessary for this . To further suppress the four-wave processes in the amplifier the gas pressure was increased to 30 atmospheres. We estimate, using the analysis below (Appendix) that this capillary was capable of enhancing the Raman gain for our multimode pump by a factor of ~4.5 compared with an unguided amplifier.

To launch the pump beam and S_1, S_2,S_3 beams into the capillary a 20cm lens was used. The launch condition was adjusted to maximise the transmission of the pump light, resulting in ~45% transmission. This was significantly less than our estimate for maximum transmission of ~85% (Appendix). It is not clear whether this discrepancy stems from the inadequacy of our rough estimate, or whether, in view of the fact that an exhaustive optimisation was not carried out, a better transmission might be possible with greater care taken. The transmission of the capillary for the S_1 (683nm), S_2(954nm) and S_3 (1.58μm) inputs was also measured, without any H_2 gas in the capillary, giving respective values of 37%, 45% ~10%. Estimates of the Raman gain for S_1,S_2,S_3 under these pump conditions, using the Raman gain coefficient $G_R = 1.85 \times 10^{-11} / \lambda_s(\mu m)$ m/w [9]

indicate that with these seed radiation intensities the cascade of Raman process should proceed to saturation for third Stokes generation. Fig. 2 shows the experimentally measured energies for S_1, S_2, S_3 emerging from the amplifier, as a function of gas pressure. At the maximum pressure of ~30 atmospheres, the generated S_3 energy, 0.58mJ,

corresponds to a photon conversion of ~ 20% if one considers only the pump radiation input to the capillary. The overall photon conversion efficiency to S_3, from the 20mJ of pump energy originally available was ~9%. The beam quality of the S_3 beam was checked by focussing the beam (after separation from S_1, S_2 by a prism), measuring the beam waist size ad the divergence from this waist. A detector and scanning slit was used for these measurements. The result showed that the S_3 beam had a smooth profile with a central maximum and none of the ring structure characteristic of four wave mixing, and a beam divergence of 1.8 times the diffraction limit. This was despite the fact that the S_3 beam generated in the oscillator had its origin in a four-wave mixing process. In fact the process of launching into the capillary and of propagation of S_3 within the capillary both have a spatial filtering action which cleaned up the S_3 beam before it underwent Raman amplification.

Conclusion

We have shown that the use of a Raman oscillator/amplifier configuration, with its ability to improve beam quality in multiple Stokes generation can be usefully extended to operation in the near infrared region. We have also shown that beam enhancement can be maintained when the amplifier incorporates a capillary waveguide. The gain enhancement provided by the waveguide has allowed us to demonstrate efficient performance with a laser of modest power. With typical

commercial pulsed dye lasers, whose powers are greater than the pump used in these experiments, this approach should permit a significant extension of the infrared tuning range.

Acknowledgements

This work has been supported by the Science and Engineering Research Council. M T T Pacheco acknowledges the support from IEAV/Centro Tecnico Aerospacial, Sao Paulo, Brasil.

Appendix: Capillary waveguide transmission and enhancement of Raman gain for a multitransverse mode pump.

An estimate of the enhancement of Raman gain provided by a capillary waveguide for a TEM_{00} mode pump has been given previously [3]. Here we derive a more general expression to include also the important case of a pump laser which is not diffraction-limited. First we consider the gain enhancement for a TEM_{00} mode pump, where it is assumed that this mode couples perfectly to the EH_{11} mode of the guide when the waist size w_0 at the guide entrance is equal to $2a/3$ where 2a is the guide diameter [10]. The Raman gain exponent G_g (ie. where exp G_g is the power gain) for a pump power P in a guide of length L is then given by [9]

$$G_g = P\, g_R\, L_{eff} / A_{eff} \qquad (1)$$

where $L_{eff} = [1 - \exp(-\alpha L)]/\alpha$ (2)

and $\alpha = 0.43\lambda_p^2/a^3$ (3)

The effective area A_{eff} is taken to be $\pi w_0^2 = 4\pi a^2/9$ [9].

If the effect of Stokes beam diffraction is ignored, then for the unguided TEM_{00} pump focussed to give a confocal parameter b, the Raman gain experiment G_u evaluated along the beam axis is [3],

$$G_u = \frac{4Pg_R}{\lambda_p} \tan^{-1}(L/b) \qquad (4)$$

To compare the values of G_g and G_u, i.e. to work out the gain enhancement factor due to the guide, $S \equiv G_g/G_u$, we assume the same spot size in the guided and unguided case. (Generally, since the value of w_0 is such that $L/b \gg 1$, hence $\tan^{-1}(L/b) \sim \pi/2$ this assumption is not restrictive) Thus S is given by

$$S = \frac{9\lambda_p\,[1-\exp(-\alpha L)]}{16\pi a^2 \alpha\, \tan^{-1}(L/b)} \qquad (5)$$

For a multimode pump we characterise the beam quality by the factor M by which the pump beam divergence exceeds the diffraction limited value $\lambda/\pi w_0$. Here w_0 refers to the $1/e^2$ intensity radius of the multimode pump beam. The guide loss for such a multimode excitation can be estimated by a simple application of a ray analysis. Such an analysis has been shown [11] to give a remarkably good agreement with the loss calculated for individual guide modes by the full e.m. wave treatment [12]. Here we model the behaviour of the multimode propagation by assuming the rays to travel at an angle to the guide axis given by $M\lambda/2a$ where this represents the divergence of a beam of diameter 2a. Then the number of reflections per unit guide length and the Fresnel reflection at each bounce can be calculated, leading to an expression for the guide loss per unit length given by $M^2\lambda^2/a^3$. Apart from a numerical factor of the order of unity this agrees for the single mode case (M = 1) with the exact wave analysis. The effect of the multimode beam is therefore essentially to replace λ by $M\lambda$. To give agreement with the single mode case the loss per unit length is taken to be $0.43M^2\lambda_p^2/a^3$. This simple model gives the guide

transmission as $\exp(-M^2\alpha L)$. It is also seen that the value G_u' taken by G_u for the unguided case is simply given by equation (4) with λ_p replaced by $M\lambda_p$ and b ($= 2\pi w_o^2/\lambda_p$) replaced by $b' = 2\pi w_o^2/M\lambda_p = b/M$ With these changes the factor S' by which the guide enhances the Raman gain for a multiple pump is

$$S' = \frac{G_g'}{G_u'} = \frac{9M\lambda p\ [1 - \exp(-M^2\alpha L)]}{16\pi a^2 M^2 \alpha \tan^{-1}(ML/b)} \qquad (6)$$

Figure 3 shows plots of S' versus guide diameter for a length L = 70cm and λ_p = 0.53μm, with M as a parameter. For the conditions of our experiment the enhancement is predicted to be ~4.

Further refinement of this model can be made by taking account of the Stokes wave diffraction loss for the unguided case. For a TEM_{00} beam equation (4) becomes [13]

$$G_u' = \left[\left(\frac{\lambda_s}{\lambda_p}\right) \tan^{-1} \left(\frac{L}{b}\right) \right] \left[\left(\frac{4P_{gR}}{\lambda_s}\right)^{\frac{1}{2}} \left(\left(\frac{4P_{gR}}{\lambda_s}\right)^{\frac{1}{2}} - 2 \right) \right] \qquad (7)$$

and G_u' for an unguided multimode beam becomes

$$G_u' = \left[\left(\frac{\lambda_s}{M\lambda_p}\right) \tan^{-1} \left(\frac{ML}{b}\right) \right] \left[\left(\frac{4P_{gR}}{\lambda_s}\right)^{\frac{1}{2}} \left(\left(\frac{4P_{gR}}{\lambda_s}\right)^{\frac{1}{2}} - 2 \right) \right] \qquad (8)$$

For large powers, ie. where $\frac{P_{gR}}{\lambda_s} \gg 1$ (8) reduces to the simpler expression (4).

References

1. P Rabinowitz, A Kaldor, R Brickman and W Schmidt, Appl.Optics 15 (1976) 2006.

2. W Hartig and W Schmidt, Appl. Phys. 18 (1979), 235.

3. A J Berry, D C Hanna and D B Hearn, Optics Commun. 43 (1982) 229

4. L Mannick and S K Brown, Optics Commun. 57, (1986) 360.

5. H Komine and E A Stappaerts, Optics Letts, 4 (1979) 398.

6. H Komine and E A Stappaerts, Optics Letts., 7 (1982) 157.

7. H Komine, E A Stappearts, S J Brosnan and J B West, Appl.Phys. Lett., 40 (1982) 551.

8. D C Hanna, M T T Pacheco and K H Wong, Optics Commun. 55, (1985) 188.

9. D C Hanna, D J Pointer and D J Pratt, IEEE J.of Quantum Electron. QE-22, (1986) 332.

10. R L Abrams, IEEE J.of Quantum Electron. QE-8 (1972) 838.

11. M J Adams 'An Introduction to Optical Waveguides' John Wiley & Sons 1981.

12. E A J Marcatili and R A Schmeltzer, Bell Syst.Tech.J. 43 (1964), 1973.

Captions

Figure 1. Schematic arrangement of Raman oscillator/waveguide amplifier.

Figure 2. Pulse energy for S_1 (683nm), S_2 (954nm), S_3 (1.58μm) versus H_2 pressure in the Raman amplifier.

Figure 3. Enhancement of Raman gain due to the waveguide, as a function of capillary diameter. The parameter M specifies the extent to which the pump beam divergence exceeds the diffraction limit.

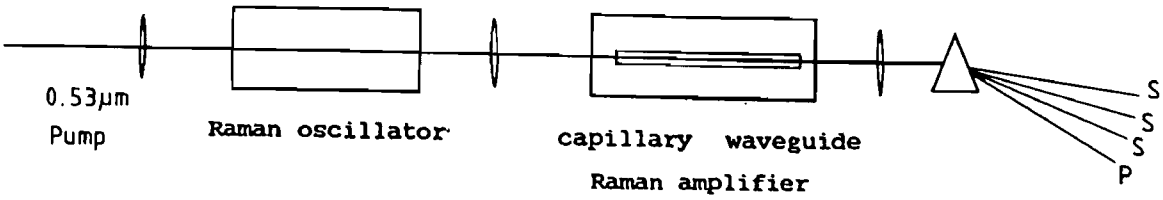
0.53μm
Pump
Raman oscillator
capillary waveguide
Raman amplifier
S
S
S
P

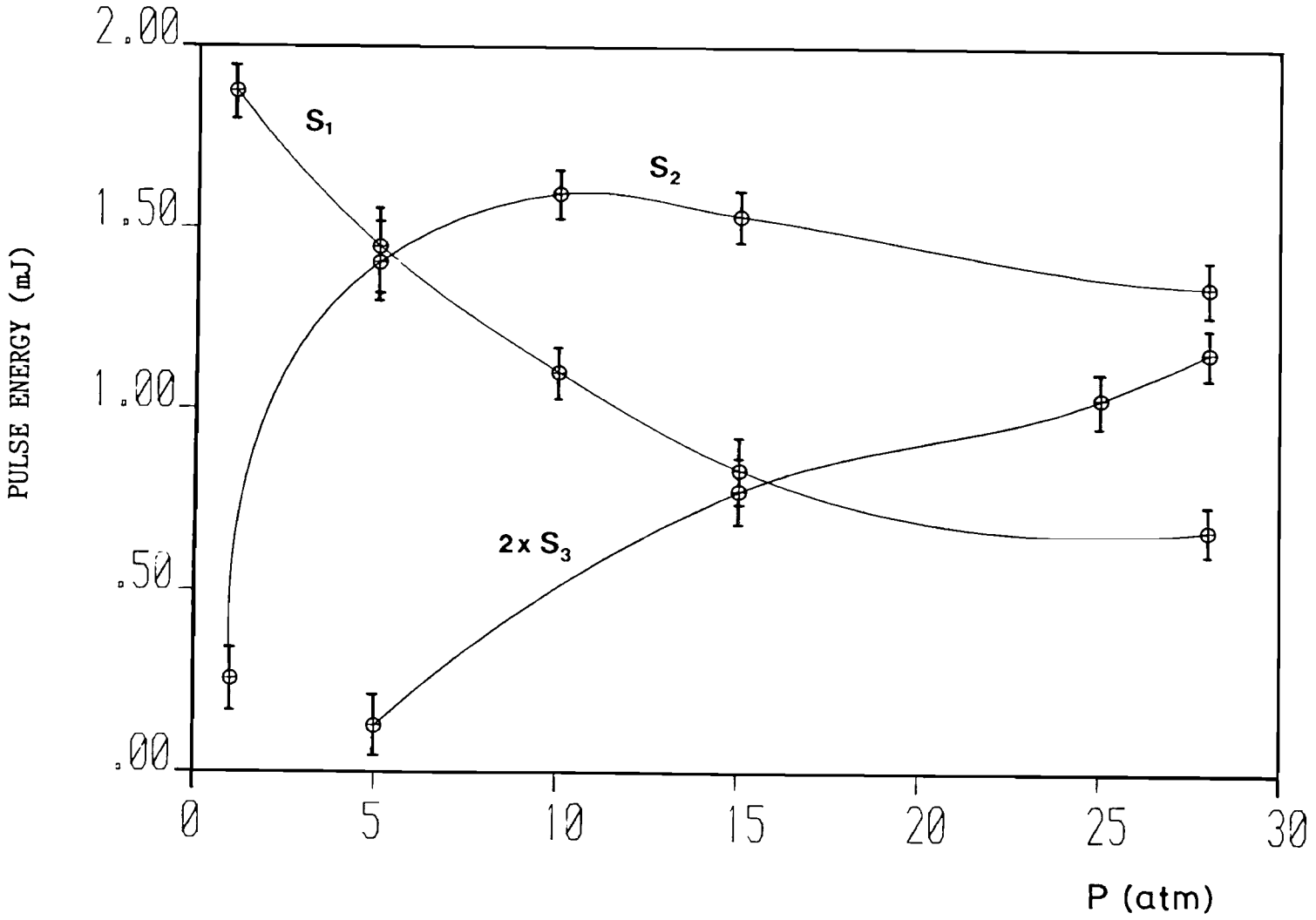
2.00
1.50
1.00
.50
.00
PULSE ENERGY (mJ)
S1
S2
2x S3
0
5
10
15
20
25
30
P (atm)

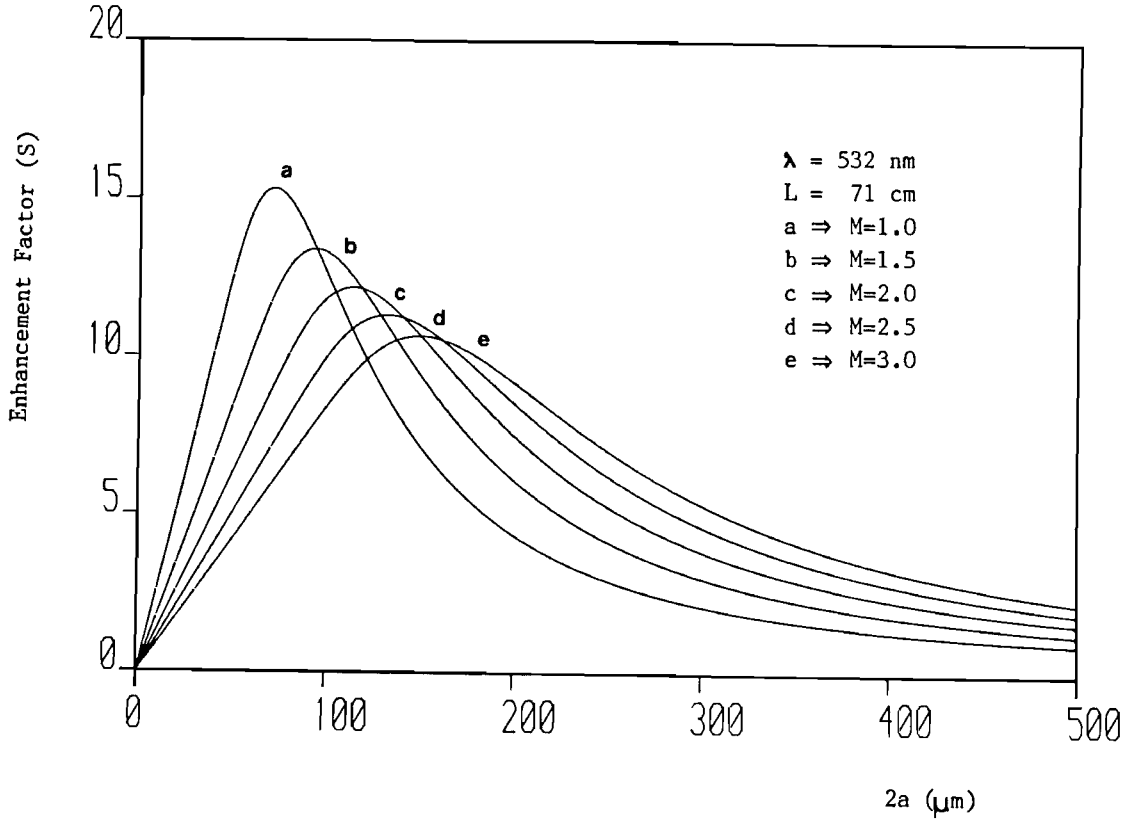
Enhancement Factor (S)
20
15
10
5
0
0
100
200
300
400
500
2a (μm)
λ = 532 nm
L = 71 cm
a ⇒ M=1.0
b ⇒ M=1.5
c ⇒ M=2.0
d ⇒ M=2.5
e ⇒ M=3.0
a
b
c
d
e

REFERENCES

R.L.Abrams, IEEE Journal of Quant. Elect. QE-8, 11 (1972)

S.A.Akhmanov, Yu.E.D'Yakov, and L.I.Pavlov, Sov. Phys. JETP,39 (1974)

R.R.Alfano and S.L.Shapiro, Phys. Rev. A 2, 6(1970)

BDH catalogue 1985/1986

A.F.Bernhardt and P.Rasmussen, Appl. Phys. B26, (1981)

A.J.Berry, D.C.Hanna and D.B.Hearn, Optics Commun. 43 (1982)

A.J.Berry and D.C.Hanna, Optics Commun. 45 (1983)

S.J.Brosnan, R.N.Fleming, R.L.Herbst and R.L.Byer, Appl. Phys. Lett. 30 (1977)

P.N.Butcher, Nonlinear Optics of free Atoms and Molecules,(1964)

V.S.Butylkin, V.G.Venkin, V.P.Protasov, P.S.Fisher, Yu G. Khronopulo and M.F.Shalyaev, Sov. Phys. JETP, 43, 3 (1976)

V.S.Butylkin, V.G.Venkin, L.L.Kulyuk, D.I.Maleev, Yu G.Khronopulo, and M.F.Shalyaev, Sov. J. Quantum Electron., 7, 7 (1977)

R.L.Carman, M.E.Mack, F.Shimizu, and N.Bloembergen, Phys. Rev. Letters 23 (1969)

I.D.Carr and D.C.Hanna, Appl. Phys. B 36 (1985)

I.D.Carr, PhD thesis, Southampton University (1985)

M.J.Colles, Opt. Commun., 1,4 (1969)

M.J.Colles and J.E.Griffiths, The Journal of Chem. Physics, 56, 7 (1972)

D. Cotter, D.C.Hanna and R. Wyatt, Appl. Phys. 8 (1975)

G.Eckhardt, R.W.Hellwarth, F.J.McClung, S.E.Schwarz, D.Weiner, and E.J.Woodbury, Phys.Rev.Letters, 9 (1962)

G.Eckhardt, IEEE J.of Quantum Electronics, QE-2, 1 (1966)

W.R.Fenner, H.A.Hyatt, J.M.Kellan, and S.P.S.Porto, J. Opt. Soc. Am. 63 (1973)

D.G.Fouche, R.K.Chang, Appl. Phys.Lett. 20 (1972)

T.Govindanunny, Appl. Phys. 23 (1980)

E.P.Ippen, Appl.Phys. Lett. 16, 8 (1970)

G.Hall and J.M.Watt (eds.), Modern Numerical Methods for Ordinary Differential Equations, Clarendon Press, Oxford (1976)

P.R.Hammond, IEEE Journal of Quant. Elect. QE-15, 7 (1979)

D.C.Hanna, P.A.Karkkainen and P.Wyatt, Opt. Quant. Elect. 7 (1975)

D.C.Hanna, M.A.Yuratich and D. Cotter, Nonlinear Optics pf Free Atoms and Molecules, Springer-Verlag Series in Optical Sciences 17 (1979)

D.C.Hanna, C.G.Sawyers and M.A.Yuratich, Opt. Commun. 37 (1981)

D.C.Hanna, private communication (1984)

D.C.Hanna, D.J.Pointer and D.J.Pratt, IEEE Journal of Quant. Elect. QE-22, 2 (1986)

T.W.Hansch, Appl.Opt.,11 (1972)

W.Hartig and W.Schmidt, Appl.Phys., 18 (1979)

W.Kaiser and M.Maier, Laser Handbook, chapter E2 edited by F.T.Arecchi and E.O.Schulz-Dubois (1972)

H.Kamiyama, S.Okano, N.Maruyama, paper III-5 at VIth Int. Laser Radar Conf., Sendai, Japan (1974)

T.Kasuya, T. Suzuki and K. Shimoda, Appl. Phys., 17 (1978)

H.Kogelnik and T. Li, appl. Optics, 5 (1966)

H.Komine and E.A.Stappearts, Opt. Lett., 4, 12 (1979)

H.Komine and E.A.Stappearts, Opt. Lett., 7, 4 (1982)

A.V.Krumin'sh, D.N.Nikogosyan, and A.A.Oraevskπ, Sov. J. Quantum Elect., 14, 7 (1984)

L.C.Laycock, PhD thesis, Southampton University (1978)

P.Lorrain and D. Corson, Electromagnetic Fields and Waves, W.H. Freeman and Company (1970)

E.A.J.Marcatili and R.A.Schmeltzer, Bell Syst. tech. J. 43 (1964)

T.J.Mckee and D.J.Janes, Can. J. Phys., 57 (1979)

J.G.Meadors and M.A.Poirier, IEEE J. of Quant. Electronics, 12 (1972)

C.A.Moore and C.D.Decker, J.Appl.Phys., 49 ,1 (1978)

C.G.Morgan, Chem. Soc. Reviews, 8, 3 (1979)

J.Mostowski and M.G.Raymer, Opt. Commun., 36 (1981)

W.F.Murphy, W.Holzer and H.J.Berstein, Appl. Spectrosc. 23 (1969)

L.G.Nair, Opt. Commun., 23 (1977)

J.H.Newton and G.M. Schindler, Opt. Lett., 6 (1981)

S.Yu Nikitin, Sov. J. Quant. elect., 12, 3 (1982)

A.Owyoung, Opt. Lett., 2, 4 (1978)

E.R.Peck and S.Huang, J. Opt. Soc. Am., 67, 11 (1977)

C.M.Penney, L.M.Goldman and M.Lapp, Nature Phys. Sc., 235 (1972)

D.J.Pointer, private communication (1985)

D.J.Pratt, PhD thesis, Southampton University (1985)

B.Racz, Zs. Bor, S. Szatmari and G. Szabo, Opt. Comm. 36 (1981)

E.Sahar and D.Treves, IEEE J. Q. Elect., QE-13 (1977)

H.W.Schrotter and H.W.Klockner, Chapt. 4, Raman Spectroscopy of gases and Liquids, Springer-verlag (1979)

C.V.Shank, A.Dienes and W.T.Silfvast, Appl. Phys. lett., 17, 7 (1970)

Y.R.Shen and N.Bloembergen, Phys.Rev. 137, 6A (1965)

Y.Taira, K.Ide and H.Takuma, Chem. Phys. Letts., 91 (1982)

H.Telle and W.Huffer, Opt. Comm., 38 (1981)

V.I.Tomin, Opt. Comm., 26 (1978)

B.V.Zhdanov, L.L.Kulyuk and S.M.Pershin, Sov. J.Quantum Electron., 6, 5 (1976)

ACKNOWLEDGEMENTS

Firstly, I am indebted to my supervisor, Dr. David C. Hanna, for his invaluable advice and continuous encouragement during the period of this work. Many thanks are due to other members of the laser group at Southampton University, in particular Ian David Carr and Kin Hung Wong for their help, Ruth Holder for technical assistance, David Pointer, D. Shepherd, L.Bromley, M.Phillips, H.Gong and Dr. A.I.Ferguson.

Financial support was provided jointly by the Science and Engineering Research Council and The Instituto de Estudos Avancados (Brazil).